Membrane-Mediated Cell Biological Communication Mechanisms in Reproduction

A Thesis submitted in fulfilment of the requirements
for the degree of D.Phil. in Physiology, Anatomy and Genetics

Felix Castellanos

St Edmund Hall

Hilary Term 2018

Supervisor: Professor Clive Wilson

Department of Physiology, Anatomy and Genetics

University of Oxford

i. Acknowledgments

First and foremost, I would like to thank my supervisor, Professor Clive Wilson, for his enormous support, brilliant guidance and unwavering encouragement. I cannot thank him enough for always believing in me, and for giving me the wonderful opportunity to be a part of his research group. He is one of the greatest mentors I had the opportunity to work with, he is truly inspirational. My sincere gratitude to him.

I am also utmost grateful to my examiners for taking time from their busy schedules to assess my thesis.

I would also like to thank my current and former members of the Wilson laboratory, a special thanks to Benjamin Kroeger and Shih-Jung Fan. I want to acknowledge the support from Mark Wainwright, Deborah Goberdhan, Kristie McCormick, Josephine Hellberg and Carina Gandy, to whom I am indebted in more than one way.

I am very grateful to my friends in Oxford, in particular Siddharth Arora, John Delaney, Thomas More Mann, Matthias Mang, Laura Bernal Bermudez, Athanasios Tsanas, Laura Canevari, Carlos Rios Ocampo, Felipe De La Parra and Christos Krastev, for being so helpful and kind.

I am obliged to thank Luis Sanchez-Pulido (MCR Human Genetics Unit, The University of Edinburgh), L. Peacock and W. Gibson from the School of Biological Sciences at the University of Bristol.

I am extremely fortunate and thankful to have the support from Jane Clark, Alexandra Brown and Katherine Noren-Curtis.

T. brucei work was performed at the Sir William Dunn School of Pathology in the Gluenz and Gulls Labs. My special thanks to Vladimir Varga, Helen Farr and Michael Fiebig for insightful discussions.

This project is made possible through the generous funding of COLCIENCIAS, Colombia.

Last but not the least, I want to thank my mother, Isabel Suarez, and my family for being with me all along this journey. Their love, support, sacrifices and belief in me has made this day possible. Many people have shaped my thinking, their guidance and invaluable support has helped me achieve my goals of becoming a biologist. I only hope that I can justify all the love and support I have received over the years, and contribute to the society through my research.

ii. Abstract

Phospholipid bilayers play a critical role in many fundamental aspects of cell biology. They provide the barrier that separates cells and the scaffold upon which many of the molecules that allow cell-cell communication are located. Furthermore, they delimit the boundaries of intracellular organelles, including those responsible for secretory processes, which communicate with the plasma membrane. My thesis focuses on two aspects of membrane-mediated cell-cell communication: cell-cell fusion and the establishment of dense-core granule (DCG) compartments, which package cargos directed for regulated secretion, for example in pancreatic β-cells.

In my first results chapter, I consider an important stage in the life cycle of the parasite *Trypanosoma brucei* (Euglenozoa: Kinetoplastea), the causative agent of African trypanosomiasis, which is transmitted by tsetse flies. Infectious forms of the parasite are found in the salivary gland of the fly, where genetic exchange between parasites has been shown to occur. While plasma membrane fusion between mating competent cells is likely to be the keystone process leading to this exchange, its cellular mechanisms have remained elusive. Bioinformatic analyses had shown that HAP2(GCS1), a gamete-specific factor related to sex cell fusion originally identified in plants, is conserved in trypanosomes. Here I further study the structure of HAP2(GCS1) in *T. brucei* and other organisms and identify new domains in this molecule. Furthermore, I present an analysis of ectopic and endogenous expression of *Tb*HAP2(GCS1), which suggests that high levels of expression may be detrimental to the parasite. Overexpression can alter the nuclear content of parasitic forms, consistent with a role in fusion, while YFP tagging may inactivate the normal function of the protein. However, I was not able to set up an *in vitro* system to track this fusion process, making it difficult to take this work forward.

In the other two results chapters, I analyse the process of dense-core granule compartment biogenesis using a new *in vivo* genetic model to study this process, the *Drosophila* prostate-like secondary cell. In addition to the powerful genetics available in this system, including the ability to knockdown genes of interest specifically in these cells in adults, secondary cells have very large DCG compartments. In collaboration with another graduate student in the group, Benjamin Kroeger, I show for the first time in any *in vivo* system, that the formation of individual compartments can be visualised in real-time. I characterise a series of new live markers to follow this process and define the secretory trafficking pathways in these cells. I then test the function of some of the known conserved genes reported to be involved in DCG biogenesis by adult secondary cell type-specific knockdown. Using this approach, I not only show that the role of these genes is conserved, but also dissect out more specific roles for the AP-1 adaptor complex and the small G-protein Arf1, both of which are involved in important trafficking events. Furthermore, I test the function of new candidate regulatory genes and report a new association between the formation of intraluminal vesicles inside DCG compartments and core formation.

In summary, the second part of my thesis work reveals that the secondary cell has considerable potential to genetically dissect the processes of DCG biogenesis and secretion. In the future, it should be possible to use this system to find novel genes with key roles in these events, which can then be tested for similar functions in mouse models of human disease such as diabetes and neurodegenerative disorders.

iii. List of Abbreviations

(Abd-B) Abdominal-B
(Acp) Accessory gland proteins
(Acp70A) Accessory gland-specific peptide 70A
(AFF-1) Anchor cell fusion failure-1
(AG) Accessory gland
(ALiX) Apoptosis linked factor X
(AnCE) Drosophila Angiotensin I-converting Enzyme
(APs) Adaptor proteins
(Arf1) ADP-ribosylation factor 1
(BMP) Bone morphogenetic protein
(CFP) Cyan fluorescent protein
(Chp) Chaoptin
(DCG) Dense-core granule
(Dpp) Decapentaplegic
(dsRNA) Double-stranded RNA
(Dsx) Doublesex
(Dve) Defective proventriculus
(ED) Ejaculatory duct
(EE) Early endosomes
(EFF-1) Epithelial fusion failure-1
(ER) Endoplasmic reticulum
(ESCRT) Endosomal sorting complexes required for transport
(GCS1) Generative Cell Specific 1
(GFP) Green fluorescent protein
(GLMMPQL) Generalised Linear Mixed Model fitted using Penalised Quasi-Likelihood
(GnRH) Gonadotropin-releasing hormone
(GPI-APs) GPI-anchored proteins
(GPI) Glycosyl-phosphatidyl inositol
(HAP2) Haploid-disrupting, Hapless 2
(iLE) Immature late endosome
(ILV) Intra-luminal vesicle
(K) Kinetoplast
(LAMP) Lysosome-associated membrane protein
(LE) Late endosomes
(LFA-3) Lymphocyte function-associated antigen 3
(LH-RH) Luteinising hormone-releasing hormone
(LPH) Rabbit Lactase-phlorizin Hydrolase

(MC) Main cell
(MDCKs) Madin-Darby Canine Kidney Epithelial cells
(mMVBLs) MultiVesicular Bodies/Lysosomes
(mRNA) Messenger RNA
(MVB) Multivesicular body
(N) Nucleus
(PCFs) Procyclic forms
(PIG) Phosphatidyl Inositol Glycan
(PLs) Promastigote-like cells
(rER) Rough endoplasmic reticulum
(RBP6) RNA-binding protein 6
(RFP) Red fluorescent protein
(RNAi) RNA interference
(RSVP) RNAi Stock Validation and Phenotype
(SC) Secondary cell
(SFPs) Seminal fluid proteins
(SmOx) Single Marker Oxford
(SNARE) Soluble N-ethylmaleimide-sensitive factor attachment protein receptor
(SP) Sex Peptide
(Spi) Spitz
(TGN) Trans-Golgi network
(TRiP) Transgenic RNAi Project
(UAS) Upstream activation sequence
(VAMP) Vesicle associated membrane protein
(Wt) Wild-type
(YFP) Yellow fluorescent protein

Table of Contents

1. Introduction

1.1. Membranes in Cell-Cell Communication

Cell-cell communication underpins almost all aspects of animal biology. For such communication to take place, cells must either interact via direct cell-cell contact or release signalling molecules that act either locally or at a distance. All these events are influenced by membranes, both the membranes at the surface of cells and those surrounding intracellular compartments. While for small molecules like nitric oxide and hydrophobic ligands, such as steroids, diffusion through membranes may be sufficient to allow signalling, more complex mechanisms are involved for other signals. These include ligands that interact with cell surface receptors, signals that are packaged in membrane-bound vesicles, and signalling interactions between surface molecules on adjacent cells. In the most extreme cases, these interactions can lead to the phagocytosis or even fusion of cells, as is observed in fertilisation.

In my thesis, I have focused on two very different forms of cell-cell communication processes that occur in insects and relate to reproductive biology. In the first, I analyse the molecular mechanisms by which mating-competent cells of the parasite *Trypanosoma brucei* fuse in the salivary gland of the tsetse fly, allowing the exchange of genetic material. In the second, I study the mechanisms by which signalling molecules, destined for secretion from the secondary cells of the *Drosophila* male accessory gland, are packaged into dense-core granules inside membrane-bound secretory compartments prior to release into seminal fluid. Previous analysis of dense-core granule biogenesis, as well as the studies I report here, suggests an important role for specific biomolecules and membranes in this packaging process.

Since both aspects of my work focus on insects, their role as disease vectors and the control of their fertility, it is potentially of significance in biotechnological applications and disease control. However, I also demonstrate that many of the molecules involved in these processes are highly evolutionarily conserved, meaning that my studies may be relevant to many other areas of biology and medicine where cell-cell communication is involved.

1.1.1. Eukaryotic cells employ multiple trafficking routes of membrane and secreted protein

The classical eukaryotic secretory pathway primarily involves the rough endoplasmic reticulum (rER), where new membrane and secreted proteins are

synthesised, the smooth ER, where many lipids are produced, and the Golgi apparatus, where proteins are modified by glycosylation, complex oligosaccharides are made and ultimately macromolecules are trafficked into specific secretory compartments.

Many animal cells are polarised, having apical and basolateral faces, and this polarity is critical to their function. This means that these cells require mechanisms to ensure that apical and basolateral proteins are trafficked to the appropriate part of the plasma membrane. Several reports have identified important motifs for such selective trafficking, for example the roles of dileucine in basolateral targeting (Mellman and Nelson 2008, Stoops and Caplan 2014), and the importance of *N*- and *O*-linked oligosaccharides in apically directed proteins (Mellman and Nelson 2008, Vagin, Kraut et al. 2009, Stoops and Caplan 2014). These two distinct membrane domains are separated by junctional complexes that link adjacent cells and prevent simple diffusion from one domain to the other (Shin, Fogg et al. 2006, Mellman and Nelson 2008, Trimble and Grinstein 2015).

The establishment of polarity ensures that many signals (and other macromolecules) are released into the appropriate extracellular space, e.g. apically into the lumen of a gland or basally into the circulation through the basement membrane. Secretion can be constitutive, but it can also be regulated, for example in cells that secrete hormones or release substances into the lumen of an exocrine gland. Regulated secretion involves storage of secreted molecules in secretory compartments, often packaged into aggregated masses called dense-core granules (DCGs)(Dikeakos and Reudelhuber 2007). These compartments fuse to the plasma

membrane in response to an activating stimulus, such as a hormonal or neuronal signal. As we will see (Section 1.1.4), the dense-core granule biogenesis pathway is distinct from the constitutive pathway, and perhaps surprisingly, involves the presence of specific lipids, although the mechanistic explanation for this link remains unresolved.

Since secretion involves the fusion of secretory compartments with the plasma membrane, thus increasing plasma membrane area, it is important that mechanisms exist to internalise this membrane again. The endocytic system provides that balance, trafficking membrane and associated proteins into early endosomes from where they can be returned to the cell surface by a number of recycling pathways or sent to late endosomes and lysosomes (Grant and Donaldson 2009, Scott, Vacca et al. 2014). Trafficking pathways also exist to recycle specific proteins back to the Golgi apparatus, for example the mannose-6-phosphate receptor, which directs lysosomal hydrolases to the lysosome from the trans-Golgi network (TGN), and then must be returned to the Golgi to perform this role again (Arighi, Hartnell et al. 2004). The late endosomes contain many small vesicles formed by inward budding of the limiting membrane, producing a so-called multivesicular body. In the lysosome, these structures can be efficiently degraded; breakdown of macromolecules into their building blocks, like amino acids, allows these molecules to be transported back into the cytosol to be used again (Scott, Vacca et al. 2014). However, there is increasing evidence that late endosomes and lysosomes are also involved in intracellular signalling, for example through the nutrient-sensing mTORC1 pathway (Goberdhan, Wilson et al. 2016) and in intercellular signalling, through secretion of

the intraluminal vesicles as exosomes (Colombo, Raposo et al. 2014, Corrigan, Redhai et al. 2014).

Important regulators of these different secretory and endosomal trafficking routes are the small GTPases known as Rabs, many of which are highly conserved from yeast to humans. They associate with specific types of compartment and are involved in vesicular trafficking to and/or from these compartments (Hutagalung and Novick 2011, Pfeffer 2013). For example, Rab5 regulates the formation of early endosomes, while Rab11 controls one of the recycling endosome pathways in addition to playing roles in secretory trafficking from the trans-Golgi. Another Rab that will be important in my study is Rab6, which is one of the Rabs associated with secretory compartments leaving the trans-Golgi (Hutagalung and Novick 2011, Pfeffer 2013).

Rabs have been studied in many organisms. Recently gene trap lines have been produced for all the *Drosophila* Rabs, which mark the endogenous proteins with an N-terminal YFP tag (Dunst, Kazimiers et al. 2015). These tools have been useful in part of my study of dense-core granule biogenesis in secondary cells, because they allow specific compartments to be marked with fluorescent molecules expressed at endogenous levels, which permits their recognition in living cells.

1.1.2. Cell-cell communication via secreted molecules

Hormones and other signalling molecules involved in cell-cell communication can be classified into several chemical classes, for example steroids, proteins and peptides, small molecule amines, such as noradrenaline and dopamine, and even gases like nitric oxide. Due to their chemical differences, these are synthesized in different parts of the cell and potentially secreted in different ways.

Proteins and peptides are typically translated in the rough ER, are glycosylated as they pass through the ER and Golgi and then can be secreted via constitutive or regulated pathways. These molecules include insulin, growth factors, many of the developmental ligands like Hedgehogs, Wnts and TGF-beta superfamily members, to name but a few. In endocrine and exocrine glands, the key hormones and proteases that are released by the gland are frequently stored so they can be released on demand. They are often packaged within secretory compartments into electron-dense structures called dense-core granules (DCGs; see Section 1.1.4), a process that is still relatively poorly understood.

For many other secreted molecules, it is becoming increasingly clear that they are also not simple soluble ligands. For example, both Hedgehog and Wnt ligands have lipid anchors, which allow them to embed into lipid bilayers once secreted, but also influence their route through the secretory system. They can be carried in complexes with lipoproteins, but can also attach to secreted vesicles like exosomes. As we will see, one aspect of secondary cells that particularly attracted me to this system, is that intraluminal vesicles form inside DCG compartments as well as late endosomal

and lysosomal compartments, and there is an interesting interaction between these vesicles and the core, whose function is unclear. Although ultimately much of my work has focused on the biogenesis of DCGs, I also made several observations concerning the associated vesicles as the project progressed.

The potential for cells to secrete exosomes brings a whole new dimension to secretory biology with ligands, receptors, intracellular signalling molecules and nucleic acids being potential cargos (Colombo, Raposo et al. 2014). The cytosolic molecules can all enter target cells upon exosome fusion, while the ligands may be able to act at the cell surface to activate intracellular signalling cascades (Colombo, Raposo et al. 2014, van Niel, D'Angelo et al. 2018).

Classically signalling molecules like steroids are made in the smooth ER on demand and are therefore thought to be controlled in a very different way to soluble ligands. However, it should be noted that recent work in *Drosophila* has indicated that this model may be oversimplified, with evidence suggesting that the steroid ecdysone, synthesized in the prothoracic gland of the developing late larva and pupa, is pumped into membrane-bound secretory compartments prior to release (Yamanaka, Marques et al. 2015). Secondary cells may synthesise ecdysone (Hentze, Moeller et al. 2013), and so the secondary cell model may also ultimately prove to be useful in developing an understanding of this surprising mechanism.

Although this will not be a focus of my thesis, I will briefly overview how secreted signals function in cell-cell communication. They must ultimately interact with receptors in order to produce a response in target cells. For hydrophilic ligands like

proteins and amines, these receptors are typically transmembrane proteins located at the cell surface, which activate an intracellular signalling cascade, which either controls local events within the cell, such as calcium ion or cAMP release, or controls processes like transcription and protein translation. By contrast, hydrophobic molecules, such as steroids, can bind to intracellular cytosolic or nuclear receptors, which regulate transcription, while soluble gases have more local subcellular effects, promoting cGMP production in the case of nitric oxide.

Given my interests in reproduction, I focused much of my DPhil work on secondary cells of the fly accessory glands, which produce secreted proteins as part of the seminal fluid (see Section 1.3). These are particularly appropriate cells to study the processes of secretion because of the very large secretory compartments they contain. Furthermore, the rate of secretion from these cells must be regulated by mating, when a proportion (perhaps one third to one half) of the luminal content of the accessory glands is transferred to females and must be replenished rapidly. Studying these processes might not only be important in understanding the general control of regulated secretion, but might also suggest pest control strategies in the future, given the fundamental role of the glands in reproduction and the common use of artificially introduced fertility-compromised males in current strategies.

1.1.3. Cell-cell fusion as a mechanism of cell enlargement and communication

Membrane fusion between lipid bilayers is an essential biophysical mechanism widely conserved in a variety of cellular systems (Martens and McMahon 2008, Kim, Jin et al. 2015, Hernandez and Podbilewicz 2017). The minimal functional unit catalysing cell fusion reactions has been called a fusogen (Chen and Olson 2005, Chernomordik and Kozlov 2008, Martens and McMahon 2008, Evans 2012, Hernandez and Podbilewicz 2017). Fusogens include a range of specialised molecules or molecular complexes directly involved in membrane merging (Chen and Olson 2005, Chernomordik and Kozlov 2008, Martens and McMahon 2008).

Cellular fusion is a multistep process that begins with a pre-fusion contact. Proteins mediate the recognition between fusionable membranes bringing them into closer proximity. Once membrane protrusions are formed, and the hydration repulsion diminished, membranes start fusing (Martens and McMahon 2008). The next stage includes a transitional structure, where proximal monolayers are fused whereas the distal remain unmerged. Subsequently, the distal monolayers fuse forming a fusion-pore opening and allowing the cytoplasmic content to come into contact (Chernomordik and Kozlov 2008, Martens and McMahon 2008).

Even though the structural features of fusogens are varied, all the known structures mediating membrane fusions follow the same conserved biophysical principles, wherein the merger of two contiguous monolayers belonging to two membranes

have to overcome energy barriers between outer leaf-lets (Chernomordik and Kozlov 2008, Martens and McMahon 2008, Avinoam, Fridman et al. 2011).

Based on genetic and structural studies, consensus has been reached in terms of the functional conditions that a fusogen must meet (Oren-Suissa and Podbilewicz 2007, Hernandez and Podbilewicz 2017). This mechanistic approach seeks to differentiate *bona fide* fusogens from other molecules involved in pre-fusion events (e.g. tethering or adhesion). Thus, a fusogen should be essential and sufficient for membrane merge, and being expressed at the time and site where membrane fusion takes place (Oren-Suissa and Podbilewicz 2007, Aguilar, Baylies et al. 2013). Additionally, a fusogen must be capable of inducing a membrane merge in a heterologous system that does not normally undergo fusion (Oren-Suissa and Podbilewicz 2007, Aguilar, Baylies et al. 2013, Hernandez and Podbilewicz 2017, Valansi, Moi et al. 2017).

Membrane fusion events can occur between intracellular compartment and based on the similarity of the merged pairs, they can be designated either as homotypic (e.g. between outer and inner mitochondrial membranes or including two endosomes) or heterotypic (e.g. synaptic vesicle exocytosis)(Martens and McMahon 2008). Members of the SNARE (soluble N-ethylmaleimide-sensitive factor attachment protein receptor) protein superfamily are well-characterised fusogens. At a given fusion site, four helices contributed by 3-4 different SNAREs form a very stable SNARE complex which overcomes energetic barriers and ultimately leads to the fusion of the two membranes. Interestingly, both SNAREs and a subunit of the influenza virus which is a class I viral fusion proteins known as

hemagglutinin HA2 use a common α-helical bundle structure to promote membrane fusion (Martens and McMahon 2008, Hernandez and Podbilewicz 2017). However, unlike some of the other fusogens discussed below, which are involved in cell-cell fusion, the fact that SNARE-mediated fusions occur in the cytosol means that they involve the fusion of lipid bilayers, which make contact through the cytosol-facing leaflet and are topologically equivalent to the inner leaflet of the plasma membrane.

Cell fusion is also the mechanism responsible for merger between gametes in fertilisation and the formation of multinuclear cells (e.g. skeletal muscle and the placental syncytiotrophoblast)(Chen and Olson 2005). Our understanding of the functional specificities of a number of families of *bona fide* fusogens catalysing cell-cell fusion has advanced remarkably in recent years (Hernandez and Podbilewicz 2017). A first category includes the *Caenorhabditis elegans* fusion family proteins anchor cell fusion failure-1 (AFF-1) and epithelial fusion failure-1 (EFF-1). Both proteins are essential for developmental cell-cell fusion in *C. elegans*. AFF-1 is involved on fusion of embryonic epidermal cells while EFF-1 catalyses the fusion of epithelial and muscle cells (just to name a subset of the events where they have been described) (Avinoam, Fridman et al. 2011, Hernandez and Podbilewicz 2017, Oren-Suissa, Gattegno et al. 2017). AFF-1 and EFF-1, when expressed in insect or mammalian cultured cells, induce membrane fusion (Hernandez and Podbilewicz 2017).

Another category includes the human syncytins, a group of proteins essential for the fusion of the epithelial placental trophoblast (syncytiotrophoblast) (Hernandez and Podbilewicz 2017). Similarly, skeletal muscles in mammals are syncytia formed by

the fusion of myoblasts where myomaker, a multispan plasma membrane is both essential and sufficient to induce membrane fusion reactions (Millay, O'Rourke et al. 2013).

Finally, recent experimental evidence has shown that the ancestral HAP2(GCS1) (*Haploid-disrupting, Hapless 2,* also named GENERATIVE CELL SPECIFIC 1 - GCS1) is also a *bona fide* fusogen playing an essential role in fertilisation in the major eukaryotic taxa (Fedry, Liu et al. 2017, Pinello, Lai et al. 2017, Valansi, Moi et al. 2017). In section 1.2.3 and Chapter 3, I will provide further information on the role of HAP2(GCS1) in sexual reproduction via gamete fusion.

1.1.4. Dense-core granule compartments

Bioactive peptides and proteins that are destined for regulated secretion, particularly those in secretory cells of glands and neurons, are typically loaded into specific compartments at the surface of the trans-Golgi network (TGN). For these compartments to be ready for secretion, they must first mature, a process requiring exchange of selected proteins and lipids with other compartments and then the protein content must condense into DCGs (Kim, Gondre-Lewis et al. 2006, Bonnemaison, Eipper et al. 2013).

Most experiments undertaken to study this process have employed primary culture and specific secretory cell lines, most notably endocrine adrenal chromaffin cells (PC12) (Houy, Estay-Ahumada et al. 2015), pituitary corticotrophs (AtT-20) (Chen,

Wang et al. 2014), pancreatic beta cells (e.g. MIN6) (Tsuchiya, Hosaka et al. 2010), exocrine pancreatic acinar cells (AR42J) (Binker, Richards et al. 2015) and neurons (e.g. SH-SY5Y) (Giudici, Sher et al. 1992). Although the key functional cargos that are loaded into these DCGs are clearly different, these studies have highlighted a number of common mechanisms that appear to regulate DCG biogenesis and release (Kim, Gondre-Lewis et al. 2006).

For example, clustering of cargos into immature dense-core compartments (DCCs), which takes place in the TGN, is dependent on cholesterol (Tsuchiya, Hosaka et al. 2010). It appears to involve enzymes associated with lipid metabolism, notably phospholipase D1 and diacylglycerol kinase, and it has been suggested that lipid raft structures may play a central role (Siddhanta, Backer et al. 2000, Kim, Gondre-Lewis et al. 2006). Another critical group of proteins thought to be involved in the formation of dense-core compartments and subsequent biogenesis of DCGs consists of the granins (Day and Gorr 2003). Granins play a role in assembling other cargos within the cores.

Cytosolic adaptor proteins that co-operate in trafficking molecules to the maturing DCG compartments and removing molecules that are not cargos include the clathrin adaptor AP-1A, the small G-protein Arf1 and the Golgi-localising, γ-adaptin ear homology domain, ARF-binding proteins (GGAs) (Bonnemaison, Eipper et al. 2013).

In regard to adaptor proteins (APs), they constitute one of the main groups of clathrin-associated complexes (Boehm and Bonifacino 2001, Bonifacino 2014, Nakatsu, Hase et al. 2014). AP complexes are widely conserved in Eukaryotes

(Boehm and Bonifacino 2001) and seven different ones have been described to date: AP-1A, AP-1B, AP-2, AP-3A, AP-3B, AP-4 and AP-5 (Nakatsu, Hase et al. 2014). Each of these complexes is a heterotetrameric structure formed by two large size subunits of ~90-130 kDA (α, β_{1-5}, γ, δ, ε or ζ) and two units of medium and small size (μ_{1-5} of ~50kDa and σ_{1-5} of ~20kDa respectively) (Boehm and Bonifacino 2001, Nakatsu, Hase et al. 2014).

AP-1 complexes are involved in a wide range of key cellular processes and they promote constitutive secretion of TGN-derived vesicles directed to the cell surface (Burgess, Jauregui et al. 2011), are involved in trafficking of the mannose 6-phosphate receptors that target newly synthesized lysosomal enzymes to the lysosomes from the TGN (Arighi, Hartnell et al. 2004, Kametaka, Sawada et al. 2010, Burgess, Jauregui et al. 2011, Kametaka and Waguri 2012), sort basolateral cargos in recycling endosomes of polarised epithelial cells (Bonifacino 2014), are involved in the clathrin binding of immature secretory granules of secretory cells where missorted proteins are retrieved during the maturation process (Morvan and Tooze 2008), and are required for the formation and maturation of regulated dense-core granules in specialised secretory cells (e.g. Weibel-Palade bodies of endothelial cells and *Drosophila* mucin granules from the salivary glands) (Lui-Roberts, Collinson et al. 2005, Burgess, Jauregui et al. 2011).

APs play an important role in allowing clathrin to interact with and stabilise the membranes of specific compartments, and in the case of AP-1A, these compartments are formed at the trans-face of the Golgi. The Arf1 protein is involved in stabilising coatomer proteins, including the GGAs, around vesicles, particularly

those vesicles involved in intra-Golgi traffic and exit from the Golgi. The functions of both the AP-1 complex and Arf1 in *Drosophila* will be considered further in Chapter 5.

Maturation of DCGs also requires a series of changes in the intraluminal microenvironment including a reduction in pH (Wu, Grabe et al. 2001) and an increase in [Ca^{2+}] (Yoo and Albanesi 1990). Finally, mature DCG compartment fusion to the plasma membrane has been extensively characterised in multiple systems: it requires Ca^{2+}-dependent synaptotagmins and vesicle-associated membrane proteins (VAMPs) (Messenger, Falkowski et al. 2014). Even though the basic genetic characterisation of DCG biogenesis processes has identified a series of important molecular steps, the limited resolution of techniques available to visualise the processes of DCG formation, particularly in living cells, means that the precise functions and dependencies of these steps has yet to be defined and almost certainly, many key genes still remain to be identified.

1.2. Cellular and Molecular Role of HAP2 in the Genetic Exchange of *Trypanosoma brucei* Parasites

1.2.1. *T. brucei* life cycle

T. brucei is an extracellular protozoan parasite affecting mammals in rural areas of sub-Saharan Africa. Sleeping sickness (Human African Trypanosomiasis) is the classical form of the infection in humans. Recent estimates indicate that about 10% of the total African population is at risk of contracting this disease (Malvy and Chappuis 2011, Simarro, Cecchi et al. 2012).

The *T. brucei* life cycle (Fig. 1.1) involves its mammalian hosts and insect vectors (tsetse flies, *Glossina* species), and comprises different developmental stages of alternating proliferative and non-proliferative phases (Vickerman 1985, Sharma, Peacock et al. 2008). An undulating parasitaemia of Bloodstream Forms (BSFs) consisting of proliferative slender and transmissible stumpy trypomastigotes has been described in infected mammals (MacGregor, Szoor et al. 2012). After being ingested by the fly vector, parasites migrate towards the insect midgut, where stumpy forms, initially arrested in G0-G1, differentiate into procyclic forms (PCFs) (Vickerman, Tetley et al. 1988, MacGregor, Szoor et al. 2012). PCFs constitute a population of proliferative trypomastigotes where the cell surface is no longer covered in variable surface glycoproteins, and procyclins are found as the prevailing surface proteins (Sharma, Peacock et al. 2008). Subsequently, PCFs move across the peritrophic membrane of the gut to the ectoperitrophic space in the direction of

the proventriculus and become non-proliferative elongated mesocyclic trypomastigotes (Vickerman, Tetley et al. 1988). During migration towards the salivary glands, trypomastigotes differentiate into epimastigotes in which the kinetoplast (K, a mitochondrial DNA-containing organelle only present in Kinetoplastea) is located between the nucleus (N) and the anterior end of the cell. These epimastigotes divide asymmetrically, giving rise to long and short epimastigotes. Once in the salivary gland of the fly, the short epimastigotes attach to the epithelium microvilli, and further cell division and differentiation occur, resulting in non-proliferative metacyclic trypomastigotes (Sharma, Peacock et al. 2008, Sharma, Gluenz et al. 2009). Metacyclics are infective forms that complete the entire life cycle once the fly vector feeds from mammalian blood again (Vickerman 1985, Vickerman, Tetley et al. 1988).

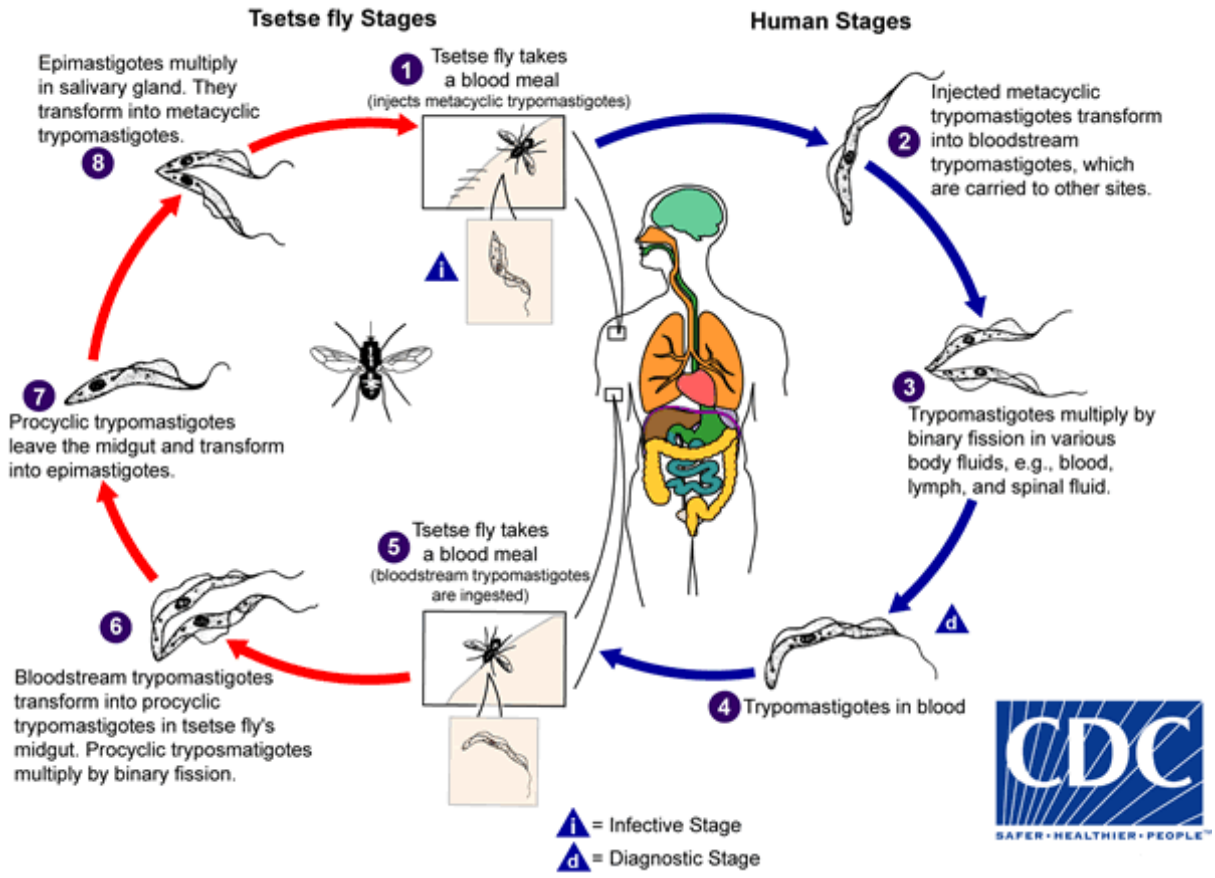

Figure 1.1 **Life cycle of *T. brucei*.** Schematic representation of the different developmental stages of the *T. brucei* parasite in the fly vector (tsetse flies, *Glossina* species) and a mammalian host (e.g. humans, cattle, horses or wild animals). Illustration courtesy of the Centers for Disease Control and Prevention.

1.2.2. Genetic exchange in *T. brucei* parasites

T. brucei parasites can undergo genetic exchange and produce hybrid progeny in the salivary gland of the vector (Jenni, Marti et al. 1986, Gibson, Peacock et al. 2008, Peacock, Ferris et al. 2009, Sharma, Gluenz et al. 2009). The production of hybrid phenotypes as a result of crossing two independent parental stocks with homozygous markers was first identified using enzyme markers and screening for

electrophoretic variations (Jenni, Marti et al. 1986). Subsequently, experimental crosses between independent clones of *T. brucei* expressing the Green Fluorescent (GFP) and Red Fluorescent (RFP) proteins produced yellow progeny, and provided further confirmation of a Mendelian inheritance pattern of fluorescent markers (Gibson, Peacock et al. 2008).

In addition to the evidence of hybrid progeny, an uncharacterized meiotic cell-type of the *T. brucei* life cycle has been described in tsetse salivary glands through the detection of meiosis-specific proteins (MND1, DMC1 and HOP1) in the nucleus of dividing cells (Peacock, Ferris et al. 2011). Subsequently, by tracking the dynamics of expression of these meiotic proteins, a novel life cycle stage of the parasite was identified and the cells designated as promastigote-like (PL) cells (Peacock, Ferris et al. 2011, Peacock, Bailey et al. 2014). The main characteristics of PLs are: (1) oval-shaped cell body with a long anterior free flagellum; (2) three different DAPI patterns, namely 1N1K (where the kinetoplast is located between the nucleus and the anterior end of the cell), 1K1N1K (where Ks are at opposite ends of the cell and separated by a single N), and 2K2N in dividing PLs; and (3) haploid DNA content (Peacock, Bailey et al. 2014). PLs are observed actively interacting when independent parental clones from the salivary glands are mixed, forming part of clusters where cells intertwine their flagella and place their cell bodies in close proximity (Peacock, Bailey et al. 2014, Peacock, Ferris et al. 2014).

Despite the progress in identifying these PLs, the cellular and molecular mechanisms leading to the formation of hybrid progeny remain elusive. It is not yet known how the exchange of cytoplasmic content occurs and what molecules or

molecular complexes are directly involved in membrane merging. However, cellular fusion between different phospholipid bilayers is likely to be a key process leading to the production of hybrid parasites in tsetse salivary glands.

1.2.3. Cell-cell fusion and the functional role of HAP2(GCS1)

In eukaryotes, cellular fusion between different phospholipid bilayers is the process responsible for fertilisation (Chen and Olson 2005, Martens and McMahon 2008, Hernandez and Podbilewicz 2017). Fertilisation is a fundamental phase of sexual reproduction, in which sex cells or gametes acquire functional competency to undergo cell-cell fusion, triggering the exchange of parental genetic information and forming hybrid cells (e.g. mammalian zygotes) (Primakoff and Myles 2007, Evans 2012, Satouh, Inoue et al. 2012).

Although several molecules have been involved with fertilisation (e.g. CD9 and Izumo1) (Evans 2012, Satouh, Inoue et al. 2012), current experimental evidence only supports the role of HAP2(GCS1) as a fusogen catalysing actual membrane fusion (Oren-Suissa and Podbilewicz 2007, Fedry, Liu et al. 2017, Hernandez and Podbilewicz 2017, Pinello, Lai et al. 2017, Valansi, Moi et al. 2017).

HAP2(GCS1) is a gamete-specific factor related to sex cell fusion affecting late stages of pollination in plants and also identified in mating-competent cells of the malaria parasite *Plasmodium*, the social amoeba *Dictyostelium discoideum*, the unicellular algae *Chlamydomonas reinhardtii* and *Gonium pectorale, Tetrahymena*

thermophila and *Nematostella vectensis* (Johnson, von Besser et al. 2004, Mori, Kuroiwa et al. 2006, Liu, Misamore et al. 2010, Mori, Hirai et al. 2010, Cole, Cassidy-Hanley et al. 2014, Ebchuqin, Yokota et al. 2014, Kawai-Toyooka, Mori et al. 2014, Okamoto, Yamada et al. 2016, Pinello, Lai et al. 2017). Loss-of-function analyses in *Arabidopsis*, *Plasmodium, Tetrahymena* and *Chlamydomonas* have revealed that HAP2(GCS1) mutant male gametes fail to fuse their plasma membrane counterparts and are infertile (Mori, Kuroiwa et al. 2006, Hirai, Arai et al. 2008, Liu, Tewari et al. 2008, Mori, Hirai et al. 2010, Wong and Johnson 2010, Cole, Cassidy-Hanley et al. 2014).

In species exhibiting gamete dimorphism such as *A. thaliana,* HAP2(GCS1) is detected in sperm (Johnson, von Besser et al. 2004, Mori, Kuroiwa et al. 2006, von Besser, Frank et al. 2006). However, HAP2(GCS1) can be also present in both mating parts as in the case of *T. thermophile* (Cole, Cassidy-Hanley et al. 2014). Furthermore HAP2(GCS1) is found in all the seven mating types characterised for *T. thermophile* (Cole, Cassidy-Hanley et al. 2014, Pinello, Lai et al. 2017). Fig. 1.2 summarises the mechanistic model by which the cellular fusion discussed above occurs.

Figure 1.2 **Mechanistic model of HAP2(GCS1)-dependent gamete fusion in eukaryotes. A.** Schematic representation of membrane fusion between gametes in the unicellular green algae *Chlamydomonas reinhardtii.* During the activation stage **(a)**, *C. reinhardtii* flagella of the minus and plus gametes adhere placing the two cells in close proximity. The tubular mating structures located between the flagella of each gamete extend **(b)** and the tips finally adhere **(c)** leading to the fusion of the phospholipid bilayers from the interacting gametes. In the next stage **(d),** the cytoplasmic content comes into contact and subsequently a zygote is formed **(e)**. Note that HAP2(GCS1) (red arrow), is found at the tip of the mating structure protruding from the minus gamete. Black arrows indicate directionality of the cellular fusion (Diagram from Fedry, Liu et al. 2017). **B.** Representation of the crystal structures of *C. reinhardtii* HAP2(GCS1) and *Arabidopsis thaliana* HAP2(GCS1) illustrating a conserved domain organisation within the ectodomains of the two homologues; the three polypeptide segments corresponding to domains I (red), II (yellow), and III (blue) are indicated. HAP2(GCS1) structures were aligned with respect to a highly conserved *α2*-helix present in domain III (Diagram from Fedry, Forcina et al. 2018). **C.** Schematic representation of the cellular stage preceding gamete fusion in *A. thaliana.* The colour code of *A. thaliana* HAP2(GCS1) ectodomains represented by ovals is as described above. The entire HAP2(GCS1) protein is drawn in green and a hypothetical interactor molecule is shown attaching to the plasma membrane of the egg (Diagram from Valansi, Moi et al. 2017).

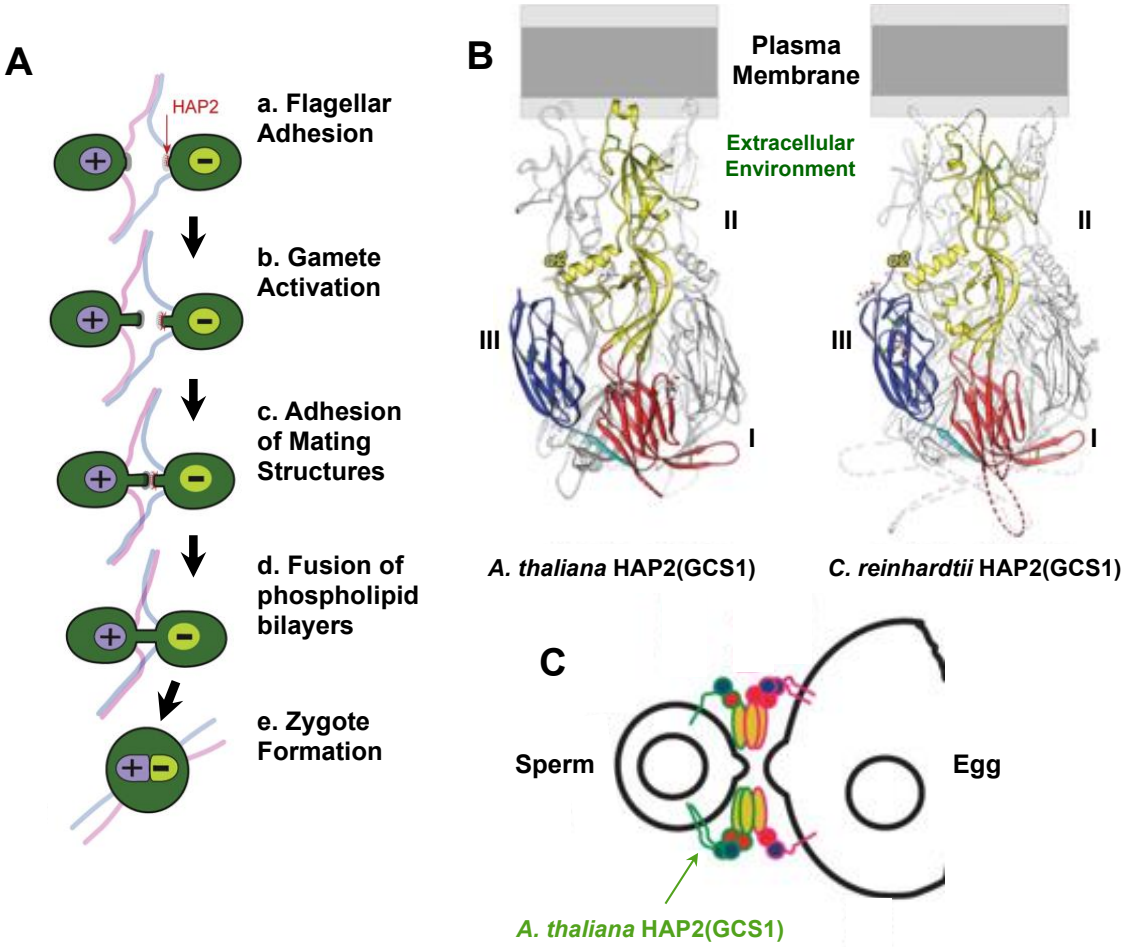

Recent bioinformatic, structural and functional studies undertaken in *A. thaliana, C. reinhardtii* and *T. thermophile* indicated structural homology between class II viral fusogens (e.g. dengue virus E glycoprotein) and the sequences of the HAP2(GCS1) ectodomain in these species. These findings allowed the identification of three β-sheet containing domains analogous to sequence fragments already characterised in class II viral fusogens. In all cases, two loops detected in Domain II were found to be critical for gamete fusion. These fusion loops are also found in class II viral fusion proteins where they are critical for the insertion of the virus into the host membrane (Fedry, Liu et al. 2017, Pinello, Lai et al. 2017, Valansi, Moi et al. 2017). These homology predictions seemed to be maintained within other

HAP2(GCS1) orthologues. Interestingly, 95% structural homology between class II viral fusion proteins and *T. brucei* HAP2(GCS1) was also predicted (Pinello, Lai et al. 2017).

Given that Trypanosomes also have a HAP2(GCS1) orthologue, a prime goal of my early thesis work was to characterise HAP2(GCS1) expression and then to test the effects of HAP2(GCS1) overexpression in specific forms of the parasite. These results will be presented in Chapter 3.

1.3. The Accessory Gland of *Drosophila* provides a unique system for the study of secretory cells and cellular trafficking

1.3.1. *Drosophila* and the characterisation of gene function

Since the beginning of the 20th century, the fruit fly *Drosophila melanogaster* has progressively become a powerful model system for studies in basic and applied biology. To date, the ground-breaking findings in fly genetics have benefitted the understanding and treatment of a wide variety of human diseases (Hales, Korey et al. 2015). Research with flies enjoys great advantages since they are highly prolific, adapt well to laboratory conditions and have a short life cycle that allows access to adult progeny in just over a week.

The genome sequence of *D. melanogaster* comprises 120 Mb of euchromatin (of a total size estimated of 180 Mb) which is distributed on four chromosomes and encodes nearly 13920 protein-coding genes (Adams, Celniker et al. 2000). The detailed study of the genome of flies and straightforward techniques for genetic manipulation have enabled the development of several experimental tools to advance our understanding (Hales, Korey et al. 2015, Heigwer, Port et al. 2018).

Amongst the genetic tools used to study the genes and molecular pathways analysed in this thesis, it is worth highlighting the GAL4-UAS system for restricted transgene expression. GAL4 is a potent transcriptional activator from yeast that has no endogenous targets in flies (Brand and Perrimon 1993). The GAL4 coding sequence is placed downstream of a tissue-specific promoter (e.g. *spitz* or *doublesex* give highly specific expression in the secondary cells of the male fly accessory gland, which are a main topic of my thesis), either in the endogenous gene locus or in a construct that is integrated into the fly genome, to create a fly line expressing this transcriptional driver (e.g. *spitz-GAL4)* (Corrigan, Redhai et al. 2014, Hales, Korey et al. 2015). The second part of this system contains multiple copies of the GAL4 binding site known as the upstream activation sequence (UAS) located upstream of a gene of interest connected to a basal promoter. A transgene under a UAS promoter remains silent in the absence of GAL4 (Brand and Perrimon 1993, del Valle Rodriguez, Didiano et al. 2012). Transgenic fly lines carrying either of the two independent components can be crossed together and as a result, GAL4 will turn on the expression of a gene of interest in a cell type-specific fashion in the progeny (Brand and Perrimon 1993, Hales, Korey et al. 2015).

The GAL4-UAS system can be used to express genetically encoded fluorescent tags, such as GFP and mCherry (characterised in Chapter 4), and for specific temporal and spatial expression of UAS-RNAi transgenes with or without other marker proteins (Chapter 5).

For *in vivo* RNA interference (RNAi) screens, a given stock line contains a UAS-regulated transgene encoding a double-stranded RNA (dsRNA) that is complementary to a specific endogenous gene (Heigwer, Port et al. 2018). Silencing of gene expression (knockdown) occurs through the RNAi pathway and is induced under GAL4 control, ultimately leading to degradation of the targeted messenger RNA (mRNA) in the cells of interest. Through this system there is no permanent modification of the gene's coding sequence (Heigwer, Port et al. 2018). Several UAS-regulated transgenic libraries of dsRNAs have been generated (Dietzl, Chen et al. 2007, Ni, Markstein et al. 2008, Perkins, Holderbaum et al. 2015, Vissers, Manning et al. 2016). Further methodological insights into my RNAi screen are provided in Chapter 2.

1.3.2. The *Drosophila* male reproductive system

The internal reproductive system of the male *D. melanogaster* is located in the abdominal region of the body (Fig. 1.3A and B). It comprises a pair of long spiralled testes, with the seminal vesicles located at the proximal end of each testis. The seminal vesicles are inserted medially to the anterior ejaculatory duct, where the paired accessory glands attach laterally (Fig. 1.3B). The male external genitalia

connect with the ejaculatory bulb, a pump-like structure attached to the posterior part of the ejaculatory duct.

Each of the five internal organ types (testes, seminal vesicles, accessory glands, ejaculatory duct and ejaculatory bulb) in the reproductive system in *D. melanogaster* has a distinctive proteomic profile (Takemori and Yamamoto 2009), and contributes to form the secretory products that will ultimately be transferred to female flies during mating (Leopold 1976, Avila, Sirot et al. 2011, Avila, Sánchez-López et al. 2016).

Initially, sperm from the testes are directed to the seminal vesicles where their maturation and storage take place (Avila, Sánchez-López et al. 2016). At least 1108 proteins have been detected in the sperm proteome of *D. melanogaster* (Wasbrough, Dorus et al. 2010). As might be anticipated, the major protein classes detected in fly sperm are involved in metabolism (e.g. hydrolases, transferases and oxidoreductases), DNA and RNA binding, cytoskeletal structure (αTub84B and βTub85D) and protein structural maintenance (including molecular chaperones such as Heat shock protein 83, Hsp60B and Hsp60C) (Takemori and Yamamoto 2009, Wasbrough, Dorus et al. 2010).

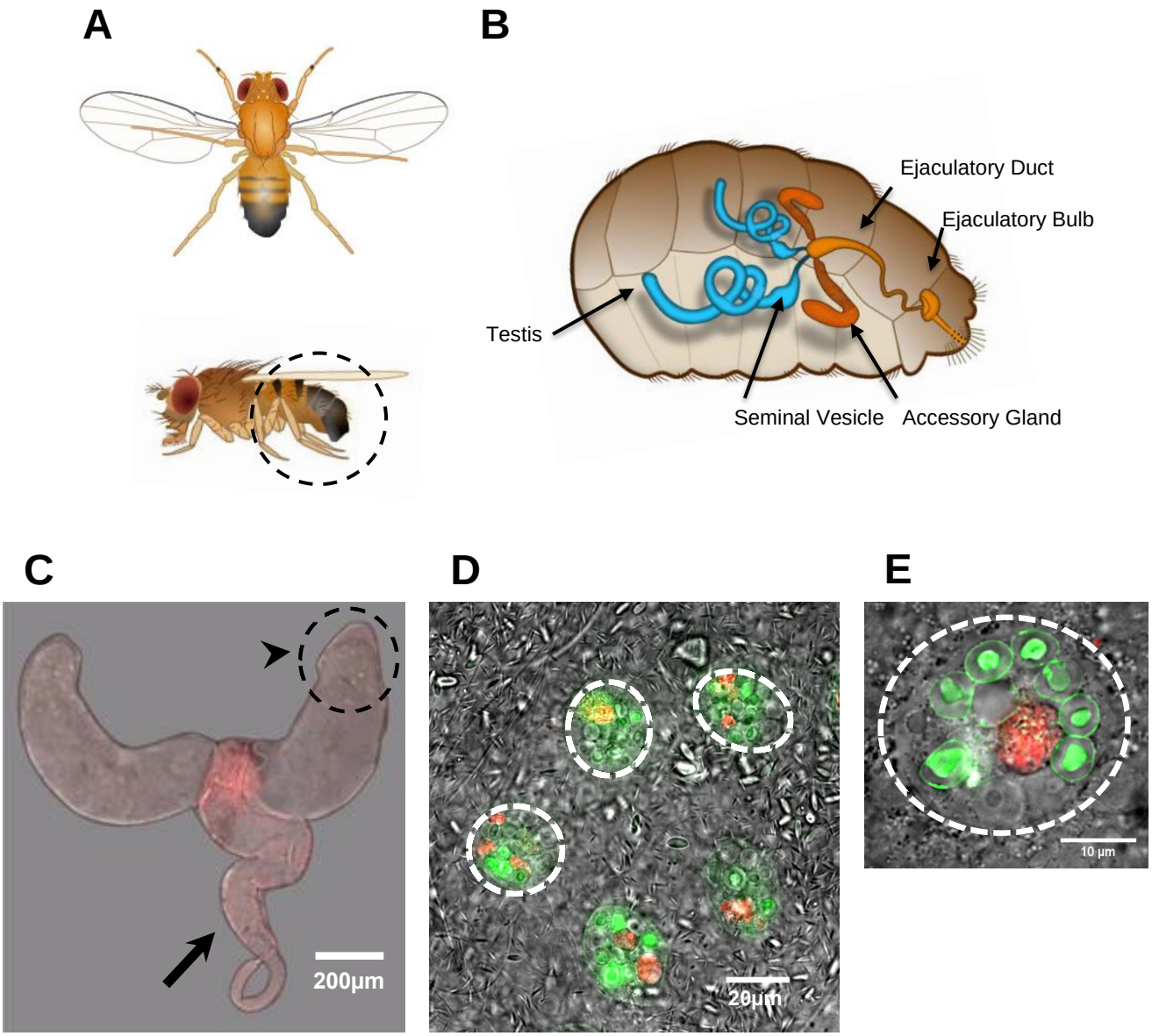
A
B
Ejaculatory Duct
Ejaculatory Bulb
Testis
Seminal Vesicle
Accessory Gland
C
200µm
D
20µm
E
10 µm

Figure 1.3 **The *D. melanogaster* male reproductive system includes the male accessory glands and the secondary cells within them. A, B**. Schematics of adult male *Drosophila melanogaster* highlighting the abdominal region (A) and the reproductive organs and tract (B), including the testes and seminal vesicles (blue), the accessory glands (dark orange), the ejaculatory duct (light orange tube linked to testes and accessory glands) and bulb (posterior, light orange rounded structure). **C.** Fluorescence and DIC combined low magnification image of the paired accessory glands (black arrowhead points to the outlined distal tip of the AG) and the ejaculatory duct (black arrow) from a 6-day-old adult male expressing GFP-GPI in SCs. **D.** Image of the epithelium in AG; cell outlines of three GFP-positive SCs are indicated by white dashed ellipses. **E.** High magnification view of a single SC where several membrane-bound compartments can be clearly identified (approximate position of SC plasma membrane is indicated by a white dashed ellipse). Genotype of virgin males, which were incubated at 29^{o}C following eclosion for 6 days, is *w; spi-GAL4 tub-GAL80^{ts}; UAS-GFP-GPI.* Acidic compartments stained with LysoTracker (red). Scale bars as shown in panels.

At the ejaculatory duct, during mating, the sperm that had been stored in the seminal vesicles, come into contact with the seminal fluid whose bulk is mostly from the accessory glands (Fig 1.3C) (Chen 1984, Gillott 2003, Avila, Sánchez-López et al. 2016, Wilson, Leiblich et al. 2017). The ejaculatory duct also performs a secretory role, contributing to the formation of the seminal fluid (Wilson, Leiblich et al. 2017). The antibacterial proteins andropin and cecropin are two of the molecules synthesised and secreted by the ejaculatory duct (Lung, Kuo et al. 2001, Avila, Sánchez-López et al. 2016). Although their specific mechanisms of action are not fully understood yet, a protective role to guarantee reproductive success in flies seems likely.

Similarly, Carboxylesterase Esterase-6 (Est-6, FlyBase CG6917, UniProt P08171) has been detected in the proteome of the ejaculatory duct (Takemori and Yamamoto 2009). Est-6 is a highly glycosylated 544-residue (61KDa) protein characterised as an odorant-degrading enzyme with substrates that include a range of short fatty acid esters (Younus, Fraser et al. 2017). Est-6 is transferred to the female tract after mating and it is implicated in the inhibition of re-mating and stimulation of egg-laying, however the specific substrates involved are still unknown (Younus, Fraser et al. 2017).

The columnar epithelium of the ejaculatory bulb (Guiraudie-Capraz, Pho et al. 2007, Sasikumar and Roy 2009) also has a secretory role that contributes to the seminal fluid (Wilson, Leiblich et al. 2017). Products of the ejaculatory bulb include the male pheromone *cis*-vaccenyl acetate (cVA) that is transferred into the female tract during mating and influences male courtship behaviour (Guiraudie-Capraz, Pho et al. 2007, Avila, Wong et al. 2015), and a set of proteins involved in the formation of the posterior mating plug in the uterus of *D. melanogaster* (whilst the anterior mating plug consists largely of proteins secreted from the accessory gland) (Avila, Wong et al. 2015). Among the posterior mating plug constituents, the ejaculatory bulb protein PEB-me (CG2668) (Takemori and Yamamoto 2009) has a key role in the formation of the plug and is critical for normal fertility because it maintains the ejaculate in the tract of mated females (Avila, Wong et al. 2015).

1.3.3. The accessory gland of the male *Drosophila* is a major contributor to the production of the seminal fluid

Two morphologically different populations of binucleated secretory cells, main cells and secondary cells, form a monolayered epithelium in the accessory glands (AGs). (Chen 1984, Bertram, Akerkar et al. 1992). The main cells constitute the most abundant cell type in the epithelium of the gland, with about 1000 hexagonal cells in each lobe (Bertram, Akerkar et al. 1992). The less abundant (~5%) and larger, rounded secondary cells (SCs), localise at the distal ends of the AG (Fig. 1.3C) (Chen 1984, Bertram, Akerkar et al. 1992). Both cell types are kept tightly interconnected by desmosomes and septate junctions, and enclosed by a mononucleated, striated, circular muscular sheath that through contraction, plays a fundamental role in the release of the secretory contents (Happ 1984, Bertram, Akerkar et al. 1992, Susic-Jung, Hornbruch-Freitag et al. 2012).

It has been established that functionally sperm from the testis and seminal fluid proteins produced by the AG are interdependent and complementary; hence male fertility is drastically reduced when AG function is disrupted (Xue and Noll 2000, Chow, Avila et al. 2015). The seminal fluid has an essential role in sperm capacitation (Chen 1984, Xue and Noll 2000) that is required for fertilisation. A large body of experimental evidence has shown that seminal fluid also induces a short-term response in mated females, leading to increased ovulation and the formation of a mating plug that prevents sperm escape and potentially blocks remating.

In addition, a combination of sperm and seminal fluid induces long-term post-mating effects. These include an increase in ovulation and egg-laying, decreased receptivity to re-mating, increased food intake and intestinal transit, modification of the immune response and promotion of sperm storage. Many of the key secreted seminal proteins involved in these processes are produced by the accessory gland (Chapman and Davies 2004, Ravi Ram, Ji et al. 2005, Avila, Sirot et al. 2011, Wilson, Leiblich et al. 2017).

Among the protein components found in the secretions of the AGs, three categories based on molecular size have been proposed (Gillott 2003): (1) short chains that do not exceed more than 100 amino acids. In *D. melanogaster*, sex peptide (SP), a protein secreted by the AG main cells is included in this group (Avila, Sánchez-López et al. 2016). SP is also known as Accessory gland-specific peptide 70A (Acp70A) and is a 6.8 kDa 55-residue protein (CG17673, UniProt P05623), which is trimmed to a 36 amino acid peptide during the secretory process and whose key role in reprogramming the female behaviour after mating has been widely studied (Wilson, Leiblich et al. 2017); (2) proteins with a primary structure ranging from 200-400 amino acids. This category includes a significant number of glycosylated proteins such as Acp26Aa (CG8982, UniProt P10333), another main cell protein also known as Ovulin, which is a regulator of ovulation in *Drosophila* that increases the release of eggs from the ovary to the uterus and the egg-laying rate in the first 24-48 h after mating (Rubinstein and Wolfner 2013); (3) a category that includes enzymes and larger proteins. Acp36DE (FlyBase CG7157, UniProt Q9V3R1), a 102kDa glycoprotein secreted by the main cells of the AG is included in this category. Acp36DE takes part in the formation of the anterior mating plug and

induces uterine morphological changes after mating required for the accumulation of the ejaculate in the female storage organs (Avila and Wolfner 2017).

The accessory gland also secretes substantial quantities of lipid and sugars into its lumen, as well as more complex signalling structures, such as exosomes (see below:(Corrigan, Redhai et al. 2014). It is believed that proteins and lipids are targets for the proteases and lipases secreted by the AG, but their hydrolysis may primarily only occur in females after mating to activate signalling molecules and release nutrients. As highlighted above, many of the secreted molecules produced by the AG and found in seminal fluid are made exclusively or primarily in main cells. But the small number of secondary cells in each gland also appear to play a critical role in seminal fluid production, as evidenced by a series of genetic experiments in the last seven years. In fact, studies have suggested parallels between SC secretory and signalling biology with the prostate epithelium, some of which will be discussed below (Wilson, Leiblich et al. 2017).

1.3.4. Functional Significance of *Drosophila* Secondary Cells (SCs)

Studies that specifically focus on SC biology and function can broadly be separated into two categories. In the first, genes involved in the development of SCs have been analysed by studies of mutants or knockdown from pupal stages onwards. In the second, SC-specific knockdown has been regulated by the inducible GAL80^{ts} system, so that RNAis are only expressed post-eclosion. Several studies in the

Wilson group suggest that there are significant changes in the secretory biology of SCs in the first three days post-eclosion (e.g. S. Redhai, DPhil thesis), with many of the large compartments that are characteristic of these cells being absent at eclosion. Therefore, these post-eclosion experiments also assess a type of developmental differentiation process, even though the SC cell type is believed to be specified during pupal development.

In the studies that have focused on the early development of SCs to date, two SC-specific transcriptional regulators have been characterised in the *Drosophila* male AGs. Defective proventriculus (Dve, Flybase CG5799) is a transcriptional repressor strongly expressed in SCs, where it is required for normal SC development. Loss-of-function *dve* males exhibited reduced AGs, loss of SCs and a significant reduction of fertility (Minami, Wakabayashi et al. 2012). The mutant males also appear to have defects in the main cells, and some of these effects are cell autonomous.

Abdominal-B (Abd-B) is a transcription factor, which in the AG is specifically expressed in SCs. Removal of *iab6,* an enhancer regulating the expression of *Abd-B*, leads to almost complete loss of compartments in adult SCs and a subsequent failure to alter the female's long-term post-mating responses, including stimulation of ovulation and reduced receptivity (Gligorov, Sitnik et al. 2013, Sitnik, Gligorov et al. 2016). Interestingly, AGs with mutant SCs also fail to glycosylate accessory gland main cell proteins such as Ovulin (Gligorov, Sitnik et al. 2013), suggesting that SCs may be involved in some of the post-translational modifications of these molecules via mechanisms that remain to be characterised.

The studies carried out in the Wilson laboratory have contributed to uncover key aspects of the subcellular morphology and functional characteristics of the SCs post-eclosion (Leiblich, Marsden et al. 2012, Corrigan, Redhai et al. 2014, Redhai, Hellberg et al. 2016, Wilson, Leiblich et al. 2017). One property of SCs, which shares parallels with prostate cells, is that they continue to grow in the adult, unlike the surrounding main cells, and this growth is promoted by BMP signalling (Leiblich, Marsden et al. 2012). Furthermore, the use of fluorescent acidotropic probes and *in vivo* confocal microscopy have allowed the differentiation of large compartments with high lumen acidity. Acidic labelled organelles include late endosomal multivesicular bodies (MVBs) and lysosomes. These compartments are also marked by a YFP-tagged Rab7, which is a marker for these compartments (Corrigan, Redhai et al. 2014).

The conspicuous Dense-core Granule (DCG) compartments are the most numerous non-acidic large intracellular SC organelles. The limiting membrane of DCG compartments contains Rab11 and can be labelled by a YFP-tagged Rab11 protein expressed under GAL4/UAS control (Redhai, Hellberg et al. 2016). Although, the mechanisms for bioactive molecule storage in *Drosophila* DCG compartments are still mostly unknown, AnCE, the fly homologue of the mammalian angiotensin-converting enzyme (ACE) has been detected localising to the cores (Rylett, Walker et al. 2007, Corrigan, Redhai et al. 2014). Interestingly, ACE expression has been associated with susceptibility of prostate cancer (Xie, You et al. 2014).

In *D. melanogaster*, bone morphogenetic protein (BMP) signalling is activated in SCs during mating and is implicated in the formation of new DCG compartments in

adult flies to replenish those that are lost following mating. Dpp (Decapentaplegic), a fly BMP ligand is expressed in SC, and is detected in DCGs from where it regulates DCG biogenesis via a primarily autocrine mechanism (Redhai, Hellberg et al. 2016). Finally, recent studies suggest that a GPI-anchored form of GFP is primarily trafficked to DCGs in SCs (Redhai, Hellberg et al. 2016); although the mechanisms controlling this process are unknown, this has proved a useful live imaging marker and is used extensively in this thesis.

BMP signalling is also involved in the biogenesis of exosomes in SCs. Exosomes detected *in vivo* inside late endosomal multivesicular bodies (MVBs) are secreted into the AG lumen, transferred along with sperm and subsequently found associated with the epithelial cells of the female reproductive tract (Corrigan, Redhai et al. 2014). More recent studies in the group have suggested that exosomes can also be formed inside other large secretory compartments, including the DCG compartments (see Chapter 4).

Interestingly, blocking BMP signalling specifically in adult SCs, suppresses the ability of males to inhibit female receptivity after mating (Leiblich, Marsden et al. 2012), implicating secretion from DCG compartments in this process. It does not affect long-term stimulation of ovulation, unlike genetic manipulations where SCs are lost in development (Gligorov, Sitnik et al. 2013). When the conserved Endosomal Sorting Complexes Required for Transport-0 (ESCRT-0) protein Hrs (Hepatocyte growth factor-regulated tyrosine kinase substrate), implicated in mammalian and *Drosophila* exosome biogenesis, was depleted selectively in SCs by knockdown, not only was exosome biogenesis reduced in SCs, but also the ability

of males to inhibit female receptivity (Corrigan, Redhai et al. 2014). Therefore exosomes appear to be involved in some of the reprogramming events involved in the female post-mating response. However, this does not eliminate the possibility that DCGs may also be involved in these processes.

As discussed in Section 1.1.4, a number of genes have been identified that play roles in DCG biogenesis in mammalian secretory cells. Studies in SCs are at a very early stage with the SNAP-25 orthologue, SNAP-24, implicated in DCG release (Redhai, Hellberg et al. 2016), as it is in mammals, but with no molecules involved in mammalian DCG formation yet tested in SCs. A primary goal of my thesis work was to test candidate genes implicated in mammalian DCG biogenesis to determine whether their functions were conserved, which would suggest that the *in vivo* SC model might be able to provide new clues about this process. Furthermore, since SCs have unique cell biology as regards their formation of extremely large DCG compartments, I hoped that this analysis might suggest more specific functions for some of these genes.

1.4. Overall Aims and Objectives

In light of my interests in membrane-mediated cellular events, I set out to use the *Trypanosome* and *Drosophila* SC systems to address several unexplored aspects of membrane biology.

1. In Trypanosomes, I wanted to test whether the evolutionarily conserved fusogen HAP2(GCS1) is expressed in *T. brucei* at a stage when these parasitic cells appear to fuse in the salivary gland of the tsetse fly.

2. Having shown this, as a first test of the function of HAP2(GCS1), I aimed to investigate whether overexpressing HAP2(GCS1) might alter the cell biology of *T. Brucei* cells in the forms normally found in the salivary gland.

3. In *Drosophila* SCs, I aimed to develop and characterise a series of live markers for DCG biogenesis that would allow me to follow the process of DCG maturation.

4. Using these markers, I wanted to test whether conserved genes involved in mammalian DCG biogenesis played a similar role in SCs, and if so, to more precisely characterise the functions. Furthermore, I hoped to identify other genes that affect DCGs, which had not previously been implicated in this process.

In general, all these aims were successfully achieved, and in particular, I present a range of data suggesting that the SC offers a remarkably powerful new model to study DCG biogenesis and its links to other subcellular processes.

2. Materials and Methods

This chapter is divided in to two main sections. The first one covers the methodology implemented for the characterisation of the cellular and molecular function of HAP2(GCS1) in the genetic exchange of *T. brucei* parasites (Section 2.1). The second section includes the material and methods used for the study of *Drosophila* SCs whose results are presented in Chapter 4 and 5 (Section 2.2).

2.1. Characterisation of Functional Role of *Tb*HAP2(GCS1) in Genetic Exchange

2.1.1. Bioinformatics

Protein orthologs in *Trypanosoma* were identified with the Basic Local Alignment Search Tool (BLAST http://blast.ncbi.nlm.nih.gov/). Reciprocal sequence searches were run on TriTrypDB (http://tritrypdb.org) or on other specialised databases for model organisms. Protein domains were defined starting from these multiple sequence alignments and performing a profile-to-sequence analysis on HMMer2. Sequences in FASTA format were blasted on UniRef 50 to provide non-redundant hits. The *E*-values obtained are estimators of the number of better matches expected in our search by chance (Sanchez-Pulido and Ponting 2011).

Signal peptide prediction was done using SignalP 4.1 Server (http://www.cbs.dtu.dk/services/SignalP/). Transmembrane domains were predicted using TMHMM Server v. 2.0 (http://www.cbs.dtu.dk/services/TMHMM/) and TOPCONS (http://topcons.cbr.su.se/). Pfam ID for the HAP2(GCS1) family is PF10699. Disulfide bond position was predicted by DISULFIND (http://disulfind.dsi.unifi.it/). Multiple alignments performed with Jalview 2.10.2b1 (http://www.jalview.org/).

2.1.2. *Trypanosoma* Cell Culture

Procyclic forms (PCFs) were cultured at 28ºC in SDM-79 medium supplemented with 10% v/v inactivated foetal bovine serum (Gibco) (Brun and Schonenberger 1979). Cell densities were quantified using a CASY Cell Counter and Analyzer (Roche Applied Science). Cells were subcultured to maintain logarithmic phase growth (densities within $1x10^5$ and $2x10^7$ cells ml^{-1}). Lister 427 (29-13)- (Wirtz, Leal et al. 1999) and Single Marker Oxford (SmOx) P927- (Poon, Peacock et al. 2012) expressing T7 RNA polymerase and the tetracycline repressor were used as parental cell lines for ectopic gene expression assays. Cells were induced by the addition of doxycycline to a final concentration of 1 µg ml^{-1}. All cell cultures were kept on supplemented medium with the appropriate selection drugs before induction. The final concentrations were as follows: 15 µg ml^{-1} G418-neomycin, 50 µg ml^{-1} hygromycin, 5 µg ml^{-1} phleomycin, 1 µg ml^{-1} puromycin and 10 µg ml^{-1} blasticidin. *T. brucei brucei* TREU 927/4 cells were use as parental lines for fly infections.

2.1.3. *Trypanosoma brucei* Transfections

Cell culture density was $1x10^7$ cells ml^{-1} for transfection. PCFs were harvested by centrifugation at 800g for 10 min at 4ºC, washed and re-suspended at $1x10^7$ cells ml^{-1} with Zimmermann's post-fusion medium (ZPFM: 132mM NaCl, 8mM KCl, 8mM Na_2HPO_4, 1.5mM KH_2PO_4, 1.5mM Mg $(C_2H_3O_2)_2$, 90µM Ca $(C_2H_3O_2)_2$ H_2O). 10 µg of sterile linearised DNA were added to a 4mm electroporation cuvette containing $2.5x10^7$ cells. Two pulses of 1.7kV were delivered (ECM 830 BTX, Harvard Apparatus), and electroporated trypanosomes were transferred to preheated SDM-79. Selection drugs were added after 12h.

2.1.4. Molecular Biology

Chemocompetent *Escherichia coli* XL1-blue (Stratagene) and plasmid DNA were incubated on ice for 20 minutes before a 5-s heat shock at 42ºC. Transformed bacteria were transferred to LB agar plates supplemented with 100 µg ml^{-1} ampicillin and incubated overnight at 37ºC. Single colonies were selected and incubated in LB broth with 100 µg ml^{-1} ampicillin at 37ºC in a shaking incubator at 200 rpm.

Gels containing 0.8-1% w/v agarose/TAE (40 mM Tris, 20 mM acetic acid, 10 mM EDTA) and 1 µg ml^{-1} ethidium bromide were used for electrophoresis. Samples were run at 80-100V and bands were visualised on a UV transilluminator.

PCR reactions contained 1 pg - 1µg of *T. brucei* genomic DNA, 0.2 mM of each dNTP, 10 µM of each primer, 5 U ml^{-1} of Taq DNA polymerase (Roche Expand High Fidelity^{PLUS}) and 1.5 mM Mg^{2+}. The thermocycler was set to perform an initial denaturing cycle (94^{o}C 3 min) and 30 successive cycles of 94^{o}C, 30 sec; 55^{o}C, 30 sec; and 72^{o}C (1min per 1kb). PCR products were visualised in agarose gels, cleaned and digested accordingly.

For ectopic expression of C-terminally tagged proteins, full-length ORFs were inserted in frame with YFP-TY between the *Bam*HI and *Hind*III restriction sites into pDex577 (Kelly, Reed et al. 2007) and pLew100 (Kelly, Reed et al. 2007). For the expression of genes from their endogenous loci with a C-terminal YFP-TY tag, the 3' intergenic fragment behind the stop codon and the 3' end of the gene were inserted between the *Hind*III and *Spe*I restrictions sites of pEnT6B (Kelly, Reed et al. 2007). Plasmid maps are presented in Appendices 2 and 3.

2.1.5. Protein Biochemistry

Cell pellets with 2.5x10^{5} cells were resuspended in Laemmli buffer (2% w/v SDS, 10% v/v glycerol, 50mM Tris-HCl pH 7.2, 0.002% bromophenol blue, 400mM β-mercaptoethanol) and incubated at 95^{o}C for 5 min. Samples were stored at -20^{o}C.

Protein samples were resolved in gels with 30% v/v acrylamide mix, 1.5M Tris-HCl pH 8.8, 10% w/v SDS, 10% w/v ammonium persulfate and 6µl v/v *N,N,N',N'* – Tetramethylethylenediamine (TEMED). Stacking gels (5%) were prepared with 30%

v/v acrylamide mix (taking 1.34 mL of the mix for a total volume of 10mL), 0.5M Tris-HCl pH 6.8, 10% w/v SDS, 10% w/v ammonium persulfate (APS) and 4µl v/v TEMED. Resolving gels (10%) were prepared with 30% acrylamide mix (taking 3.4 mL of the mix for a total volume of 10mL), 1M Tris-HCl pH 8.8, 10% w/v SDS, 10% w/v ammonium persulfate (APS) and 4µl v/v TEMED. Molecular weight was established by Precision Plus Protein markers (BIO-RAD). Samples were run at a constant current of 20 mA in running buffer (25 mM Tris, 250 mM glycine, 0.1% SDS).

After SDS-PAGE completion, proteins were transferred onto a nitrocellulose membrane (Whatman) by semi-dry blot in Towbin transfer buffer (25mM Tris, 192mM Glycine, 20% Methanol, 0.1% SDS) at 0.8 mA cm^{-2}. PonceauS staining (Sigma) was used to confirm protein transfers.

For antigen detection, membranes were blocked for 30 min with 5% v/v non-fat dry milk in TBS-Tween (10 mM Tris, pH 7.4, 150 mM NaCl and 0.05% v/v Tween) and incubated afterwards with 1:50 BB2 primary antibody (Bastin, Bagherzadeh et al. 1996) diluted in 1% non-fat dry milk in TBS-Tween. Anti-mouse IgG peroxidase antibody produced in rabbit (Sigma) diluted in 1% v/v non-fat dry milk TBS-Tween (1:1000) was used as a secondary antibody. Membranes were treated with enhanced chemiluminescence (ECL) reagent (Perkin Elmer) and exposed to film for visualisation (Kodak).

2.1.6. Microscopy of *Trypanosoma brucei*

For microscope imaging, PCFs were washed in phosphate-buffered saline (PBS), fixed in 2% paraformaldehyde for 15 min, permeabilised with 0.1% NP-40 in PBS and mounted in glycerol, 4′,6-diamidino-2-phenylindole dihydrochloride (DAPI) containing 1% (wt/vol) 1,4-diazabicyclo[2.2.2]octane (DABCO). PCFs were analysed on a Zeiss Axioplan 2 microscope with a CCD camera controlled by Micro-Manager 1.4 (http://micro-manager.org/).

Images from salivary gland extracts were imaged using a Leica DMRB microscope with a Retiga Exi camera and Volocity version 4.1 software (Improvision). Each image was taken under phase contrast and UV fluorescence at 40-100x magnification.

All measurements from the digital images were made using Image J software (Version 1.41) (http://rsb.info.nih.gov/ij/ website). For the quantification of the proportion of kinetoplasts (Ks) and nuclei (Ns) in each of the phenotypes obtained after *Tb*HAP2:TY or *Tb*HAP2:YFP:TY overexpression, the total number reported was obtained from ten different field views.

2.1.7. Tsetse Fly Work

Glossina morsitans morsitans were kept at 25^{o}C and 70% relative humidity. Flies were fed with infected, defibrinated horse blood through a silicone membrane 24-

48 h after eclosion and dissected at 22-23 days post-infection. After decapitation of fly males (15-17 individuals), the extracted salivary glands were fixed (4% PFA) and a thin-layer cell preparation (Cytospin 4 Cytocentrifuge, Thermo Scientific) was stained with DAPI. The glands were analysed to verify the life cycle status of the parasites.

2.2. Membrane-mediated Cell Biological Mechanism in Reproduction

2.2.2. *Drosophila melanogaster* Stocks and Genetics

Fly stocks and experimental crosses were cultured on a standard cornmeal-agar-glucose mixture at 17^{o}C unless otherwise indicated. Ectopic gene expression was achieved by the GAL4/Upstream Activation Sequence (UAS) tissue-specific modular misexpression system (Brand and Perrimon 1993).

For experiments in Chapter 5, we implemented a system that uses GAL4/UAS to control the expression of a gene fragment that has been dimerised to produce a double-stranded RNA (dsRNA) hairpin which in turn silences gene expression by RNA interference (RNAi) (Dietzl, Chen et al. 2007, Ni, Markstein et al. 2008, Perkins, Holderbaum et al. 2015).

Our system for *in vivo* targeted transgenic RNAi in SCs included the following components: (1) a fluorescent marker (e.g. *UAS-GFP-GPI*); (2) the SC driver *spi*-GAL4 for cell type-specific expression (Brand and Perrimon 1993), which has been previously established in the laboratory as a driver for gene expression in SCs (Corrigan, Redhai et al. 2014); and (3) the *tub*-GAL80^{ts}, a ubiquitously expressed temperature-sensitive transcriptional repressor (Suster, Seugnet et al. 2004). GAL80^{ts} inhibits the GAL4/UAS activity at 17^{o}C but permits transgene expression when it is inactivated by increasing the temperature to 29^{o}C.

Thus, a knockdown specifically in SCs is achieved by shifting flies to 29˚C at eclosion. In all cases virgin males were kept at 29^{o}C to ensure continued transgene expression and a standard procedure for comparison against controls.

The fly stocks used for this thesis research are summarised below:

Function	Source	Stock No	Genotype
SC driver	Kyoto112-114 (Hayashi et al. 2002)	A13006	*w; spi-GAL4* (NP0261)
SC and ejaculatory duct driver	Goodwin (Rideout et al. 2010)	A13008	*w; dsx-GAL4/TM6B*
Temperature-sensitive SC driver	(Corrigan, Redhai et al. 2014)	A15068	*w; spi-GAL4, tubGAL80^{ts}/CyO*
Actin-Gal4 (ubiq. driver)	Bl-3954	A4441	*y^{1}w*; P[w^{+mc}=Act5C-GAL4] 17bFO1/TM6B, Tb^{1}*
SC CD63-GFP driver line	(Corrigan, Redhai et al. 2014)	N/A	*w; UAS-CD63-GFP, tubulin-GAL80^{ts}; dsx-GAL4/SM5.TM6*
GPI-anchored GFP (MV marker)	Eaton (Panakova et al. 2005)	A15050	*UAS-GFPgpi2.1/CyO*
Exosome marker	Eaton (Panakova et al. 2005)	A15051	*UAS-CD63-GFP/CyO; Dr/TM3 Sb*

Gene	Stock ID	Lab ID	Genotype
Adaptor Protein complex 1, σ sigma subunit	VDRC107322	A16303 A16292	CG5864; P*[KK108869]VIE-260B*
	BDSC40895	A16181	CG5864; *y^1 sc^* v^1; P[TRiP.HMS02143]attP2* Expresses dsRNA for RNAi of AP-1 sigma under UAS control.
Adaptor Protein complex 1, μ mu subunit	VDRC24017	A16235	CG9388; *w^{1118}; P[GD14206]v24017/TM3*
Adaptor Protein complex 1, γ gamma subunit	BDSC27533	A16155	CG9113; *y^1 v^1; P[TRiP.JF02684]attP2* Expresses dsRNA for RNAi of AP-1 gamma (FBgn0030089) under UAS control.

Gene	Stock ID	Lab ID	Genotype
Arf79F	VDRC23082	A15339 A15420	CG8385; *w^{1118}*; P[*GD12522]v23082*
Arf79F	BDSC29538	A15368	CG8385; *y^1 v^1; P[TRiP.JF01809]attP2* Expresses dsRNA for RNAi of Arf79F (FBgn0010348) under UAS control, TRiP
Arf79F	VDRC103572	A15403 A15996	CG8385; P[*KK101396]VIE-260B*

Gene	Stock ID	Lab ID	Genotype
Chaoptin (*chp*)	BDSC 31276	N/A	CG1744; *y v*; P[*TRiP.JF01217]attP2* Expresses dsRNA for RNAi of *chp* (FBgn0000313) under UAS control, TRiP (RNAi1).
Chaoptin	BDSC31655	N/A	CG1744; *y v*; P[*TRiP.JF01447]attP2* Expresses dsRNA for RNAi of *chp* (FBgn0000313) under UAS control, TRiP (RNAi2).
Chaoptin	BDSC42251	N/A	CG1744; *cu^1 chp^2*

Gene	Stock ID	Lab ID	Genotype
Phosphatidyl-inositol glycan anchor biosynthesis, class C	VDRC103915	A16445	CG12077; P[*KK101771]VIE-260B*
PIG-U Phosphatidyl-inositol glycan anchor biosynthesis class U	VDRC105420	A16450	CG13089; P[*KK101552]VIE-260B*
PIG-V Phosphatidyl-inositol glycan anchor biosynthesis class V	VDRC8143 VDRC8144 BDSC51478	A16402 A16403 A15886	CG44239; *w*^{1118}; P[*GD3514]v8143/TM3* *w*^{1118}; P[*GD3514]v8144* *y v*; P[*TRiP.HMC03223]attP40*

Gene	Source	Lab ID	Genotype
AnCE gene trap	BDSC59828	N/A	CG8827; y^{1} w^{67c23}; Mi[PT-GFSTF.1] AnCE$^{MI05748-GFSTF.1}$/SM6a Recombination Mediated Cassette Exchange of a Mi (MIC) insertion results in expression of AnCE tagged with eGFP-FlAsH-StrepII-TEV-3xFlag.
***CFP-Rab6* gene trap**	(Dunst, Kazimiers et al. 2015)	N/A	
***YFP-Rab11* gene trap**	(Dunst, Kazimiers et al. 2015)	N/A	
Ubi-DE-Cad-tRFP	N/A	A16632	*Ubi-DE-Cadherin-tagRFP2-2/Cyo*

BDSC: Bloomington Drosophila Stock Center

VDRC: Vienna Drosophila Research Center, Austria

KSC: Kyoto Stock Center

KK and GD RNAi fly stocks were obtained from VDRC. KK lines belong to an RNAi library whose members carry a pKC26 vector with a site-specific integration of hairpin RNAs that was incorporated into a defined locus (40D on chromosome 2L) to ensure steady expression of RNA hairpins with the least disruptive effect of the host genes (Vissers, Manning et al. 2016).

GD lines belong to a library developed by cloning vectors with short gene fragments as inverted repeats into a pMF3 vector. The insertion of the p-element library in this case is random and therefore can be found on chromosome 1, 2 or 3 (Dietzl, Chen et al. 2007).

TRiP lines were generated by the Transgenic RNAi Project (TRiP) at Harvard Medical School. These knockdown transgenic vectors VALIUM (Vermilion-AttB-Loxp-Intron-UAS-MCS) were designed to enable the incorporation of RNAi hairpins into attP sites on the second or third chromosomes (attP40 and attP2 respectively) (Ni, Markstein et al. 2008, Perkins, Holderbaum et al. 2015).

RNAi Stock Validation and Phenotype (RSVP) database was used to verify whether our RNAi fly stocks were previously studied.

2.2.3. Microscopic Analysis of the *D. melanogaster* AG

For fluorescent live-cell imaging, six-day-old virgin male flies were anesthetised and dissected in cold PBS (1X, pH 7.4, Gibco). AGs were incubated for five minutes in a 5µM solution of LysoTracker (ThermoFisher) and subsequently washed with cold PBS.

AGs for time-lapse, wide-field and DIC microscopy were mounted onto high-precision cover glasses with thickness No. 15H (Marienfeld Superior). Specimens were placed in a small drop of cold PBS (1X, pH 7.4, Gibco) and covered with 10S Voltalef low viscosity Halocarbon oil (VWR International) which provides free diffusion of oxygen and prevents hypoxia and dehydration (Parton, Valles et al. 2010). The cover glass with the AG was secured to a custom-built metallic slide holder and the sample was kept in place by a rounded 13-mm diameter cover glass (VWR International).

For live cell imaging of DNA with SiR-DNA (Sir-Hoechst, Spirochrome), AGs were incubated for one hour at room temperature in a 2µM solution of Sir-Hoechst and 10µM of Verapamil (Spirochrome). Samples were subsequently washed with cold PBS and mounted as described above.

Dissected accessory glands collected for immunohistochemistry were fixed for 20 minutes in a 4%-paraformaldehyde (Sigma-Aldrich) solution dissolved in PBS (1X, pH 7.4, Gibco) and then washed for 20 minutes in PBST (PBS containing 0.3%

Triton X-100, Sigma-Aldrich). Samples were blocked for 30 minutes in PBSTG (10% vol/vol filtered goat serum diluted in PBST).

Fixed glands were incubated overnight at 4°C with primary antibodies as follows:

Primary Antibody/ Antigen	Dilution	Source, Reference
Polyclonal rabbit anti-fly AnCE	1:2000	(Rylett, Walker et al. 2007)
Monoclonal mouse anti-fly Chp	1:10	DSHB
Polyclonal anti-jellyfish GFP	1:2000	Abcam
Polyclonal rabbit anti-GM130, cis-Golgi matrix protein network	1:100	Abcam

Secondary antibodies anti-donkey, anti-goat, anti-mouse and/or anti-rabbit) were conjugated with Alexa Fluor 555 or 647 (Abcam). Samples were finally mounted in Vectashield with DAPI (Vector Laboratories).

Images were acquired using a DeltaVision Elite imaging system (GE Healthcare, Pittsburgh, PA) which consisted of an Olympus 1X71 inverted microscope equipped with a CCD high-resolution camera (CoolSNAP HQ^2; Photometrics), and excitation/emission filters for DAPI, CFP, GFP, YFP, TRITC, mCherry and CY5. Images were acquired using the following objectives: C-Plan 10X (Air, 0.3 NA), UPLSAPO 20X (Air, 0.75NA, 0.17mm WD FL/DIC), PLAPON 60X (Oil, 1.42NA, 0.15mm WD FL/DIC) and UPLSAPO 100X (Oil, 1.40NA, 0.13mm WD FL/DIC) (Olympus). Stacks of images were taken every 0.2-0.5µm and later deconvolved using SoftWoRx 5.5 (Applied Precision).

2.2.4. GFP-GPI Sequence Determination

Freshly eclosed transgenic flies containing the UAS:GFP-GPI construct were anesthetised, frozen, and subsequently pestle-grinded up in liquid nitrogen using an Eppendorf-sized pestle. Genomic DNA was extracted following a DNeasy protocol (QIAGEN). The regions flanking the GFP reporter were PCR-amplified from genomic DNA using the following primer pairs (Sigma, Life Science): pUAST 345 F (5'-TGCAACTACTGAAATCTGC-3') and eGFP N-ter R (5'-CGTCGCCGTCCAGCTCGACCAG-3') for the sequence upstream of GFP, and eGFP C-ter F (5'-CATGGTCCTGCTGGAGTTCGTG-3') and pUAST 495 R (5'-TGTCCAATTATGTCACACCACAGAAGTAAG-3') for the fragment downstream of GFP. PCR products were visualised on a 1.5% agarose gel, DNA bands were cut out of the gel and purified using a QIAquick Gel Extraction Kit (QIAGEN). Next, gel purified DNA was sent for sequencing (Source BioScience Sequencing, UK).

After quality-control inspection of sequencing results, a consensus DNA segment was assembled using ApE-A plasmid Editor v2.0.46 (https://ape-a-plasmid-editor.wikispaces.com/home). The DNA sequence which includes *GFP-GPI* is as follows:

5’…..>ATGGAGCTCTTTTGGAGTATAGTCTTTACTGTCCTCCTGAGTTTCTCCTGCCGG
GGGTCAGACTGGGAATCTCTGCAGTCGACGGTACCGCGGGCCCGGGATCCACCGG
TCGCCACCATGGTGAGCAAGGGCGAGGAGCTGTTCACCGGGGTGGTGCCCATCCT
GGTCGAGCTGGACGGCGACGTAAACGGCCACAAGTTCAGCGTGTCCGGCGAGGGC
GAGGGCGATGCCACCTACGGCAAGCTGACCCTGAAGTTCATCTGCACCACCGGCAA
GCTGCCCGTGCCCTGGCCCACCCTCGTGACCACCCTGACCTACGGCGTGCAGTGCT
TCAGCCGCTACCCCGACCACATGAAGCAGCACGACTTCTTCAAGTCCGCCATGCCC
GAAGGCTACGTCCAGGAGCGCACCATCTTCTTCAAGGACGACGGCAACTACAAGAC
CCGCGCCGAGGTGAAGTTCGAGGGCGACACCCTGGTGAACCGCATCGAGCTGAAG
GGCATCGACTTCAAGGAGGACGGCAACATCCTGGGGCACAAGCTGGAGTACAACTA
CAACAGCCACAACGTCTATATCATGGCCGACAAGCAGAAGAACGGCATCAAGGTGAA
CTTCAAGATCCGCCACAACATCGAGGACGGCAGCGTGCAGCTCGCCGACCACTACC
AGCAGAACACCCCCATCGGCGACGGCCCCGTGCTGCTGCCCGACAACCACTACCTG
AGCACCCAGTCCGCCCTGAGCAAAGACCCCAACGAGAAGCGCGATCACATGGTCCT
GCTGGAGTTCGTGACCGCCGCCGGGATCACTCTCGGCATGGACGAGCTGTACAAGT
ATGATCCGCGCCCAAGCAGCGGTCATTCTAGACACAGATATGCACTTATACCCATAC
CATTAGCAGTAATTACAACATGTATTGTGCTGTATATGAATGTTCTTTAATTGAGAAGA
CAATTTCTTCATTTTTAGGTATTCTGAAATGTGACAGAAAACCAGACAGAACCAACTC
CAATTGATTGGTAACAGAAGATGAAGACAACAGCATAACTAAATTATTTTAAAAACTAA
AAAGCCATCTGATTTCTCATTTGAGCTTTAGAGCACAATGGATCTCGAGGGATCTTCC
ATACCTACCAGTTCTGCGCCTGCAGGTCGCGGCCGCGGCTCGAGGGTACCTCTAGA
GG<…..3’

Sequences were translated using ApE-A plasmid Editor v2.0.46 (https://ape-a-plasmid-editor.wikispaces.com/home), and multiple alignments performed with Jalview 2.10.2b1 (http://www.jalview.org/).

2.2.5. Generation of the mCherry-GPI *Drosophila* Stock

To generate UAS:mCherry-GPI, three sequences were fused:

(i) the segment that includes the coding region for LPH signal peptide, which was amplified with the primer pairs (Sigma, Life Science): *EcoR*I - LPH F (5'-CAGAATTCCGAGCTCAAGC TTAGCTA-3') and LPH mCherry R (5'-TCCTCGCCCTTGCTCACCATGGTGGCGAC CGGTGGAT CCC-3');

(ii) a 708bp fragment coding for the mCherry reporter, with primers LPH mCherry F(5'-GGGATCCACCGGTCGCCACCATGGTGAGCAAGG GCGAGGA-3') and mCherry CD58 R (5'-CTGCTTGGGCGCGGATCATACTTGTAC AGCTCGTCCATGC-3'); and

(iii) a segment of 248bp where the coding sequence for the C-terminal region of CD58 is found, amplified with primers mCherry CD58 F (5'-GCATGGACGAGCTGTACAAGTATGATCCGCGCCCAAGCAG-3') and CD58-*Not*I R (5'-CCTCTAGAGGTACCCTCGAG-3'). All oligonucleotides were provided by (Sigma, Life Science).

All amplified fragments were included in a single PCR reaction with Q5 high-fidelity DNA polymerase (New England BioLabs). The final product of ~1.2kb was gel-purified using a Gel purification kit (Qiagen).For ectopic expression, the mCherry-GPI sequence was inserted between the *EcoR*I and *Not*I restriction sites in pUAST. (Brand and Perrimon 1993). The ligation products were transformed into NEB 5-alpha chemically competent *E. coli* cells suitable for high efficiency transformation (New England BioLabs). Bacteria were spread onto plates containing solid LB agar

with ampicillin and incubated overnight at 37°C. Positive colonies were subjected to PCR to confirm the integrity of the assembled fragments. Subsequently, selected colonies were cultured in LB liquid medium with ampicillin and high-purity DNA was obtained through Minipreps (Qiagen).

Successful ligations were verified by digestion of Miniprep DNA with *EcoR*I and *Not*I restriction enzymes and separation on a 1.5% agarose gel. Miniprep DNA from candidate clones was sequenced using primers LPH mCherry F and CD58-NotI R (Source BioScience Sequencing, UK).

The DNA construct selected was injected into flies (BestGene, USA) and nine independent transformant stocks were generated. Finally, to obtain stable stocks, transformant flies were mapped with a balancer stock. I was able to establish that 18795-1-6M and 18795-1-8M were introduced on the second and third chromosomes, respectively.

2.2.6. Statistical Analysis

The effects of variables presented in Chapter 4 analysed by GLMM were performed using R software (https://www.r-project.org/). All measurements and quantification of the digital images for statistical analysis were made using ImageJ software (Version 1.41) (http://rsb.info.nih.gov/ij/ website). Descriptive statistical analyses were computed on MATLAB software (https://uk.mathworks.com/).

3. Results Chapter: Characterisation of the cellular and molecular role of HAP2(GCS1) in the genetic exchange of *Trypanosoma brucei* parasites

3.1. Aims

To begin to assess the biological importance of *T. brucei* HAP2(GCS1) and its potential roles in membrane fusion events, I undertook an analysis with the following aims:

1. To use bioinformatics analysis to identify important conserved regions in HAP2(GCS1) from different organisms;
2. To determine whether endogenous HAP2(GCS1) is expressed in *T. brucei* parasites in the tsetse fly salivary gland;
3. To test the effects of overexpressing HAP2(GCS1) in *T. brucei* procyclic forms.

Based on my preliminary bioinformatics analysis, my hypothesis is that there are unrecognised conserved regions within the N-terminal domain of HAP2(GCS1). Furthermore, taking into consideration that meiosis-specific proteins are detected in *T. brucei* salivary gland forms (Peacock, Ferris et al. 2011) and that exchange of fluorescent markers has been observed *in vitro* (Gibson, Peacock et al. 2008), I anticipate that *Tb*HAP2(GCS1) will be detectable in the tsetse fly salivary gland forms. *Tb*HAP2(GCS1) is therefore playing a key role in gamete fusion and the subsequent formation of progeny that exhibit the Mendelian inheritance pattern observed in these parasites. Finally, I hypothesise that by overexpressing a tagged form of *Tb*HAP2(GCS1) I will also be capable of triggering cellular fusion *in vitro* in procyclic forms, a life stage that does not normally undergo fusion.

As discussed below, my analysis reveals the presence of previously unrecognised conserved regions within HAP2(GCS1) molecules and has allowed me to identify homologues in other species. In addition, I have shown that overexpressed HAP2(GCS1) can induce phenotypes in *T. brucei* that may be relevant to its proposed functions in cell-cell fusion.

3.2. Results

3.2.1. HAP2(GCS1) Domain Organisation

3.2.1.1. Bioinformatic analysis shows previously unrecognised conserved regions within HAP2(GCS1) among protist, plants and invertebrates

To gain a better understanding of the structural features of HAP2(GCS1) and compare its different homologues, a HMMer2-based analysis was performed (Eddy 1996, Sanchez-Pulido and Ponting 2011).

The predicted primary structure of the *T. brucei* orthologue (Tb927.10.10770) includes a short signal peptide within the first 27 residues, followed by a long extracellular sequence containing the HAP2(GCS1) domain and ending with a single transmembrane region at amino acids 556-577 (Fig. 3.1A-B). The putative sequence also comprises a short cytoplasmic region, which, unlike that in plants, is not enriched in histidine residues (Wong, Leydon et al. 2010). Hence, *Tb*HAP2(GCS1) can be classified as a type I transmembrane protein (Johnson, von Besser et al. 2004, Mori, Kuroiwa et al. 2006, von Besser, Frank et al. 2006).

A

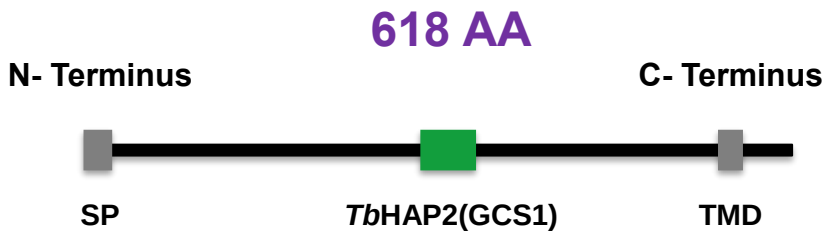
618 AA
N- Terminus
C- Terminus
SP
TbHAP2(GCS1)
TMD

B

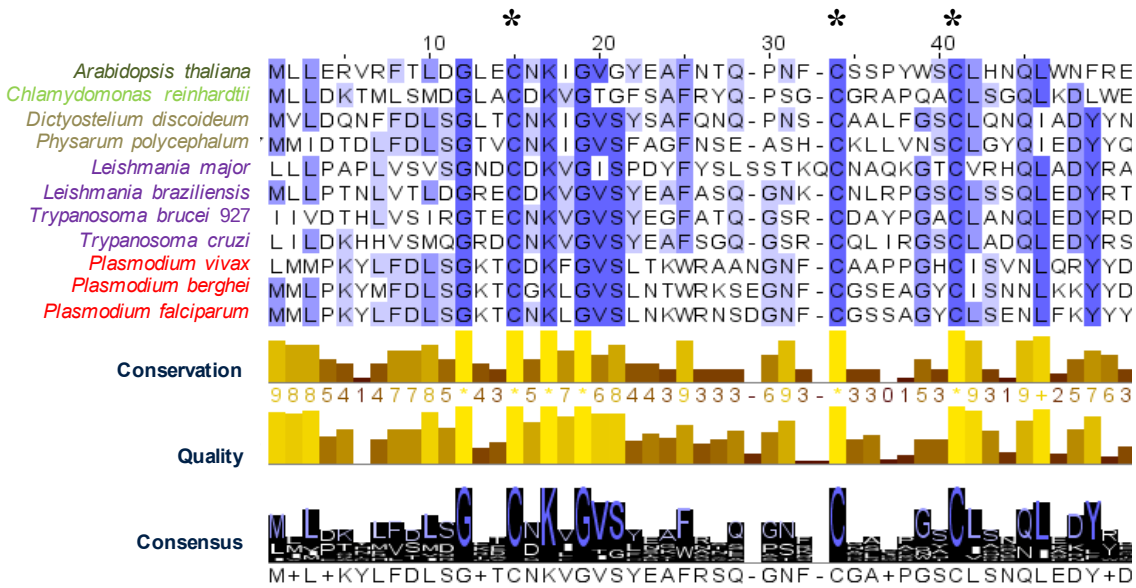
Arabidopsis thaliana
Chlamydomonas reinhardtii
Dictyostelium discoideum
Physarum polycephalum
Leishmania major
Leishmania braziliensis
Trypanosoma brucei 927
Trypanosoma cruzi
Plasmodium vivax
Plasmodium berghei
Plasmodium falciparum
Conservation
Quality
Consensus

Figure 3.1 **Predicted topology of the *T. brucei* HAP2 orthologue (Tb927.10.10770, Q389Q2, PF10699). A.** Schematic representation of the primary structure of *Tb*HAP2(GCS1) illustrating the arrangement of the N-terminal signal peptide **SP (aminoacids 0-27)** (grey rectangle), the **HAP2(GCS1) (aminoacids 297-344)** Pfam domain (green rectangle), and the transmembrane domain **TMD (aminoacids 556-577)** (grey rectangle) marking the start of a short cytoplasmic sequence. The total length of the protein is indicated in purple. **B.** Alignment of representative HAP2(GCS1) domains. Three cysteine residues (*) are conserved among the selected species. Here and in subsequent figures blue shading indicates the percentage of identity and increments according to the percentage of amino acids in each column that agrees with the consensus sequence (>80% is darker blue, >40% light blue, <40% not coloured). Multiple alignments generated using Jalview. The numerical conservation index reflects the number of physico-chemical properties conserved. The quality score measures the likelihood of observing mutations in a particular column. Consensus is the relative amount of the modal residue in each column.

3.2.1.2. Identification of novel structural features of HAP2(GCS1)

The homology search presented here started with a seed sequence alignment from the Pfam HAP2(GCS1) family. Initial results were examined for sequence conservation to avoid the inclusion of false-positives. The limits of the HAP2(GCS1) domain in the different sequences were gradually expanded in length to include conserved blocks of amino acids. Iterative profile searches on HMMer2 were done until convergence on a finite set of candidates with *E*-values of $<10^{-5}$ (within the UniRef50 protein data-base) (Sanchez-Pulido and Ponting 2011). A final list of these candidates, organised according to five major divisions of eukaryotes (Walker, Dorrell et al. 2011), is presented in Appendix 1, and their representative sequence alignments in Fig. 3.2A-C.

The first profile predicted has 57 different candidates, comprises a multiple alignment with a sequence length of 233 ± 29 (average ± SD) amino acids and was designated Box 3 (Fig. 3.2C). Two more conserved regions were subsequently identified using the same approach, delimiting a total of three conserved areas among the HAP2(GCS1) homologues (Boxes 1-3). Box 1 comprises 111 ± 7 residues while Box 2 is formed from 122 ± 28 amino acids. Finite sets include 42 and 41 candidates for Boxes 1 and 2 respectively (Appendix 1). Examples of identified homologues with statistically significant *E*-values for each box are presented in Fig. 3.3A.

Box limits were determined by exclusion, meaning that the species which have only Box 3 (e.g. Mat proteins (Bloomfield 2011) [MatD and MatT proteins are part of the mating-types II and III respectively expressed during the sexual life cycle of *D. discoideum*]), or Boxes 1 and 3 (e.g. *Drosophila melanogaster* CG34027, see architectures in Fig. 3.3 B) were not included in setting the limits for Box 2. Therefore, my database includes homologous sequences with only one box, two boxes (1 and 2, 2 and 3, or 1 and 3) or three boxes.

Previous predictions for the distribution of HAP2(GCS1) in eukaryotic species have been obtained by running profile-based iterative searches under PSI-BLAST (Hirai, Arai et al. 2008, Liu, Tewari et al. 2008, Steele and Dana 2009). This analysis was improved upon here using HMMer2 (Eddy 1996, Sanchez-Pulido and Ponting 2011), so that in the sequence between the N-terminus and the transmembrane region of HAP2(GCS1) homologues, it was possible to distinguish three different areas with significant sequence conservation. The results of my analysis indicate that the HAP2(GCS1) domain (previously defined as a ~48 residue sequence) can be expanded to include the evolutionarily conserved region identified here as Box 3. The bioinformatic results presented here broaden the current list of species where HAP2(GCS1) has been predicted across Archaeplastids, Alveolates, Excavates, Amoebozoa and Opisthokons (Hirai, Arai et al. 2008, Liu, Tewari et al. 2008, Steele and Dana 2009) (Appendix 1), and confirm its ancestral distribution.

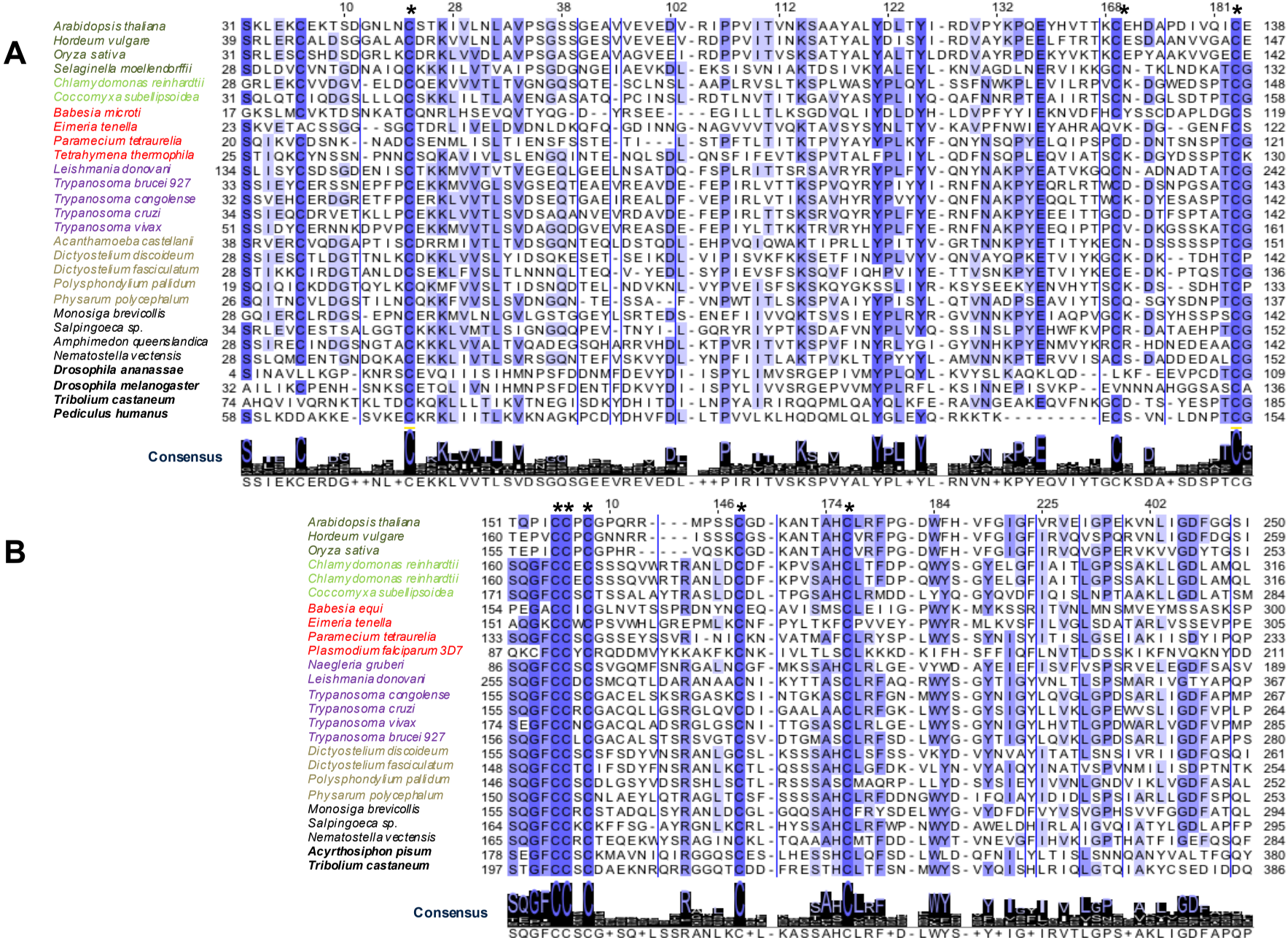
A
B
Consensus
Consensus

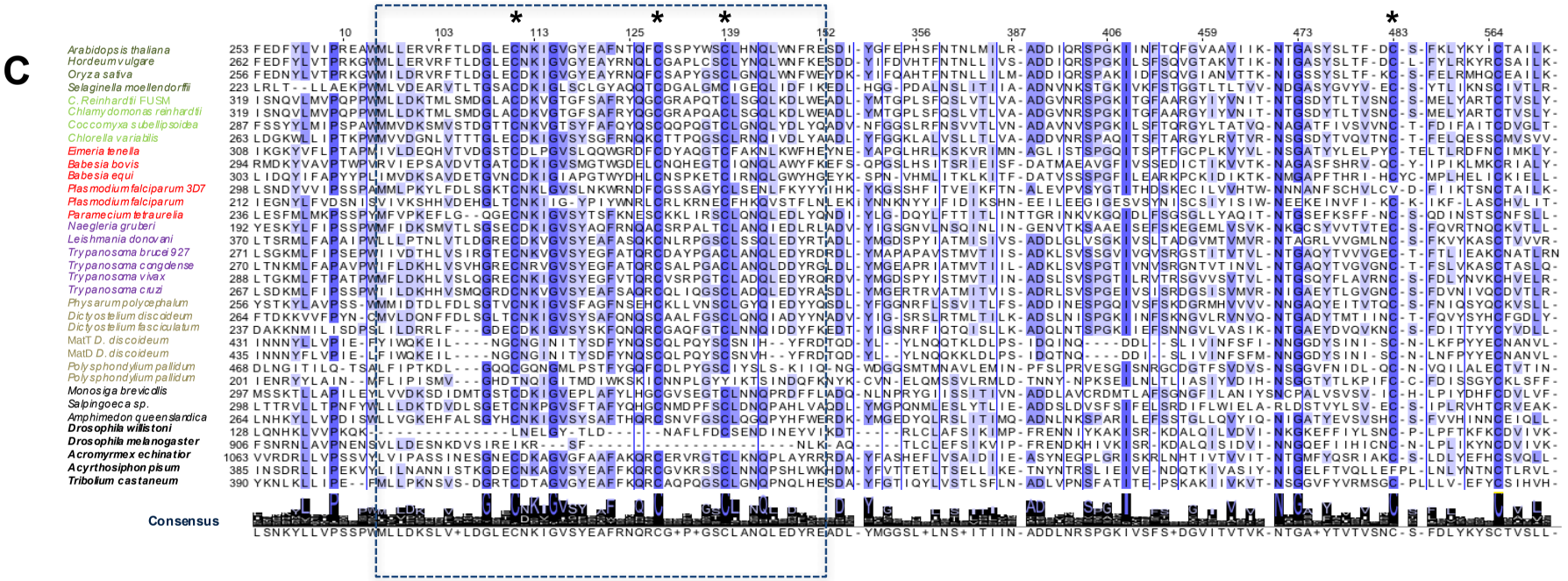

Figure 3.2 **Representative multiple sequence alignments of conserved domains in HAP2(GCS1). A.** Box 1, **B**. Box 2 and **C.** Box 3. Alignments were generated using Jalview. Box limits are indicated by flanking amino acid numbers. Aligned sequences correspond to species listed in five major divisions of eukaryotes (Walker, Dorrell et al. 2011). Species colour code represents **Archaeplastids** in green (Chlorophytes in light green and Embryophytes dark green), **Alveolates** (including Ciliates and Apicomplexa) in red, **Excavates** in purple, **Amoebozoa** in light brown and black for **Opisthokons** (including Choanoflagellates, and in bold, Metazoans: Porifera, Cnidaria and Arthropoda). The HAP2(GCS1) domain is indicated by a dashed box in **C**. The top scale shows amino acid sequence length. Blue solid lines running between amino acids down the alignments represent hidden columns excluded to facilitate visualisation. Highly conserved cysteine residues (*) obtained high scores in a prediction of disulphide bonding state for Tb927.10.10770 (Score = 8; low = 0 to high = 9).

A

Entry Name UniProtKB	Species	Box 1			Box 2			Box 3		
		Alignment		HMMer 2 Score	Alignment		HMMer 2 Score	Alignment		HMMer 2 Score
		Start	End		Start	End		Start	End	
F4JP36_ARATH	*A. thaliana (Mouse-ear cress)*	31	139	**5.1 e-40**	151	251	**1.7 e-37**	253	476	**1.2 e-87**
G0U801_TRYVY_01	*T. vivax (strain Y486)*	51	162	**2.2 e-38**	174	286	**8.2 e-41**	288	513	**1.7 e-84**
Q389Q2_TRYB2	*T. brucei (strain 927/4 GUTat10.1)*	33	144	**3.6 e-32**	156	269	**3.9 e-36**	271	495	**2.7 e-75**
Q1X7J9_LEIMA_01	*L. major*	44	165	**3.1 e-09**	177	282	**7.9 e-14**	283	523	**1.2 e-48**
A7SIM4_NEMVE	***N. vectensis (Starlet anemone)***	28	153	**1.4 e-29**	165	285	**7.6 e-37**	287	519	**2.2 e-64**

B

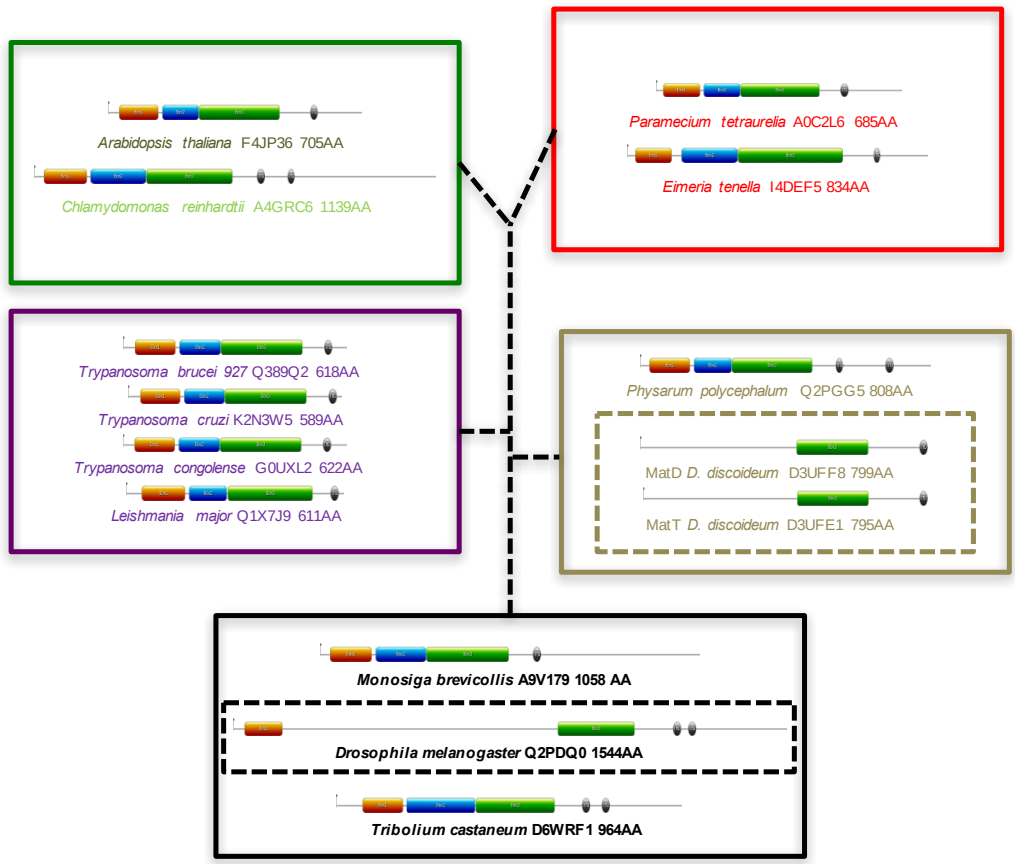

Figure 3.3 **Rearranged architecture of conserved domains within HAP2(GCS1) protein homologues. A.** HMMER2 *E*-values for homologous amino acid sequences in selected HAP2(GCS1) homologues, confirming the conservation of Boxes 1-3. **B.** Schematic representation of Boxes 1-3 of HAP2(GCS1) in five major eukaryotic divisions. Cartoons are boxed according to Walter *et al*. (2011). The green branch represents **Archaeplastids** (Chlorophytes and Embryophytes), red **Alveolates** (including Ciliates and Apicomplexa), purple **Excavates**, light brown **Amoebozoa** and black **Opisthokons** (Choanoflagellates and the Metazoans Porifera, Cnidaria and Arthropoda). Colour codes of the cartoon boxes are: orange **Box 1**, blue **Box 2** and green **Box 3**. A small flag represents a Signal peptide predicted by SignalP 4.1 Server. TMD domains were predicted on TMHMM Server v. 2.0 and TOPCONS are represented by grey ovals. Species UniProtKB ID is noted below each model followed by the total length of the amino acid sequence.

3.2.2. *In vitro* differentiation of *T. brucei* using ectopic expression of RNA-binding protein 6

My ultimate goal was to study the functions of *Tb*HAP2(GCS1) in different forms of *T. brucei* found in the tsetse fly salivary gland. However, there are major limitations in undertaking these experiments in infected flies. A system for *in vitro* differentiation of procyclic forms would advance the characterisation of *Tb*HAP2(GCS1) function, since the localisation and functions of different tagged and mutated versions of the protein and other cell markers could be easily assessed outside tsetse flies.

Recently, it was established that overexpression of RNA-binding protein 6 (RBP6) in procyclics results in the production of long and short epimastigotes and infective metacyclics (Kolev, Ramey-Butler et al. 2012). *Tb*RBP6 (Tb927.3.2930) is a 27kDa

protein with 239 residues and a well-conserved C-terminal RNA recognition motif (RRM) (data not shown). I sought to replicate the experimental conditions of Kolev *et al*. who reported a sustained production of epimastigotes during days two to seven after induction of *Tb*RBP6, followed by a gradual increase in metacyclics until day 10 of up to 32% of all cells (Kolev, Ramey-Butler et al. 2012).

To this end, 29:13 cells were transfected with a pDex577:RBP6-YFP-TY plasmid in which expression of tagged RBP6 can be induced by doxycycline. Although expression of RBP6-YFP-TY was observed after induction of two independent clones, no salivary gland forms of the parasite were produced over a period of eight days (Fig. 3.4A). The same result was obtained using a plasmid in which the YFP-TY tag was not present.

Subsequently, I tested the overexpression of *Tb*RBP6 inserted in the plasmid pLew100 and transfected into 29:13 cells, which permits expression of proteins under the control of an inducible EP1 procyclin promoter (Wirtz, Leal et al. 1999). This approach was also unsuccessful in producing developmental progression of procyclics into mature metacyclics (metacyclogenesis). A summary of representative morphologies obtained three days after induction is shown in Fig. 3.4B. The highest proportion of short epimastigote forms was 12% of a total of 131 cells, and this was obtained three days after induction (Fig. 3.4B, panels e to h). This proportion was halved by day seven (data not shown). Employing a high-cell-density culture to $1x10^7$cells ml^{-1}, a different culture medium and keeping PCFs on supplemented medium with selective drugs during induction, failed to improve these results.

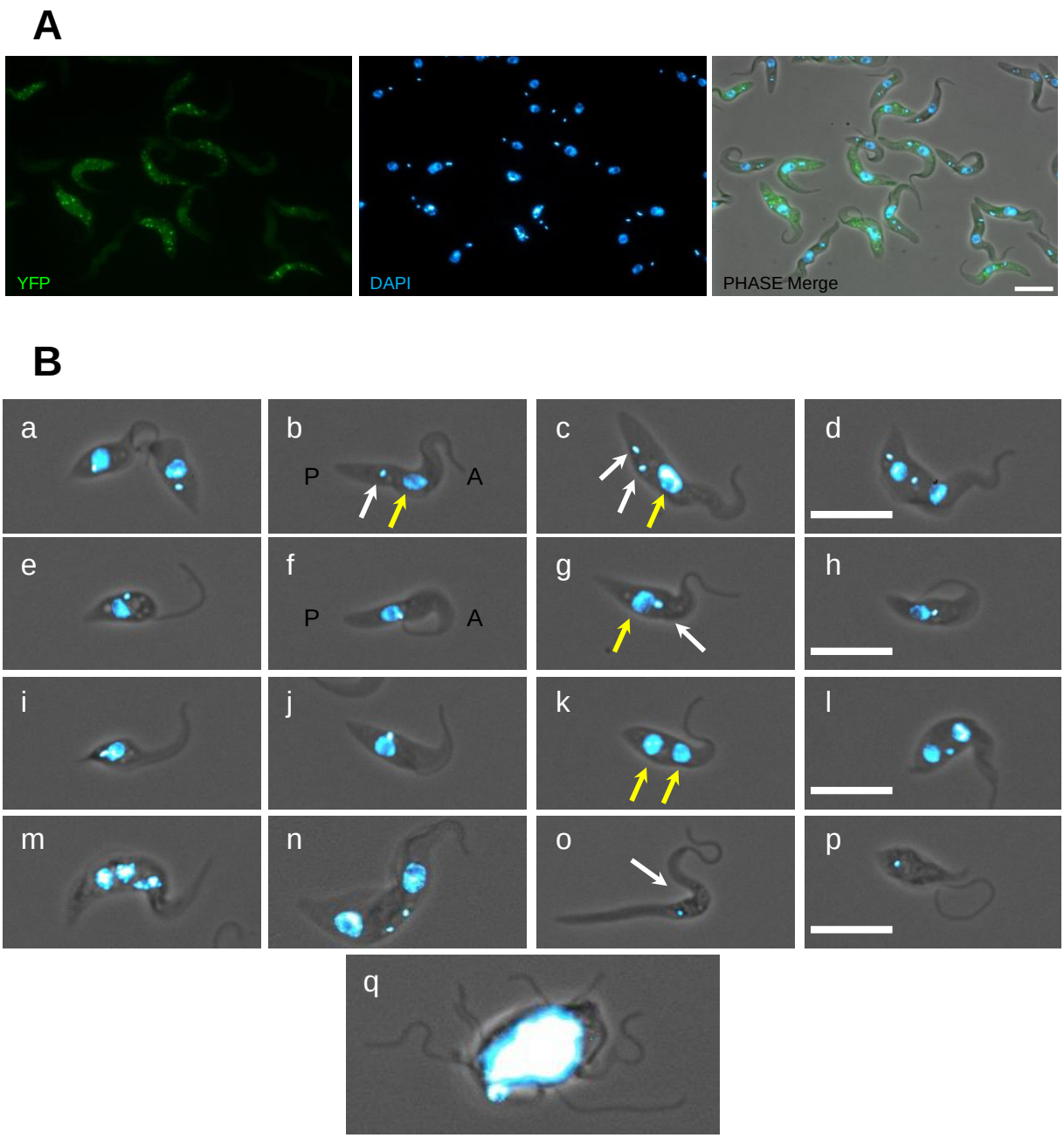

Figure 3.4 ***In vitro*** **differentiation of** ***T. brucei*** **using** ***Tb*****RBP6 ectopic expression. A.** Field of view showing multiple pDex577:RBP6:YFP:TY cells (clone 4) eight days after doxycycline induction. **B.** Representative nuclear and cellular phenotypes observed three days after inducing *Tb*RBP6 expression. These phenotypes include PCFs that are: 1K1Ns **(a-b)**, 2K1N **(c)**, 2K2N **(d)**; characteristic of a Short epimastigote forms **(e-h);** other cells with a juxtaposed kinetoplast **(i-j)**; aberrant cell types **(k-q)**. Cyan blue = DAPI staining. Scale bars in white represent 10µm. A=Anterior, P=Posterior. White arrows point to the kinetoplast (K) and yellow to the nucleus (N).

The difficulties in trying to replicate the differentiation *in vitro* of *T. brucei* procyclics using RBP6 ectopic expression underscored the importance of optimising cell culture conditions and expression systems. Because of time limitations, I decided to examine the expression, localisation and functions of *Tb*HAP2(GCS1) fusion proteins in forms of *T. brucei* isolated from the tsetse fly salivary glands.

3.2.3. *Tb*HAP2:YFP expression from the endogenous genomic locus is observed in tsetse salivary gland isolates.

I hypothesised that the *T. brucei HAP2(GCS1)* gene might be involved in membrane fusion events mediating production of hybrid progeny in the tsetse fly salivary glands. A transgenic *T. brucei* strain, in which the endogenous *Tb*HAP2 locus had been targeted by homologous recombination to generate a *TbHAP2:YFP* transgene, was generated in the Gluenz laboratory. Unpublished results had already shown that the *Tb*HAP2:YFP protein made from this locus is expressed within a fraction of parasites in tsetse salivary glands. To gain insights into the subcellular localisation of *Tb*HAP2(GCS1) by fluorescence microscopy, I characterised the phenotype of cells expressing a tagged form of HAP2(GCS1) from the endogenous locus. Male tsetse flies were infected with *T. brucei* in which endogenous HAP2(GCS1) was tagged with YFP. The flies were dissected at 22-23 days post-infection and a thin-layer preparation was obtained from their salivary glands.

A total of 1101 *T. brucei* cells were analysed, which included 17% epimastigotes and 64% metacyclic forms (both of them YFP-negative). Approximately 13% of the

cells showed a fluorescence signal. These cells were neither epimastigotes nor metacyclic forms. The frequency of YFP-positive cells at 22-23 days post-infection for these other *T. brucei* cells was significantly increased when compared to epimastigotes and metacyclic forms ($P<0.01$, Chi-squared test). Indeed, the nuclear morphology of cells in which a YFP signal was detected did not seem to correspond to the life cycle stages described extensively in tsetse salivary glands (Vickerman 1985, Vickerman, Tetley et al. 1988, Sharma, Peacock et al. 2008). However, we were able to identify 67 cells that meet the morphological characteristics recently reported for PLs (Peacock, Bailey et al. 2014, Peacock, Ferris et al. 2014)(Fig. 3.5C and D).

Figure 3.5**. *Tb*HAP2:YFP expression from endogenous HAP2 locus is observed in tsetse salivary gland isolates. A.** Tsetse fly cartoon illustrating the compartments in which different forms of the parasite are found. Ingested parasites (IN) first establish an infection in the midgut of the fly, migrating afterwards to the salivary glands to become the infectious forms that are injected (OUT) into the host. **B.** YFP-negative cells found in the salivary gland of the tsetse fly. **C., D**. Representative YFP-positive PL cell types found in the salivary gland include 1K1N1K (C) and .1N1K (D). Cells are stained with a DAPI, which marks nuclei and the kinetochores (red in merge). White arrows point to the kinetoplast (K) and yellow to the nucleus (N). In all cells, anterior is oriented to the right, A=Anterior P=Posterior. All images at same scale, the scale bar represents 2μm.

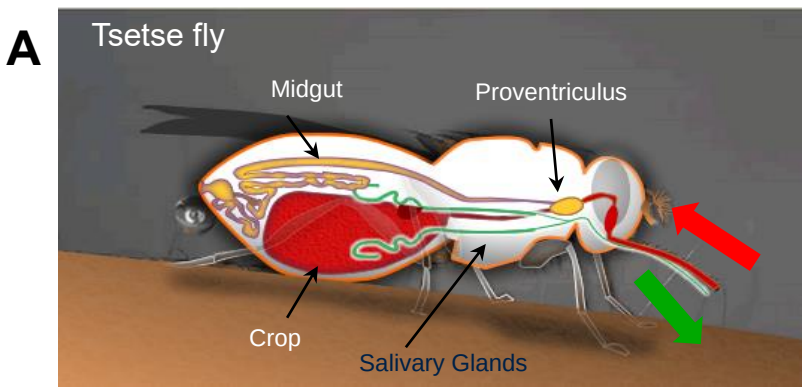

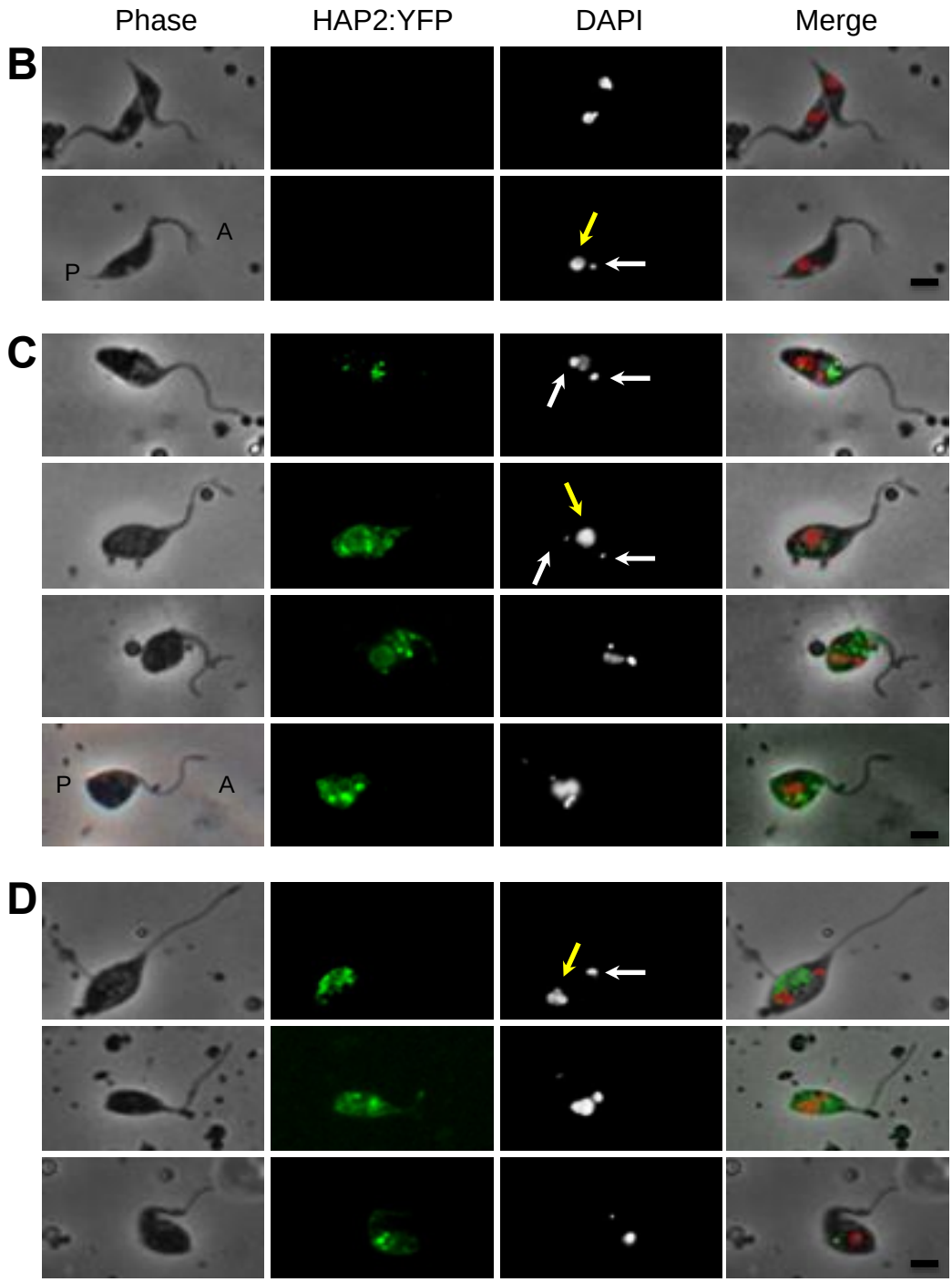

Nearly 53% of the YFP-positive cells could not be categorised as PLs (Fig. 3.6). These trypanosomes displayed at least six different nuclear morphotypes (0K1N, 1K1N, >2K>2N, 1K2N1K, 1N≥3K, as well as cells that exhibited clumps of DNA of varying size, which could indicate fragmentation of the genetic material). Even though there did not appear to be a distinctive pattern of fluorescence in all the YFP-

positive trypanosomes observed in the isolates, two common morphological features were apparent: (1) YFP signal surrounding the DNA material and (2) fluorescent loci of variable intensity distributed throughout the cell body of the parasites.

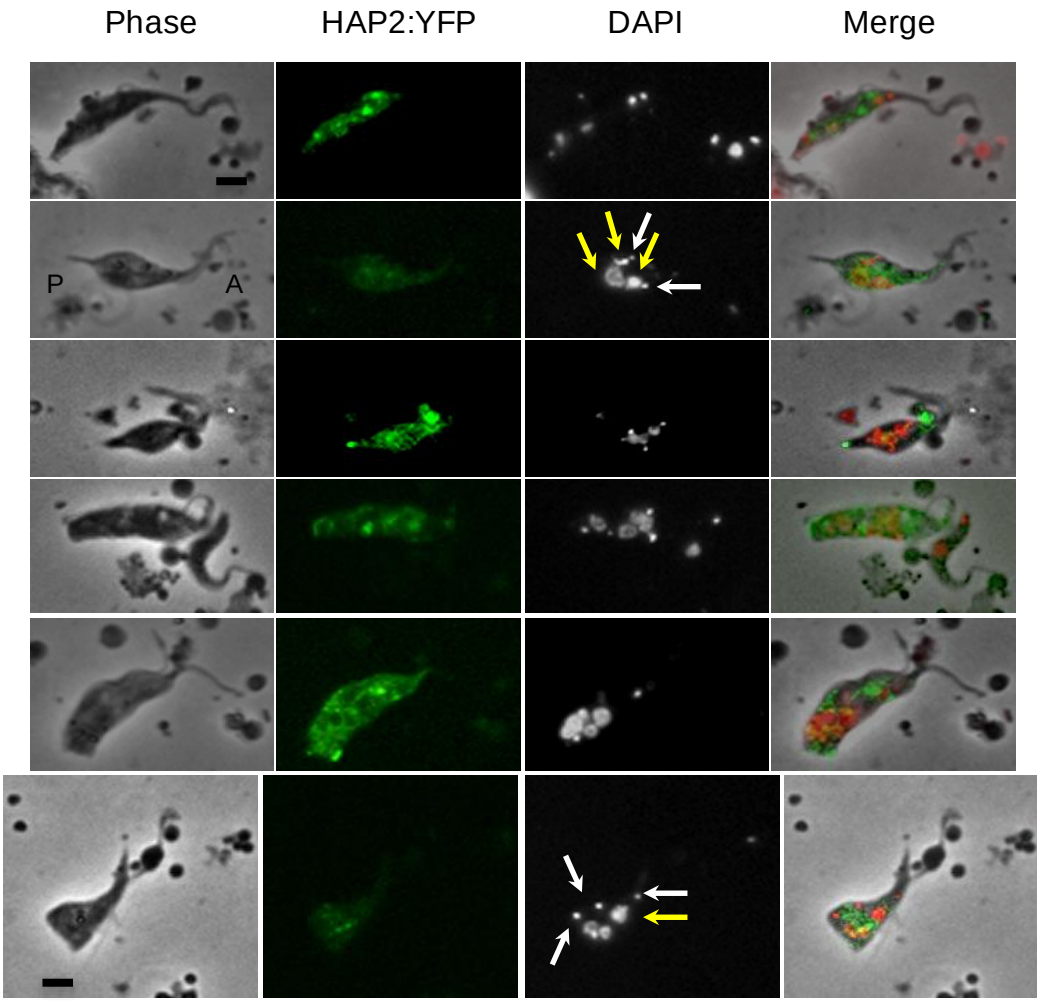

Figure 3.6 **Endogenous *Tb*HAP2:YFP expression is observed in tsetse salivary gland isolates.** Examples of other YFP-positive cell types found in the salivary gland that have abnormal KN arrangements. Cells are stained with DAPI, which marks nuclei and the kinetochores (red in merge). White arrows point to the kinetoplast (K) and yellow to the nucleus (N). In all cells, anterior is oriented to the right, A= Anterior P=Posterior. All images at same scale, the scale bar represents 2μm.

3.2.4. Expression levels, subcellular localisation and effects of inducibly expressed *T. brucei* HAP2 fusion proteins in procyclic forms

During the normal cell cycle of *T. brucei* procyclic cells, at least three nuclear morphologies are observed: (1) 1K1N cells show a single anterior nucleus (N) and a posterior single kinetoplast (K); (2) uninucleated 2K1Ns where, as a result of kinetoplast segregation, two kinetoplasts are detected at the posterior end of the cell; and (3) single cells with two Ks and two Ns (2K2Ns), where nuclear division is completed (Sharma, Peacock et al. 2008). The variations in the positioning of the kinetoplast and nucleus along the anterior-posterior cellular axis provide important morphological markers for determining the stages of the cell cycle and any morphological variations generated by *Tb*HAP2:TY overexpression.

As part of the initial attempts to characterise the expression patterns and subcellular localisation of *Tb*HAP2(GCS1), I studied the overexpression of two versions of the tagged protein: *Tb*HAP2:TY (the TY epitope is described by (Bastin, Bagherzadeh et al. 1996) and *Tb*HAP2:YFP:TY (Fig.3.7A). I reasoned that the unusual subcellular localisation of endogenous *Tb*HAP2:YFP:TY might mean that the large YFP tag was disrupting its trafficking in the cell and therefore only included the much smaller TY tag in one of the constructs.

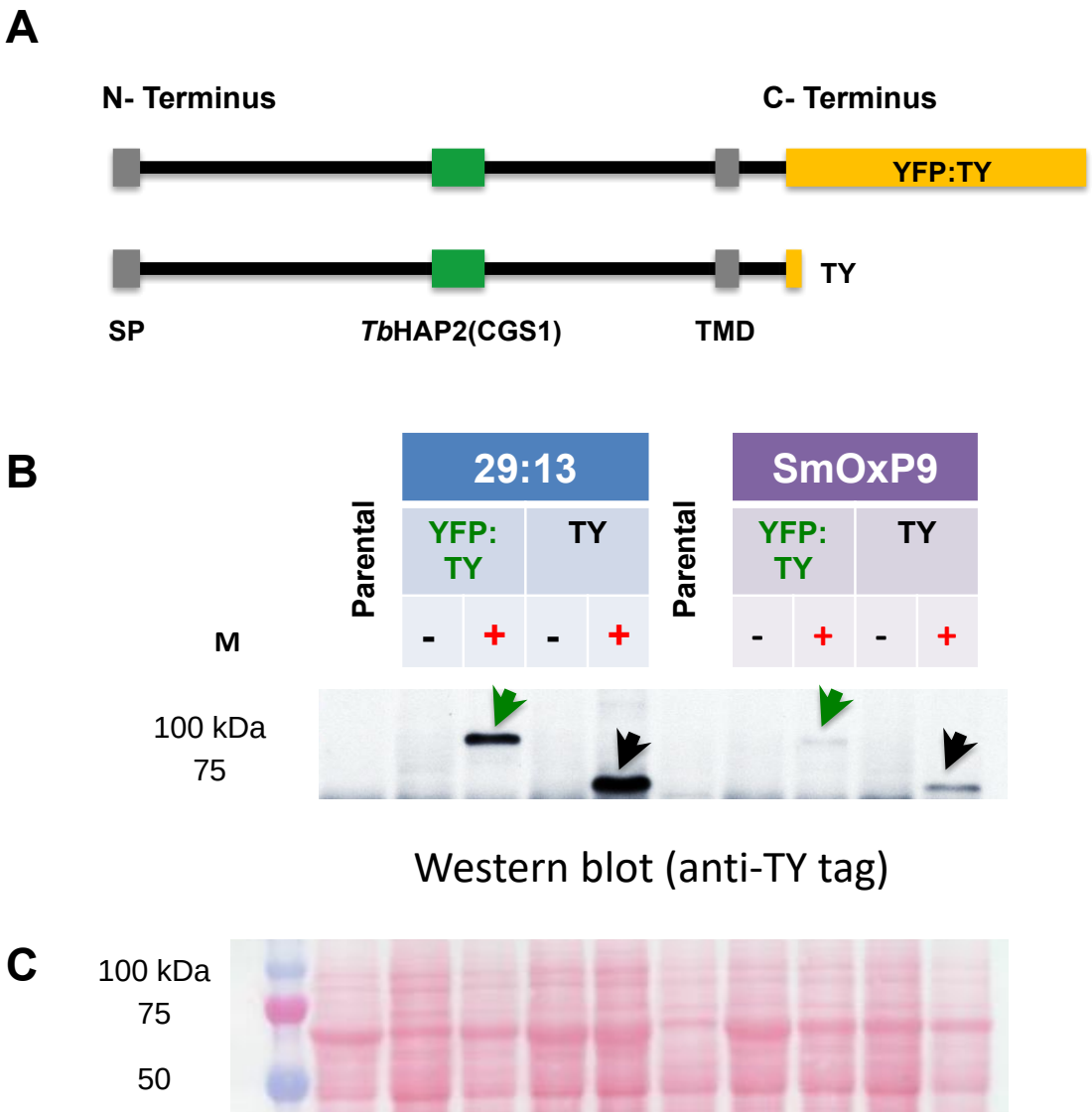

Figure 3.7 **Overexpression of *Tb*HAP2:TY and *Tb*HAP2:YFP:TY in the procyclic cell lines 29:13 and SmOxP9. A.** Schematic representations of the two versions of the tagged protein: *Tb*HAP2:TY and *Tb*HAP2:YFP:TY, illustrating the relative size of each tag in relation to the other described topological features **B**. Immunoblot of whole cell extracts probed for the TY tag with the BB2 monoclonal antibody. Blot shows that 24 hours after induction (+: Addition of doxycycline) HAP2:TY cells expressed a higher amount of tagged protein compared to HAP2:YFP:TY cells. Expression of fusion proteins was higher in the 29:13-derived cell lines. Expected band sizes are: ~100 kDa for *Tb*HAP2:YFP:TY (green arrow head), ~70 kDa for *Tb*HAP2:TY (black arrow head). *Tb*HAP2 is ~67 kDa. **C.** PonceauS staining with molecular weight markers is included as a loading control and to confirm protein transfer to nitrocellulose following SDS-PAGE.

Doxycycline-inducible expression constructs were integrated into two PCF cell lines (29:13 and SmOxP9, Fig. 3.7B-C). Given the higher expression of the transgenic protein 24 hours after induction in 29:13 cells, subsequent experiments were done only in these cells (Fig. 3.8A-D). Over an induction period of eight days, *Tb*HAP2:TY overexpression induced a reduced growth phenotype, while no difference was observed in *Tb*HAP2:YFP:TY-overexpressing cells when compared with non-induced controls. This result correlated with constant expression levels of *Tb*HAP2:TY and the decreasing levels observed for *Tb*HAP2:YFP:TY (Fig. 3.8B-D), suggesting that high expression levels of *Tb*HAP2:TY might block growth.

In the *Tb*HAP2:TY overexpression experiment, the non-induced control (n=592 cells) showed the following proportions: 73.6 ± 5.8% (average ± SD) 1K1Ns 5.6 ± 2.5% 2K1Ns, 8.4 ± 4.1% 2K2Ns, while the number of abnormal cells reached 12.3 ± 4.7% (under the same experimental conditions, 9.1% of non-transfected 29:13 cells were abnormal, data not shown). After *Tb*HAP2:TY induction, the proportion of abnormal cells increased to 31.6 ± 5.0%, whereas 1K1Ns and 2K2Ns cells diminished (13.8 and 5.2% respectively) within the first 24 hours (Fig. 3.9A and C). In addition to the decline in overall growth of induced cells at 48 hours, a pronounced reduction in 1K1Ns was observed, while cells with abnormal phenotypes increased to 70.7 ± 6.9% (Fig. 3.9A and D).

The abnormal phenotypes produced following *Tb*HAP2:TY induction included rounded cells; cells of variable size with dense packing of increased DNA content and overall loss of normal cell shape; 1K1Ns with a shifted position of kinetoplast and nuclei; 1K2Ns; and 0K1Ns (Fig. 3.10B).

In addition, two multinucleated phenotypes were highlighted: the first includes a single cell in which several rounds of DNA duplication and nuclear division occurred without cell division (Fig. 3.11A), whilst in the second, two opposed flagella are distinguishable. Here an apparent furrowing and abscission failure is likely to have occurred after DNA duplication and nuclear division (Fig. 3.11B).

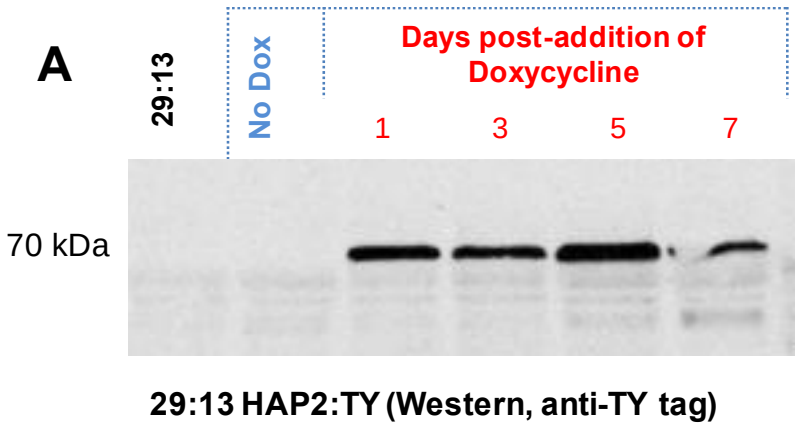

29:13 HAP2:TY (Western, anti-TY tag)

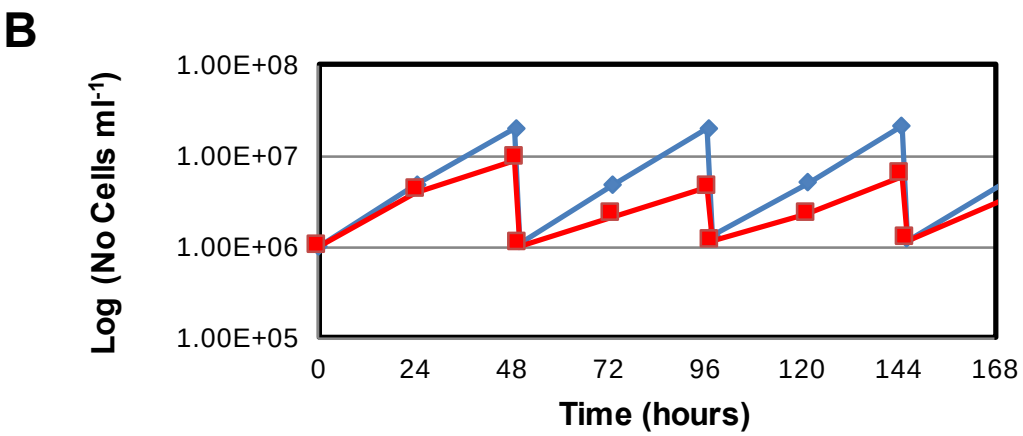

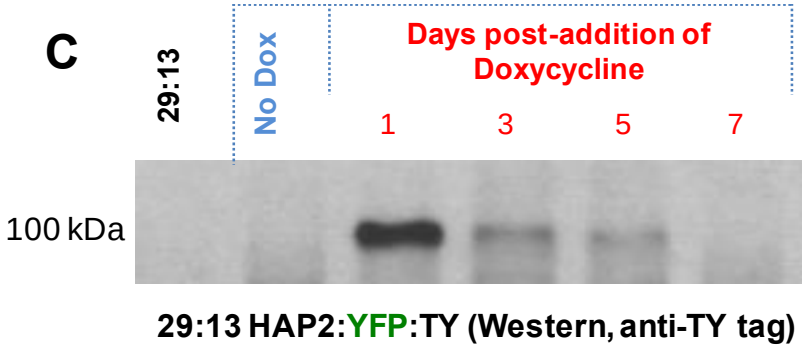

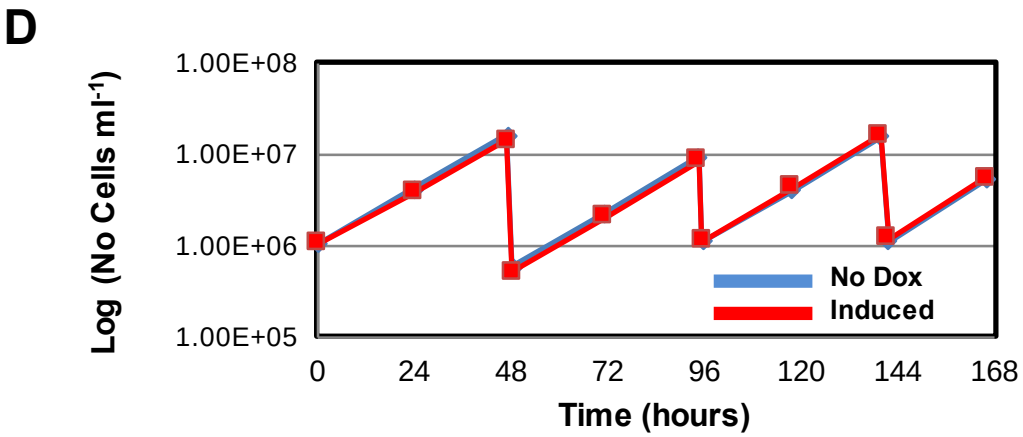

Figure 3.8 **Comparative analysis of the expression of *Tb*HAP2:TY and *Tb*HAP2:YFP:TY over time. A** and **C.** Western blot of the recombinant protein probed with BB2 monoclonal antibody directed against the TY tag in whole cell extracts of procyclic forms. The expression levels of *Tb*HAP2:TY persisted over time (from 1 to 7 days post-addition of doxycycline) (A), and resulted in a decrease in growth rate (B). **B** and **D.** Expression levels of *Tb*HAP2:YFP:TY protein decreased over this period (C) and there was no effect on growth (D). Expected band sizes are: ~100kD for *Tb*HAP2:YFP:TY and ~70kD for *Tb*HAP2:TY. Population growth was measured every 24 hours, and cells in culture diluted to $1x10^6$cells ml^{-1} every 48 hours.

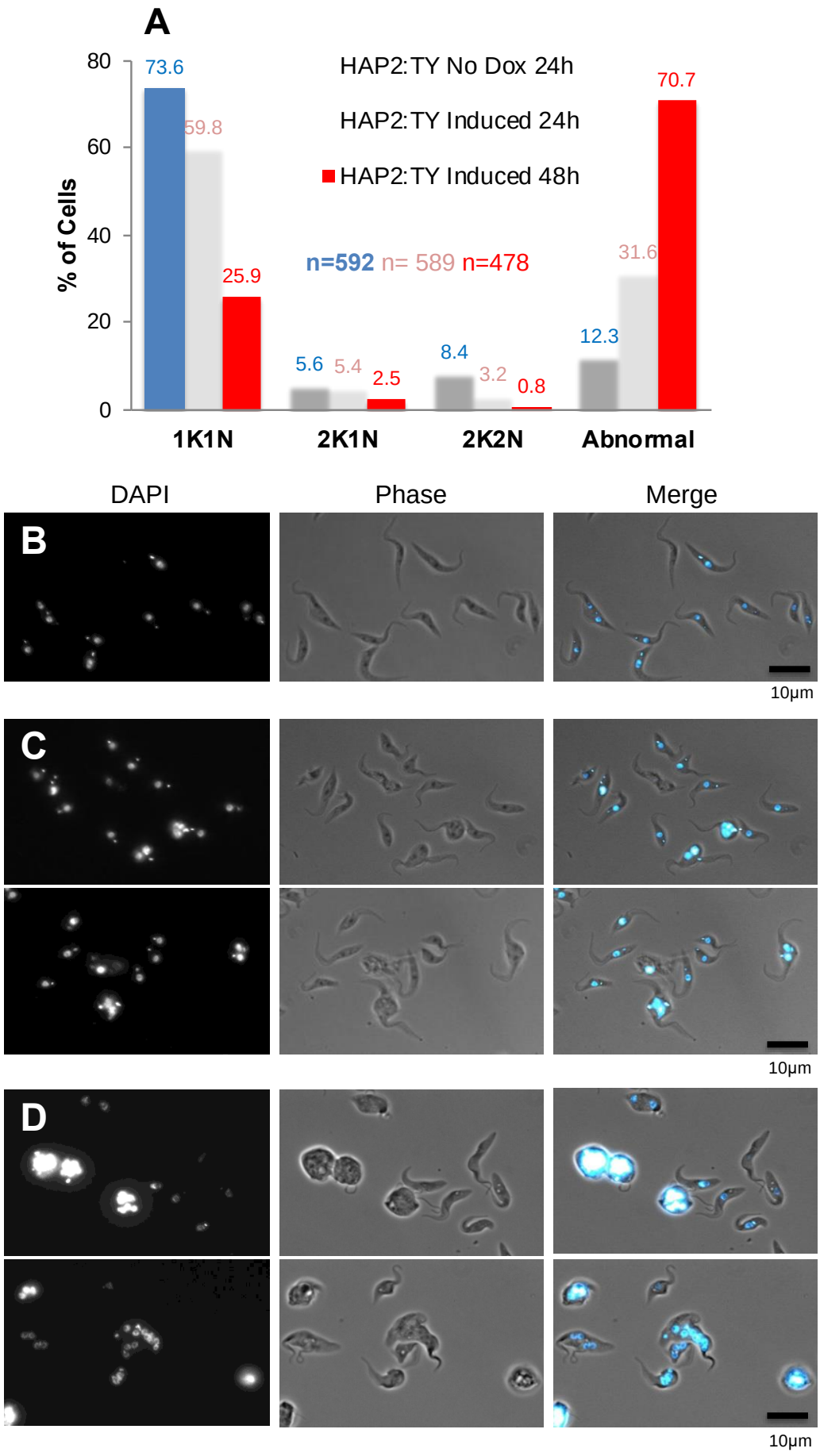
A
80
60
40
20
0
% of Cells
73.6
59.8
25.9
5.6
5.4
2.5
8.4
3.2
0.8
12.3
31.6
70.7
HAP2:TY No Dox 24h
HAP2:TY Induced 24h
HAP2:TY Induced 48h
n=592 n= 589 n=478
1K1N
2K1N
2K2N
Abnormal
DAPI
Phase
Merge
B
10µm
C
10µm
D
10µm

Figure 3.9 ***Tb*HAP2:TY overexpression leads to abnormal nuclear and cellular phenotypes. A.** Quantification of kinetoplasts (Ks) and nuclei (Ns) reveals an increase in aberrant morphologies over time after *Tb*HAP2:TY induction, whilst numbers of 1K1N and 2K2N diminished. Cell populations were sampled 24 and 48 hours after induction. **B.** Field of view of non-induced cells is presented as a control. **C, D.** Induced cells show increased abnormality over time. Cells were observed 24h (C), and 48h (D) post-doxycycline induction. Cyan blue = DAPI staining.

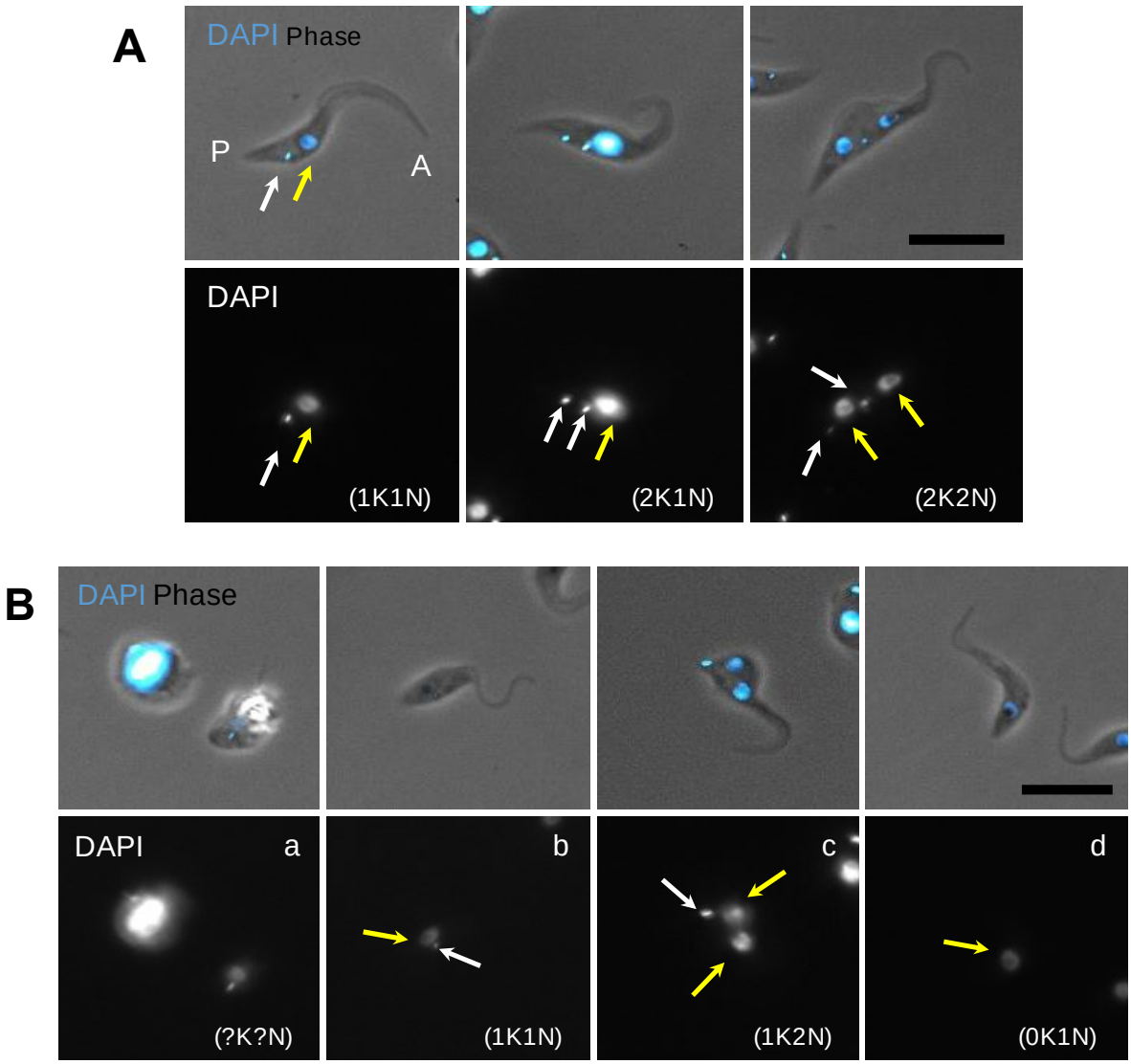
A
DAPI Phase
P
A
DAPI
(1K1N)
(2K1N)
(2K2N)
B
DAPI Phase
DAPI
a
b
c
d
(?K?N)
(1K1N)
(1K2N)
(0K1N)

Figure 3.10 **Nuclear and cellular phenotypes observed after *Tb*HAP2:TY overexpression. A.** Normal cellular and nuclear phenotypes. **B.** The abnormal phenotypes produced following *Tb*HAP2:TY induction included: **(a)** rounded cells with dense packaging of DNA content; **(b)** 1K1Ns with a shifted position of kinetoplast and nuclei; **(c)** 1K2Ns; and **(d)** 0K1Ns. Scale bars represent 10µm. Cyan blue=DAPI staining. White arrows point to the kinetoplast (K) and yellow to the nucleus (N). A = Anterior P = Posterior.

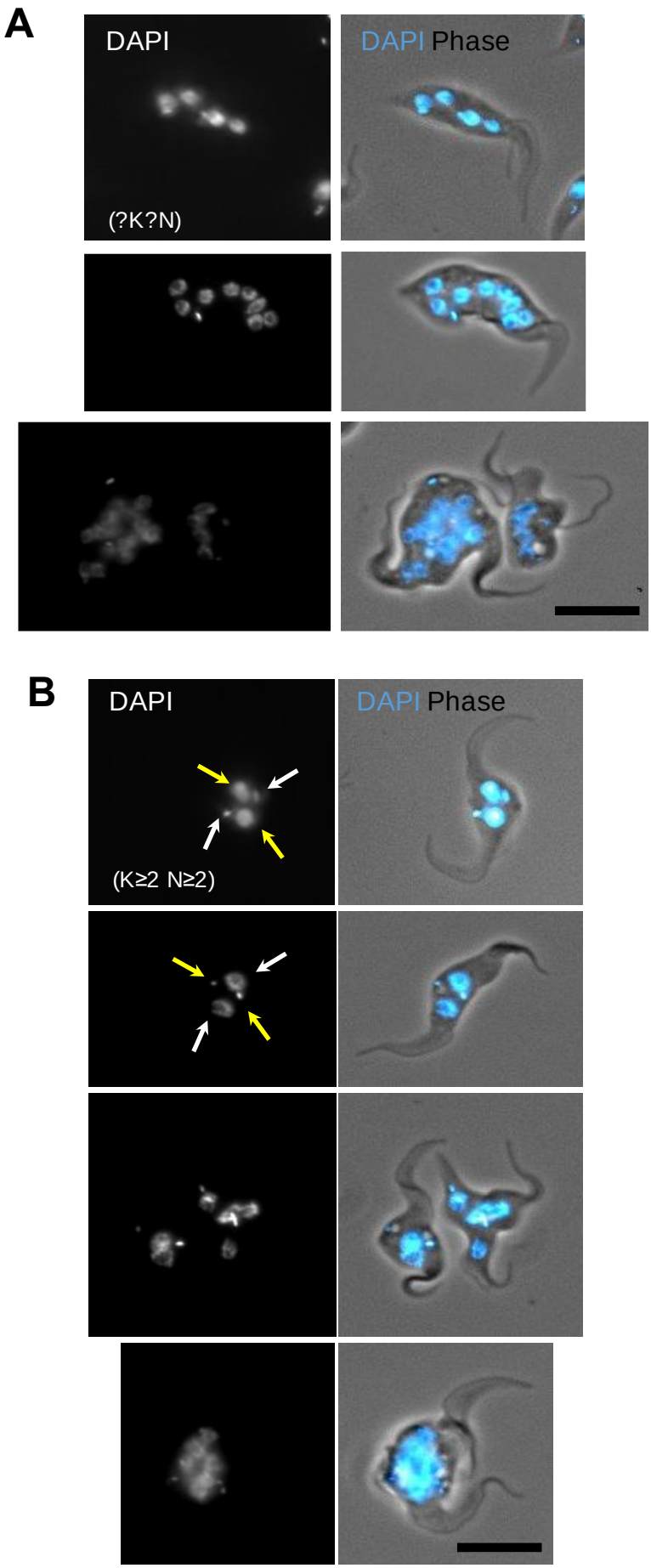
A
DAPI
DAPI Phase
(?K?N)
B
DAPI
DAPI Phase
(K≥2 N≥2)

Figure 3.11 **Nuclear and cellular phenotypes observed after *Tb*HAP2:TY overexpression.** Examples of the abnormal multinucleated phenotypes: **A.** Single cells where several rounds of DNA duplication and nuclear division occurred without cell division. **B.** Cells with two opposed flagella show an apparent furrowing and abscission failure occurred after DNA duplication. Scale bars represent 10µm. Cyan blue=DAPI staining. White arrows point to the kinetoplast (K) and yellow to the nucleus (N). A = Anterior P = Posterior.

To study the localisation of ectopic *Tb*HAP2:YFP:TY, PCFs were observed after 24 and 48 hours of induction. Only 10% of the cells showed a YFP fluorescence signal 24 hours after induction (total n=681), and this proportion decreased to 4% after 48 hours (Fig. 3.12A). Additionally, there were no detectable changes in the nuclear or cellular phenotypes after induction, even in the small number of cells that expressed YFP (Fig. 3.12B, quantification not shown). This observation correlates with the lack of apparent variation in cell growth after induction and may suggest that even when the YFP fusion is expressed, it lacks biological activity.

Two YFP patterns were identified in these cells (Fig. 3.12B): (1) reticulated cytoplasmic signal and (2) nodes with different signal intensity distributed throughout different parts of the cell body. High intensity of YFP signal in the posterior region of the cells and a perinuclear reticular cytoplasmic signal were also noted. Attempts to characterise the sub-cellular location of *Tb*HAP2 using immunofluorescence with anti-TY (BB2 monoclonal mouse antibody) (Bastin, Bagherzadeh et al. 1996), data not shown) were unsuccessful.

A

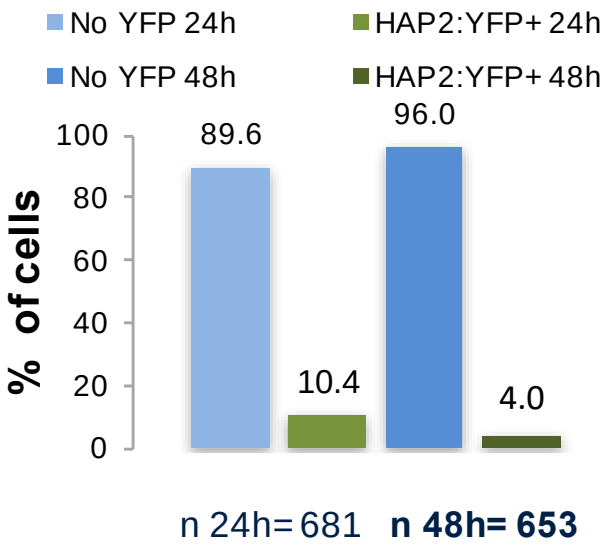
No YFP 24h
HAP2:YFP+ 24h
No YFP 48h
HAP2:YFP+ 48h
% of cells
100
80
60
40
20
0
89.6
10.4
96.0
4.0
n 24h= 681
n 48h= 653

B

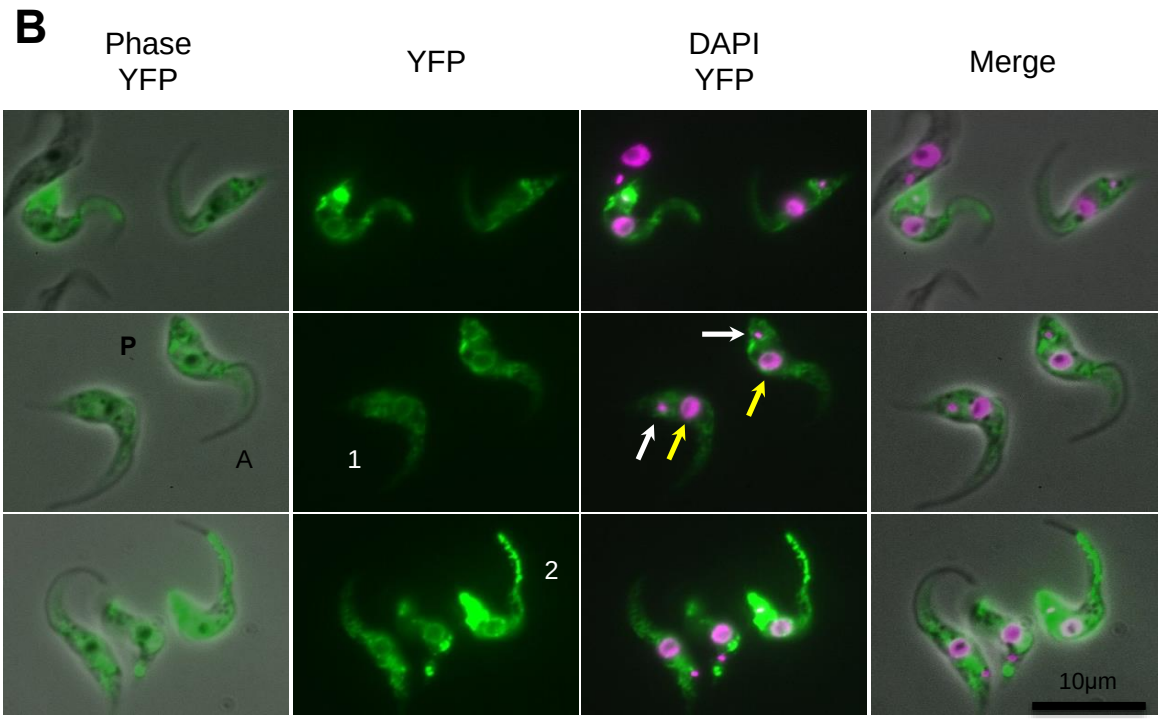
Phase
YFP
YFP
DAPI
YFP
Merge
P
A
1
2
10µm

Figure 3.12 ***Tb*HAP2:YFP:TY ectopic expression has no effect on nuclear and cellular morphology. A.** Quantification of cells showing YFP signal (green bars versus blue bars for YFP-negative) 24 and 48 hours after induction, **B.** The YFP patterns observed were: reticulated (1) or revealed concentrated puncta with different signal intensity (2). A high intensity of YFP signal was typically observed at the posterior region of the cells, and in a perinuclear reticular cytoplasmic signal. White arrows point to the kinetoplast (K) and yellow to the nucleus (N). A= Anterior P= Posterior. DNA was visualised with DAPI=magenta. Scale bars as shown in bottom right panel.

3.3. Discussion

In this chapter, I have undertaken a detailed bioinformatics analysis of the HAP2(GCS1) gene across a wide range of species, leading to the identification of three different areas with significant sequence homology. Interestingly, my results showed that the HAP2(GCS1) domain can be extended. Furthermore, I have assessed the subcellular localisation of HAP2(GCS1), first using a YFP-tagged protein expressed from the endogenous HAP2(GCS1) locus in *T. brucei*, then by employing two tagged overexpression constructs. Neither approach produced data that could be easily interpreted, but these experiments suggested that HAP2(GCS1) might be able to induce multinucleate cells when active, but that the YFP-tagged form of the protein lacked activity.

3.3.1. The RBP6 *in vitro* system did not induce a high proportion of epimastigotes and infective metacyclics *in vitro*

The weak phenotypes in my experiments compared to Kolev et al. (2012) may be the result of inadequate levels of expression of *Tb*RBP6 in the induced cells. In an effort to tackle this issue, I focused on developing new cell lines for inducible expression transforming with pDex777:RBP6 (Poon, Peacock et al. 2012) and pLew100v5:RBP6 (Kolev, Ramey-Butler et al. 2012), these two plasmids have been reported to induce high-levels expression of RBP6. Despite the various attempts I made to recreate the conditions reported for this RBP6 differentiation system, the results obtained were not satisfactory.

3.3.2. Analysis of *Tb*HAP2:YFP fusion protein localisation and function suggests it is not properly localised

My analysis of overexpressed *Tb*HAP2:TY and *Tb*HAP2:YFP:TY fusions in procyclic cell lines has led to several major conclusions. First, the YFP fusion protein was primarily expressed intracellularly, mirroring observations made with the *Tb*HAP2:YFP gene trap. Second, western analysis suggested that this protein was expressed at lower levels than *Tb*HAP2:TY and unlike the latter, expression progressively reduced over several days of induction. The low levels appear to be linked to the small proportion of cells that express the *Tb*HAP2:YFP:TY protein, and might suggest that this protein is toxic, although those cells that continued to express it did not generally exhibit abnormal morphology.

Previous studies of the subcellular localisation pattern of HAP2(GCS1) in other organisms have suggested a subcellular localisation pattern, where most of the protein is usually localised to the cell surface (Mori, Kuroiwa et al. 2006, von Besser, Frank et al. 2006, Hirai, Arai et al. 2008, Liu, Tewari et al. 2008, Mori, Hirai et al. 2010). In relation to the subcellular localisation of HAP2(GCS1), it is known that in *Lilium* and *Arabidopsis*, antibodies against a recombinant peptide from the N-terminal region of the protein detected signal surrounding the nuclei of pollen generative cells and also recognised HAP2(GCS1) in a fraction containing membrane components where this protein progressively accumulates during pollen development (Mori, Kuroiwa et al. 2006). *At*HAP2:GFP was detected as a perinuclear ring in pollen cells and at the plasma membrane (von Besser, Frank et al. 2006, Mori, Hirai et al. 2010). In the unicellular green alga *C. reinhardtii,* HAP2(GCS1) localises on the apical side of the plasma membrane, between the two flagella and at the tip of a mating-specific structure of minus gametes(Liu, Tewari et al. 2008). Whereas in *Plasmodium,* male gametocytes and gametes expressed HAP2:GFP intracellularly and in their plasma membrane(Hirai, Arai et al. 2008, Liu, Tewari et al. 2008).

In the experiments with *Tb*HAP2:YFP, I did not observe the subcellular localisation pattern described in previous studies (Mori, Kuroiwa et al. 2006, von Besser, Frank et al. 2006, Hirai, Arai et al. 2008, Liu, Tewari et al. 2008, Mori, Hirai et al. 2010). It is possible that the network-like pattern observed in *Tb*HAP2:YFP:TY-positive cells indicates the accumulation of proteins in the endoplasmic reticulum at an early stage of the secretory pathway (McConville, Mullin et al. 2002). Thus, the fluorescent tag

may be affecting the protein structure (e.g. proper folding), resulting in its degradation before reaching the intended destination. C-terminal tagging may also interfere with the final localisation of the transgenic protein (Bohme and Cross 2002), which would cause a similar result. Ultimately the likely mislocalisation observed not only means that the YFP fusion proteins cannot be used to investigate subcellular localisation of *Tb*HAP2, but it also probably explains why these proteins do not appear to be functional.

4. Results Chapter: Characterisation of the Dense-Core Granule Secretory Pathway in *Drosophila* Secondary Cells

As discussed in Chapter 1, the male accessory glands of the fruit fly *D. melanogaster* (Fig.1.3A-C) are key contributors to seminal fluid, producing much of the fluid volume and a number of seminal fluid proteins (SFPs) that are essential for fertility. Historically, much of the initial work on these glands focused on the abundant main cells and their role in producing SFPs like Sex Peptide (SP) and Ovulin (Acp26Aa), key activators of the female post-mating responses (Heifetz, Vandenberg et al. 2005, McGraw, Clark et al. 2008, Avila, Sirot et al. 2011).

However, more recently it has been shown that if SCs are ablated or reprogrammed in development, many female post-mating responses are also strongly suppressed (Sitnik, Gligorov et al. 2016). Furthermore, genetic manipulation of SCs after eclosion has revealed an essential role for BMP signalling (Leiblich, Marsden et al. 2012) and potentially for exosomes (Corrigan, Redhai et al. 2014) in suppressing female receptivity to males after mating. A subsequent analysis highlighted the roles of the BMP Decapentaplegic (Dpp) in autocrine control of Dense-core Granule (DCG) biogenesis and secretion (Redhai, Hellberg et al. 2016). More detailed analysis of secretory processes in these cells is ultimately likely to extend our

understanding of the mechanisms that modulate female post-mating responses, including those involved in the competing interests of males and females that drive sexual conflict.

4.1. The Secondary Cell as a Model to Study Dense-Core Granule Biogenesis

One remarkable feature of the DCG compartments in SCs is their large size. While these compartments in most secretory tissues are only a few hundred nanometres in diameter, those in SCs are typically about 5 µm in diameter, up to 10^4 times larger in volume than their mammalian counterparts (Wilson, Leiblich et al. 2017).

A number of different very large subcellular compartments can be identified in SCs by assessing acidity and other biochemical properties such as differential Rab GTPase localisation. For example, Rab7 localises to the surface of large acidic late endosomes and lysosomes, while Rab11 localises to the limiting membrane of non-acidic secretory compartments that contain DCGs (Corrigan, Redhai et al. 2014, Redhai, Hellberg et al. 2016). Furthermore, cores have been found to store Angiotensin I-converting Enzyme (AnCE), a protease secreted from then lumen of the male AG during mating (Rylett, Walker et al. 2007).

The size of DCG compartments and their small number in each cell, which allow them to be easily analysed and counted, led me to initiate a collaboration with another DPhil student in the Wilson laboratory, B. Kroeger, aimed at characterising

the morphogenesis and subsequent trafficking of DCG and membrane-associated proteins through the SC secretory pathway. We postulated that if this trafficking route was better understood, particularly the changes in membrane markers as maturation takes place, we would be able to test the effects of known DCG regulators much more precisely and we could also screen for new regulators.

Previous studies in the laboratory (Corrigan, Redhai et al. 2014) had indicated that it was difficult to preserve SC compartment structure following fixation and that live imaging was therefore preferable for such experiments. However, some GFP-tagged markers affect the compartments of SCs, such as the human exosome marker CD63-GFP, which increases the number of DCG compartments (Redhai, Hellberg et al. 2016). Hence a key goal of my initial studies was to identify live markers that label DCG compartments, but have minimal effects on SC secretory biology and would therefore allow me to define the trafficking events that drive DCG secretion.

4.1.1. Aims

I set out to characterise DCG compartments in SCs with the following specific aims:

1. To provide evidence on the morphogenesis of DCGs during their maturation;
2. To identify novel live fluorescent markers that label the DCG compartments without affecting the biology of these cells;

3. To characterise the trafficking of a selected DCG marker (ultimately GFP-GPI) using pulse-chase experiments, and establish the identity of intermediate compartments involved in this trafficking;
4. To compare this trafficking route with the route used by other membrane associated proteins in SCs.

From this collaborative work, I established the GFP-GPI marker as an important tool for screening for genetic defects in DCG trafficking, providing the basis for a candidate screen for genetic regulators of this process in Chapter 5.

My first hypothesis is that the non-acidic, non-cored compartments are immature stages in the compartment morphogenesis, and that the small vesicles surrounding them during the maturation process are involved in trafficking key molecules to the cores. The previous assumption that the non-acidic, non-cored compartments are sorting hubs for macromolecules destined for different SC compartments is therefore not correct.

Secondly, I propose that GFP-GPI trafficking is different to the one observed with CD63-GFP, and that this is due to the different structure of the two fusion proteins. Since GFP-GPI is an anchor protein, we anticipate that the fusion protein will be localising in some other subcellular structures such as the trans-Golgi network and ultimately different membrane localisation patterns related to the polarity of the cell will be observed.

4.2. Results

4.2.1. Analysing the overall cell biology of SCs using wide-field fluorescence and DIC imaging

To develop a more powerful imaging system to analyse SC DCG compartments, we explored the use of wide-field fluorescence microscopy using a Delta Vision Elite imaging system. As shown subsequently in this chapter, this system not only permits the identification of cell outlines, but also allows the limiting membranes of compartments and the boundaries of DCGs themselves to be visualised in living tissue in the absence of fluorescent markers.

Given that the AG epithelium is transparent in phase contrast, differential interference contrast (DIC) microscopy proved to be a suitable visualisation technique for live imaging of SCs (Fig. 4.1). By using this method, we were able to explore the AG tissue at different magnifications to the point of clearly identifying several categories of membrane-bound compartments as well as nuclei without further labelling (Fig. 4.1C-D; see Section 4.2.2).

Fig. 4.1C shows that in a distal region of the AG, a subset of cells is labelled when *spitz*-GAL4>UAS:GFP-GPI is expressed. A further characterisation at a higher magnification (Fig. 4.1.D) confirmed previous observations (Wilson, Leiblich et al. 2017) that the AG tissue at the distal tips has two cell types (main and secondary cells; MCs and SCs) arranged as a simple epithelium. Three optical sections

corresponding to different regions in the AG epithelium are presented in Fig. 4.1D. The first plane, Z1, is located apically in the epithelium and therefore includes the free surface exposed to the lumen of the gland.

By contrasting different Z-planes of the AG epithelium found around Z1, we detected large numbers of cigar-shaped structures called microcarriers in the AG lumen adjacent to the apical surface of SCs (Fig. 4.1D, white arrowheads in Z1). They had previously been identified by Dr Mark Wainwright in our laboratory as main cell-derived lipid-containing structures that deliver specific Sfps to females. In successive planes, extending from Z2 to the most basal region Z3, most of the DCG compartments marked by the GFP-GPI protein are present. Other membrane-bound organelles such as acidic compartments and the two nuclei in SCs are detected basally (Fig. 4.1D, Z2-Z3).

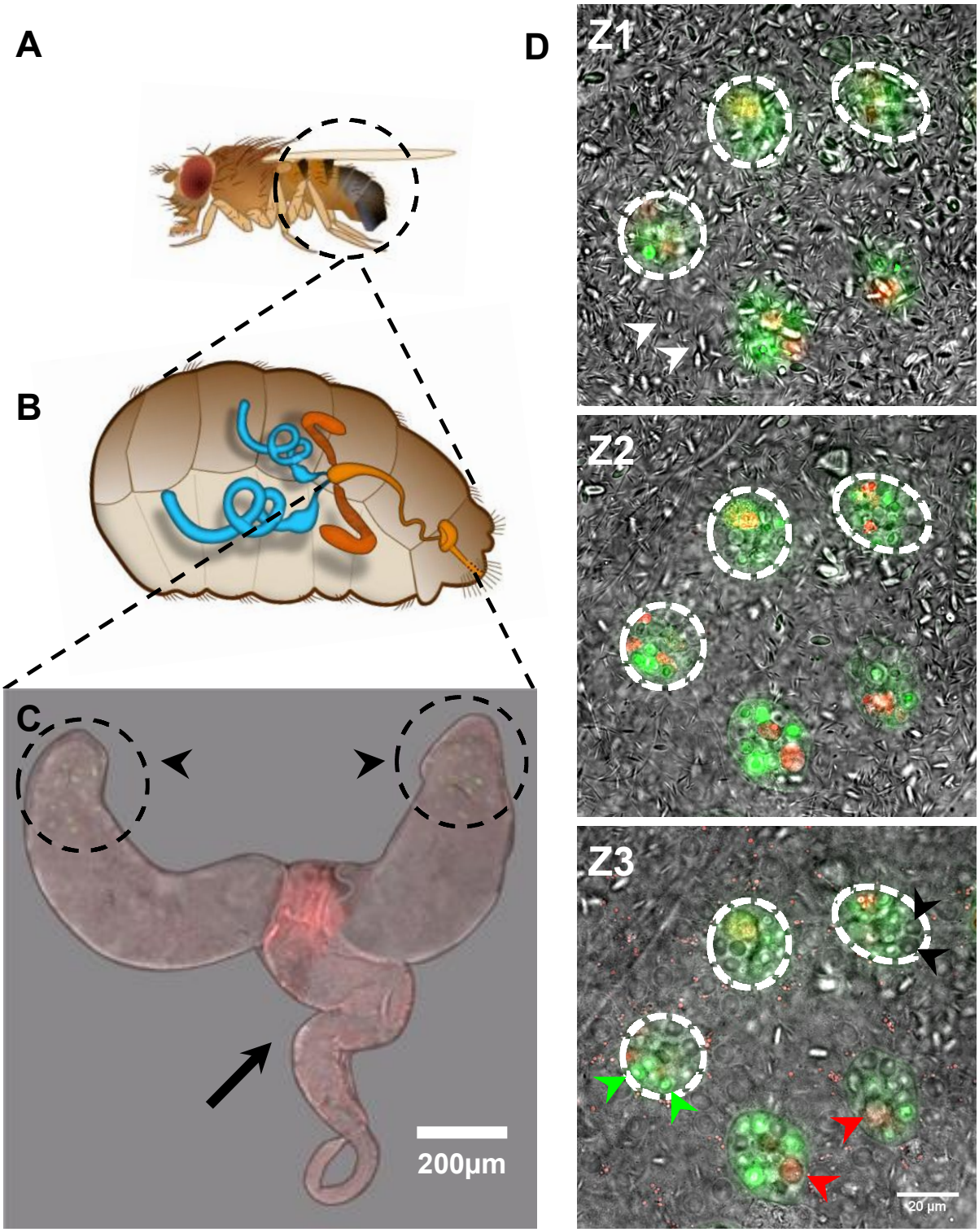
A
B
C
200µm
D
Z1
Z2
Z3
20 µm

Figure 4.1 **The accessory glands and reproductive system of a male *D. melanogaster.*** **A.** Schematic representation of a male fly, highlighting the abdominal segments of the body. **B.** Overall structure of the adult male abdomen containing the male reproductive organs and tract, including the testes (blue), the accessory glands (dark orange), the ejaculatory duct (light orange tube linked to testes and accessory glands) and ejaculatory bulb (posterior, light orange rounded structure). **C.** Wide-field fluorescence and DIC combined low magnification image of the paired accessory glands (black arrowhead points to the distal tip of each AG) and the ejaculatory duct (black arrow) from a 6-day-old adult male expressing GFP-GPI in SCs. **D.** Three different Z-plane views of SCs (outlined by white dashed circles) in the monolayered epithelium of the distal tip of the male AG (Z1 = apical, Z3 = basal). Note the large number of cigar-shaped structures in the lumen of the AG (white arrowheads in Z1; so-called microcarriers that form a large proportion of main cell secretions). More basally, the two nuclei of individual GFP-GPI-expressing SCs become visible (black arrowheads in Z3). Many of the DCG compartments in SCs are also in the basal and central parts of these cells (green arrowheads in Z3), as are the large acidic compartments (red arrows in Z3). Genotype of virgin males, which were incubated at 29^{o}C following eclosion for 6 days, is *w; spi-GAL4 tub-GAL80^{ts}; UAS-GFP-GPI.* Acidic compartments stained with LysoTracker (red). Scale bar shown in panels.

By co-expressing a ubiquitously expressed tRFP-marked form of *Drosophila* E-cadherin (DE-Cad or Shotgun [Shg]), it was possible to image some of the junctional contacts between SCs and MCs at the surface of these cells (Fig. 4.2). The junctional complexes between these cells were observed apically (Fig. 4.2C, Z1), highlighting a relatively small protrusion of the SC apical surface (less than 10 µm in diameter) into the AG lumen. Plasma membrane-localised GFP-GPI is primarily on the basolateral membrane below these junctions (Fig. 4.2C, Z2, green arrows).

One other notable feature of the DE-Cad-tRFP localisation in SCs is the presence of specific microdomain staining in the limiting membrane of each DCG compartment (Fig. 4.2C, Z2, white arrows). Although other membrane markers, like GFP-GPI, do not label these membranes entirely uniformly, this is the first example we have observed of such restricted localisation, suggesting a specialised role for DE-Cad in membrane organisation in this compartment.

Figure 4.2 **Apical/Basal Polarity of Accessory Gland Epithelial Cells. A.** Image of the distal AG epithelium from males expressing DE-Cad-tRFP ubiquitously and GFP-GPI in the SCs. Note that DE-cadherin demarcates the boundaries between MCs, but does not mark the boundaries with SCs so clearly in this plane. **B**. Schematic representation of an SC and its surrounding cells (MC: main cell and muscle layer) in transverse view showing two planes of section (Z1-Z2). **C.** High magnification wide-field views of SC in two Z-planes (Z1, apical view; Z2, basal view). Note that the apical protrusion of SCs into the AG lumen is restricted to a small central region, where GFP-GPI is not concentrated (white arrows in Z1; faintly fluorescent, out-of-focus GFP-labelled DCGs are visible, which lies underneath a thin MC layer). More basally (Z2), GFP-GPI is found in DCG compartments (green arrowheads) and the basolateral plasma membrane (green arrows). Note the highly restricted expression of DE-Cad-tRFP in subdomains on the limiting membranes of DCG compartments (white arrows). Genotype of virgin males, which were incubated at 29^{o}C following eclosion for 6 days is: *w; spi-GAL4 tub-GAL80^{ts}/Ubi-DE-Cad-tRFP; UAS-GFP-GPI*. Scale bars as shown in panels.

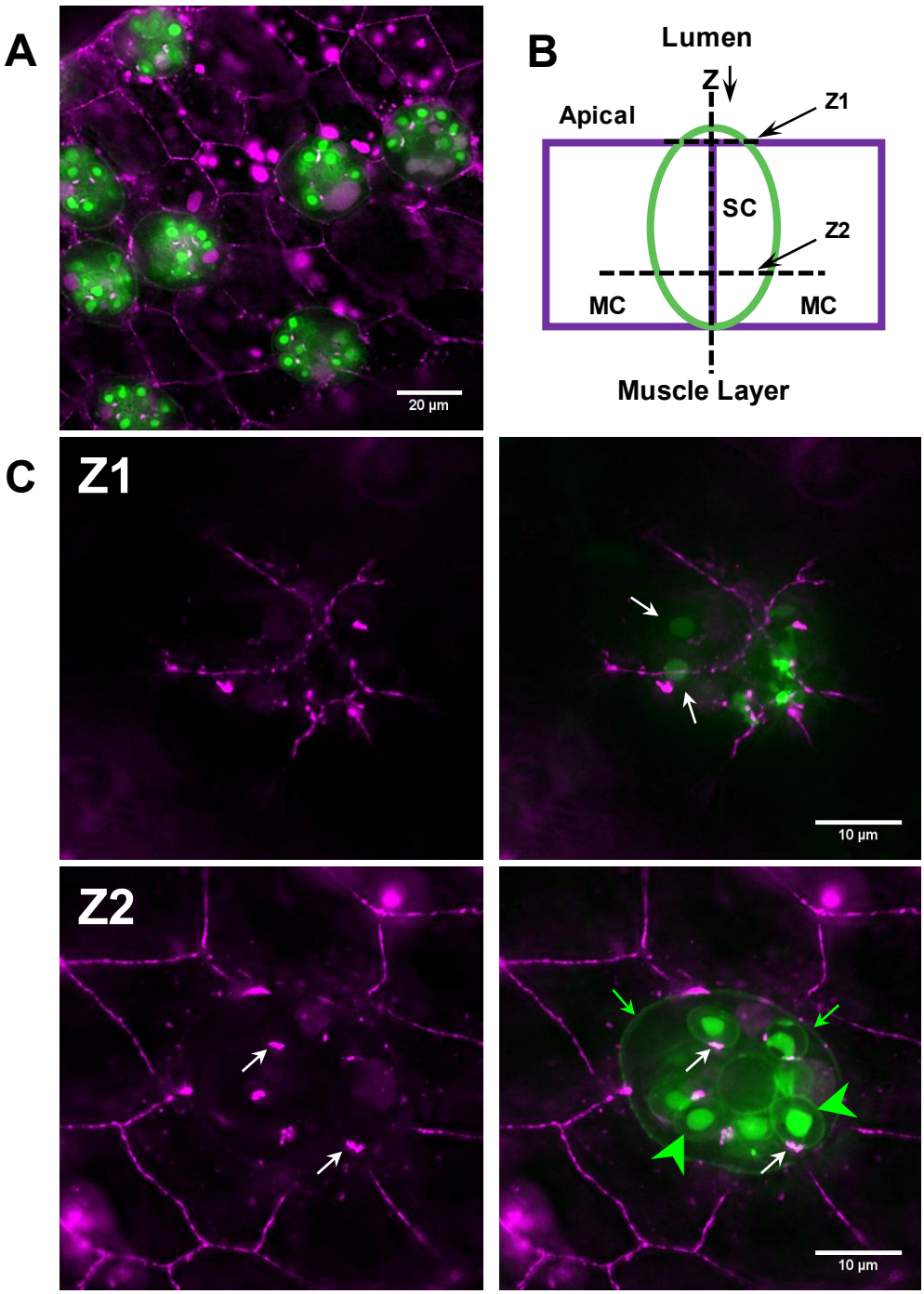
A
20 µm
B
Lumen
Z
Z1
Apical
SC
Z2
MC
MC
Muscle Layer
C
Z1
10 µm
Z2
10 µm
DE-Cad-tRFP
DE-Cad-tRFP GFP-GPI

4.2.2. Morphological characterisation of compartments in wild type SCs

In order to assess the effects of expressing different fluorescently tagged protein markers in SCs, it was essential to characterise the compartment organisation of wild type cells. This information was ultimately used as the experimental control for the phenotypic analysis of the *CFP-Rab6* and *AnCE-eGFP* gene traps and GFP-GPI-expressing SCs used in my studies. A minimal effect on the anatomy and physiology of the cells under study is an optimal property for a useful cell marker.

DIC microscopy was the method of choice for the initial assessment of the morphology of wild type SCs, since it allows the study of SC subcellular structures in the absence of fluorescent markers and fixation (Fig. 4.3A-C).

Fig. 4.3A shows high magnification DIC images of three characteristic wild type SCs from virgin males kept for six days post-pupal stage at 17ºC. These panels display the standard spatial distribution of different organelles within an area extending from the medial plane to the basal region of the SCs. At this magnification, the greatest number of DCGs is visible in addition to the nuclei, some non-cored vacuoles and various intracellular microvesicles. The SC plasma membrane can be clearly delimited as well.

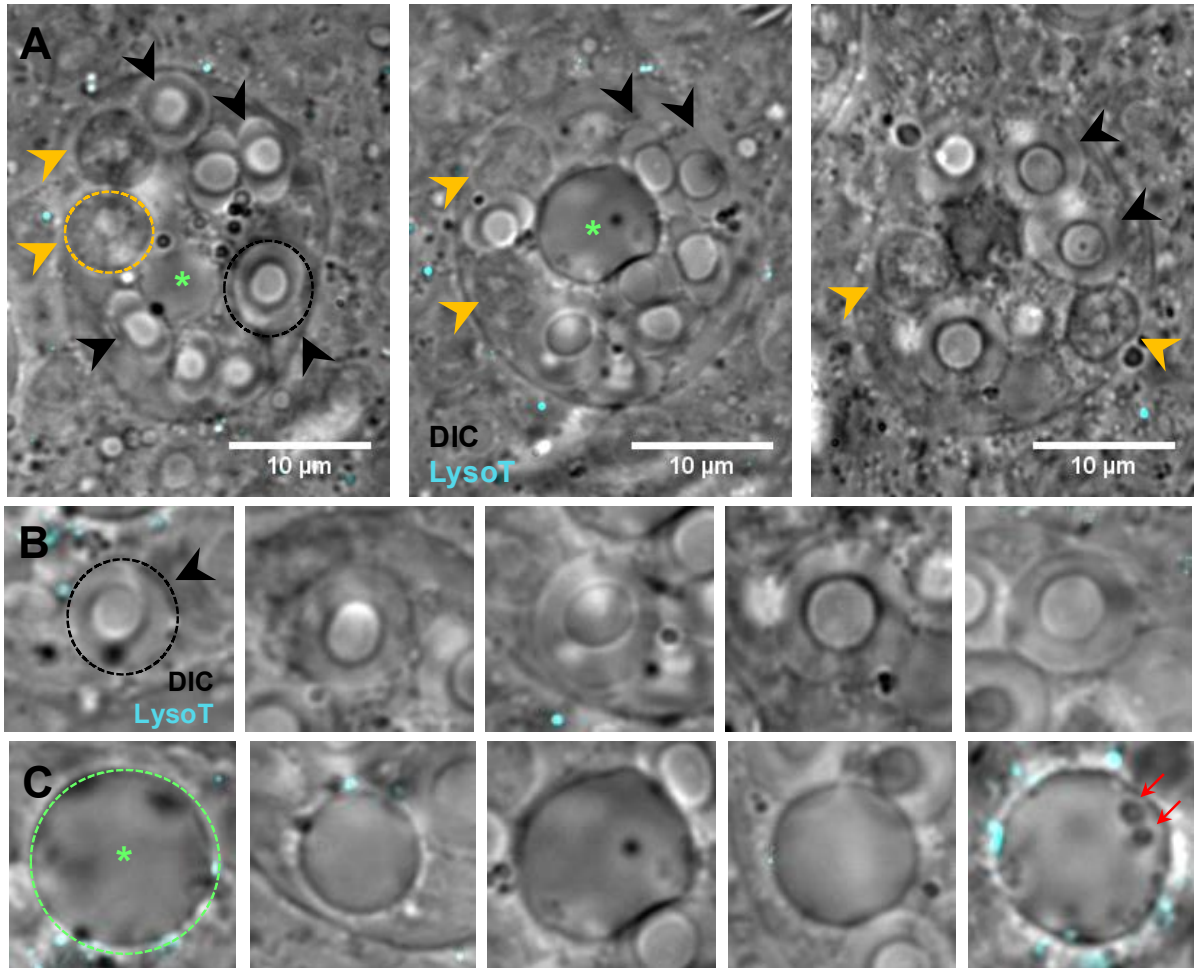

Figure 4.3 **Live imaging of wild type *D. melanogaster* SCs using DIC**. **A.** High magnification wide-field images illustrating the typical subcellular organisation of representative cells. SCs have two nuclei (indicated by orange arrowheads and dashed ellipse), DCG compartments (black arrowheads and dashed ellipse in B) and non-acidic, non-cored compartments (green asterices and dashed ellipse in C). Note the striking level of detail revealing the intracellular morphology of SCs and their compartments. Nuclei and DCG compartments are of similar size. **B.** Characteristic DCG compartments (around 5-8 µm diameter) are the most abundant large organelles (mean = 9.5 ± 1.2 per SC). **C.** Less abundant non-acidic, non-cored compartments (mean = 1.8 ± 0.8 per SC) exhibit some intraluminal vesicular structures (red arrows) and have variable size. All images are of w^{1118} (wild-type) virgin males incubated at 17ºC following eclosion for 6 days before dissection. AGs were stained with LysoTracker Red (cyan). Scale bars are shown in panels.

4.2.2.1. There are at least two types of non-acidic large compartments in SCs

The DCG compartments in SCs show two clear features (Fig. 4.3B): a central dense core and a concentric 'clear' region between the core and the limiting membrane. The nuclei in SCs are not easily distinguishable from DCGs in a single focal plane, since they can both have a very similar size and morphology, but focusing through several Z-planes allows the spherical cores of DCGs to be differentiated from the more homogeneous nucleus (Fig. 4.3A).

The overall size of the DCGs is relatively constant (around 5-8 µm diameter) with a minimum of 7 and maximum of 12 in each cell (Fig. 4.3B; mean = 9.5 ± 1.2; n=49 SCs, taken from 8 different AGs); they are the most abundant group of large membrane-bound compartments.

However, I identified a second group of non-acidic compartments, which do not have dense cores (Fig. 4.3C). The size (and shape) of these compartments varies widely and their abundance is lower than that of DCGs (mean 1.8 ± 0.8; n=49 SCs, from 8 different AGs) with one compartment often positioned in the centre of the cell.

We also noticed variations in the number of the AG compartments from flies kept at different temperatures in the laboratory. Considering that the activation of one major SC gene expression system is temperature-dependent, we decided to analyse samples from virgin males that were kept for six days post-pupal stage both at 17ºC and 29ºC.

4.2.2.2. DCG compartments are formed from non-acidic, non-cored organelles in SCs

As part of this project, we also carried out an exhaustive study of the intracellular dynamics occurring inside SCs, combining DIC and time-lapse microscopy over long periods of time. Consequently, we were able to observe cellular mechanisms such as the morphogenesis of dense cores in live SCs (Fig. 4.4).

Fig. 4.4A shows two single optical sections at high magnification from a 6-hour movie of a 6-day-old SC (from a virgin w^{1118} male kept at 17ºC) taken at the time points t_{10} and t_{88}. The main difference displayed in these images is the transformation of a compartment lacking a DCG into a new DCG compartment at the later time (Fig. 4.4A, red arrowhead).

A detailed analysis of this cellular transformation consistently identified three stages based on visible morphological changes. The first one occurs between t_{10} - t_{30}, is designated here as pre-DCG stage and is characterised by a reduction in the size of the non-cored compartment (Fig. 4.4B, green asterices). No intra-compartment content was observed at this stage.

The second stage takes approximately nine minutes, includes the images from t_{46} to t_{49} (Fig. 4.4B) and reveals intense activity of the internal contents (clustering and movement of small rounded inclusions marked with white arrowheads in Fig. 4.4B). This internal movement inside the compartment is apparent in high magnification

images t_{46} and t_{47}, where several small black nodes in the limiting membrane stay in the same place (red arrows in Fig. 4.4B), while the internal contents move.

During the final stage, from t_{49} onward, the gradual increase in the size of the dense core becomes more noticeable. This appears to be associated with cluster rotation and leads to an increase in volume of the cluster of rounded structures that in t_{57} exhibit a clover-shape arrangement. These results may support the idea that the concentration of material in the dense cores might occur through the application of a centripetal force or by the exclusion of molecules and structures that are not affected by this force.

Figure 4.4 **Non-acidic, non-cored compartments mature into DCG compartments.** Time-lapse live cell imaging, combining wide-field and DIC microscopy of a SC reveal the biogenesis of DCG compartments. Single optical sections from a movie illustrating the formation of a DCG compartment (red arrowhead) at a high level of detail. **A.** First image (t_{10}) shows the non-acidic, non-cored compartment (green asterisk) from which a DCG compartment develops at a later time (t_{88}, red arrowhead indicates this newly matured compartment). More mature DCG compartments are present in the same focal plane (black arrowheads). **B.** Serial images extracted from a six-hour movie allow the identification of three key stages during the formation of a DCG compartment: pre-DCG period between t_{10} - t_{30} where no content is observed inside the non-acidic, non-cored compartment (green asterices), t_{46}-$t_{49, a}$ nine-minute interval leading to the formation of an internal core, that rotates and accumulates internal content (white arrowheads), while material at the limiting membrane remains apparently static (red arrows), and finally t_{49}-t_{88}, characterised by a gradual increase in size of the dense core. Time-points designated in hours. A virgin male w^{1118} fly was incubated at 17^{o}C following eclosion for 6 days before dissection. AGs were stained with LysoTracker Red (cyan). Scale bars shown in panels represent 10µm.

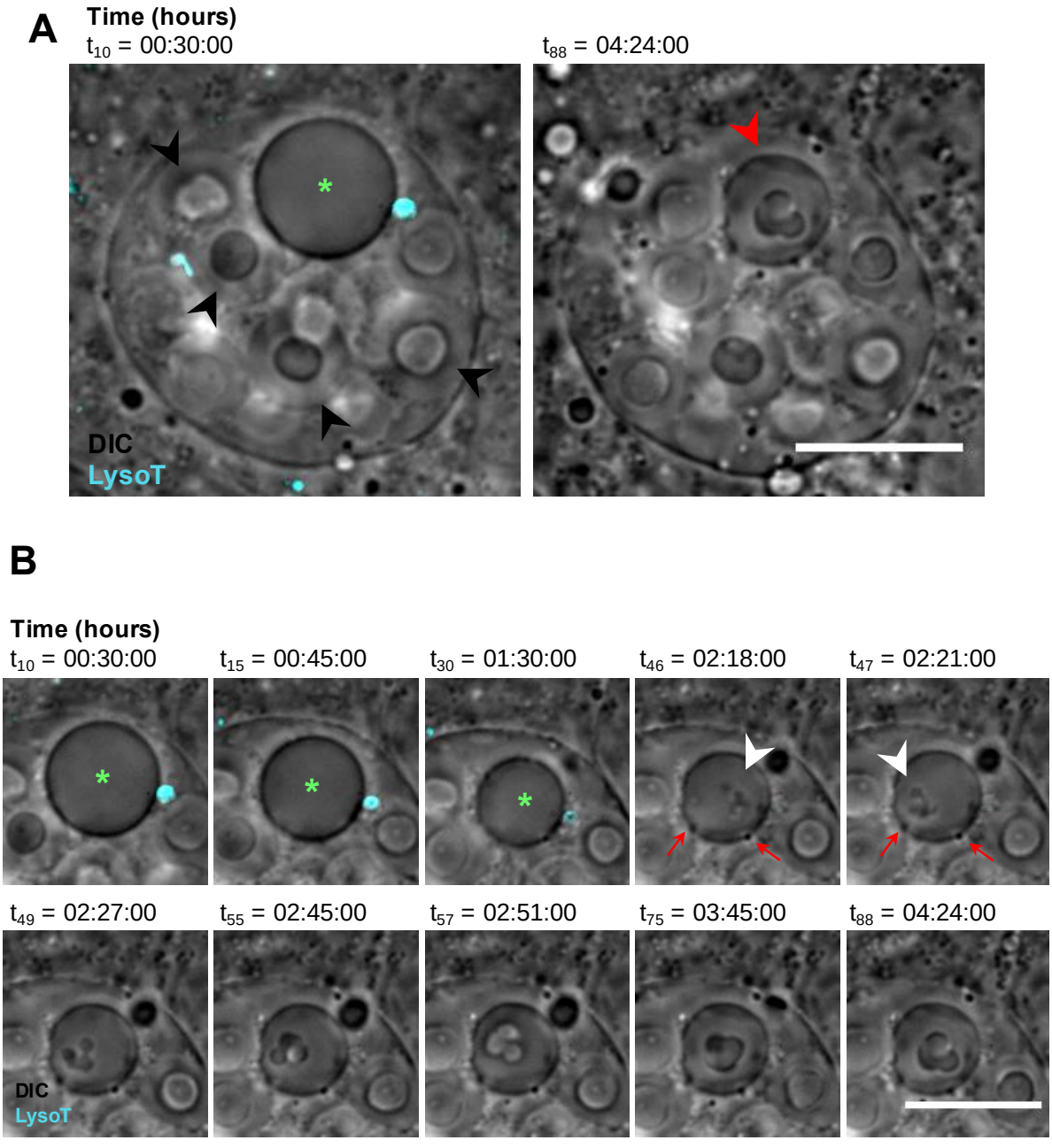
A
Time (hours)
t10 = 00:30:00
t88 = 04:24:00
DIC
LysoT
B
Time (hours)
t10 = 00:30:00
t15 = 00:45:00
t30 = 01:30:00
t46 = 02:18:00
t47 = 02:21:00
t49 = 02:27:00
t55 = 02:45:00
t57 = 02:51:00
t75 = 03:45:00
t88 = 04:24:00
DIC
LysoT

DIC and live-cell imaging together constitute a powerful tool to reveal the cellular events leading to the morphogenesis of DCG compartments in SCs. Previous work in the laboratory had led to the conclusion that a central non-cored compartment was acting as a sorting hub for DCGs (Redhai, Hellberg et al. 2016), however our current results show that these compartments constitute a precursor step in the maturation process of DCG organelles in SCs.

4.2.2.3. DIC allows the visualisation of membrane fusion between non-acidic, non-cored compartments in SCs

Fig. 4.5A displays two single optical sections at high magnification from a 6-hour movie of a 6-day-old SC (from a virgin male kept at 17°C) taken at t_{27}=01:21:00h and t_{88}=04:24:00h. The main differences observed between these two-time points is the formation of a new DCG compartment (red arrowhead) and the fusion between two of the non-acidic, non-cored compartments.

To characterise further this multistep transformation, I examined time-lapse images between the time intervals t_{27} and t_{88}. Fig. 4.5B reveals 12 images of the major subcellular events observed in this SC. At the beginning of the sequence (pre-fusion events t_{27}-t_{39}), the two non-core compartments align and are brought into closer proximity. Large intraluminal vesicular structures appear in the areas where the fusion of the two limiting membranes will take place (Fig. 4.5B, red arrows).

In t_{44}, the parts of the limiting membrane that are closest together form a fusion zone. In this area, the limiting membranes appear less refractive, and the two compartments initially come together to form a single figure eight-shaped compartment. From t_{53} onward, a single newly formed organelle with a relatively homogeneous content (except for occasional vesicles) is observed. There is a further reduction in size of the non-cored compartment that resembles the pre-DCG stage described in the previous section.

These data show that compartment fusion can be studied in SCs at an unparalleled level of detail by combining DIC and time-lapse microscopy. Although in this study the frequency with which this event occurs was not established, more than one example was observed. Detailed analysis of more SCs will allow further insights into the frequency of fusion between compartments and the molecular specificity required for this event to take place.

Figure 4.5 **Pre-DCG compartments fuse *in vivo* to form larger compartments.** Time-lapse, wide-field and DIC microscopy of a living SC allow the visualisation of membrane fusion between two non-acidic, non-cored compartments. Single optical sections from a movie illustrate the multistep formation of a single pre-DCG compartment as a result of the merger of two independent compartments. **A**. At t_{27}, three non-acidic, non-cored compartments are present (green asterices). Two that will ultimately merge share some morphological similarity (darker internal contents and some internal vesicles). At the second time point (t_{88}), the final product of the fusion is observed and the third non-cored compartment has matured into a DCG compartment (green asterisk and red arrowhead respectively). Nuclei (orange arrowheads) and a mature DCG (black arrowhead) are also indicated. **B.** Serial images extracted from the same six-hour movie allow the identification of a pre-fusion stage (t_{27} - t_{39}) where two large intraluminal vesicles (indicated by red arrows) are visualised in the fusion zone of the limiting membranes of the two non-acidic, non-cored compartments. Subsequently, a link between the two independent compartments is established (t_{44}), membranes undergo physical merging (t_{45} – t_{49}), the membrane invaginations at the fusion site are lost (t_{53}) and a newly formed non-acidic, non-cored compartment is formed. Note a gradual reduction in the size of the resulting compartment after t_{53}. Representative time-points designated in hours. A fly virgin w^{1118} male was incubated at 17^{o}C following eclosion for 6 days before dissection. AGs were stained with LysoTracker Red (cyan). Scale bars shown in panels represent 10μm.

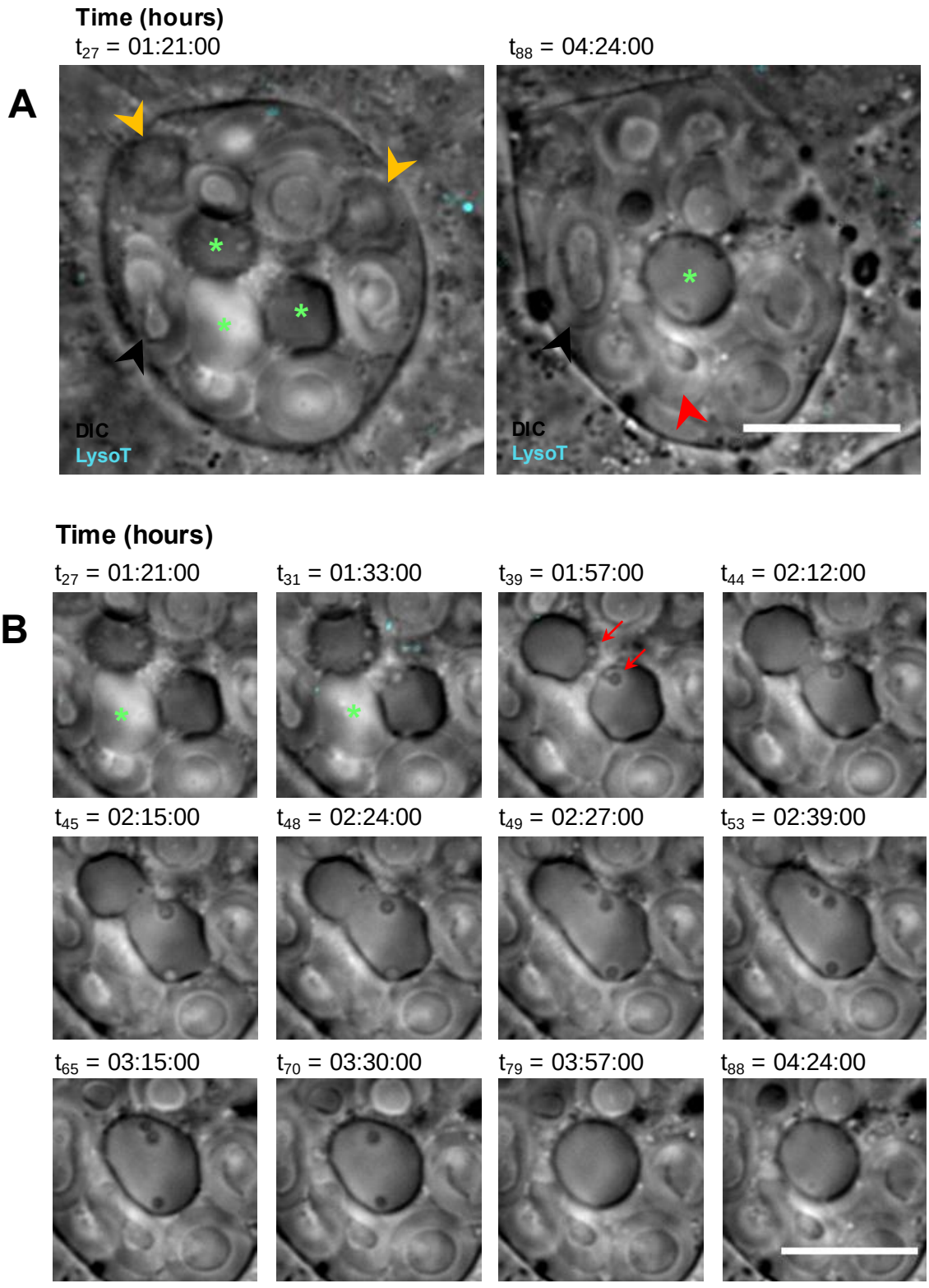
A
Time (hours)
t27 = 01:21:00
t88 = 04:24:00
DIC
LysoT
DIC
LysoT
B
Time (hours)
t27 = 01:21:00
t31 = 01:33:00
t39 = 01:57:00
t44 = 02:12:00
t45 = 02:15:00
t48 = 02:24:00
t49 = 02:27:00
t53 = 02:39:00
t65 = 03:15:00
t70 = 03:30:00
t79 = 03:57:00
t88 = 04:24:00

4.2.2.4. A far-red DNA stain clearly reveals nuclei in living SCs

Through the analysis of DIC images from SCs of different genetic backgrounds, I found that in several cases it was difficult, if not impossible, to differentiate between DCG compartments and nuclei from single Z-planes. Both cellular organelles show a similar size (5-8 µm diameter), are surrounded by a limiting membrane and their internal contents have increased density centrally (in Fig. 4.3A-B).

Until recently, no fluorescent nuclear probes were accessible for live-cell multicolour imaging (Nakamura, Takigawa et al. 2014). Major limitations of conventional DNA fluorescent probes include high cytotoxicity, significant cellular auto-fluorescence and restricted cell selectivity (Nakamura, Takigawa et al. 2014, Lukinavicius, Blaukopf et al. 2015). An alternative for DNA staining is Hoechst 33342 attached to a carboxylated silicon-rhodamine (SiR); it overcomes the limitations mentioned above and has recently become available (Lukinavicius, Blaukopf et al. 2015).

To test the applicability this DNA-binding probe in SCs, I first attempted to establish a suitable protocol with varying time, temperature and concentrations. For this purpose, I considered the experimental conditions that are used for the incubation of other cell probes in the laboratory, such as LysoTracker (Corrigan, Redhai et al. 2014).

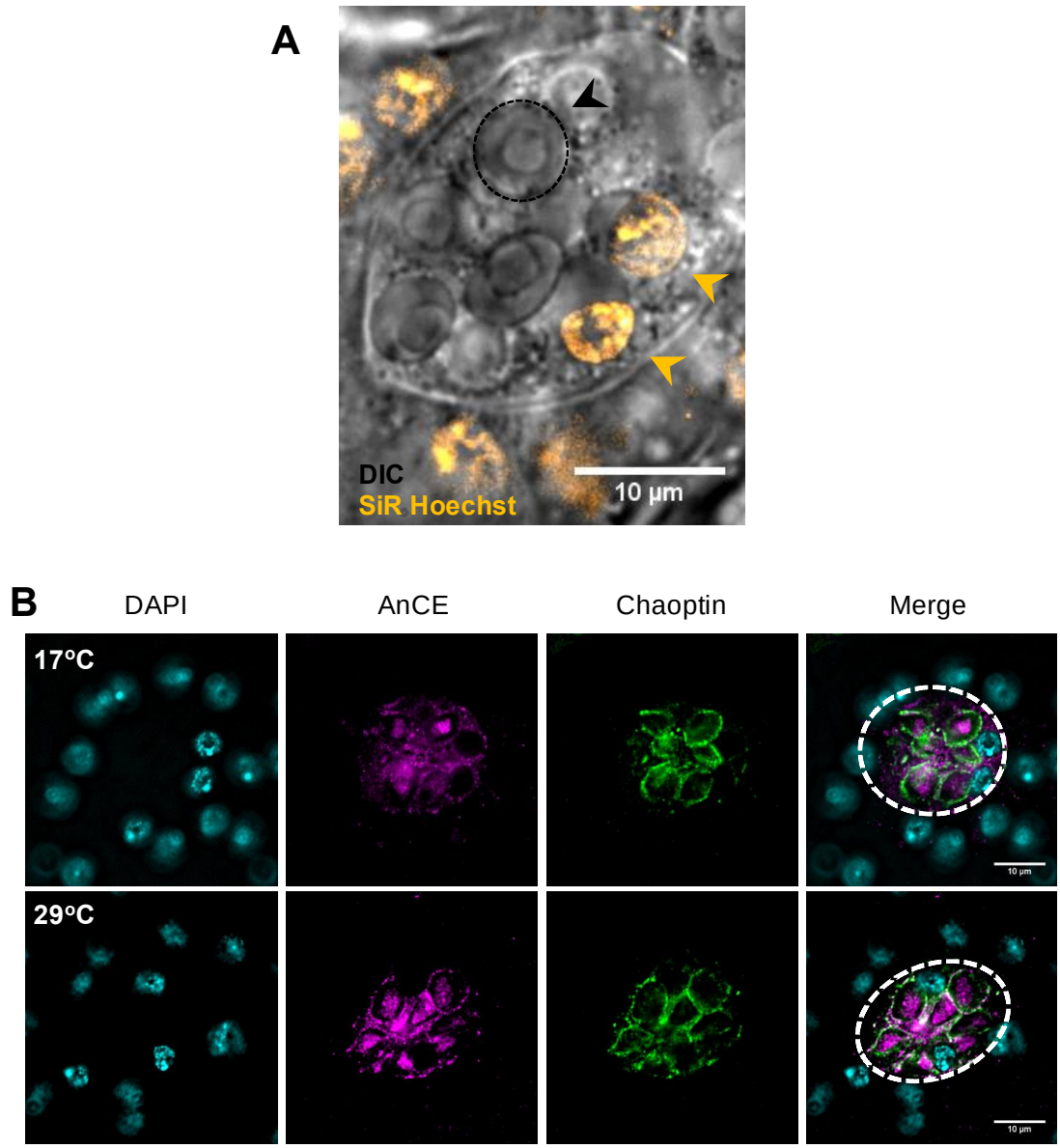

Figure 4.6 **SiR-Hoechst, anti-AnCE and anti-Chaoptin are useful markers for wide-field imaging of SC organelles. A.** Wide-field and DIC microscopy of a living cell stained with SiR-Hoescht (orange), which labels SC and MC nuclei, and does not disrupt DCG compartments. Nuclei are indicated by orange arrowheads. A representative DCG compartment (black arrowhead) is outlined by a dashed ellipse **B.** Both anti-AnCE (magenta) and anti-Chaoptin (green) label the DCG compartments of SCs from flies kept at 17°C and 29°C. AnCE is primarily located in the DCGs, while Chaoptin is associated with the limiting membrane and internal puncta. AGs were stained with DAPI (cyan). For both datasets, virgin w^{1118} males were incubated at the appropriate temperature (29°C in A) following eclosion for 6 days before dissection. Scale bars shown in panels represent 10µm.

Fig. 4.6A presents a SC imaged at high magnification combining DIC and fluorescence following one hour incubation in 2µM SiR-Hoechst at room temperature. It was possible to clearly differentiate between nuclei (Fig. 4.6A, orange arrowheads) and DCGs. The nuclei of main cells were also detected in this serial optical section. Thus, SiR-Hoechst specifically labels nuclei in the AG epithelium without detectable effects on cell morphology, enabling further imaging characterisation.

4.2.2.5. Anti-AnCE and Anti-Chaoptin Antibodies Mark DCG Compartments

As an additional tool to analyse DCG compartments further, I also characterised the SC staining patterns for two antibodies at 17ºC and 29ºC. Fig. 4.6B shows two SCs from six-day-old virgin wild type male flies maintained at two different temperatures and then fixed for immunohistochemistry. This approach does not provide the very high resolution and uniformity for DCGs observed with live imaging due to the methodology implemented. The characteristic binucleate pattern of the nuclei, stained with DAPI, is clearly distinguished.

One antibody employed was the previously characterised rabbit polyclonal antibody against *D. melanogaster* angiotensin I-converting enzyme (AnCE) using an Alexa 555 secondary (Fig. 4.6B). Mammalian AnCE is a zinc- and chloride-dependent carboxypeptidase whose known substrates include angiotensin I, the vasodilator bradykinin, the gonadotropin-releasing hormone (GnRH) and the luteinising hormone-releasing hormone (LH-RH) (Sturrock, Natesh et al. 2004). In the germ

cells of the fly testes, AnCE is required for the differentiation and individualisation of spermatids (Hurst, Rylett et al. 2003). AnCE was already reported to be localised to DCGs in SCs (Rylett et al. 2007; Corrigan et al., 2014).

SC immunohistochemistry revealed the localisation of the AnCE protein in the limiting membranes and dense cores of DCG compartments. Even though low level non-specific staining is observed in cytosolic regions, a defined dotted arrangement of fluorescence delineates the DCG limiting membranes and variable, but dense, clusters of the AnCE protein are revealed inside these compartments.

Encouraged by the interesting localisation of GFP-GPI in SCs, my supervisor had searched for GPI-anchored proteins that are expressed in the AG using the FlyAtlas database (Chintapalli, Wang et al. 2007). Chaoptin is a major GPI-anchored protein expressed in the fly eye (Reinke, Krantz et al. 1988, Van Vactor, Krantz et al. 1988) (Gurudev, Yuan et al. 2014), but microarray data also suggested that it is expressed in AG at lower overall levels. Following preliminary tests in collaboration with other laboratory members, I analysed mouse monoclonal anti-fly Chaoptin (DSHB: 24B10; (Fujita, Zipursky et al. 1982) localisation in SCs in detail, using an Alexa Fluor 647 secondary antibody (Fig. 4.6B). Remarkably, Chaoptin is expressed exclusively in SCs of the AG and is trafficked to the limiting membrane of DCG compartments and some internal puncta. Therefore, although this protein is trafficked to the same compartments as GFP-GPI, it is not incorporated into DCGs.

4.2.3. Characterisation of SC morphology in cells expressing fluorescent markers for non-acidic compartments

4.2.3.1. A CFP-Rab6 protein expressed from a gene trap localises on non-acidic compartments, some of which do not have a DCG

Previous studies in the laboratory have demonstrated that the small GTPase Rab11 is localised on the limiting membrane of DCG compartments (Corrigan et al., 2014; Redhai et al., 2016). B. Kroeger in the laboratory had screened through a number of targeted gene trap insertions in *Rab* genes (Dunst, Kazimiers et al. 2015) and identified Rab6 as a marker of large non-acidic compartments. To assess the localisation pattern of Rab6 protein in *Drosophila* AGs and SCs, I analysed expression of an endogenous CFP-tagged *rab6* allele (a gift from Elodie Prince [Geneva] and Suzanne Eaton [Dresden]).

Analysis of the tissue localisation of this N-terminally tagged protein showed that it is primarily expressed in SCs (Fig. 4.7A). By combining my analysis of cells with DIC, I confirmed that this marker is expressed only in non-acidic compartments and does not induce apparent changes in the morphology of SCs at either 17ºC or 29ºC (Fig. 4.7A) in 6-day-old males compared to controls.

Importantly, the marked compartments included the non-acidic compartments that I had already observed in wild type cells (Fig. 4.3C), which lack a DCG (Fig. 4.7A-B,

green asterices). My analysis of high magnification images from cells expressing the CFP-Rab6 protein in SCs led us to establish two main categories of compartments expressing CFP: (1) non-DCG compartments (pre-DCGs) which are variable in size and sometimes irregular in shape, and contain distinctive CFP-Rab6-positive invaginations (seen as foci of CFP signal associated with the limiting membrane) and large ILV structures (both indicated with white arrows in Fig. 4.7B) and (2) a more numerous group of compartments where DCGs are visualised by DIC and CFP signal is present on the limiting membrane, and labelling some peripheral regions of the dense core, potentially in differently sized microvesicles (Fig. 4.7B, yellow arrows; previous work by B. Kroeger had shown that transmembrane CD63-GFP also internalises within these compartments, and super-resolution microscopy has confirmed that this is associated with intraluminal vesicles). In this group of compartments, there were some DCG compartments with weaker and less continuous staining on the limiting membrane (Fig. 4.7B, yellow dotted arrows), which might be losing this molecule from their surface. There were always some DCG compartments that did not carry CFP-Rab6 (Fig. 4.7B, indicated with yellow asterices).

These data show that the CFP-tagged *rab6* allele can be used to categorise non-acidic compartments in SCs and allows a clear differentiation of their maturation stages. Additionally, CFP-Rab6 can be considered as a suitable marker at the range of temperatures employed in my studies with no detectable morphological effects in SCs.

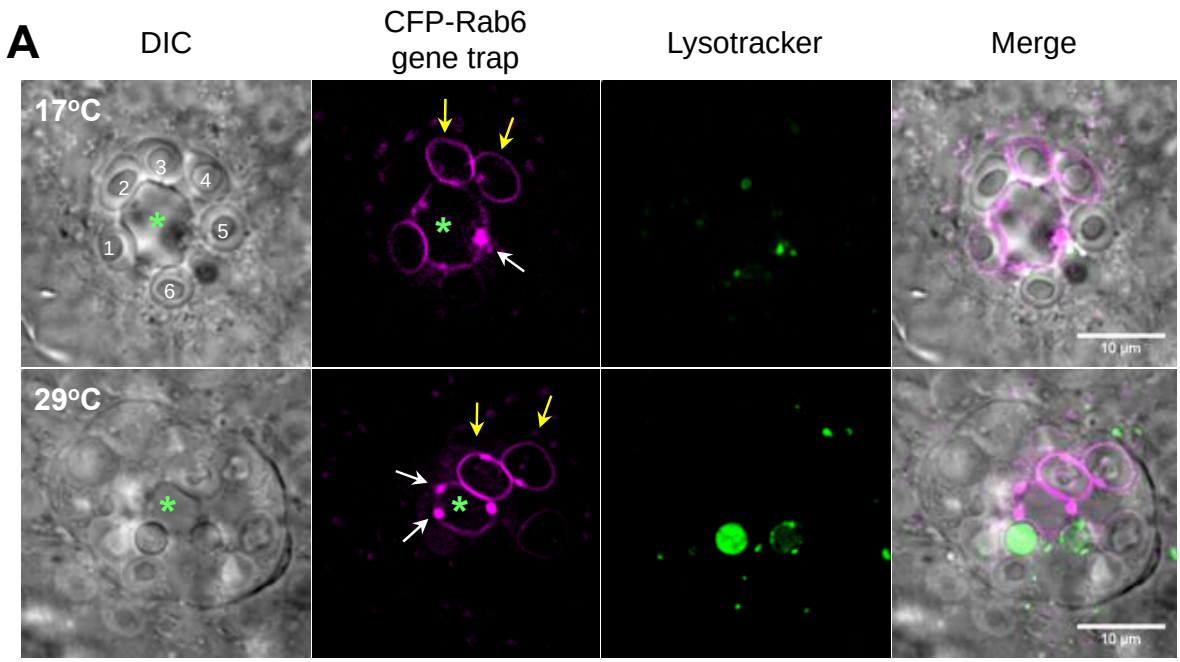
A
DIC
CFP-Rab6
gene trap
Lysotracker
Merge
17°C
29°C
1
2
3
4
5
6
10 µm
10 µm

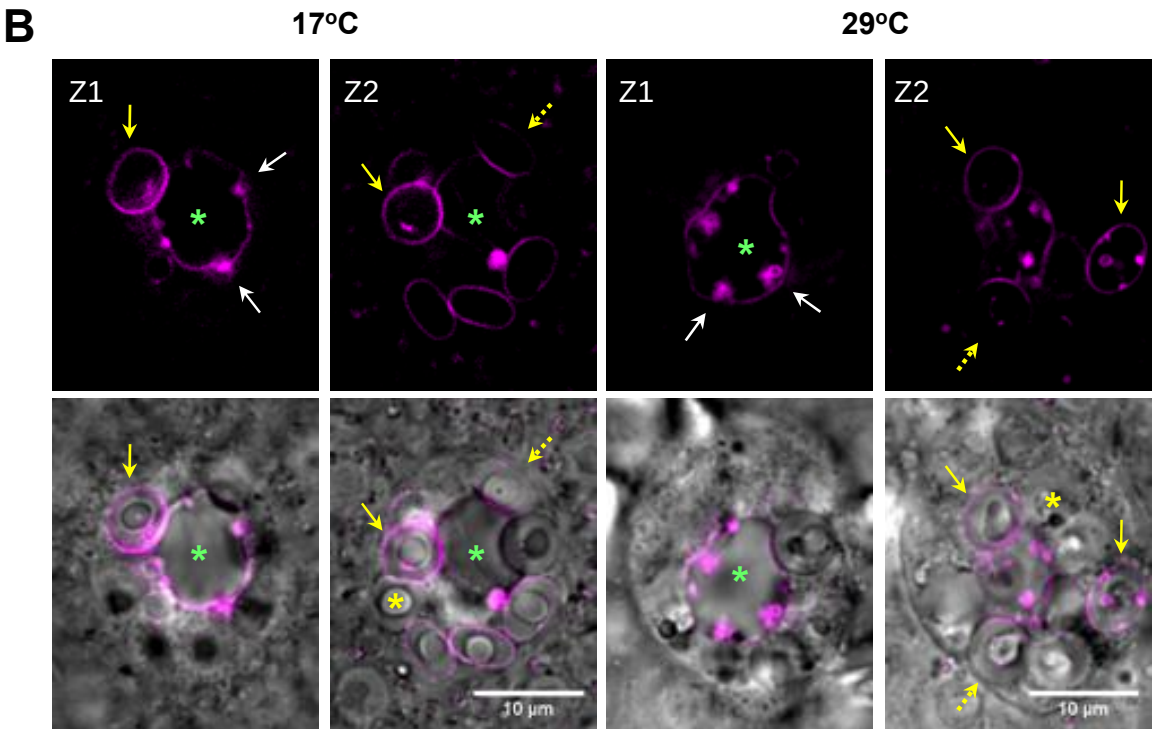
B
17°C
29°C
Z1
Z2
Z1
Z2
10 µm
10 µm

Figure 4.7 **Fusion protein expressed from a *CFP-Rab6* gene trap marks large non-acidic, non-cored compartments and some DCG compartments in SCs.** Wide-field and DIC microscopy of living SCs at 17ºC and 29ºC expressing a *CFP-Rab6* gene trap (magenta). **A.** At both temperatures, CFP-Rab6 localises to the limiting membrane and internal puncta (white arrows) in large non-acidic, non-cored compartments (green asterices). It also marks the limiting membrane and some structures around the dense core in a subset of DCG compartments (yellow arrows highlight strong staining, dashed arrows mark weaker staining in B). **B.** Higher magnification views of representative SCs at two different planes (Z1 is more apical than Z2; the latter is towards the mid-plane of the cell where the greatest number of DCG compartments is visible) allows further detail of the subcellular structures marked with CFP. Yellow asterices mark DCG compartments with no CFP staining. Virgin *CFP-Rab6* gene trap males were incubated at the appropriate temperature following eclosion for 6 days before dissection. AGs in A were stained with LysoTracker Red (green). Scale bars are shown in panels.

4.2.3.2. An AnCE-eGFP gene trap can be used to mark DCGs

Even though the expression of AnCE has been studied in AGs, such studies are limited to fixed tissue. I set about characterising a newly available *AnCE-eGFP* gene trap produced as part of a major project designed to mark genes and disrupt the fly genome using transposable elements (BDSC stock 59828 = Flybase genotype= *y* [1] *w*[67c23]; Mi [PT-GFSTF.1] AnCE [MI05748-GFSTF.1]/ SM6a) (Nagarkar-Jaiswal, Lee et al. 2015).

I studied AGs from six-day-old virgin males kept at 17 and 29ºC (n=55 SCs in each case) (Fig. 4.8A). At 17ºC the AnCE-eGFP protein is incorporated into DCGs as expected, though it also shows some cytosolic distribution, consistent with AnCE antibody staining patterns (Fig. 4.6B). Surprisingly, this pattern was drastically altered at 29ºC, where AnCE-eGFP was largely excluded from the DCGs, even though these structures were present by DIC (Fig. 4.8A).

There was also a significant diminution in the number of DCGs at 29ºC (Fig. 4.8A; see section 4.2.4 and Fig. 4.10 for a detailed quantification). A number of other changes were apparent (Fig. 4.8B), including an increase in the number of acidic compartments and trafficking of GFP signal into these compartments, suggesting that in this gene trap line, either more protein (including GFP-tagged AnCE) is trafficked to late endosomes and lysosomes or it is less efficiently degraded.

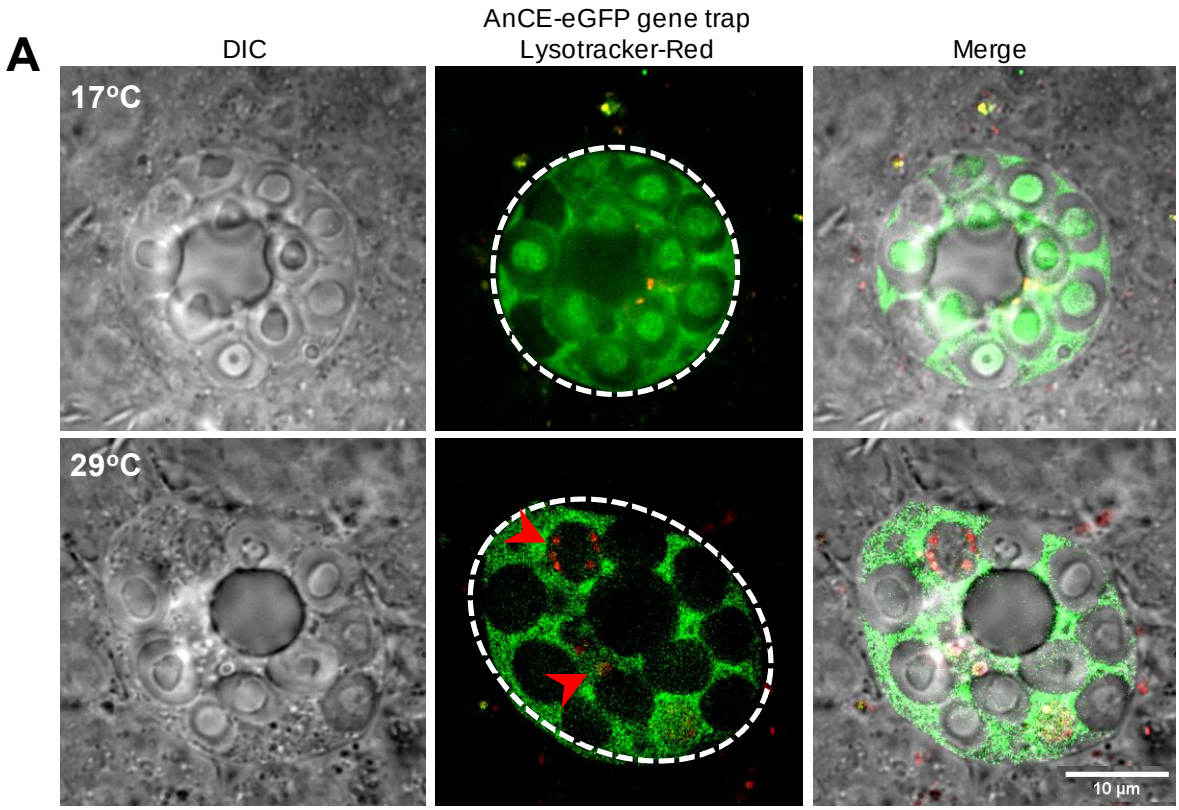
A
DIC
AnCE-eGFP gene trap
Lysotracker-Red
Merge
17°C
29°C
10 µm

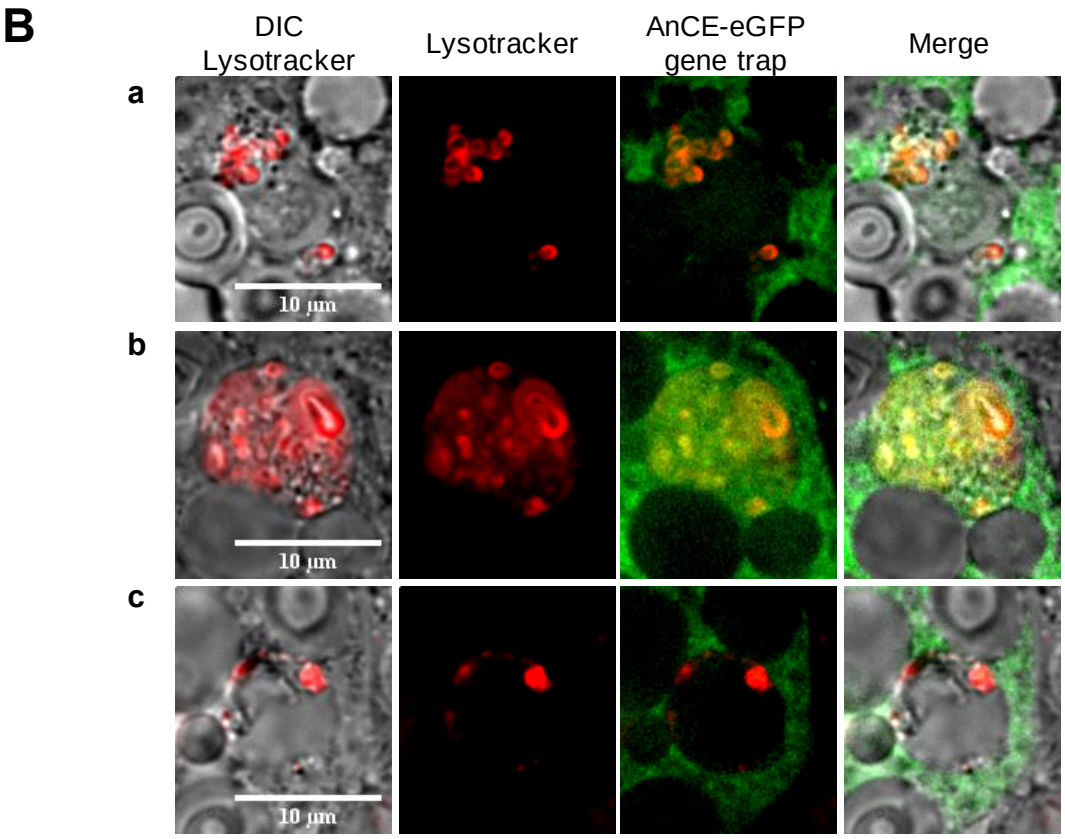
B
DIC
Lysotracker
Lysotracker
AnCE-eGFP
gene trap
Merge
a
b
c
10 µm
10 µm
10 µm

Figure 4.8 **Fusion protein expressed from an AnCE-eGFP gene trap is incorporated into DCGs at 17ºC. but not at 29ºC.** Wide-field and DIC microscopy of living SCs at 17ºC and 29ºC expressing an *AnCE-eGFP* gene trap (green) and stained with LysoTracker Red (red). **A.** At 17ºC, eGFP is trafficked to the DCGs of SCs and is also present in the cytoplasm outside the large compartments. At 29ºC, DCG fluorescent staining is lost (even though DCGs compartments are still detected by DIC), but the cytoplasmic staining remains. There is a general increase in acidic compartments (red arrowhead). **B.** Higher magnification views of SCs at 29ºC, showing three categories of acidic compartments (LysoTracker-positive): **(a)** small vesicles which are less than 2µm in diameter; **(b)** AnCE-eGFP-positive mMVBLs (>2µm in diameter); and **(c)** a novel category of compartments with around 6-10 µm diameter that do not have eGFP and lack the granular appearance of mMVBLs. The accumulation of eGFP in some acidic compartments, especially the large compartment in **b**, but also some smaller compartments **(a)** suggests that AnCE-eGFP may be trafficked at higher levels to late endosomal/lysosomal compartments. Virgin *AnCE-eGFP* gene trap males were incubated at the appropriate temperature following eclosion for 6 days before dissection. Scale bars are shown in panels.

4.2.3.3. AnCE-eGFP SCs allow the identification of three categories of acidic compartments

The increase in size and number of acidic compartments constitutes a remarkable difference between SCs kept at 17^{o}C or 29^{o}C (Fig. 4.8 A, red arrowheads). To gain a better understanding of the characteristic changes responsible for this variation, I studied the acidic compartments of SCs from males maintained at 29^{o}C throughout adulthood.

In the Wilson laboratory, a protocol for labeling and tracking of acidic organelles in live cells was originally established for SCs expressing the fluorescent CD63-GFP marker (Corrigan, Redhai et al. 2014). This highly selective technique comprised the use of a fluorescent dye (LysoTracker-Red) and enabled the identification of two morphological categories: (1) immature late endosome (iLE) compartments, of less than 2µm in diameter (<2µm) and (2) GFP- and LysoTracker-positive maturing, MultiVesicular Bodies/Lysosomes (mMVBLs), which are larger than >2µm in diameter and are positive for both the GFP marker (fluorescence on the limiting membrane) and the LysoTracker probe (Corrigan, Redhai et al. 2014).

For this study, AGs of males expressing the AnCE-eGFP protein and kept at 29^{o}C were stained with LysoTracker. Fig. 4.8B presents acidic compartments belonging to SCs imaged at high magnification in which DIC is combined with two fluorescent channels. Amongst all the SCs under study (n= 55 SCs), I was able to detect at least three different categories of acidic compartments: (1) compartments with less than 2µm in diameter either in isolation or clustered. Although many of these small

compartments clearly show the presence of LysoTracker, it was difficult to establish if all of them are eGFP positive (Fig. 4.8B, panel a); (2) maturing MultiVesicular Bodies/Lysosomes (mMVBLs) which are >2µm in diameter and are positive for both the AnCE-eGFP marker and LysoTracker-Red (Fig. 4.8B, panel b), and (3) a novel category that does not have eGFP signal but presents a sequence of red dots delimiting the membrane of the compartment. The compartment size is similar to that of DCGs (around 8 µm diameter, Fig. 4.8B, panel c). These compartments lacked the granular appearance observed with mMVBLs under DIC and therefore may represent an earlier stage of less mature endosome to which AnCE-eGFP has not been trafficked.

Therefore, by combining the different tools available for the study of SCs and their acidic compartments, I have found evidence for the presence of at least one new category of large acidic compartments in AG.

4.2.3.4. Characterisation of the GFP-GPI marker in SCs

4.2.3.4.1. The primary structure of the GFP-GPI fusion includes fragments of three different proteins

GFP-GPI is a fusion protein originally designed as a marker of subcellular trafficking, which is transported to the apical domain in polarised Madin-Darby Canine Kidney Epithelial cells (MDCKs) in a membrane-associated form (Keller, Toomre et al.

2001). This GFP-GPI cDNA was previously incorporated into a pUAST vector and expressed in *Drosophila* transgenics (Greco, Hannus et al. 2001).

Having found that GFP-GPI is trafficked to the dense-core granules of SCs, confirming the nucleotide sequence coding for GFP-GPI became an important aspect of my analysis. To this end, I extracted genomic DNA for sequencing from flies carrying the GFP-GPI construct.

As a result, I was able to identify a DNA sequence of 72 nucleotides upstream of the GFP coding sequence, corresponding to 24 amino acids (MELFWSIVFTVLL SFSCRGSDWES), 19 of which coded for the signal peptide of the Rabbit Lactase-phlorizin Hydrolase (LPH), a single-pass type I membrane protein that splits lactose in the small intestine. At the 3' end of the GFP-GPI coding sequence, I identified two sequences encoding peptides originally from CD58, a human protein also known as Lymphocyte function-associated antigen 3 (LFA-3), which functions as a Ligand of the T-lymphocyte CD2 glycoprotein (Seed 1987).

These peptides are:

(1) a fragment of 33 amino acids (PSSGHSRHRYALIPIPLAVITTCIVLYMNVL$_{END}$) coding for a part of Isoform 2 that features a GPI-anchored amidated asparagine (N) followed by valine (V, 236) and leucine (L, 237), and

(2) 15 residues of Isoform 1 (GILKCDRKPDRTNSN$_{END}$) that include three amino acids of the transmembrane domain followed by 12 residues (239-250) of the

cytoplasmic domain. Isoform 1 is a single-pass type I membrane protein (UniProt P19256-2).

DNA sequences belonging to the pUAST vector and eGFP were also detected in the appropriate location, confirming sequencing accuracy.

Altogether, these results allow prediction of the primary structure of the GFP-GPI fusion protein (Fig. 4.9A).

4.2.3.4.2. The GFP-GPI fusion protein is a reliable marker for specific large compartments in living SCs

The temporal control of the expression in SCs of GFP-GPI driven by the GAL4/UAS system (Brand and Perrimon 1993) was achieved using the *tub*-GAL80^{ts} ubiquitously expressed temperature-sensitive transcriptional repressor (Suster, Seugnet et al. 2004). GAL80^{ts} inhibits the GAL4/UAS activity at 17^{o}C, but allows transgene expression when it is inactivated by increasing the temperature to 29^{o}C. Cell specificity was attained utilising an SC promoter (*spitz*-GAL4) which has been identified in the laboratory to drive gene expression in the SCs (Corrigan, Redhai et al. 2014).

To gain insight into the expression of GFP-GPI in SCs, I studied AGs from six-day-old virgin males kept at 29^{o}C after eclosion (n=60 SCs, taken from 13 different AGs).

Fig. 4.9B shows two representative GFP-GPI-expressing cells at high magnification combining DIC and two fluorescent channels.

Based on these data, I categorised the compartments where the GFP signal is visible as follows:

(1) non-acidic, non-cored compartments which conform to the description of pre-DCGs in Section 4.2.3.1. They exhibit GFP signal outlining their entire limiting membrane and contain GFP-GPI-positive invaginations seen as foci of GFP signal close to the limiting membrane (indicated by a white arrow in Fig. 4.9B). The mean number of these organelles is 1.6 ± 0.7 per SC (n=60 SCs, from 13 different AGs). All large non-acidic compartments lacking a DCG (by DIC) were GFP-positive.

(2) DCG compartments (mean 7.5 ± 1.3 per SC; n=60 SCs, from 13 different AGs), comprising the most abundant category of large membrane-bound organelles in SCs, of more than 3μm in diameter. Strikingly, 99 ± 4% of DCGs identified by DIC were labelled by GFP-GPI, although at variable levels. In these organelles, the green fluorescent signal is observed throughout the dense cores, labelling also some peripheral regions of the core that can extend to the limiting membrane (Fig. 4.9B, white arrows). Additionally, GFP-positive, intra-luminal microvesicles are also observed (Fig. 4.9B, green dashed arrows) and the limiting membranes frequently carry thickened accumulations of GFP fluorescence in discrete sub-domains (Fig. 4.9B, yellow arrows). Some DCGs are more weakly stained with GFP (Fig. 4.9B, yellow dotted arrows). They might be either accumulating the GFP molecule at this

stage or losing fluorescence (by quenching) or losing GFP-GPI itself. This may suggest the existence of different maturation states for these DCG compartments.

(3) acidic compartments belonging to the morphological categories proposed in section 4.2.3.3 (Fig. 4.9B, red arrows), i.e. (i) compartments of less than 2µm in diameter either in isolation or clustered. Although these small compartments clearly show the presence of LysoTracker, not all of them are GFP-positive; (ii) large acidic compartments, mMVBLs (>2µm in diameter), which are positive for LysoTracker-Red and contain variable levels of GFP signal in distinct regions; (iii) compartments that do not have GFP signal but present a number of red puncta close to the limiting membrane of the compartment. Their size is similar to that of DCGs and they do not have the granular appearance observed with other acidic compartments under DIC; (iv) an additional group (Fig. 4.9B, red dashed arrow), very similar to the previous category but revealing a weak GFP signal, a dense core with DIC, and a few small internal LysoTracker-positive puncta. Acidic compartments were detected in all 60 SCs under study, but representatives of groups iii and iv were only observed in a total of five cells).

(4) the basolateral plasma membrane is seen as a thin continuous line in central zone in the plane of the epithelium (Fig. 4.9B, white arrowhead), while the apical membrane exhibits an irregular appearance which would suggest a more invaginated structure.

Taken together, these data show that the GFP-GPI is a reliable marker for several key large compartments in SCs. By combining DIC and fluorescence microscopy for

the assessment of this marker, it is possible to recognise the various compartments present in SCs. This analysis suggests that SCs may contain DCG compartments at different stages of maturity and that these compartments may become acidified in some cases, and their contents broken down in mMVBLs. In addition, expression of the GFP-GPI fusion protein does not affect SC morphology, and so it can be considered as a suitable live cell marker of SC compartments, a conclusion confirmed in Section 4.2.4.

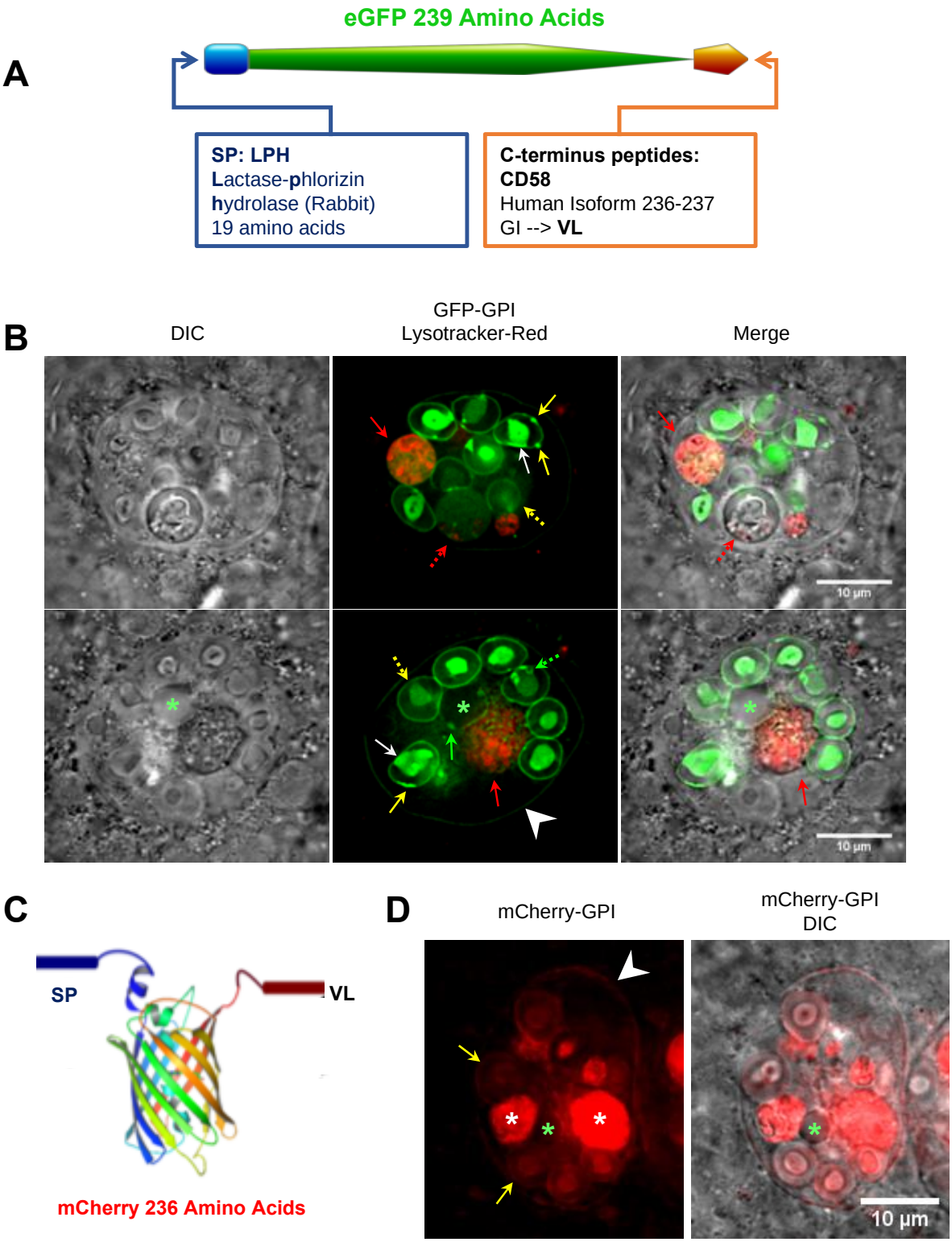
A
eGFP 239 Amino Acids
SP: LPH
Lactase-phlorizin
hydrolase (Rabbit)
19 amino acids
C-terminus peptides:
CD58
Human Isoform 236-237
GI --> VL
B
DIC
GFP-GPI
Lysotracker-Red
Merge
10 µm
10 µm
C
SP
VL
mCherry 236 Amino Acids
D
mCherry-GPI
mCherry-GPI
DIC
10 µm

Figure 4.9 **The GFP-GPI fusion protein is a suitable live-cell marker for SCs. A.** Schematic representation of the primary structure of GFP-GPI displaying the assembly of three different components: N-terminal signal peptide (SP) sequence from Rabbit Lactase-phlorizin Hydrolase (LPH, blue rectangle), followed by eGFP (green pentagon), and a C-terminal region from CD58 (orange pentagon). The residues G (glycine) and I (Isoleucine) are replaced by V (Valine) and L (Leucine) in the GPI-anchored isoform of CD58. **B.** Wide-field and DIC high magnification images illustrating the subcellular organisation of representative GFP-GPI-expressing SCs. GFP signal is detected in the limiting membrane and invaginations (green arrow) of pre-DCG compartments (green asterices, mean = 1.6 ± 0.7 per SC). In DCG compartments (mean 7.5 ± 1.3 per SC), green fluorescent signal is found in the dense cores and their limiting membranes. Note that some cores are 'connected' to their limiting membranes by accumulations of GFP (white arrows) and that foci of fluorescent signal are present in some limiting membranes (yellow arrows). Putative intra-luminal microvesicles (green dashed arrow) are also present. Basolateral plasma membrane is indicated by a white arrowhead. Yellow dashed arrows show weaker stained DCG compartments, perhaps illustrating different maturation states. LysoTracker-positive (red) compartments exhibit variable levels of GFP (red arrows). Interestingly, DCG compartments with limited LysoTracker staining and weak homogeneous GFP were also identified (dashed red arrows). Genotype of virgin males, which were incubated at 29ºC following eclosion for 6 days is: *w; spi-GAL4 tub-GAL80^{ts}; UAS-GFP-GPI*. **C.** 3D representation of the structure of mCherry-GPI illustrating the three sequences forming the red fusion protein: the fluorescent mCherry reporter is flanked by SP from LPH at the N-terminus and a C-terminal sequence from CD58 where the GPI-anchor (VL) can be found at the opposite end. **D.** Wide-field and DIC microscopy of a living cell expressing mCherry-GPI under the control of *dsx*-GAL4 *tub-GAL80^{ts}*. High magnification images show mCherry localisation in DCG compartments (yellow arrows), pre-DCGs (green asterisk) and the basolateral plasma membrane (white arrowhead). Higher levels of red signal are detected in mMVBL-like compartments (white asterices). Virgin males were incubated at 29ºC following eclosion for 6 days before dissection. Scale bars are shown in panels.

4.2.3.4.3. A red fluorescent GPI-anchored fusion protein permits double-labelling of secretory compartments in SCs

Once I determined the sequence coding for GFP-GPI, I was able to propose a strategy to replace the fluorescent reporter and engineer a red version of the marker. Importantly, the availability of a dual fluorescence system (e.g. green and red) allows studies to further understand the dynamics of GPI-anchored cargos in SCs by combining with molecules such as endogenously tagged Rab proteins expressing YFP or GFP (Dunst, Kazimiers et al. 2015).

To generate the pUAST: mCherry-GPI construct, three sequences were fused: (i) includes the signal peptide (SP) of LPH, (ii) an mCherry reporter, and lastly (iii) a segment of the C-terminal region of CD58 (Fig. 4.9C).

After successfully incorporating the UAS: mCherry-GPI pUAST construct into *D. melanogaster* (undertaken by BestGene), nine transgenics were examined by fluorescence microscopy for mCherry expression following crosses to a SC>GAL4 driver, and two stable expressing stocks were finally selected. The expression of mCherry-GPI in SCs was studied in AGs from six-day-old virgin males kept at 29^{o}C after eclosion. Fig. 4.9D shows a high magnification view of a representative mCherry-GPI-expressing cell.

These preliminary data showed that although overall expression levels of the mCherry version appeared to be lower in non-acidic compartments, it is possible to observe fluorescence signal localising in DCG compartments, pre-DCGs and on the plasma membrane (Fig. 4.9D, yellow arrows, green asterices and white arrowhead, respectively). A very high level of red signal was observed inside compartments that appear to be acidic mMVBLs, because of their granular appearance with DIC (Fig. 4.9D, white asterices).

At first glance, the two versions of the GPI-anchored marker exhibit very different expression patterns. The underlying explanation may be that red fluorescent proteins generally appear to traffic more readily to mMVBLs in secondary cells. These results suggest that additional adjustments should be explored to study the expression of the mCherry-GPI, for example by analysing the trafficking of a protein pulse. Regardless, detectable morphological defects in non-acidic compartments were not observed in SCs expressing this construct, suggesting that it may in the future be useful to employ with green fluorescent proteins in studies of DCG formation.

4.2.4. Quantitative analysis provides additional support of the robustness of GFP-GPI as a reliable marker for SC compartment analysis

Studies in the Wilson Laboratory have indicated that the expression of fluorescent markers can induce phenotypic modifications in SCs (Redhai, Hellberg et al. 2016).

Among such changes, one relevant and easily characterised change is the effect on the number of DCG compartments, which for example, is significantly increased by CD63-GFP expression (Redhai, Hellberg et al. 2016). Quantification of these organelles is easily achievable in different genetic backgrounds when DIC data are available for contrast with fluorescence channels.

To test the effects of the new fluorescent markers I had characterised and study the variability in the number of DCG compartments across SCs from six-day-old virgin male flies kept at 17 and 29^{o}C, I built a database with counts of DCG compartments (a discrete variable) grouped by genetic background (w^{1118}, SC>*GFP-GPI*, *AnCE-eGFP* gene trap and *CFP-Rab6* gene trap), AG and incubation temperature. This produced seven different categories/conditions (genotype and temperature), containing a total of 378 SCs (i.e. from individual cell images, with DIC and including the corresponding marker if present, see Fig. 4.10).

Preliminary statistical analysis of these data indicated that there was no homogeneity of variance across groups, and the distribution of the DCG compartment counts was non-normal. Therefore, the best alternative for data analysis was to implement a Generalised Linear Mixed Model fitted using Penalised Quasi-Likelihood (GLMMPQL) (McCullagh and Nelder 1989, Breslow and Clayton 1993, Wolfinger and Oconnell 1993, Bolker, Brooks et al. 2009). This approach was carried out following the advice of Dr Daniel Lunn from the Department of Statistics at the University of Oxford.

GLMMPQL incorporates two methods for statistical analysis: linear mixed models and generalised linear models. In brief, a linear mixed model allows fixed and random effects to be taken into consideration (Breslow and Clayton 1993, Wolfinger and Oconnell 1993, Bolker, Brooks et al. 2009). For this model, DCG compartments (fixed effects) were set as the response variable in order to establish its variability among the different genetic backgrounds at two different temperatures. Gland (AG) was used in the random effect part of the model given that for each AG several counts of DCGs from different SCs were quantified. This was done because counts from the same gland are predicted to have a correlation that needs to be accounted for (Bolker, Brooks et al. 2009). In addition, to fulfil the requirements of the model, input data were fitted to a Poisson distribution.

The output of the GLMMPQL is shown in Fig. 4.10. The mean values of DCG compartments and their respective confidence intervals at 95% allow the data sets to be divided into two groups based on mean similarity. The first group includes the categories 1 (wild-type w^{1118}), 4 (flies expressing the *AnCE-eGFP* gene trap), and 6 (flies expressing the *CFP-Rab6* gene trap). All of them kept at 17^{o}C for six days after eclosion (Fig. 4.10A-B).

Category 7, which accounts for flies expressing the *CFP-Rab6* gene trap and kept at 29^{o}C for six days after eclosion, also falls within the range of this group, however further analysis is required to explain this finding (Fig. 4.10A-B).

A

Genotype	Category	T°C	*n*	Confidence Intervals for number of DCG compartments (95%) Mean	Lower Bound	Upper Bound
w^{1118}	1	17	49	9.6	8.9	10.2
	2	29	51	7.3	6.9	7.9
SC>GFP-GPI	3	29	60	7.5	7.0	7.9
AnCE-eGFP	4	17	55	9.3	8.7	9.8
gene trap	5	29	55	7.8	7.4	8.3
CFP-Rab6	6	17	60	9.5	8.9	10.1
gene trap	7	29	48	9.1	8.5	9.7

B

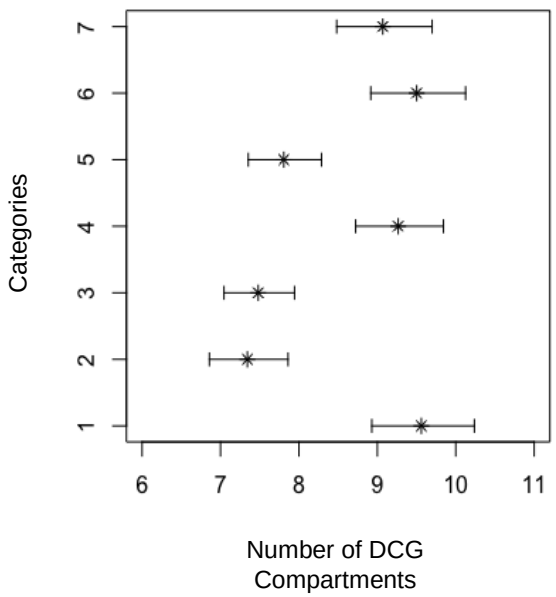

C

Cat	1	2	3	4	5	6	7
1							
2	0.0000						
3	0.0000	0.6842					
4	0.4950	0.0000	0.0000				
5	0.0000	0.1821	0.3184	0.0001			
6	0.8944	0.0000	0.0000	0.5692	0.0000		
7	0.2753	0.0000	0.0001	0.6371	0.0014	0.3183	

Figure 4.10 **Comparative analysis of the number of DCG compartments across different genetic backgrounds suggests different markers do not affect these compartments. A.** GLMMPQL Output depicts the mean values and limits for a 95% confidence interval calculated for the number of DCG compartments per SC. Database included observations from 378 different SCs belonging to four different genotypes that were grouped into seven different categories based on incubation temperature. SCs from six-day-old virgin male flies kept at 17ºC or 29ºC; their genetic backgrounds were w^{1118}, SC>*GFP-GPI*, *AnCE-eGFP* gene trap and *CFP-Rab6* gene trap. **B.** Plot depicts mean values and their confidence intervals. **C.** Pairwise analysis among means allows the estimation of significant differences between categories. *p*-values <0.01 indicate a significant difference. The only significant differences are found between males kept at different temperatures.

The second group takes account of the categories in which a smaller number of DCG compartments is observed. The range of values in this group is between approximately 7-8 DCG compartments per SC, and includes categories 2 (wild-type w^{1118}), 3 (GFP-GPI-expressing flies), and 5 (flies expressing the *AnCE-eGFP* gene trap). All of them kept at 29ºC for six days after eclosion.

Taking into account that there is a significant difference between the observed counts at 17 and 29ºC in wild-type flies (group 1 versus 2; *p*-values are <0.0001, Fig. 4.10C), it can be concluded that the incubation temperature has an effect on the decrease of DCG compartments in SCs.

The similarity in counts of DCG compartment observed when comparing wild-type w^{1118} kept at 29ºC to GFP-GPI-expressing flies (categories 2 and 3 respectively), and the significant difference of these two (*p*-values are <0.0001, Fig. 4.10C) with

w^{1118} flies kept at 17ºC provide evidence of the reliability of this data analysis and contribute robust reference values for further assessments (e.g. study of DCG biogenesis regulators in Chapter 5).

The confidence intervals established for number of DCG compartments along with the pairwise comparison among the means (respective *p*-values depicted in Fig 4.10C) allow to validate the model implemented here in terms of precision and accuracy. Therefore, I can confirm that number of DCG compartment is an informative variable for the study of SCs capable of capturing variability between groups from different backgrounds and culture conditions.

Altogether, the reference data obtained in this section is particularly valuable since it allows comparisons to establish whether the modification of a wild-type genotype (via introduction of coding sequences for cellular markers) or any changes in the environment (response to environmental stressors) induce a phenotypic effect on DCG compartments and therefore on the secretory function of SC. This is then a key starting point for any further functional characterisation of the AG.

4.2.5. Pulse-chase of the GFP-GPI fusion protein in SCs reveals cargo trafficking between different compartments within the cell

Having shown that there are both non-cored and core-containing large non-acidic compartments in SCs (sections 4.2.2.1 and 4.2.3.4.2), I sought to determine

whether these compartments are linked by trafficking or represent separate trafficking routes in these cells. A pulse-chase strategy was implemented to characterise the trafficking routes of fluorescently tagged proteins in SCs (Corrigan, Redhai et al. 2014). Standardly, a pulse of protein expression is produced by increasing to 29^{o}C the incubation temperature of six-day-old virgin male flies for 8-14 hours. During the course of the pulse, the GAL80^{ts} transcriptional repressor is inhibited (Suster, Seugnet et al. 2004), allowing localised protein expression driven by the GAL4/UAS system (Brand and Perrimon 1993). After the pulse, flies are placed back at 17^{o}C to allow transcriptional repression through GAL80^{ts}. The fluorescent marker is then imaged after different time points using microscopy to assess how it traffics through the cell's secretory and endolysosomal systems; glands were co-stained with LysoTracker Red.

To characterise the trafficking of GFP-GPI through the SC, an 8 h-pulse was carried out using virgin males that were kept at 17^{o}C for six days after eclosion until the pulse was induced on the sixth day. After the pulse, the expression of the fluorescent marker was chased at 0, 16, 24 and 48 hours at 17^{o}C. Fig. 4.11 shows high magnification images of four SCs regions extending from the apical pole (Z1) towards the basal end (Z4) within a SC at these four different time points.

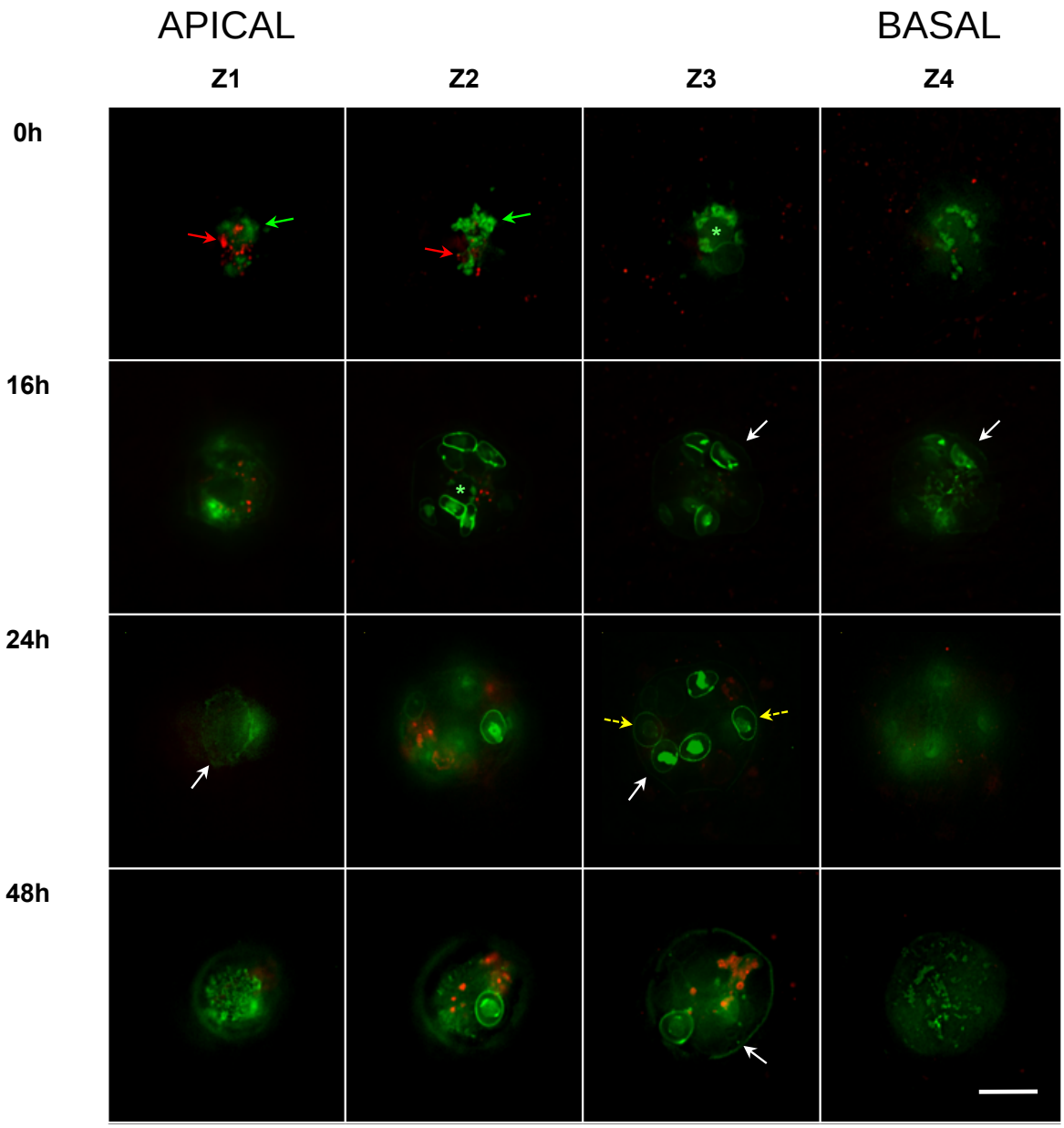

Figure 4.11 **Pulse-chase analysis allows the trafficking routes of GFP-GPI through the secretory pathway in SCs to be visualised.** A pulse to induce the expression of GFP-GPI was achieved by increasing the incubation temperature of 6-day-old-virgin male flies from 17ºC to 29ºC for 8 h. Subsequently, flies were placed back at 17ºC and the expression of the GFP-GPI was chased at 0, 16, 24 and 48 h. Wide-field high magnification images from the chase time points across four cellular z-planes extending from the apical (Z1) towards the basal (Z4) pole reveal the subcellular progression of the fluorescent cargo in living SCs. At time 0 h, acidic and

non-acidic granular structures are detected clustering apically and towards the mid-plane of the SC (green and red arrows in Z1-Z2). A pre-DCG is also labelled at this stage (green asterisk in Z3). At 16 h, GFP is labelling a pre-DCG (green asterisk in Z2), several DCG compartments and the basolateral plasma membrane (indicated by white arrows in Z3-4). After 24 h chase, differences in the localisation of GFP at the apical and basolateral domains of the plasma membrane become clearly visible (discontinuous versus continuous respectively; white arrows). Yellow dashed arrows show weaker stained DCG compartments, potentially highlighting different maturation states. In this SC, no GFP-positive pre-DCG compartments were detected. At 48 h post-pulse, a different localisation of GFP on the apical and basolateral (white arrow) domains of the plasma membrane is displayed. The number of GFP-positive DCG compartments is decreased. Genotype of virgin males, which were kept at 17ºC following eclosion for 6 days before pulse was: *w; spi-GAL4 tub-GAL80^{ts}; UAS-GFP-GPI*. AGs were stained with LysoTracker Red. Scale bar shown represents 10μm.

At time 0 h, numerous foci of green and red fluorescent signal were observed clustering in the centre of the apical area of the SC (Fig 4.11, indicated by green and red arrows at 0h in Z1-Z2). Moreover, one large and many small GFP-positive central non-acidic compartments were typically observed towards the mid-plane of the cell, where the greatest number of DCG compartments is visible (Z3).

Fig. 4.12A offers further insights into the trafficking of GFP around Z3 in three different SCs at this early stage. These images have been organized to illustrate three potential stages in the trafficking progression of GFP within the cell (Fig. 4.12A a-c): (a) initially, the GFP signal is seen distributed in microvesicular structures surrounding a non-acidic, non-cored central compartment (Fig. 4.12A panel a, pre-DCG green asterisk). GFP signal is not present on the limiting membrane at this stage; (b) fluorescent signal clearly delineates the entire limiting membrane of a

large non-acidic, non-cored compartment. GFP-positive microvesicles and foci of signal are observed in direct contact with various sectors of this membrane, and weak diffuse fluorescence is seen inside the compartment; and (c) a similar structure to that seen in (b) is observed again, but GFP foci and microvesicles surrounding the limiting membrane are more conspicuous (Fig. 4.12A panel c, white arrows). In addition, the limiting membrane and dense core of a newly formed DCG compartment are also labelled with GFP (yellow arrow).

In Fig. 4.11, after a 16 h chase, weak localisation of GFP was seen for the first time in the basolateral plasma membrane (Fig. 4.11, white arrow). At this time point, the number of GFP-positive DCG compartments had increased notably. A labelled non-cored, non-acidic compartment was also present (Fig. 4.11, green asterisk), but unlike the previous time point, GFP-positive microvesicular structures surrounding its limiting membrane were less visible.

At 24 h post-pulse, the apical plasma membrane had become clearly labelled. However, the localisation pattern of GFP in the apical and basolateral membranes was different. Apically, it appeared irregular, with a denticulate appearance, while basally there was a well-defined and continuous line of fluorescence (Fig. 4.11, 24 h, Z1 and Z3 respectively, white arrows). At this time, the proportion of GFP-positive pre-DCG compartments has decreased substantially to 26% (from 54 SCs analysed, only 14 exhibited GFP labelling) contrasting with the percentage observed during the previous time point of 98% (where 42 out of 43 SCs were GFP-positive). Another major point is that in DCG compartments, GFP localisation patterns were variable (e.g. some were weakly labelled with GFP in the cores, Fig. 4.11, 24 h, Z3,

yellow dashed arrows). This may suggest different maturation states for these organelles, although it is important to note that some variability is seen even with continuous expression of the GFP-GPI construct.

By 48 h, a cluster of GFP-positive puncta was associated with the membrane in the apical region (Fig. 4.11, 48 h, Z1), whereas the basolateral membrane was clearly delimited as a continuous circle of fluorescence (Fig. 4.11, 48 h, white arrow in Z3). One important aspect at 48 h chase was the significant reduction in the number of GFP-positive DCG compartments. Fig. 4.12B shows two additional examples of SCs at this stage, in which it is possible to confirm by DIC that numerous DCG compartments no longer have GFP signal. Fig. 4.12B also reveals several acidic compartments with acidic microvesicles and dispersed GFP signal (indicated by red arrows).

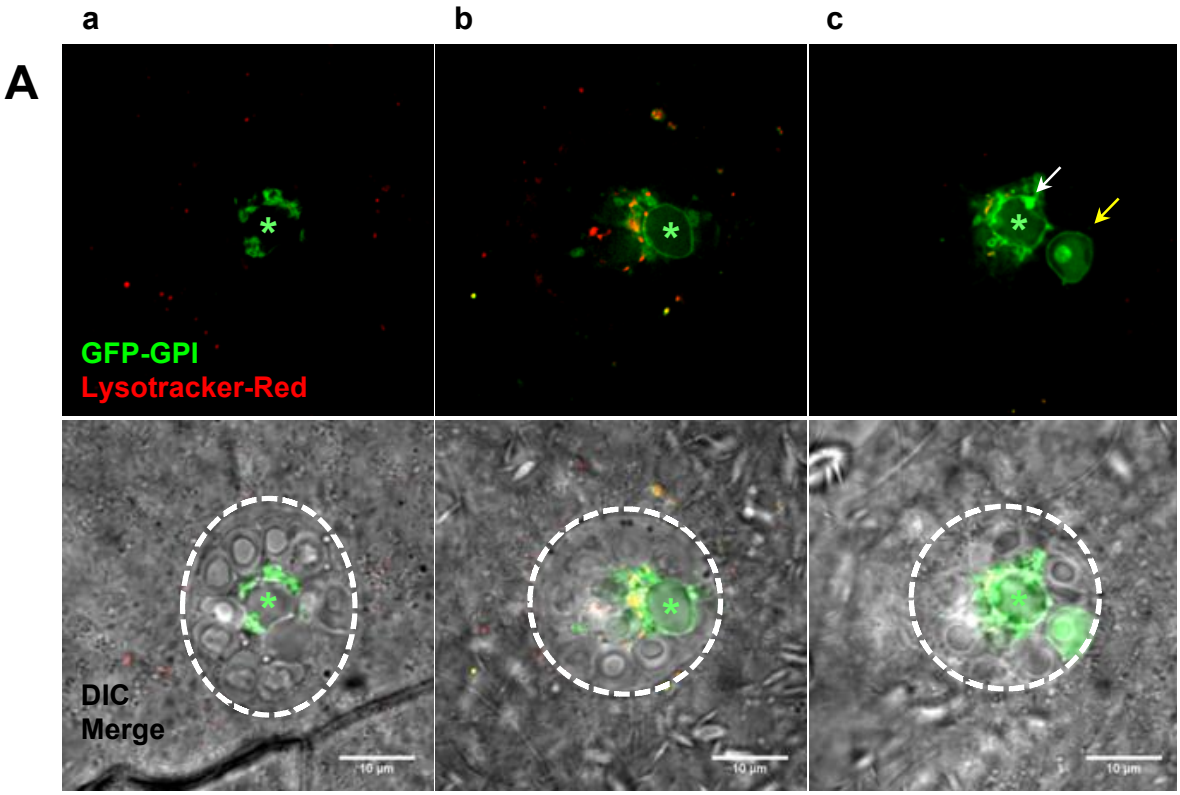
a
b
c
A
GFP-GPI
Lysotracker-Red
DIC
Merge
10 µm

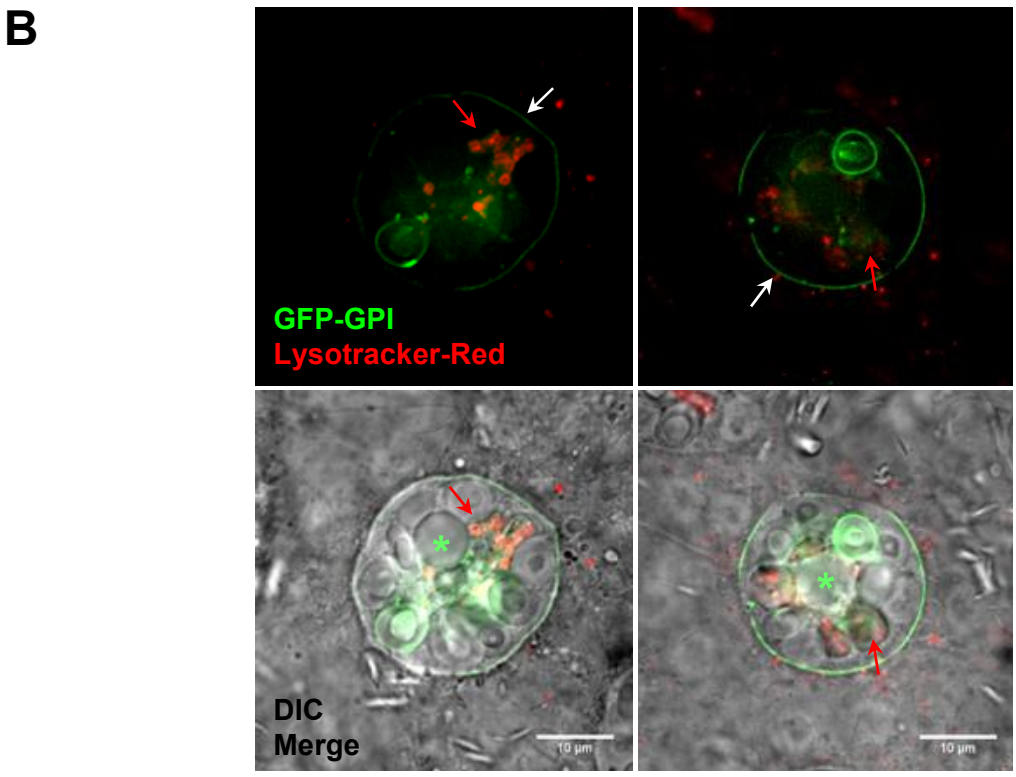
B
GFP-GPI
Lysotracker-Red
DIC
Merge
10 µm

Figure 4.12 **Trafficking progression of GFP-GPI through the SC in pulse-chase analysis.** Wide-field fluorescence and DIC images of SCs expressing GFP-GPI under *spi*-GAL4 control. **A.** Sequence of trafficking of GFP observed at the mid-plane of SCs reveals how GFP is initially trafficked after an 8-h pulse (time point 0 h): **(a)** firstly, GFP-positive microvesicular structures are detected surrounding a pre-DCG compartment (green asterisk); **(b)** secondly, GFP is outlining the entire limiting membrane of a pre-DCG compartment and clusters of green signal are detected around the limiting membrane; and **(c)** brighter GFP labelling is detected at the limiting membrane of a pre-DCG (green asterisk) wherein well-defined microvesicles and membrane invaginations (white arrow) are evident. A DCG compartment, which has a small DCG and presumably has only recently been formed, is indicated by a yellow arrow. Even though several DCG compartments are detected by DIC, most of them are not stained with GFP. **B.** SCs at 48 h post-pulse exhibit a low proportion of GFP-positive compartments (this is confirmed by the DIC/Merge panels where several DCG compartment are displayed). Note that no GFP signal is detected in the pre-DCG compartments (green asterices) and a clearly delimited basolateral plasma membrane is visible (white arrows). Enlarged mMVBLs are present and some of them exhibit diffuse GFP signal (red arrows). An 8 h-pulse was produced in 6-day-old virgin males kept at 17ºC following eclosion by increasing the incubation temperature to 29ºC. The expressed marker was chased at 17ºC. Genotype of males was: *w; spi-GAL4 tub-GAL80^{ts}; UAS-GFP-GPI*. AGs were stained with LysoTracker Red. Scale bars are shown in panels.

4.2.5.1. A multilevel model suggests how GFP is trafficked into DCG compartments of the SCs

In analysing the results obtained by pulse-chase of GFP-GPI, a measurable variable that allows assessment of the fluorescent protein progression through the SC is the proportion of GFP-positive DCG compartments (calculated as number of GFP-

positive DCG compartments / total number of DCG compartments observed by DIC).

To study the variation in this proportion of GFP-expressing DCG compartments during a GFP-GPI pulse-chase experiment, a total of 194 pulsed SCs from the time points defined in the previous section were quantified (respective *n* values per time point are indicated in Fig. 4.13). Preliminary analysis led to the implementation of a GLMMPQL analysis, where data were fitted to a binomial distribution (McCullagh and Nelder 1989).

For this multilevel model the proportion of GFP-positive DCG compartments during the chase time was set as a fixed effect for the model. The data collected for each gland account for random effects, given that quantification of DCG compartment number within the same gland is likely to have some correlation and needs to be accounted for to avoid pseudoreplication (McCullagh and Nelder 1989).

The mean and 95% coefficient intervals for the proportion of positive DCG compartments for the four chase time points are depicted in Fig. 4.13A and C. These data show that all observed ratios at the time points under analysis were significantly different from each other (all *p*-values are <0.0001). The width of the confidence intervals for each time point can also be used as a direct indicator of the variability observed at each sampling point (e.g. at 16 h the greatest variability in terms of the proportion of DCG compartments where GFP is expressed is observed).

At 0 hours after the pulse, approximately 2.5% of DCG compartments showed GFP signal. This ratio increased rapidly over the next 16 hours to 60%, and achieved a maximum of 81% at 24 hours after the end of the pulse. Finally at 48 hours only 20% of DCG compartments still had GFP signal.

The confidence intervals established for the proportion of GFP-positive DCG compartments along with their *p*-values (for each time point, they were <0.0001) validated the model in terms of precision and accuracy for the assessment of the movement of this marker through the DCG compartments over time.

Altogether, these results suggested a simple model in which GFP-GPI chases into DCG compartments for about 24 h following the pulse of expression, but the number of positive compartments then decline, presumably because of secretion and trafficking to degradative compartments. This model satisfactorily explains the trafficking of GFP-GPI within SCs under the conditions set above. It is also consistent with the real-time imaging data shown earlier, which suggests that non-cored non-acidic compartments are pre-DCG compartments.

Finally, Fig. 4.13B shows that the results presented here can be fitted to a trend-line and can therefore be used to generate a predictive equation that could enable future comparisons with trafficking of other molecules in SCs.

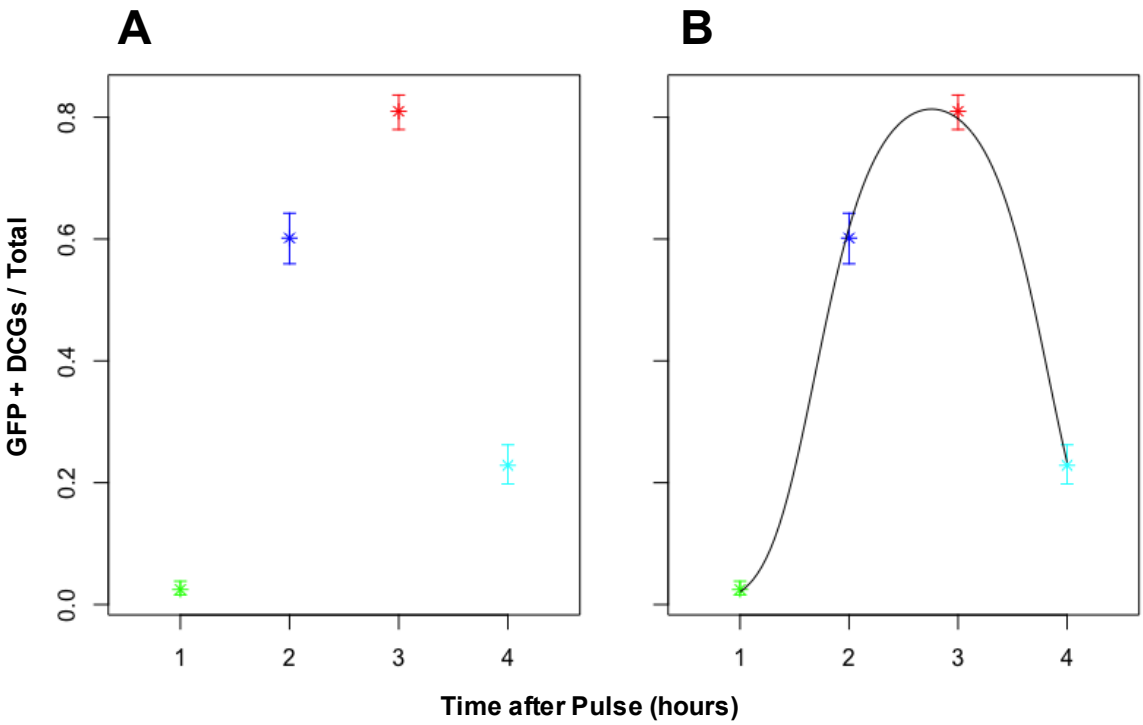

C

Time after Pulse (hours)	SCs (n)	AG (n)	Confidence Intervals for proportion of GFP-positive DCG compartments (95%) Mean	Lower	Upper
0	50	11	0.0250	0.016	0.038
16	43	12	0.6020	0.559	0.642
24	54	13	0.8100	0.780	0.836
48	47	10	0.2280	0.198	0.262

Intercept= 0.0672, Residual= 0.7866;
p-values estimated for each time point are <0.0001

Figure 4.13 **Analysis of the pulse-chase results provides further insights into the progression of GFP-GPI through the DCG compartments of SCs. A.** Plot using a GLMMPQL depicts striking differences among the four chase time points (1-4 refers to 0, 16, 24 and 48 h after pulse). Each point illustrates the mean values and limits for a 95% confidence interval calculated for the proportion of GFP-positive DCG compartments (GFP-positive DCG compartments / total number of DCG compartments detected by DIC). **B.** Trend-line indicating the change in GFP-GPI–positive DCG compartments over time. **C.** Model output presenting the numerical data plotted in A and B. Database included a total of 194 pulsed SCs. An 8 h-pulse was produced by increasing the incubation temperature of 6-day-old virgin males previously kept at 17ºC following eclosion to 29ºC. The expression of the fluorescent marker was chased at 17ºC. Genotype of males was: *w; spi-GAL4 tub-GAL80^{ts}; UAS-GFP-GPI*. *p*-values <0.01 indicate a significant difference.

4.2.5.2. GFP-GPI and mCherry-GPI labelling kinetics can be studied simultaneously in SCs

A pulse-chase approach was implemented to provide a preliminary assessment of the trafficking routes follow by GFP-GPI and mCherry-GPI when simultaneously expressed in a SC. The standard method described in section 4.2.5 was applied to six-day-old virgin male flies, adjusting the pulse time to 14 h. This was done to take into consideration findings in the Wilson laboratory and elsewhere indicating that the maturation time required for mCherry in *D. melanogaster* AGs is greater than for GFP.

After a 14 h-pulse, the expression of both fluorescent markers was chased at 17^{o}C through the time points 0, 24 and 48 hours. Fig. 4.14A shows high magnification images of characteristic SCs illustrating an overview of the chase results.

At 0 h, GFP and mCherry signals were not colocalising completely, indicating that the two markers were expressed and subsequently trafficked at different rates or along different pathways. GFP was detected in fewer compartments (Fig. 4.14A-B, numbers 1-4). Among the GFP-positive compartments detected at this time point, there was a pre-DCG compartment in which GFP signal was found at the limiting membrane, in membrane invaginations and in microvesicular structures around the compartment (Fig 4.15A-B, number 1). mCherry was localised similarly. A second, more rounded pre-DCG compartment displaying a stronger GFP and mCherry signal at the limiting membrane and fewer invaginations was also detected (Fig 4.15A-B, number 2). There was a very faint GFP-expressing DCG compartment in which the mCherry signal localised brightly at the core and limiting membrane (Fig 4.15A-B, number 3), while one other DCG compartment showed only mCherry signal in the core and at the limiting membrane (Fig 4.15A, number 4).

At this stage, both fluorescent markers were weakly detected at the apical and basolateral (Fig. 4.15A, yellow arrows) domains of the plasma membrane, suggesting that these markers are also rapidly trafficked to the cell surface, potentially independently of the DCG trafficking route.

By 24 h post-pulse, the basolateral plasma membrane had become clearly labelled with GFP and mCherry (Fig. 4.15A, yellow arrows). However, the localisation pattern

at the apical membrane was only detectable with GFP (data not shown). At this stage, the highest level of co-localisation in pre-DCG and DCG compartments was observed. In addition, not all DCG compartments showed fluorescence (Fig 4.15A, yellow asterices). Interestingly, one large acidic compartment sometimes had accumulated mCherry, but fluorescence from the GFP marker was never visible (Fig 4.15A, white arrows).

Lastly, at 48 h post-pulse, GFP and mCherry were still observed in the basolateral membrane (Fig 4.15A). Fluorescent signals were faint or absent in pre-DCG compartments (Fig 4.15A, white asterices) and it was possible to visualise occasional compartments in which only GFP was present (Fig 4.15A, yellow dashed arrow), while all the remaining fluorescent compartments carried both markers.

Altogether, these results reveal that both GFP-GPI and mCherry-GPI can be simultaneously expressed in the secretory compartments of the same SC. They traffic similarly, but surprisingly, mCherry seems to progress rather more rapidly, despite its longer maturation time. It also accumulates in large acidic compartments, although the absence of GFP from these compartments may be due to quenching at lower pH. Therefore, the mCherry-expressing system might be suitable to combine with other GFP markers to study differential trafficking, although there was insufficient time for me to pursue this during my thesis work.

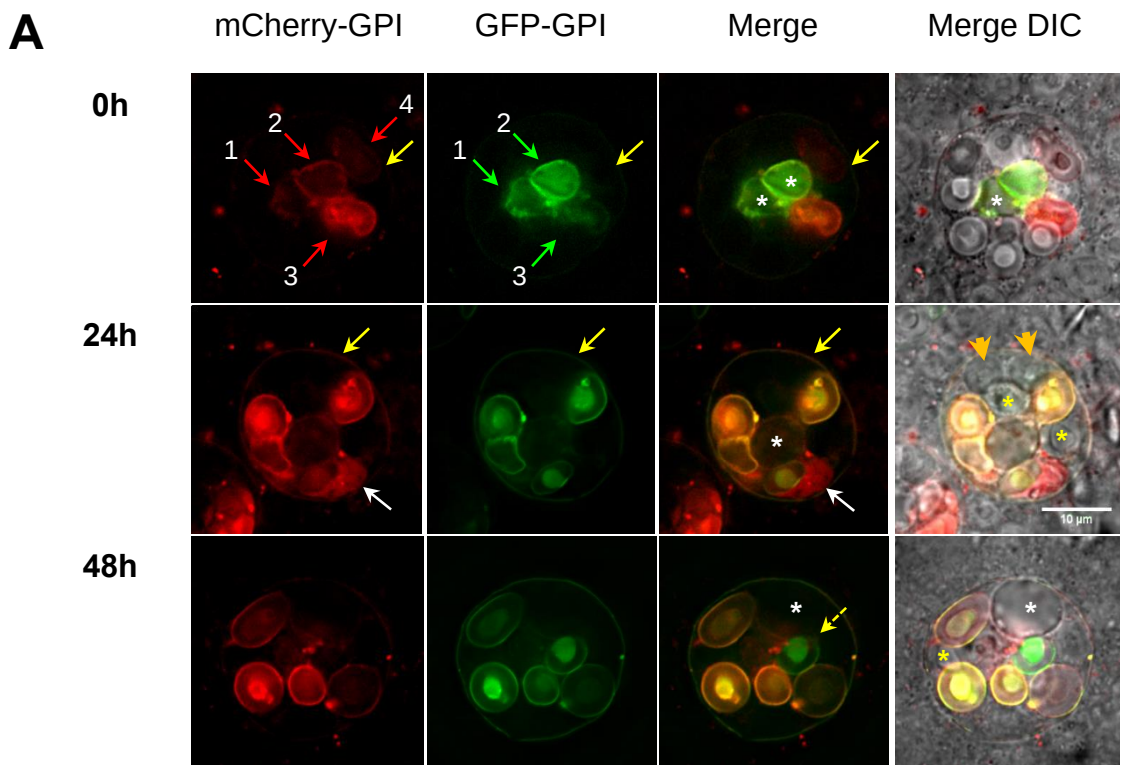
A
mCherry-GPI
GFP-GPI
Merge
Merge DIC
0h
24h
48h
1
2
3
4
10 µm

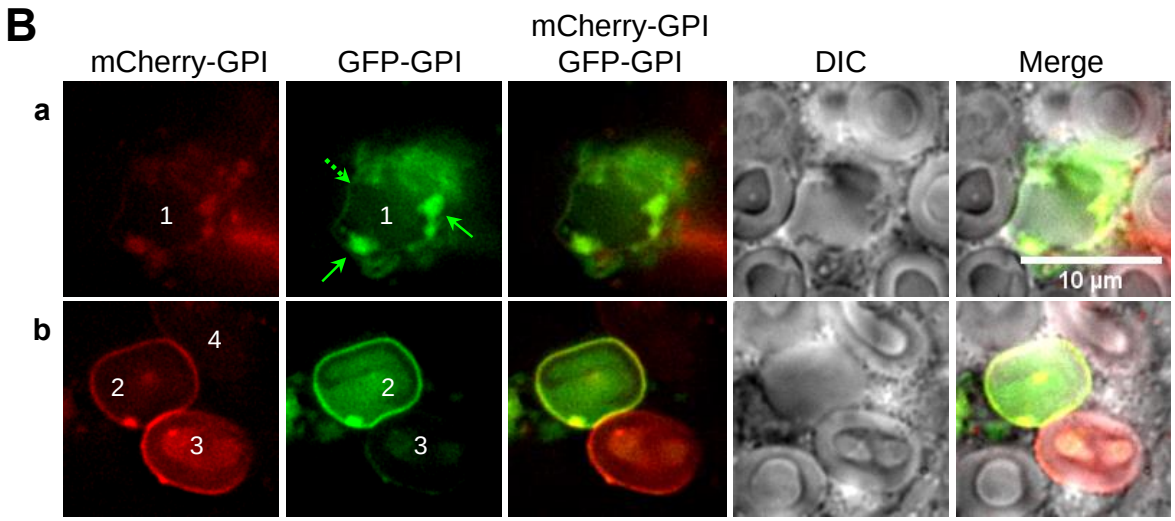
B
mCherry-GPI
GFP-GPI
mCherry-GPI
GFP-GPI
DIC
Merge
a
b
1
2
3
4
10 µm

Figure 4.14 **Pulse-chase experiment to follow simultaneous traffic of GFP-GPI and mCherry-GPI in SCs. A.** Wide-field and DIC high magnification images illustrating the simultaneous expression of GFP-GPI and mCherry-GPI after a 14-h pulse at 29ºC. The markers were chased for 0, 24 and 48 hours. **B.** Higher magnification views of the pre-DCG and DCG compartments observed at 0 h post-pulse. In **B** at 0 h, the subcellular labelling was as follows (indicated by numbers 1 and 4): GFP and mCherry were detected on a pre-DCG **(1),** in internal GFP- and mCherry-positive microvesicular structures and in foci of green signal in different regions of the limiting membrane (panel **Ba**, green arrows and green dashed arrows respectively); in a second pre-DCG **(2)**, displaying strong and continuous GFP and mCherry signals in the limiting membrane (**Bb**), while the content of this compartment appears weak and diffuse, and it is only marked with GFP except for a membrane invagination at bottom left; in a very faint GFP-expressing DCG compartment **(3)** where mCherry signal was localising more brightly at the core and limiting membrane; and finally in **(4)**, a compartment expressing only weak mCherry signal. At this stage, weak localisation of both fluorescent markers was seen in the basolateral plasma membrane (yellow arrows). At 24h (**A**), GFP and mCherry signals were clearly detected at the basolateral membrane (yellow arrows). At this time point all the non-acidic large compartments that were fluorescent carried both fluorescent tags (a pre-DCG is indicated with a white asterisk). An mMVBL (identified by DIC) labelled with mCherry signal was also present (white arrows). Not all the DCG compartments detected in this field of view were stained with fluorescent markers (yellow asterices, nuclei are indicated with orange arrowheads). At 48 h post-pulse, both markers were still found at the basolateral membrane, but were not clearly detected in the pre-DCG compartment (white asterisk). It was possible to visualise a DCG compartment in which only GFP was detected (yellow dashed arrow) whilst in this field of view, all the remaining fluorescent DCG compartments exhibited colocalisation of GFP and mCherry. Note that not all the DCG compartments were stained with fluorescent markers (yellow asterisk). The experiment was carried out using 6-day-old virgin males kept at 17ºC following eclosion until the pulse. The expression of the fluorescent marker was chased at 17ºC. Genotype of males was: *w; spi-GAL4 tub-GAL80^{ts}; UAS-GFP-GPI; mCherry-GPI*. Scale bars are shown in panels.

4.2.5.3. mCherry-GPI trafficking progression can be studied in SCs expressing the YFP-Rab11 gene trap

A further option for a multicolour study of SC membrane protein trafficking can be implemented using mCherry-GPI in combination with an endogenous YFP-tagged Rab11 protein (Dunst, Kazimiers et al. 2015), whose expression pattern in SCs has been studied in the Wilson laboratory. Overexpressed *YFP-Rab11* marks larger non-acidic compartments in SCs (Corrigan, Redhai et al. 2014, Redhai, Hellberg et al. 2016) and the gene trap has a similar expression pattern.

To investigate the trafficking dynamics of the GPI-mCherry when combined with the *YFP-Rab11* gene trap, I implemented a pulse-chase experiment using the strategy employed previously. Fig. 4.15 shows high magnification images of representative SCs, illustrating an overview of the chase results.

In general terms, the kinetics of mCherry-GPI trafficking were very similar to those in cells co-expressing GFP-GPI. Thus, at 0 h post-pulse, red signal was detected in the limiting membrane and membrane invaginations of a pre-DCG compartment. Rab11 only colocalised with mCherry within the invaginations and small compartments around the pre-DCG (Fig. 4.15). At this stage, mCherry had already been rapidly trafficked to the apical and basolateral domains of the plasma membrane (Fig. 4.15), suggesting an independent trafficking route to that observed in DCG compartments.

At 24 h there was more labelling of DCGs and their compartments by mCherry-GPI. In the image shown, there are two pre-DCG compartments with only the peripheral one displaying strong YFP-Rab11 staining, consistent with it being at a later stage of maturation. By 48 h, the proportion of mCherry-positive DCG compartments had decreased (Fig. 4.15, green asterices).

In summary, these results show that both mCherry-GPI and YFP-Rab11 can be simultaneously expressed in the same SC. Thus, engineering a red version of the GPI-anchored marker unlocks further options for multicolour live cell and real-time studies using molecules YFP or GFP, as well as mCherry-GPI.

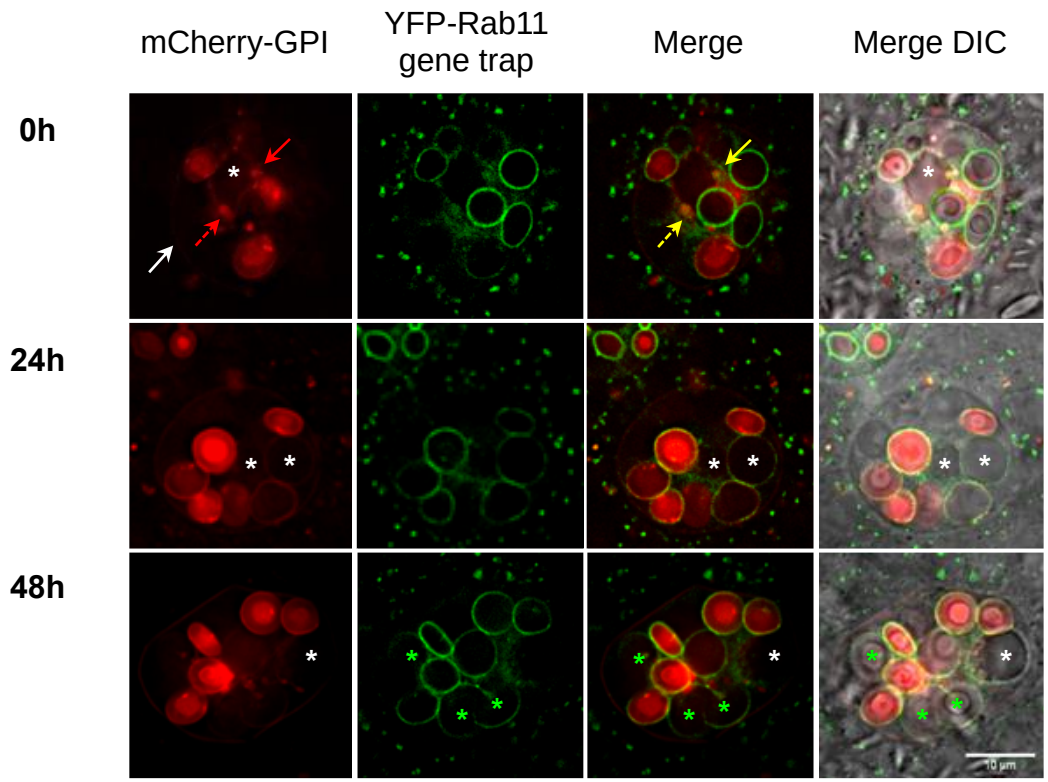

Figure 4.15 **mCherry-GPI in combination with YFP-Rab11 provides a multicolour system for the study of cargo trafficking in SCs.** Wide-field and DIC high magnification images illustrating mCherry-GPI trafficking when combined with the *YFP-Rab11* gene trap. A 14-h pulse at 29ºC was carried out using six-day-old virgin males kept at 17ºC from eclosion. After the pulse, the expression of the fluorescent marker was chased at 0, 24 and 48 hours at 17ºC. At 0 h, red signal is detected at the limiting membrane and in a membrane invagination (red arrow) inside a pre-DCG compartment (white asterices) and in structures around the compartment (red dashed arrow). Note that in the pre-DCG compartment, Rab11 seems to colocalise with mCherry at the invagination of the limiting membrane (yellow arrow) and in surrounding compartments (yellow dashed arrow). At this stage, red signal is detected at the basolateral plasma membrane (white arrow). At 24 h, the number of DCG compartments labelled with mCherry has increased. YFP-Rab11 is localised on the limiting membrane of one (right-hand) of the two pre-DCG compartments observed at this time point (white asterices), potentially illustrating different maturation with the more mature pre-DCG exhibiting a well-outlined limiting membrane. Variability in the localisation patterns of mCherry in DCG compartments (e.g. some dense cores were weakly labelled with mCherry) suggests different

maturation states for these organelles. By 48 h, more DCG compartments displayed only YFP expression (green asterices). Genotype of is: *w; spi-GAL4 tub-GAL80^{ts}; YFP-Rab11; mCherry-GPI*. Scale bars are shown in panels.

4.2.6. Loading of AnCE-eGFP into Dense-Core Granules appears to be Inhibited at 29^{O}C

In Section 4.2.3., I showed that the distribution of eGFP expressed from an *AnCE-eGFP* gene trap is completely transformed in male flies kept for six days at 29ºC (Section 4.2.3.2). In this experimental group, I was able to establish that none of the DCG compartments had eGFP inside the dense cores (Fig. 4.8A, n=55 SCs, from 13 different AGs), while at 17ºC all DCG compartments have eGFP signal (Fig. 4.8A). One possible explanation is that the AnCE-eGFP protein cannot be loaded on new DCGs at this high temperature. Alternatively, high temperatures might lead to the diffusion of AnCE-eGFP out of previously formed DCGs. Since most SC experiments in the laboratory are performed at 29ºC, I sought to investigate this issue further.

I applied a 14 h 29ºC temperature shift to males expressing both the *AnCE-eGFP* and CFP-tagged *rab6* gene traps, and subsequently documented changes in the location patterns of the fluorescent markers at three time points at 17ºC (0, 16 and 48 h). We reasoned that CFP-Rab6 marks recently formed large non-acidic compartments in SCs (Section 4.2.3.1; Fig. 4.7) and would therefore highlight the

most immature compartments. These include compartments that do not contain a DCG (pre-DCG compartments). Unlike the *YFP-Rab6* gene trap, several DCG-containing compartments are also marked, suggesting that CFP-Rab6 may be abnormally retained on DCG compartments during early stages of their maturation. Using this gene trap as a marker of recently formed DCG compartments in combination with DIC, I tested which compartments failed to incorporate AnCE-eGFP following a temperature pulse (Fig. 4.16).

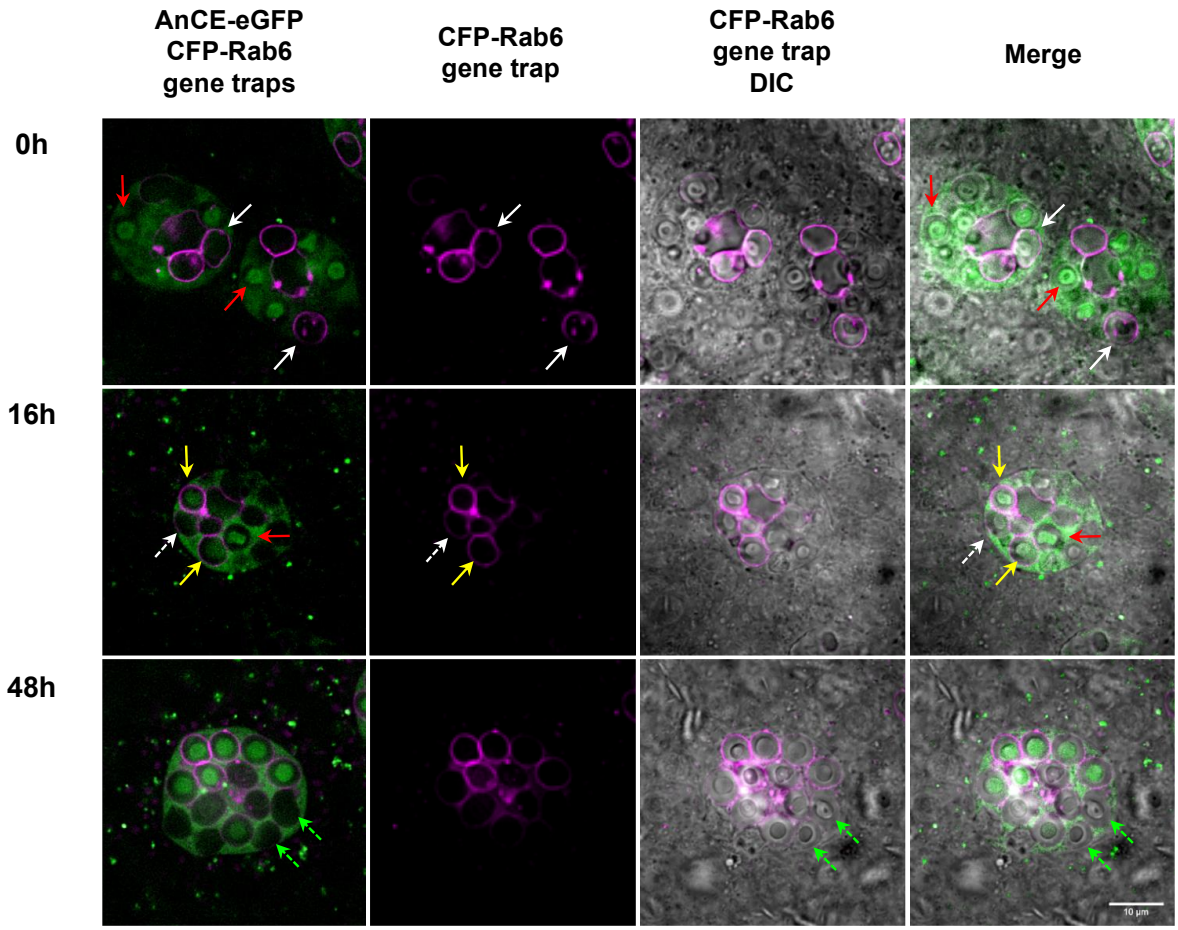

Figure 4.16 **High temperature affects the localisation of the AnCE-eGFP protein in the cores of newly formed DCGs compartments in SCs**. Wide-field fluorescence and DIC high magnification images of SCs expressing the *AnCE-eGFP* and CFP-tagged *rab6* gene traps simultaneously. A temperature shift to 29ºC

was applied for 14 h to 6-day-old-virgin male flies previously kept at 17ºC following eclosion. Flies were returned to 17ºC and the expression of the fluorescent markers was studied at 0, 16 and 48 hours. At 0 h, recently formed DCG compartments differentially labelled with Rab6 did not exhibit eGFP localisation in the dense cores (0h, white arrows) whilst in mature DCG compartments eGFP was detected in DCGs (0h, red arrows). After 16 h, eGFP was present in the core of newly formed Rab6-positive DCG compartments (yellow arrows). Interestingly, at this stage, no eGFP labelling was found in some more mature DCG compartments (weaker CFP-Rab6 is detected in their limiting membrane; indicated by white dashed arrows). eGFP-positive, Rab6-negative DCG compartments are also displayed (red arrow). Lastly, at 48 h only in the most mature (CFP-negative) DCG compartments have no eGFP (green dashed arrows). Scale bar is shown in the lower right panel.

SCs imaged immediately after males were returned to 17ºC (0 h) did not contain any eGFP-positive DCGs in Rab6-positive compartments (Fig. 4.16, white arrows), suggesting that the DCGs formed at 29ºC had not incorporated AnCE-eGFP. By contrast, many other presumably more mature DCG compartments did contain AnCE-eGFP (Fig. 4.16, red arrows), indicating that the temperature shift did not lead to the dispersion of GFP from more mature DCGs. Consistent with this idea, by 16 h, the time required to make roughly two new DCG compartments, Rab6-positive DCG compartments contained AnCE-eGFP (Fig. 4.16, yellow arrows), while there were some more mature DCG compartments that did not include eGFP (Fig. 4.16, white dotted arrows). These are likely to contain DCG compartments that were formed at 29ºC, while eGFP-positive, Rab6-negative DCGs (red arrows) are most likely to have been formed prior to the temperature shift.

By 48 h, even in SCs where most of the DCG compartments are marked by CFP-Rab6, only the Rab-negative DCGs are eGFP-negative, consistent with them representing the most mature DCGs in the cell that have not yet been released.

Taken together, I can conclude that DCGs formed at 29^{o}C do not appear to incorporate AnCE-eGFP, but preformed DCGs do not lose this protein when the temperature is raised. My data are most consistent with the contents of each DCG being stable after formation. Although there is no evidence that there are major effects on male fertility at 29^{o}C, my data do suggest that DCGs in SCs may change their contents at this temperature. However, there is no evidence that localisation of endogenous AnCE is altered under these conditions, so it is possible that this phenomenon reflects a fusion protein-specific event, perhaps due to protease cleavage of the molecule. Nevertheless, it would be interesting in the future to compare post-mating responses in females in more detail using males at different temperatures to test whether there is any detectable effect on these physiological processes.

4.3. Discussion

At the start of this chapter, I set out to develop the *Drosophila* secondary cell system of the male accessory gland as a new model to study dense-core granule biogenesis and secretion. My study was driven by several previous observations and the goal to advance these further. First, SCs have remarkably large DCGs, potentially permitting these structures to be analysed in unparalleled detail. Second, although some characterisation of SC DCGs had already been reported (Rylett, Walker et al. 2007, Corrigan, Redhai et al. 2014, Redhai, Hellberg et al. 2016), major issues, such as how the morphologically different compartments in SCs might be functionally linked, had not been addressed. And third, if SC studies could be developed further, it would provide a new *in vivo* model to analyse the fundamental mechanisms by which DCGs are formed, a topic addressed in the following chapter. Furthermore, if real-time imaging could be pioneered in this system, it might provide the first opportunity in any model to visualise the formation of DCGs as each compartment matures.

Although I analysed a small number of markers for SC DCG compartments using antibodies, I found that live cell fluorescent markers associated with gene traps and GAL4/UAS overexpression constructs provided much more powerful tools that frequently did not disrupt SC cell biology. Furthermore, using Delta Vision Elite imaging system, I was able to combine DIC and fluorescence microscopy (Section 4.2.2) and use DIC to confirm that the phenotypes observed by fluorescence were maintained in cells that were not expressing fluorescent constructs. Ultimately, this live cell imaging approach allowed me to characterise the trafficking route by which

DCG compartments are formed and permitted the visualisation of DCG biogenesis in real time.

4.3.1. Live markers for *in vivo* SC biology

In this chapter, I report the SC expression patterns of fluorescent markers, including UAS-regulated GPI-anchored GFP and mCherry, AnCE-eGFP, DE-Cad-tRFP, and YFP- and CFP-tagged *Rab* gene traps. By assessing the numbers of DCG compartments in these genetic backgrounds and wild type cells, I demonstrate that unlike CD63-GFP (Redhai, Hellberg et al. 2016), these constructs do not significantly affect the numbers of DCGs in SCs. In fact, the variable that does alter DCG number is temperature, with more DCGs observed in SCs at 17^{o}C compared to 29^{o}C (Section 4.2.4), suggesting that temperature must be carefully controlled in experiments using these cells. I also demonstrated that SiR-Hoechst could be used to mark SC nuclei in living glands.

Importantly, however, the trafficking and/or stability of individual markers can be affected by the fluorescent tag. For example, a GPI-anchored form of mCherry appears to traffic much more extensively into SC acidic compartments. The aggregation of red fluorescent proteins is sometimes linked to toxicity (Shemiakina, Ermakova et al. 2012), which may explain this different behaviour. The *CFP-Rab6* gene trap provided another interesting example, since it not only marked non-acidic, non-cored large compartments strongly, but was also observed on several DCG compartments. Anti-Rab6 antibody staining and the *YFP-Rab6* gene trap did not

pick up such extensive DCG localisation, suggesting that the CFP tag might be stabilising the Rab6 protein on compartments from which it would normally be lost. My findings do not exclude the use of these markers in DCG analysis, but they highlight that care must be taken in interpreting differential trafficking of markers that may primarily be explained by the fluorescent tag rather than the tagged protein.

One other surprising observation was that fusion protein from the *AnCE-eGFP* gene trap is not incorporated into DCGs at 29^{o}C, but is trafficked normally at lower temperatures. This suggests that there are temperature-dependent trafficking mechanisms that remain to be characterised in SCs or that the integrity of the AnCE-eGFP marker in these cells is sensitive to temperature. Fortunately, only AnCE-eGFP exhibited this unusual behaviour, while the DCGs appeared normal, and AnCE itself was still trafficked to DCGs at high temperatures, indicating that there is no fundamental problem with analysing DCG biogenesis at 29^{o}C, where many of our previous experiments have been performed.

Overall, my analysis confirmed that I could use several distinct fluorescent markers to identify different compartments in SCs, allowing me to make two major conclusions: (1) Non-acidic, non-cored compartments are precursors for DCG compartments; (2) DCG markers like GFP-GPI can be followed as they traffic through the DCG secretory compartment and appear to accumulate in these compartments at more than one stage of maturation. Both points are considered in more detail below.

4.3.2. Non-acidic, non-cored large compartments in SCs are precursors for DCG compartments

Initially by using DIC microscopy of living SCs in collaboration with B. Kroeger, I was able to demonstrate that non-cored, non-acidic compartments in SCs convert into DCG compartments over a period of about 4 hours. Notably, these non-cored compartments mature through a number of stages (Section 4.2.2.2). Although initially irregular in morphology, they round up and then shrink in size, prior to the beginning of internal condensation events that form the DCG. Importantly, these findings eliminate the hypothesis that the non-acidic, non-cored compartments are sorting hubs for macromolecules destined for different SC compartments. Instead, they appear to be immature stages in compartment maturation, and the small vesicles that surround them during the maturation process are presumably involved in trafficking key molecules to and from these structures. Whether these central compartments always become DCG compartments remains to be fully investigated, but since DCG compartments are the most abundant compartments formed in SCs, it seems likely that this maturation event is commonplace.

These conclusions were backed up by my analysis of the *CFP-Rab6* gene trap. YFP-Rab6 was identified in a screen of *Rab* gene traps by B. Kroeger as a marker for non-cored, non-acidic compartments; CFP-Rab6 provided a convenient alternative marker that could be combined with green fluorescent markers to analyse the maturation process. Its presence on a discrete subset of DCG compartments is consistent with the idea that these compartments may be less mature than CFP-Rab6-negative DCG compartments. This hypothesis should now

be testable by undertaking GFP-GPI pulse-chase experiments in a *CFP-Rab6* background, but is already supported by the temperature-shift experiments I have undertaken with the *AnCE-eGFP* and *CFP-Rab6* gene traps.

4.3.3. Pulse-chase experiments suggest complex trafficking routes for DCG cargos

To further confirm that cored and non-cored non-acidic compartments are functionally linked, I undertook a series of pulse-chase experiments, particularly focusing on the GFP-GPI fusion. These experiments clearly showed that GFP-GPI reached the non-acidic, non-cored compartments prior to DCG compartments, consistent with the maturation process discussed above.

One other interesting observation in these experiments was the high level of accumulation of GFP-GPI in dense cores, much higher than is ever seen at the limiting membrane. This suggests that GFP-GPI continues to be trafficked into these compartments once the DCG starts to form. Subsequent experiments from B. Kroeger are consistent with the idea that these compartments receive input from the endosomal system as they mature, suggesting that GFP-GPI may traffic by multiple routes into these structures.

Overall, my analysis demonstrates that live fluorescent markers combined with DIC can be used in SCs to visualise DCG biogenesis, and has identified a new step in maturation that can be distinguished by Rab6. In addition, my work has identified

highly specific protein localisations, such as that observed with DE-Cad-tRFP, which suggest a previously unsuspected complexity of membrane organisation on DCG compartments that will require much more detailed analysis in the future. For example, one interesting observation is that this DE-Cad staining appears to coincide with positions where intraluminal vesicles bud off from the limiting membrane of DCG compartments. It will be extremely interesting to test whether this association has a functional link.

Armed with the newly characterised fluorescent markers described above, I set out to test whether DCG compartment formation in SCs might parallel events observed in mammalian DCG-containing cells, an analysis described in the next chapter.

5. Results Chapter: Secondary Cells as an *in vivo* system to study regulation of DCG biogenesis and maturation

In Chapter 4, I presented my analysis of several fluorescent markers for DCG compartments in SCs and discussed how they could be visualised in living cells to analyse the maturation of DCG compartments. I also described some real-time and pulse-chase analyses in this system, which led me to the conclusion that DCG compartments form from pre-DCG compartments that are Rab6-positive. These findings suggest that the SC model could provide a new and powerful genetic system to dissect out the *in vivo* regulation of DCG biogenesis and maturation.

However, for this to be the case, the process of DCG formation in these unusual cells containing huge DCG compartments would ideally need to be conserved with the process observed in mammalian cells, so that observations made in flies can be translated to more complex systems and perhaps inform human and clinical studies.

With this in mind, I set out to test the role of several genes that have previously been implicated in DCG formation in mammals, namely the components of the AP-1

adaptor complex and the small G-protein Arf1 involved in ER/Golgi traffic and secretion.

5.1.1. The Drosophila AP-1 complex

Drosophila encodes a AP-1 complex formed by the subunits AP-1γ, β-adaptin (encoded by CG12532), AP-1μ1 (also known as AP-47) and AP-1σ (Benhra, Lallet et al. 2011, Nakatsu, Hase et al. 2014).

Depletion of *AP-1γ*, *AP-1μ1* and *AP-1σ* by RNAi induced a misalignment of photoreceptor neuronal cells in larvae that subsequently affected the development of the adult compound eyes. In addition, these results contributed key evidence to establish a functional role of the AP-1 complex in the intracellular trafficking of Notch during the development of the compound eye in *D. melanogaster* (Kametaka, Kametaka et al. 2012). In epithelial cells of the *Drosophila* salivary glands, the biogenesis of mucin secretory granules is AP-1-dependent (Burgess, Jauregui et al. 2011).

In the *Drosophila* Sensory Organ Precursors *loss-of-function* and knockdown by RNAi screenings of the subunits *AP-1σ1*, *AP-1μ1* and *AP-1γ* have shown that the AP-1 complex is required for cell fate acquisition and is a negative regulator of Notch signalling (Benhra, Lallet et al. 2011).

5.1.2. *Drosophila* Arf79F, the homologue of mammalian Arf1

Arf1 belongs to the highly conserved ADP-ribosylation factor (ARF) family of GTP-binding proteins that are ubiquitously expressed in eukaryotic cells (D'Souza-Schorey and Chavrier 2006, Donaldson and Jackson 2011). ARF function is controlled by active-GTP- and inactive-GDP-bound cycles (D'Souza-Schorey and Chavrier 2006, Donaldson and Jackson 2011). Arf1 is involved in the formation of two forms of vesicles: Coat protein complex I (COPI)-vesicles that are trafficked through the Golgi and the *cis*-Golgi towards the ER, and clathrin-coated vesicles which are directed from the TGN to other membrane systems and the plasma membrane (D'Souza-Schorey and Chavrier 2006, Rodrigues, Shao et al. 2016).

Arf79F is the *Drosophila* homologue of Arf1 (ADP-ribosylation factor 1). In *Drosophila* adult wings and eyes, Arf79F and its interactor AP-1complex are essential regulators in the formation of membrane domains in polarised epithelial tissue (Carvajal-Gonzalez, Balmer et al. 2015). Arf79F is also required for correct conformation of the Golgi structure and biosynthesis of cleavage furrow in the development of the *Drosophila* early embryo (Rodrigues, Shao et al. 2016).

5.1.3. Screening for novel genes involved in DCG biogenesis

As a first step in identifying new genes that might control DCG formation in SCs, I decided to test the hypothesis that GPI-anchored proteins might play a role in this process. In Chapter 4, I provided evidence that the GPI-anchored protein Chaoptin is loaded into DCG compartments where it is found on intraluminal vesicles.

Furthermore, overexpressed GFP-GPI traffics to the dense cores themselves, although it remains unclear whether the GFP in the cores is GPI-anchored, because there is no evidence for membranes or lipids in these structures. To test the functional significance of these associations, I decided to test the role of genes involved in GPI addition, as well as Chaoptin, in the DCG biogenesis process.

The *chaoptin* gene (*chp*; FlyBase CG1744) encodes a 1315 amino acid (UniProt, P12024) Glycosylphosphatidylinositol (GPI)-anchored protein which has at least 13 N-glycosylation sites (Kanie, Yamamoto-Hino et al. 2009) and 38 Leucine-rich repeats (LRRs) - a conserved arrangement that accounts for 90% of the full-length protein (Reinke, Krantz et al. 1988, Rosenbaum, Brehm et al. 2012). The LRRs have been implicated in homotypic interactions on the extracellular side of the lipid bilayer. *chp* is very specifically expressed in the epithelial photoreceptor cells of the adult fly eye, where it performs crucial functions as a cell adhesion molecule and it is required for morphogenesis (Rosenbaum, Brehm et al. 2012, Gurudev, Yuan et al. 2014). Mutations in *chp* have been implicated in a severe reduction and disorganisation of the microvilli in the apical domain of photoreceptor cells (Van Vactor, Krantz et al. 1988, Gurudev, Yuan et al. 2014), resulting in retinal degeneration (Rosenbaum, Brehm et al. 2012). In light of its structure, it seems likely that this defect is caused by disruption of intermembrane contacts that may be required for the stereotypic microvilli organisation of photoreceptors.

A number of *PIG* genes have been implicated in the biosynthesis of the Glycosylphosphatidylinositol (GPI) moiety and its attachment to GPI-anchored proteins (GPI-APs) (Kinoshita 2014). GPI-APs are ubiquitous in eukaryotes, where

they can function as hydrolytic enzymes, virulence factors, adhesion molecules, extracellular receptors or extracellular matrix components (Kinoshita 2014, Ferguson, Hart et al. 2015, Kinoshita and Fujita 2016).

Fig. 5.1 illustrates the major biochemical reactions involved in the synthesis and subsequent attachment of GPI-APs to the ER membrane (Kinoshita 2014, Kinoshita and Fujita 2016).

Ethanolamine phosphate, three mannoses, glucosamine and inositol phospholipid constitute the highly conserved glycolipid core of GPI, which in turn is posttranslationally attached by a covalent bond to the C-terminal end of a protein to form a GPI-AP (Kinoshita 2014, Ferguson, Hart et al. 2015, Kinoshita and Fujita 2016).

Figure 5.1 **GPI anchor biosynthesis.** Schematic representation of the assembly process of a GPI-anchored protein in mammals. Numbers in brackets indicate 11 reactions for the synthesis and transfer of a GPI anchor to a protein on the endoplasmic reticulum (ER) membrane. The widely conserved core structural components are depicted in the lower part of the diagram and include a phosphatidylinositol (PI) moiety, a glucosamine moiety, three mannoses and ethanolamine phosphate. *Phosphatidyl Inositol Glycan* (*PIG*) genes linked to each reaction are indicated (red boxes denote PIGs assessed in this study, diagram from Kinoshita 2014).

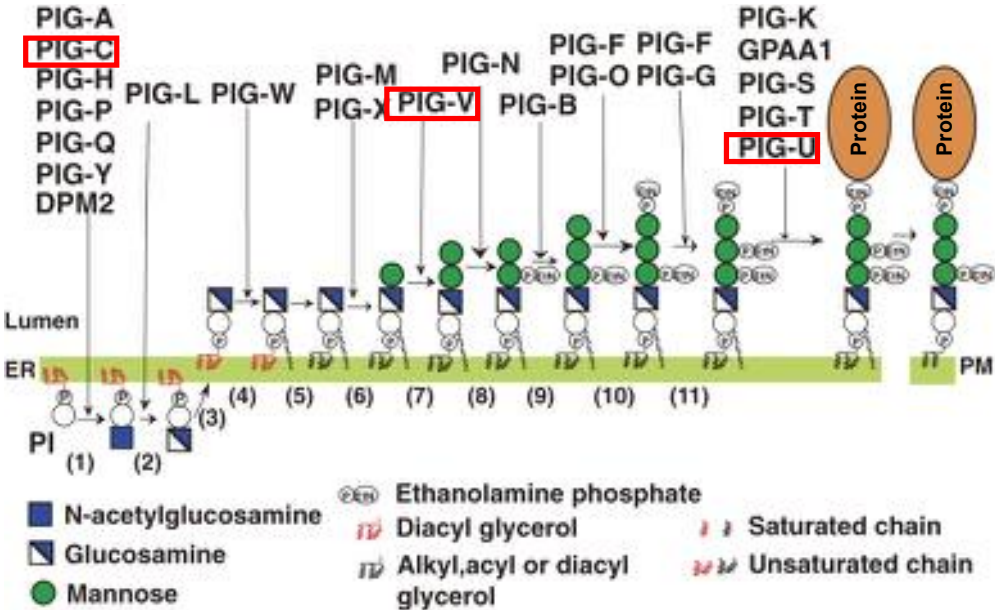

The reactions implicated in the formation of the common structural core of GPI-APs are widely conserved in eukaryotes (Ferguson, Hart et al. 2015, Kinoshita and Fujita 2016). In *Drosophila*, the biosynthesis of GPI anchors in *Drosophila* is not well characterised, but several reagents, particularly GAL4/UAS-regulated knockdown constructs have become available.

5.2. Aims

My key aims in this chapter were to test the functions of a number of different genes, some previously linked to mammalian DCG biogenesis in DCG formation using inducible (GAL80ts-mediated) SC-specific RNAi knockdown in the GFP-GPI genetic background to image DCGs in living cells. Those genes included:

1. Genes encoding components of the AP-1 complex
2. the Arf1 homologue Arf79F
3. representatives of the PIG gene family
4. the *chaoptin* gene, an SC-specific GPI-anchored protein

My hypothesis is that the genetic disruption of the conserved mammalian key regulators of DCG biogenesis also triggers changes in SCs in *Drosphila.* In addition, I hypothesise that knocking down genes involved in the GPI anchor biosynthesis, such as the members of the PIG family, would have an effect in the subcellular localisation of the GFP-GPI marker in SCs.

Thirdly, I hypothesise that depleting *chp* will cause a phenotypic effect in SCs given that it is expressed in AGs and seemed to play a functional role in the formation of DCGs and SC intracellular trafficking.

Overall my findings allow me to conclude that the SC system is well suited to the study of conserved mechanisms of DCG formation. Indeed, my results show a more detailed explanation for the mechanisms by which known DCG regulators function, suggesting that this model will be useful in dissecting out the in vivo genetics of DCG biogenesis in the future.

5.3. Results

5.3.1. Functional role of the Adaptor Protein-1 (AP-1) components in the biogenesis of DCG compartments

5.3.1.1. The *AP-1γ* subunit affects DCG biogenesis in SCs

Adaptor Protein complex 1, gamma subunit (FlyBase CG9113) encodes the AP-1γ subunit for which nine different transcriptional variants have been annotated to date (FlyBase AP-1γ-R_{A-E}; UniProt: Q9W388, Q86B59, Q7KVR7 and Q7KVR8). AP-1γ has been implicated in trafficking of cargos between the *trans*-Golgi network (TGN) and endosomes (Hirst, Sahlender et al. 2009). In Schneider's *Drosophila* Line 2 (S2) cells, AP-1γ localisation overlaps with the *cis*-Golgi GM130 marker. It is involved in protein loading into clathrin-coated vesicles, a role that is performed together with GGAs [Golgi-localised, γ-ear containing, ARF (ADP-ribosylation factor)-binding proteins] (Hirst, Sahlender et al. 2009).

To gain insight into the role of the AP-1*γ* subunit in the biology of SCs and test its functional role in the biogenesis of DCGs, I studied the effect of tissue-specific depletion of *AP-1γ* expression in SCs. These experiments were implemented in GFP-GPI-expressing AGs from six-day-old virgin males kept at 29ºC after eclosion

(n=30 SCs imaged from 6 different AGs; knockdown RNAi line is the TRiP line JF02684, BDSC 27533)

Fig. 5.2 shows representative high magnification images combining DIC and two fluorescent channels of SCs expressing both the GFP-GPI marker and *AP-1γ-RNAi* under *spitz*-GAL4 control. *AP-1γ*-depleted SCs exhibited severe phenotypic abnormalities with a consistent loss of normal morphology observed. The number of DCG compartments per SC dramatically decreased (n=30 SCs, taken from 6 different AGs; almost all cells had no DCG compartments). This was in striking contrast with control cells where the mean number of DCG compartments per cell was 7.5 ± 1.3 (n=60, in 13 different AGs).

A common novel phenotype observed in SCs depleted of *AP-1γ* was the presence of both oversized acidic and GFP-positive non-acidic, non-cored compartments with dimensions that frequently occupied nearly half of the SC area (indicated by white arrows in Fig. 5.2), and in some cells reached around 80% of the total cross-sectional area. These compartments were observed in 63% (n=19/30) of the cells under study. They exhibited a limiting membrane and an inner non-localised (diffuse) GFP signal, however none of the ILVs or GFP-GPI-positive invaginations that characterise control cells (Fig. 5.2) are present.

In 33% of *AP-1γ*-deficient SCs (n = 10/30), GFP-positive small to medium-sized compartments (around 3 µm in diameter) were also detected clustering around the medial plane of the cell and extending towards the basal region. In this group, it was possible to distinguish three different classes of compartment: (1) non-acidic, non-

cored compartments, (2) non-acidic compartments whose contents resembled dense cores, and (3) acidic compartments (Fig. 5.2, yellow, white and red dashed arrows respectively). In addition, some normal-sized DCG-like compartments were observed, however they exhibited a hazy GFP internal signal whose dense core could not be identified by DIC (Fig. 5.2, green arrows).

Enlarged acidic compartments, mMVBLs (≥10μm in diameter and positive for LysoTracker-Red; Fig. 5.2, red arrows) were found in 87% of the cells under analysis. Also, often the greatest GFP intensity in these cells was in the mMVBLs (Fig. 5.2, red arrows). However, the GFP in these compartments was homogeneously localised.

Finally, in knockdown SCs, the GFP signal in the apical and basolateral plasma membrane domains was abnormal. In 20% of the cells no GFP signal was detected at the plasma membrane, and in the other cases, the membrane expression was seen to be discontinuous and associated with vesicle-like structures (data not shown).

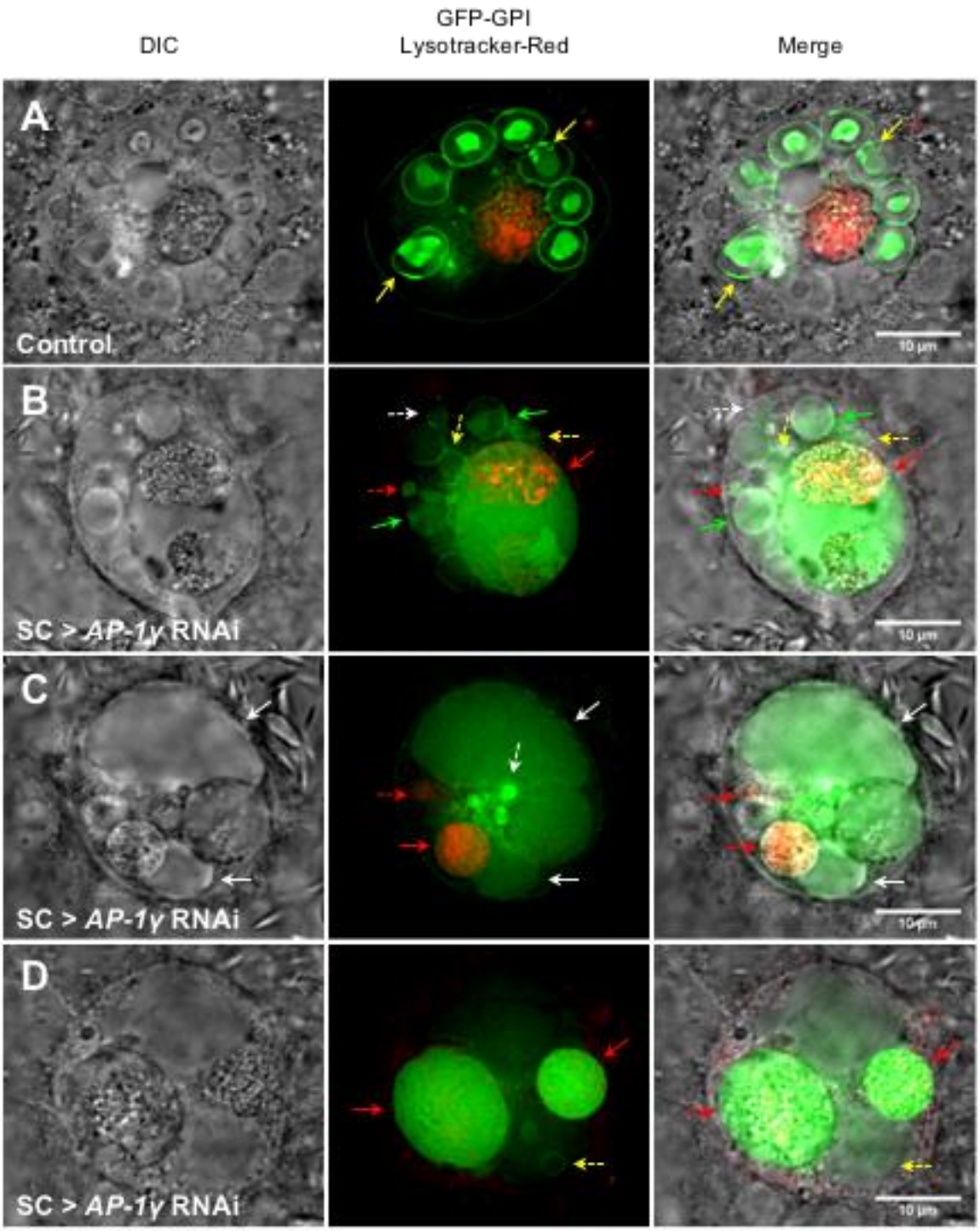
DIC
GFP-GPI
Lysotracker-Red
Merge
A
Control
B
SC > AP-1γ RNAi
C
SC > AP-1γ RNAi
D
SC > AP-1γ RNAi

Figure 5.2 ***AP-1γ* knockdown induces a pleiotropic phenotype affecting DCG compartments in SCs.** Wide-field fluorescence and DIC images of SCs expressing GFP-GPI under *spi*-GAL4 control with and without *AP-1γ*-RNAi. A. GFP-GPI-expressing control. Representative DCG compartments observed by DIC and GFP-GPI incorporation are indicated with yellow arrows. B-D. Remaining panels show SCs expressing *AP-1γ*-RNAi. GFP-positive compartments observed in *AP-1γ*-depleted SCs included: oversized non-acidic, non-cored compartments (white arrows), normal-sized DCG-like compartments, but with no DCG (green arrows in B), and small to medium-sized non-acidic (with and without internal content indicated by white and yellow dashed arrows respectively) as well as small acidic compartments (red dashed arrows). Large acidic mMVBLs were also found (red arrows). All virgin males were incubated at 29^{o}C following eclosion for 6 days. AGs were stained with LysoTracker Red. Genotype of knockdown males is: *w; spi-GAL4 tub-GAL80^{ts}; UAS-GFP-GPI/AP-1γ- RNAi*. Control does not express a UAS-RNAi construct. Scale bars are shown in panels.

5.3.1.2. Knockdown by RNAi of *AP-1µ1* also induces severe morphological abnormalities in SCs

To gain insight into the functional role of AP-1µ1 (FlyBase CG9388, also known in Drosophila as *AP-47*) in SCs, I examined the effect of knocking down the expression of this gene in GFP-GPI-expressing AGs from six-day-old virgin males kept at 29ºC after eclosion (n=42 SCs taken from 8 different AGs, GD14206 (VDRC 24017) RNAi line). Fig. 5.3 shows representative high magnification images combining DIC and two fluorescent channels of SCs expressing both the GFP-GPI marker and *AP-1µ1-RNAi* under *spitz*-GAL4 control.

The main morphological phenotype observed in these cells when compared with controls (Fig. 5.3) was a drastic decrease in the number of DCG compartments per SC (from a mean of 7.5 ± 1.3, n=60 SCs from 13 different control AGs to 1.8 ± 1.4, n=42 from 8 different AGs). Most resulting DCG compartments also exhibited aberrant morphologies with a few exceptions. For example, DIC microscopy revealed dense cores that were not characteristically positioned in the centre of the DCG compartment, maintaining one or several contact points with the limiting membrane. Additionally, the GFP signal in the limiting membrane of DCGs often appeared reduced or even absent (indicated by yellow dotted arrows in Fig. 5.3B-C).

The GFP-positive intra-luminal vesicles associated with DCG compartments in control cells (indicated by yellow arrows in Fig. 4.9B and in Fig. 5.3A) were frequently absent or difficult to identify in knockdown cells. Typically, these vesicles

link the DCG with the limiting membrane in control cells, but in knockdown cells, these links seemed to be extensions of the core structure itself.

Although some normal-sized non-acidic, non-cored compartments were observed (mean 0.45 ± 0.74; n=42 SCs taken from 8 different AGs), such organelles did not conform to the description of pre-DCGs outlined in Section 4.2.3.1. They exhibited a weak homogeneous internal GFP signal and did not contain GFP-GPI-positive invaginations or GFP foci at the limiting membrane. Enlarged and small-sized non-acidic, non-cored compartments were also detected in *AP-1μ1*-deficient SCs (Fig. 5.3B, white dashed arrows).

Large acidic compartments, mMVBLs (>2 μm in diameter and positive for LysoTracker-Red; Fig. 5.3, red arrows) were present in all knockdown cells under analysis. Their abundance was very similar to that scored for DCGs. In the majority of SCs studied, the organelles that exhibited the greatest overall GFP intensity were mMVBLs (Fig. 5.3B, red arrows). However, the localisation of GFP inside these compartments was homogeneous.

In these SCs, GFP signal in the apical and basolateral plasma membrane was also abnormal. In 30% of the cells no GFP signal was detected at the plasma membrane, and in all the other cases the membrane labelling was discontinuous and involved vesicle-like structures.

Figure 5.3 ***AP-1µ1* knockdown disrupts DCG compartment biogenesis in SCs.** Wide-field fluorescence and DIC images of SCs expressing GFP-GPI under *spi*-GAL4 control with and without *AP-1µ1*-RNAi. A. GFP-GPI-expressing control. Representative DCG compartments observed by DIC and GFP-GPI incorporation are indicated with yellow arrows. B-C. Remaining panels show SCs expressing *AP-1µ1*RNAi. GFP-positive compartments observed in depleted cells included: DCG compartments (mean = 1.8 ± 1.4 per SC; indicated by yellow dashed arrows, most of which exhibited aberrant morphologies) and non-acidic, non-cored compartments of variable size (white dashed arrows in B). Large mMVBLs were also detected (red arrows). All virgin males were incubated at 29ºC following eclosion for 6 days. Nuclei are indicated by yellow asterices. AGs were stained with LysoTracker Red. Genotype of knockdown males is: *w; spi-GAL4 tub-GAL80^{ts}; UAS-GFP-GPI/AP-1µ1- RNAi*. Control does not express a UAS-RNAi construct. Scale bars are shown in panels.

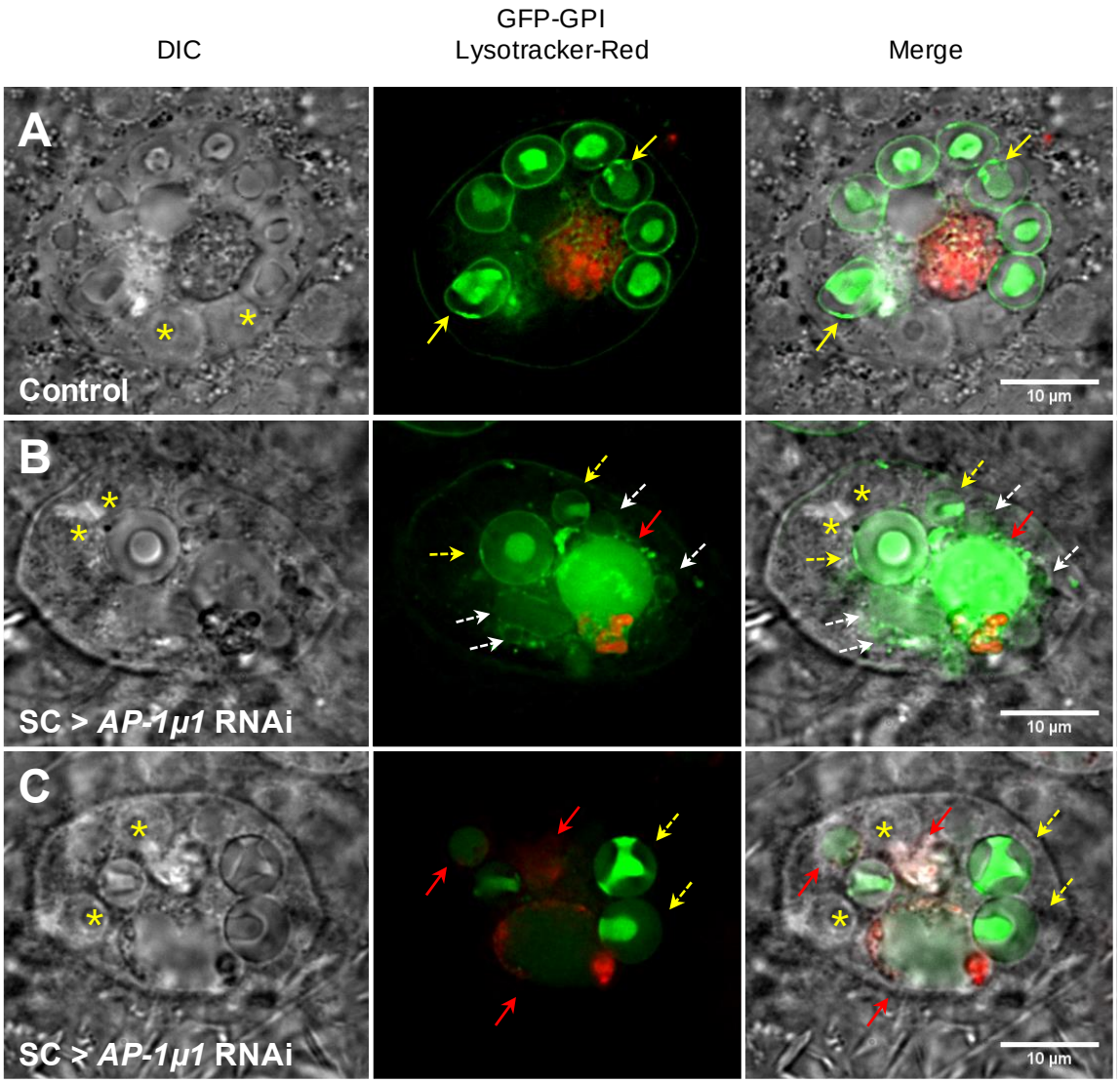
DIC
GFP-GPI
Lysotracker-Red
Merge
A
Control
B
SC > AP-1μ1 RNAi
C
SC > AP-1μ1 RNAi
10 μm
10 μm
10 μm

To better understand the effect of *AP-1µ1* depletion in SCs, I studied SCs that were simultaneously expressing the *YFP-Rab-11* gene trap (Dunst, Kazimiers et al. 2015) and *AP-1µ1-RNAi* under *spitz*-GAL4 control. Fig. 5.4 shows representative images combining DIC and two fluorescent channels of these SCs. *AP-1µ1*-depleted SCs exhibited the same severe phenotypic abnormalities observed with the GFP-GPI marker. In this case, abnormal DCG compartments carried Rab11 at their limiting membrane, consistent with a model in which they mature more normally than compartments in *AP-1γ* knockdown SCs, but still fail to make DCGs of normal morphology. I conclude that like *AP-1γ*, *AP-1µ1* is required for normal DCG biogenesis in SCs.

Figure 5.4 **YFP-Rab11 localises at the limiting membrane of DCG compartments in *AP-1µ1*-deficient SCs**. Wide-field fluorescence and DIC images of SCs expressing the *YFP-Rab11* gene trap and *AP-1µ1-RNAi* under *spi*-GAL4 control. A. YFP-Rab11-expressing control showing the characteristic localisation of the endogenous YFP-tagged protein at the limiting membrane of DCG compartments. B-C. *AP-1µ1*-RNAi-expressing SCs exhibiting a drastic reduction in the number of DCG compartments. YFP-Rab11 localised at the limiting membranes of non-acidic, DCG and non-DCG-containing compartments that exhibited abnormal morphologies (yellow dashed arrows). Some YFP-positive small-sized non-acidic compartments were also detected (around 3 µm in diameter, indicated by white dashed arrows). Enlarged mMVBLs were detected that did not appear to be YFP-positive (red arrows). All virgin males were incubated at 29ºC following eclosion for 6 days. AGs were stained with LysoTracker Red. Genotype of knockdown males is: *w; spi-GAL4 tub-GAL80^{ts}; YFP-Rab11/AP-1µ1- RNAi*. Control does not express a UAS-RNAi construct. Scale bars are shown in panels.

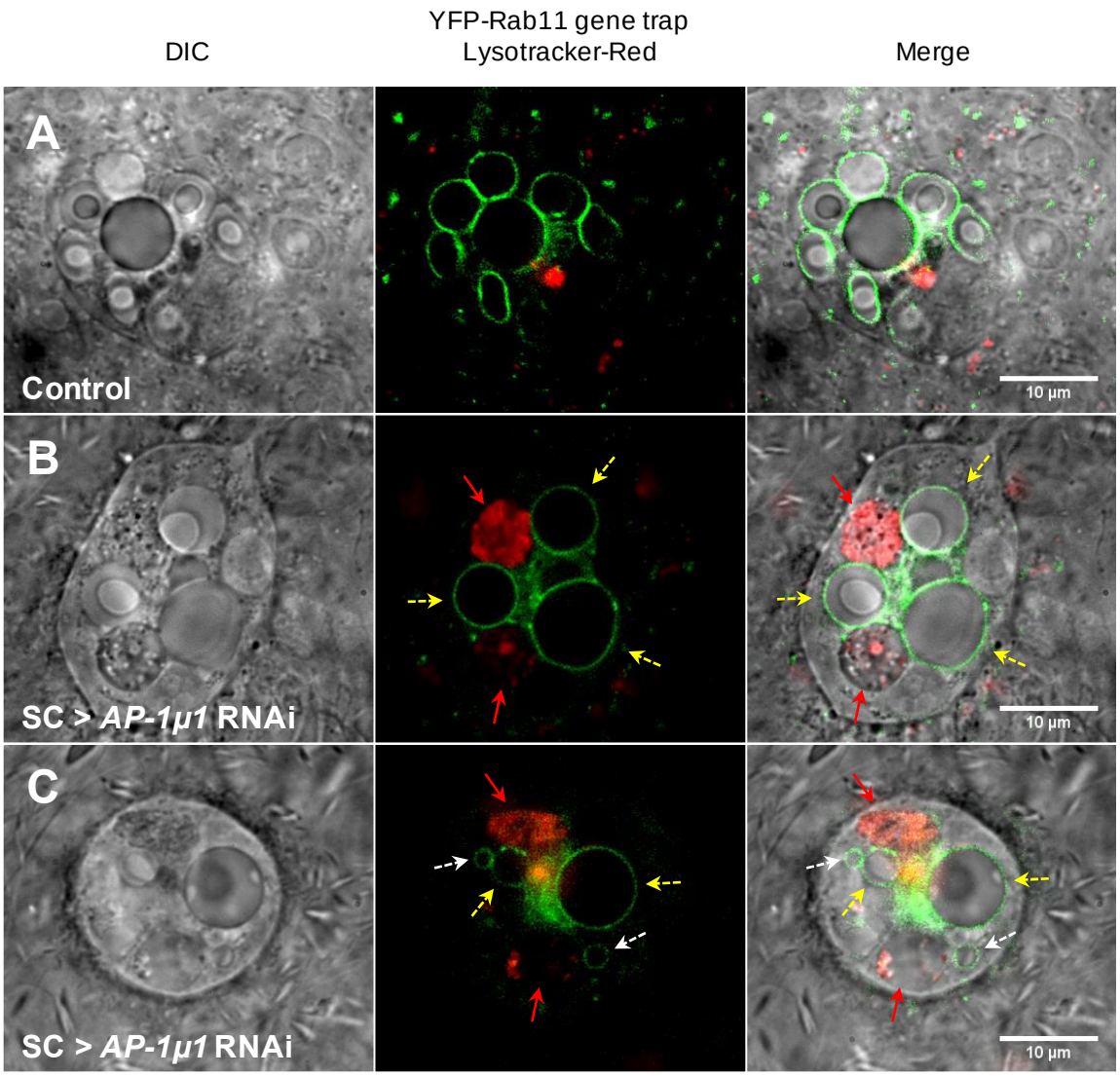
DIC
YFP-Rab11 gene trap
Lysotracker-Red
Merge
A
Control
10 µm
B
SC > AP-1µ1 RNAi
10 µm
C
SC > AP-1µ1 RNAi
10 µm

5.3.1.3. Knockdown by RNAi of the *AP-1σ1* subunit has no detectable effect on SCs

To gain insight into the functional role of *AP-1σ1* (FlyBase *CG5864*) in SCs, I tested two independent RNAi lines for this gene (RNAi1 is KK108869, VDRC107322, belongs to the Vienna library, n=40 SCs from 8 glands; RNAi2 from the TRiP library designated as HMS02143, BDSC40895, n=30 SCs from 6 glands). My results suggested that there was no phenotypic effect of knockdown in *spitz-GAL4-GAL80^{ts}* SCs from six-day-old virgin males kept at 29^{o}C following eclosion when compared with GFP-GPI-expressing controls (Fig. 5.5).

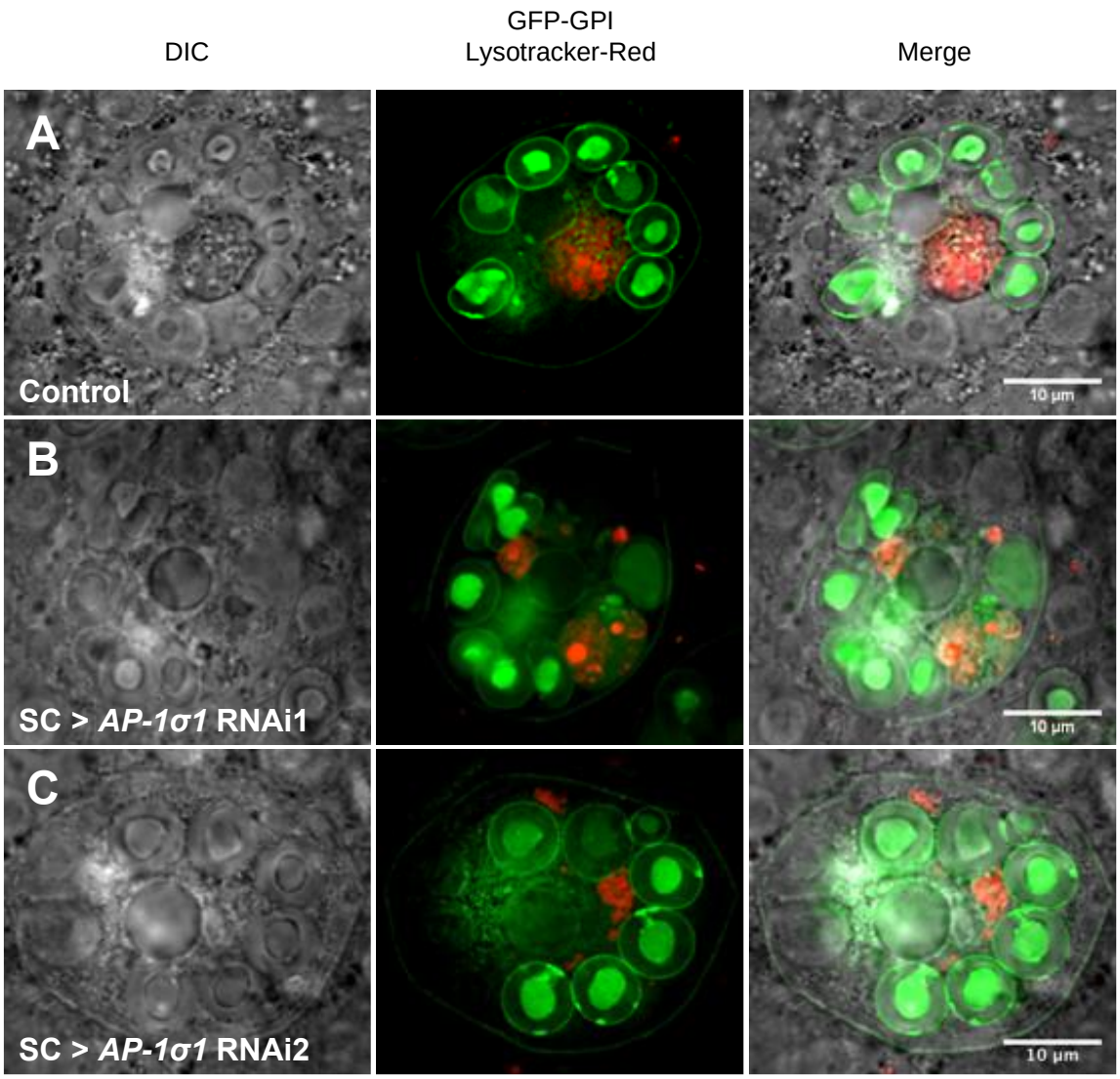

Figure 5.5 ***AP-1σ1* knockdown has no consistent phenotypic effect on SCs.** Wide-field fluorescence and DIC images of SCs expressing GFP-GPI under *spi*-GAL4 control with and without *AP-1σ1*-RNAi. **A.** GFP-GPI-expressing control. **B-C.** Remaining panels show SCs expressing two different *AP-1σ1*-RNAi lines whose genotypes are: *w; spi-GAL4 tub-GAL80^{ts}/ AP-1σ1- RNAi1; UAS-GFP-GPI* and *w; spi-GAL4 tub-GAL80^{ts}; UAS-GFP-GPI/AP-1σ1- RNAi2*. All virgin males were incubated at 29^{o}C following eclosion for 6 days. AGs were stained with LysoTracker Red. Control does not express a UAS-RNAi construct. Scale bars are shown in panels.

5.3.2. The *Arf79F* subunit affects DCG biogenesis in SCs

To study the functional role of Arf79F in the biology of SCs and determine whether it might function in the biogenesis of DCG compartments, I studied the effect of tissue-specific knockdown by RNAi of Arf79F. These experiments were implemented in AGs expressing both GFP-GPI and Arf79F-RNAi under *spitz*-GAL4 control. Three independent RNAi lines (1-3 respectively) were tested, v23082 (GD12522), v103572 (KK101396) and TRiP line JF01809, the first two of which produced very strong phenotypic effects on DCGs.

Knockdown with both RNAi1 (Fig. 5.6) and RNAi2 (Fig. 5.7) produced SCs that typically did not contain normal DCG compartments. Most notably, there was no concentration of GFP-GPI in the core regions and there were no normal visible DCGs by DIC. Instead, GFP-GPI was distributed diffusely in these compartments. Although the number and size of these non-acidic compartments was quite variable for RNAi1 (Fig. 5.6B-D), it was more consistent for RNAi2 and comparable to control cells in many cases (Fig. 5.7B-D). Changes to acidic compartments were more variable. By contrast, knockdown with RNAi3 had subtle, if any, effects on SCs with the most consistent change being the more variable morphology of DCGs in some compartments (Fig. 5.8).

Since two RNAis give very similar and unusual phenotypes in SCs, which have not been observed with many other RNAis tested, it seems likely that Arf79F is required for the establishment of DCG compartments. The much weaker phenotypes observed with RNAi3 (Fig. 5.8 B-D) presumably indicate that this RNAi has much

less effect on Arf79F expression. Notably a subsequent analysis undertaken by B. Kroeger and presented in his DPhil thesis indicated that the ‘empty’ non-acidic compartments produced by RNAi1 are not Rab11-positive, suggesting that the maturation of large non-acidic compartments in this background is impaired and potentially explaining the absence of DCGs.

Figure 5.6 ***Arf79F* knockdown disrupts DCG compartment biogenesis in SCs.** Wide-field fluorescence and DIC images of SCs expressing GFP-GPI under *spi*-GAL4 control with and without *Arf79F*-RNAi1, v23082. **A.** GFP-GPI-expressing control. Representative DCG compartments observed by DIC and GFP-GPI incorporation are indicated with yellow arrows. **B-D.** SCs expressing *Arf79F*-RNAi1. Note that all cells lack normal GFP-GPI-labelled DCG compartments. Large non-acidic compartments of variable size are present, some of which contain diffuse GFP fluorescence, but DCGs are completely absent, as judged by DIC as well as GFP-GPI staining (yellow dashed arrows). Acidic compartments are not consistently altered (red arrows). All virgin males were incubated at 29ºC following eclosion for 6 days. Nuclei are indicated by yellow asterices. AGs were stained with LysoTracker Red. Genotype of knockdown males is: *w; spi-GAL4 tub-GAL80^{ts}; UAS-GFP-GPI/Arf79F-RNAi1*. Control does not express a UAS-RNAi construct. n=50 SCs from 10 AGs. Scale bars are shown in panels.

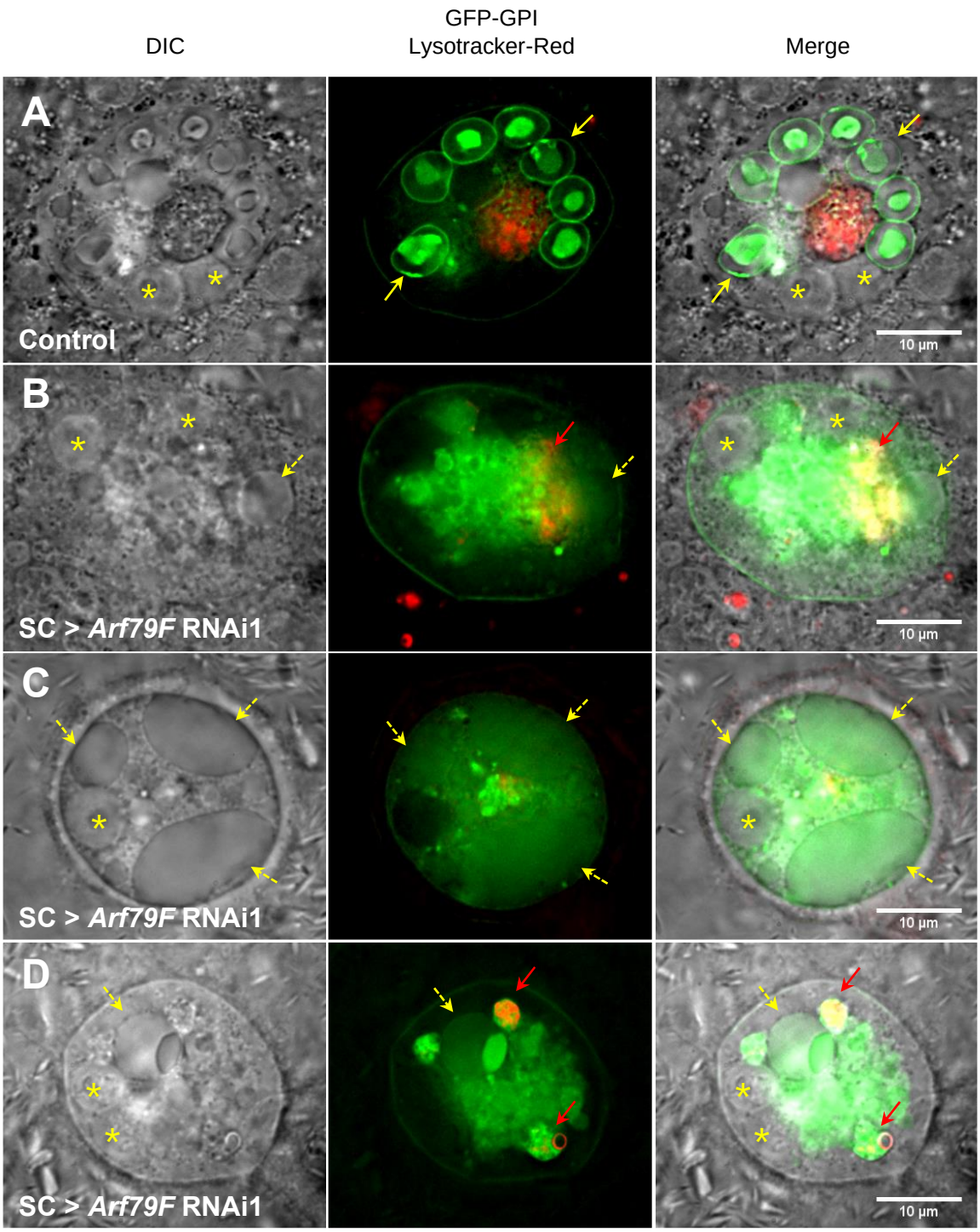
DIC
GFP-GPI
Lysotracker-Red
Merge
A
Control
B
SC > Arf79F RNAi1
C
SC > Arf79F RNAi1
D
SC > Arf79F RNAi1
10 µm
10 µm
10 µm
10 µm

Figure 5.7 ***Arf79F* knockdown with a second RNAi disrupts DCG compartment biogenesis in SCs.** Wide-field fluorescence and DIC images of SCs expressing GFP-GPI under *spi*-GAL4 control with and without *Arf79F*-RNAi2, v103572. **A.** GFP-GPI-expressing control. **B-D.** SCs expressing *Arf79F*-RNAi2. While in some cells (B), a relatively normal pattern of DCG compartments is observed, many SCs lack normal DCG compartments (by DIC and fluorescence) and instead contain diffuse GFP in their lumen. Note that all cells lack normal GFP-GPI-labelled DCG compartments (abnormal compartments are indicated by yellow dashed arrows). In some cases, there are near-normal numbers of large non-acidic compartments. No major effects on acidic compartments were observed (red arrows). All virgin males were incubated at 29^{o}C following eclosion for 6 days. Nuclei are indicated by yellow asterices. AGs were stained with LysoTracker Red. Genotype of knockdown males is: *w; spi-GAL4 tub-GAL80^{ts}; UAS-GFP-GPI/Arf79F-RNAi2*. Control does not express a UAS-RNAi construct. n=32 SCs from 7 AGs. Scale bars are shown in panels.

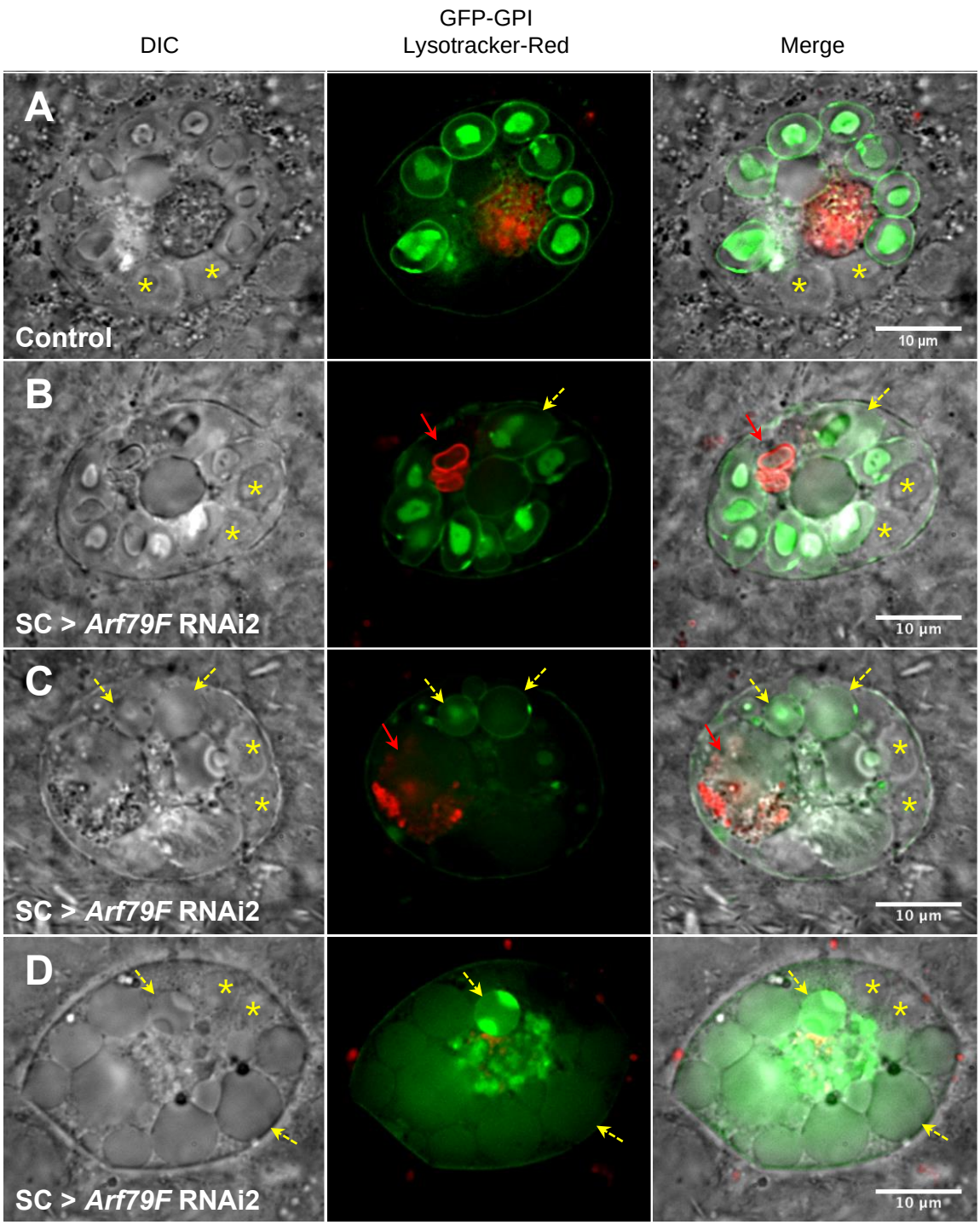
DIC
GFP-GPI
Lysotracker-Red
Merge
A
Control
10 µm
B
SC > Arf79F RNAi2
10 µm
C
SC > Arf79F RNAi2
10 µm
D
SC > Arf79F RNAi2
10 µm

Figure 5.8 ***Arf79F*** **knockdown with a third RNAi has more minor and less consistent effects on DCG compartment biogenesis in SCs.** Wide-field fluorescence and DIC images of SCs expressing GFP-GPI under *spi*-GAL4 control with and without *Arf79F*-RNAi3, v103572. **A.** GFP-GPI-expressing control. **B-D.** SCs expressing *Arf79F*-RNAi3. Many SCs have relatively normal numbers of DCG compartments (B-C), though the morphology of the DCGs may be more variable than in controls. Some SCs have more abnormal morphology and reduced DCG compartments (some abnormal compartments are indicated by yellow arrowheads). All virgin males were incubated at 29^{o}C following eclosion for 6 days. Nuclei are indicated by yellow asterices. AGs were stained with LysoTracker Red. Genotype of knockdown males is: *w; spi-GAL4 tub-GAL80^{ts}; UAS-GFP-GPI/Arf79F-RNAi3*. Control does not express a UAS-RNAi construct. n=46 SCs from 10 AGs. Scale bars are shown in panels.

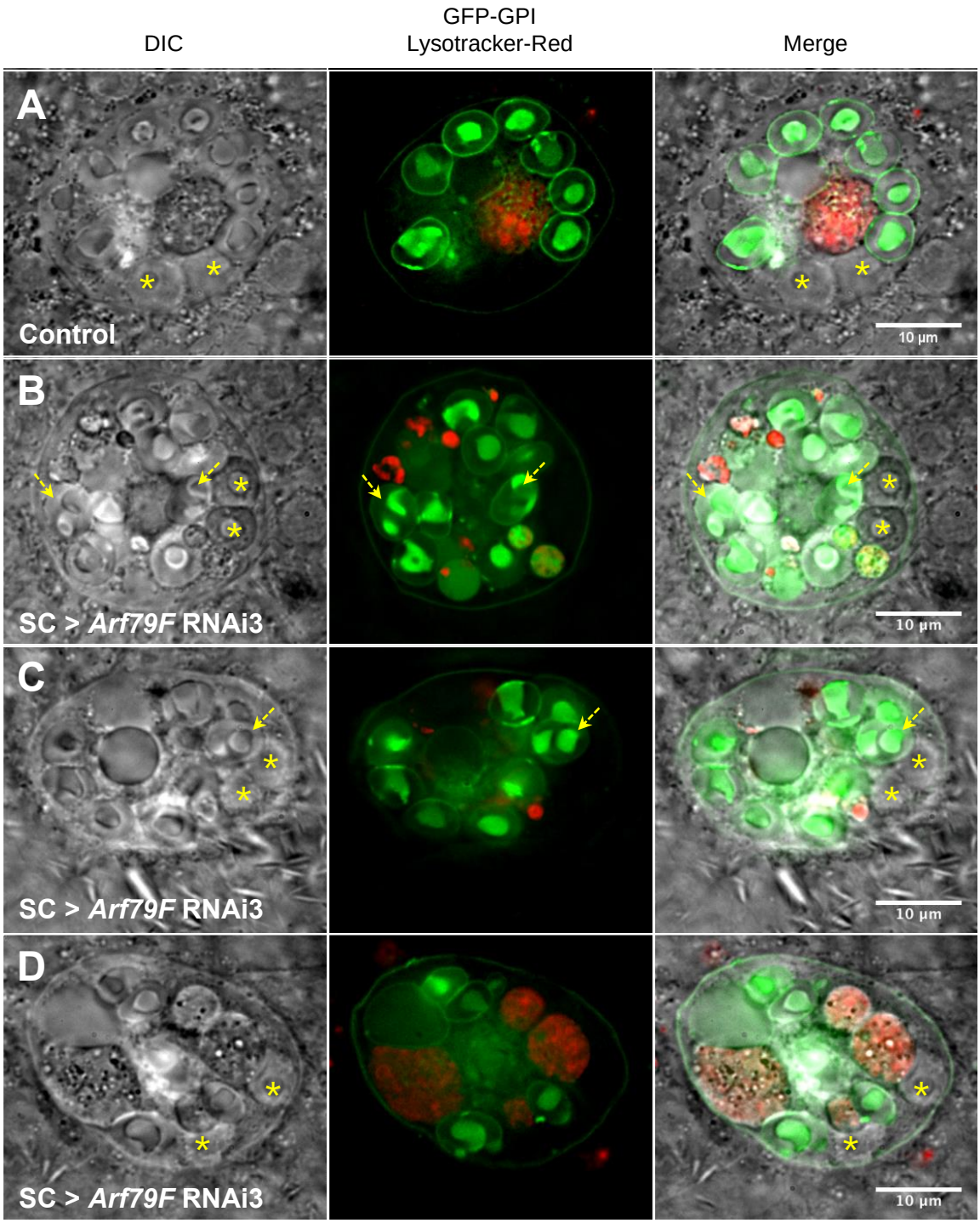
DIC
GFP-GPI
Lysotracker-Red
Merge
A
Control
B
SC > Arf79F RNAi3
C
SC > Arf79F RNAi3
D
SC > Arf79F RNAi3
10 µm

5.3.3. Preliminary analysis of the functional role of Chaoptin in the formation of DCGs

In *Drosophila* adult flies, mRNA data has shown that *chp* is also expressed at a detectable level in AGs (Chintapalli, Wang et al. 2007). Moreover, I showed in Section 4.2.2.5 that Chaoptin protein is expressed selectively in the DCG compartments of SCs and is associated with the intraluminal puncta that are distinct from the dense cores. Therefore, we wanted to investigate whether depleting *chp* expression causes a phenotypic effect in SCs.

To this aim, I expressed two different *chp*-RNAi lines in SCs for 6 days post-eclosion, using GFP-GPI as a read-out in virgin males (RNAi1 (TRiP line JF01217), n=35 SCs, taken from 8 different AGs; RNAi2 (TRiP line JF01447), n=10 SCs, taken from 3 different AGs; Fig. 5.9A).

In addition, I studied AGs (n=13 SCs, taken from 3 different AGs, Fig. 5.9B) from male adult flies carrying the null allele chp^2 (Van Vactor, Krantz et al. 1988, Gurudev, Yuan et al. 2014). The chp^2 allele carries a deletion 3' of exon 6 in the *chp* gene, which removes the remaining coding sequence encoded by a further 10 exons, including the GPI anchor site. Mutants have a severe reduction in the number and length of microvilli in *Drosophila* photoreceptor cells (Gurudev, Yuan et al. 2014), and no Chp protein has been detected by immunohistochemistry in these flies (Van Vactor, Krantz et al. 1988, Gurudev, Yuan et al. 2014).

In our hands, none of the experimental manipulations described above showed an obvious phenotypic effect on DCGs in SCs (Fig. 5.9). However, these results are still at a preliminary stage, and further study is required to gain a better understanding of the functional role of *chp* in SCs.

Figure 5.9 **The *chp*^{2} mutant and *chp* knockdown in SCs using RNAi have no detectable phenotypic effect on DCG compartment biogenesis in SCs.** Wide-field fluorescence and DIC images of SCs with or without genetic manipulation of *chp*. **A.** Upper row shows a GFP-GPI-expressing control cell. Lower two rows are SCs expressing two different *chp*-RNAi lines. SCs exhibit normal morphology and numbers of DCG compartments. Genotype of knockdown males is: *w; spi-GAL4 tub-GAL80*^{ts}*; UAS-GFP-GPI/chp-RNAi1* (TRiP JF01217) and *w; spi-GAL4 tub-GAL80*^{ts}*; UAS-GFP-GPI/chp-RNAi2* (TRiP JF01447). **B.** *chp*^{2} mutant SCs show no obvius defects in DCGs by DIC imaging. Knockdown virgin males were incubated at 29^{o}C following eclosion for 6 days. AGs were stained with LysoTracker Red. Scale bars are shown in panels.

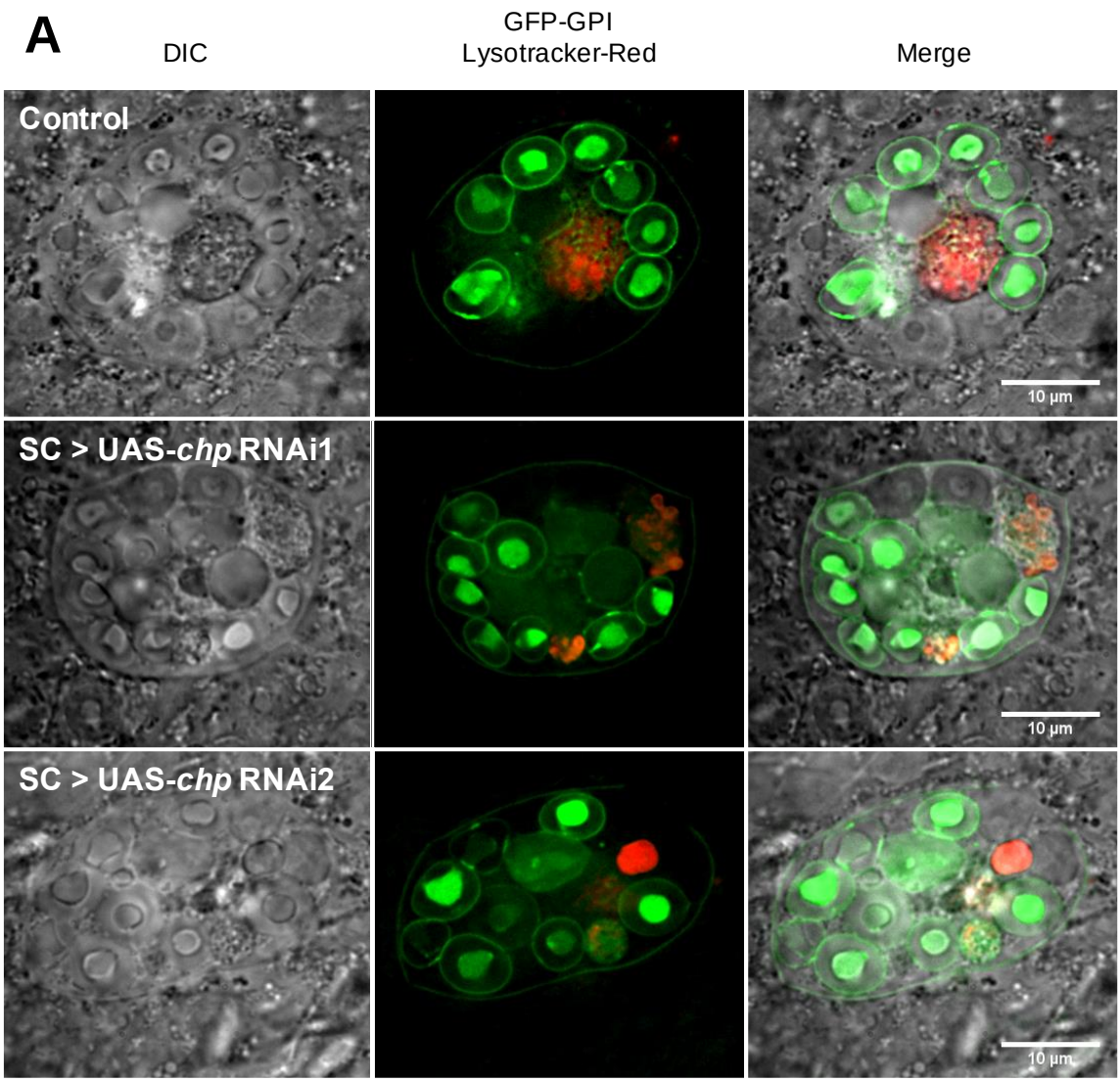
A
DIC
GFP-GPI
Lysotracker-Red
Merge
Control
SC > UAS-chp RNAi1
SC > UAS-chp RNAi2
10 µm
10 µm
10 µm

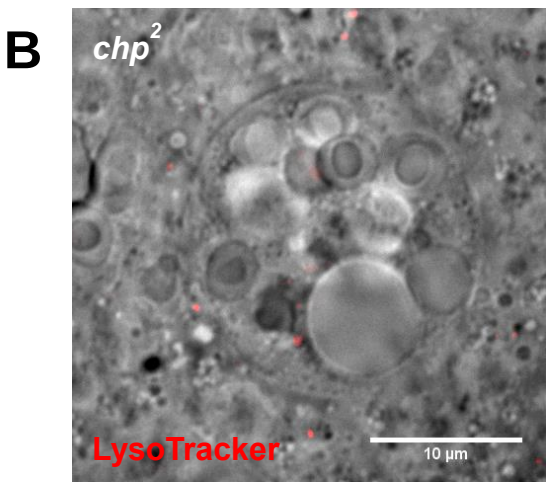
B
chp2
LysoTracker
10 µm

5.3.4. Preliminary analysis of the functional role of Phosphatidyl Inositol Glycan (PIG) genes in the formation of DCGs

Given the distinctive localisation of the GPI-anchored Chp in DCG compartments of SCs, I reasoned that other GPI-anchored proteins (GPI-APs) were likely to be trafficked similarly. I aimed to establish whether disruption in the biosynthesis of GPIs can cause changes in DCG formation. For our preliminary screening, I decided to test RNAi lines for three PIG genes that are involved in different steps in the synthesis of GPI-APs: PIG-C, PIG-U and PIG-V. In addition, because of the biochemical nature of the GFP-GPI marker, we wanted to establish whether *PIG* gene disruption affects the subcellular localisation and trafficking of GFP-GPI in *Drosophila* SCs.

PIG anchor biosynthesis class C (PIG-C; FlyBase CG12077, UniProt Q9VZR1) is one of the subunits of the GPI-GlcNAc transferase, which catalyses the first reaction in the synthesis of a GPI anchor at the cytoplasmic face of the endoplasmic reticulum (Satoh, Inagaki et al. 2013, Kinoshita 2014, Kinoshita and Fujita 2016). In addition to *PIG-C*, five more PIG genes take part in the GPI-GlcNAc transferase step in mammals (Kinoshita 2014, Kinoshita and Fujita 2016). Defective or no synthesis of GPI-APs is observed in mutant cells for PIG-C (Kinoshita 2014). In humans, three different *PIC-C* mutations were identified in patients suffering from a developmental delay and seizure disorder. Furthermore, synthesis of these defective variants of human *PIG-C* led to a reduction of GPI-APs on the surface of mouse lymphoma cells (Edvardson, Murakami et al. 2017).

Phenotypic assessment of SCs expressing a *PIG-C*-RNAi for 6 days post-eclosion in a GFP-GPI background in virgin males (n=19 SCs, taken from 7 different AGs expressing KK101771, VDRC103915) revealed no obvious changes in DCGs when compared with controls (Fig. 5.10B versus Fig. 5.10A).

PIG class U (PIG-U; FlyBase CG13089, UniProt Q9VLK0) is a subunit of glycosylphosphatidylinositol (GPI) transamidase complex, which mediates GPI anchoring in the endoplasmic reticulum (Kinoshita 2014). *PIG-U* is an essential component of the GPI-transamidase (Hong, Ohishi et al. 2003) which is overexpressed in human bladder cancer (Guo, Linn et al. 2004). *PIG-U* mutant mammalian epithelial cells exhibited no detectable activity of the GPI transamidase complex and a drastic reduction in the amount of GPI-APs on the cell surface (Hong, Ohishi et al. 2003).

In SCs, *PIG-U* knockdown by RNAi also did not show a phenotypic effect on DCGs (Fig. 5.10C, n=15 SCs taken from 6 different AGs expressing KK101552, VDRC105420).

PIG subunit V (PIG-V; FlyBase CG44239, UniProt Q9V7W1) is also known as Phosphatidylinositol glycan anchor biosynthesis class V, and is a GPI mannosyltransferase 2 (GPI-MT2), an enzyme controlling transfer of a second mannose to the glycolipid core (GPI) (Kinoshita and Fujita 2016). *PIG-V*-defective mammalian cells showed a reduce expression of critical GPI-APs (Kinoshita 2014). In humans, loss of *PIG-V* function induces a reduction in the anchoring of alkaline phosphatase (ALP) which in turn induces elevated serum ALP (Satoh, Inagaki et al.

2013). *PIG-V* mutations have been identified in patients affected with the hyperphosphatasia mental retardation syndrome that is characterised by elevated serum ALP and several neurologic abnormalities (Krawitz, Schweiger et al. 2010).

In *D. melanogaster* GPI-MT2 is required for a proper association of Chaoptin with the microvillar membrane of photoreceptor cells. In *PIG-V* mutants, Chaoptin fails to be trafficked to the surface of photoreceptor cells which ultimately leads to retinal degeneration (Rosenbaum, Brehm et al. 2012).

In our hands, knockdown by RNAi using three different lines over six days post-eclosion (RNAi1: GD3514, VDRC8143; n=22 SCs, taken from 9 different AGs; RNAi2: GD3514, VDRC8144; n=10 SCs, taken from 3 different AGs, and RNAi3: TRiP HMC03223, n=19 SCs, taken from 6 different AGs) did not have a phenotypic effect on DCGs in SCs from virgin males (Fig. 5.10D).

The results presented here are preliminary, but the simplest interpretation is that PIGs are not required for normal DCG biogenesis.

Figure 5.10 ***PIG-C, PIG-U or PIG-V*** **knockdowns have no phenotypic effect on SCs.** Wide-field fluorescence and DIC images of SCs expressing GFP-GPI under *spi*-GAL4 control with and without RNAis targeting different *PIG* genes. **A**. GFP-GPI-expressing control. **B-D.** Remaining panels show SCs expressing *PIG-C*-RNAi (B)*, PIG-U*-RNAi (C) and *PIG-V*-RNAi1 (D) whose genotypes are: *w; spi-GAL4 tub-GAL80^{ts}/UAS-PIG-C-RNAi; UAS-GFP-GPI; w; spi-GAL4 tub-GAL80^{ts}/UAS-PIG-U-RNAi1; UAS-GFP-GPI* and *w; spi-GAL4 tub-GAL80^{ts}; UAS-GFP-GPI/UAS-PIG-V-RNAi1.* All virgin males were incubated at 29^{o}C following eclosion for 6 days. AGs were stained with LysoTracker Red. Controls did not express a UAS-RNAi construct. Scale bars are shown in individual panels.

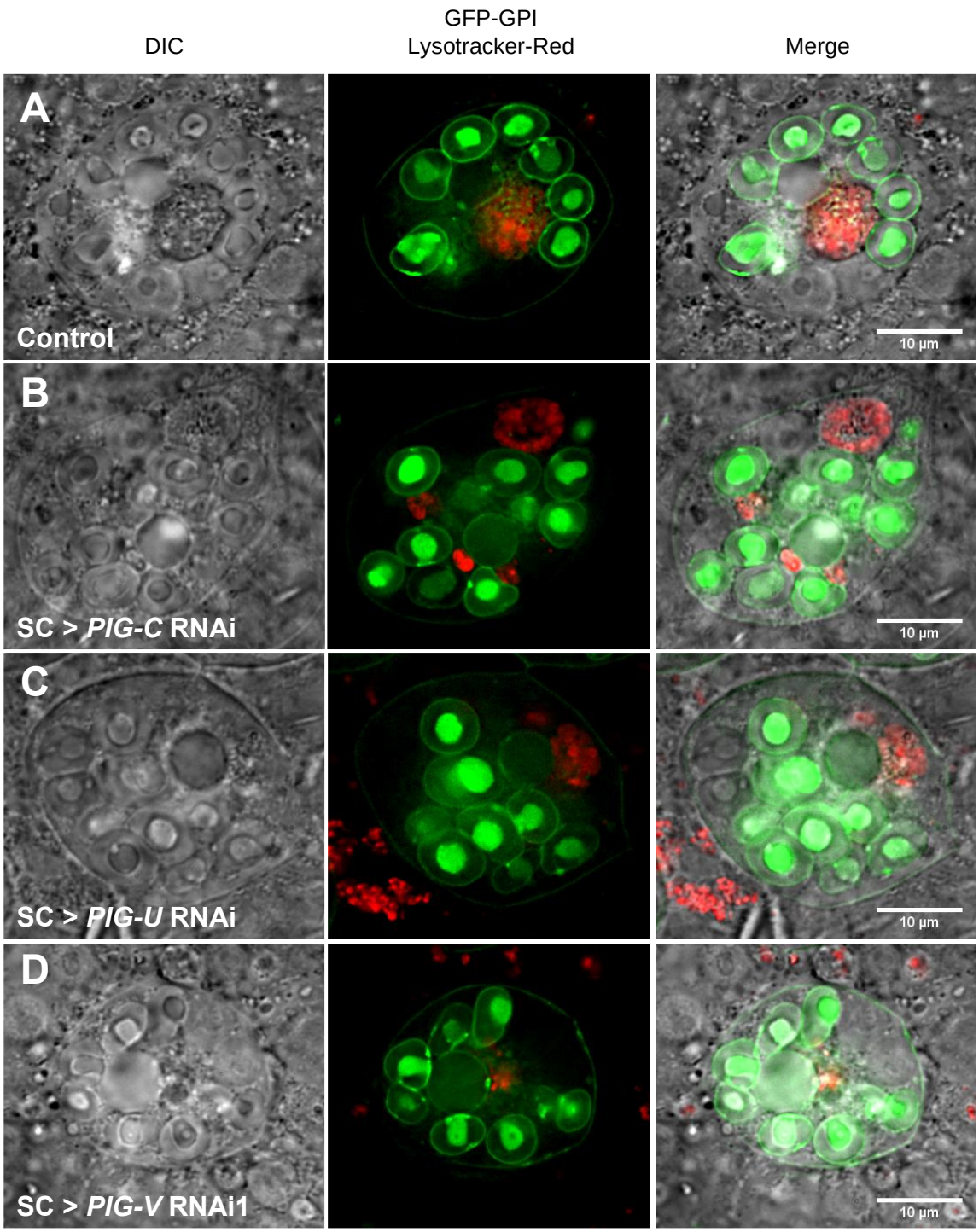
GFP-GPI
Lysotracker-Red
DIC
Merge
A
Control
10 μm
B
SC > PIG-C RNAi
10 μm
C
SC > PIG-U RNAi
10 μm
D
SC > PIG-V RNAi1
10 μm

5.4. Discussion

Having characterised the *Drosophila* secondary cell as a new system to study the formation of dense-core granules in Chapter 4, in this chapter, I employ the versatile genetics of the fly to test whether genes that have already been associated with DCG biogenesis in mammalian systems are also involved in the same processes in SCs. Furthermore, the high resolution imaging available in SCs has allowed me to dissect out some of the subcellular changes that accompany the removal of key regulators such as the AP-1 complex and Arf79F. Since my analysis of protein expression in SCs revealed that the GPI-anchored protein Chaoptin is trafficked to the limiting membrane and ILVs of large non-acidic compartments in SCs and that a GPI-anchored form of GFP traffics to the same locations and also to the DCGs themselves, I tested the roles of Chaoptin and the GPI biosynthesis pathway in DCG biogenesis. However, the latter experiments did not highlight any roles for these molecules in the DCG biogenesis process.

Overall I conclude that the SC system offers new opportunities to dissect out the genetics of DCG formation, and that the tools I have characterised in my thesis will greatly facilitate the mechanistic characterisation of this regulation.

5.4.1. The AP-1 complex plays a conserved role in DCG biogenesis

The AP-1 complex is formed four different subunits, AP-1γ, AP-1μ1 (also known as AP-47), AP-1σ and β-adaptin (encoded by CG12532). Here I tested the roles of all but the last subunit and found that loss of AP-1γ and AP-1μ1 produced extremely

severe DCG phenotypes. Although these phenotypes were only observed with a single RNAi, the fact that both subunits generated a related phenotype that had not been observed following knockdown of many other genes in SCs suggests that loss of the AP-1 complex is responsible.

However, knockdown of *AP-1σ* with two independent RNAis failed to induce a phenotype (Carvajal-Gonzalez, Balmer et al. 2015). It seems unlikely that AP-1σ is not part of the AP-1 complex in SCs and so further analysis is required to understand this discrepancy.

Previous studies have indicated that Clathrin and the AP-1 adaptor complex are required to form DCGs in *Drosophila* salivary gland cells (Burgess, Jauregui et al. 2011) where they appear to act at the trans-Golgi network to promote the accumulation of DCG proteins into specific compartments. AP-1 forms a protein coat around the secretory compartments to which clathrin is recruited, as well as being involved in other vesicle assembly events in the endomembrane system (Bonifacino 2014).

The phenotypes associated with *AP-1γ* and *AP-1μ1* knockdown suggest that the AP-1 complex is not required to form large non-acidic compartments in SCs, but it is needed to allow these to mature into DCG compartments. Loss of *AP-1γ* produced cells with several large non-acidic compartments, but none contained DCGs. Subsequent analysis by B. Kroeger (reported in his thesis) has demonstrated that these compartments do not carry YFP-Rab11 expressed from the *YFP-Rab11* gene trap, suggesting that Rab11 cannot be transferred to these compartments during

the maturation process. However, they are Rab6-positive. It is unclear whether the large acidic compartments present in these knockdown cells are produced by fusion with these defective compartments, but their morphology suggests this, because they frequently contain domains of acidic and non-acidic, GFP-positive contents inside them.

AP-1µ1 knockdown produced a less dramatic phenotype in which three or four enlarged non-acidic compartments were formed, some of which contained morphologically distorted DCGs. Importantly, these compartments were Rab11-positive, suggesting that this less extreme phenotype may be generated because the loading of Rab11 on to non-acidic compartments is not completely blocked in these cells, perhaps because the knockdown is incomplete.

Overall, I conclude that in SCs, the AP-1 complex is required for maturation of DCG compartments, once they are formed on the trans-face of the Golgi. Interestingly, one important role of AP-1 appears to be the recruitment of Rab11 to these compartments, a process that has been shown to be essential for DCG formation (B. Kroeger, DPhil thesis). It will now be interesting to test whether a similar role can be deciphered in other secretory cells, where immune-EM may be required to confirm these findings.

5.4.2. The AP-1-interacting protein Arf79F also controls DCG compartment formation, but produces a different SC phenotype

Knockdown of the gene encoding Arf79F, the homologue of mammalian Arf1, also blocked the production of normal DCG compartments with two of the three independent RNAis employed leading to complete loss of DCG-containing compartments in the most extreme cases. Large non-acidic compartments remained, many of which contained diffusely localised GFP expressed from the GFP-GPI construct. Unlike the *AP-1*-associated knockdown phenotypes, large and non-homogeneous acidic fusion compartments were not commonly seen when Arf79F expression was blocked.

Further analysis by B. Kroeger (DPhil thesis) has indicated that the non-acidic compartments observed in *Arf79F* knockdown cells do not carry either Rab6 or Rab11 fusion proteins expressed from their respective gene traps, in contrast to the *AP-1* knockdown phenotypes. This suggests that the primary step in DCG biogenesis that is regulated by Arf79F is not the same as the one controlled by the AP-1 complex, and in fact may occur earlier in the process. Nevertheless, large non-acidic compartments still appear to bud off from the TGN in Arf79F knockdown cells, but they are not coated by the appropriate Rabs, a defect that may also prevent them from fusing with acidic compartments.

5.4.3. Chaoptin and the PIG proteins do not appear to be involved in DCG biogenesis

Knockdown experiments with two RNAis targeting the gene encoding the GPI-anchored protein Chaoptin did not appear to affect DCG formation. Of course, absence of phenotypes might be explained because there is insufficient knockdown of the *chp* gene. However, in this case an amorphic and viable mutant of the gene, chp^{2}, allowed me to confirm that it is not required for DCG biogenesis. Chaoptin is a homophilic cell adhesion molecule containing 36 leucine-rich repeats, which participate in protein-protein interaction.

In photoreceptors, where Chp is specifically and highly expressed, it plays an important role in assembling the complex microvilli structure known as the rhabdomere. One possible role in SCs is that it is involved in connecting the elaborate ILV network inside DCG compartments, where these vesicles appear to form chains. Alternatively, since these vesicles are secreted, Chp could play a role in target cell recognition when the resulting exosomes are transferred to females. Both these hypotheses require further investigation.

My analysis of multiple PIGs using knockdown failed to produce any consistent phenotypes in SCs. There is some redundancy in the GPI biosynthesis pathway, but for some of the genes I tested, previous studies have suggested that the *PIG* RNAis employed do generate phenotypes. Although there are further PIG genes that should be tested, currently the evidence presented here suggests that GPI-anchored proteins do not play a critical role in DCG biogenesis.

6. Conclusions

Cell-cell interactions are central to the biology of multicellular eukaryotic organisms, and as these organisms have increased in complexity during evolution, the range of mechanisms involved has expanded. In my thesis, I have focused on specialised cell-cell interaction mechanisms in reproduction and the roles of membranes in these processes, either as the mediators of cell-cell fusion events or as the foundation for membrane trafficking events that control secretion. The key conclusions from this work have been overviewed at the end of Chapters 3-5. Here, I briefly summarise my results and look forward to their implications in future studies of cell-cell communication.

6.1. *T. brucei* HAP2(GCS1)

Ultimately the inability to induce different forms of *T. brucei* relevant to infectivity and meiosis *in vitro* meant that my studies were restricted to the analysis of HAP2(GCS1) fusion proteins from samples derived from the parasite host, limiting the scope of my work. Furthermore, I was unable to assess whether the tagged forms of HAP2(GCS1) that I expressed had normal function or indeed any function at all. At this point, I made a decision to divert my analysis to a completely different insect reproductive system, which I had become aware of, in which membranes play a range of different roles in controlling secretory processes in the cell. The remaining work in my thesis is focused on a series of questions associated with this alternative model.

My interest in cell-cell fusion in reproduction led me to consider other mechanisms by which membranes might facilitate reproductive physiology. In this regard, the *Drosophila* secondary cell was a particularly attractive system. Studies had already shown that these cells secrete exosomes that fuse with sperm and interact with female tissues after mating (Corrigan, Redhai et al. 2014), and more detailed analysis by B. Kroeger, described in his DPhil thesis, had indicated that these exosomes are not only formed in late endosomal compartments, but also in large compartments that contain dense-core granules. Given the genetic tools available to study these cells and the emergence of high resolution wide-field fluorescence microscopy as an approach to study SCs, I set out to characterise how these DCG compartments are formed and mature and the roles of membrane proteins and trafficking in these events.

6.2. The Drosophila secondary cell as a unique genetic model to study DCG and exosome biology

When I initiated my studies in the Wilson laboratory, I set out with two major aims: first, to determine whether the transgenic tools available to study SC biology affected secretory trafficking in these cells; and second, to employ these tools to investigate whether SCs could be used as a model for dissecting out the basic genetic processes that control DCG biogenesis and associated exosome formation in DCG compartments.

My analysis of the tools confirmed that unlike CD63-GFP, whose overexpression increases the number of non-acidic and DCG compartments in SCs, markers like overexpressed GFP-GPI and CFP-Rab6 (expressed from a gene trap) did not significantly alter compartment numbers or identities as judged by DIC analysis of dense cores and staining with LysoTracker Red. Furthermore, it showed that using living tissue produces much higher definition images of SC compartments than fixed samples, which has influenced many of the subsequent studies in the laboratory.

I then successfully used the GFP-GPI marker in Chapter 5 to show that the AP-1 complex and Arf79F, which both have key functions in mammalian DCG formation, play important roles in DCG biogenesis in SCs. Moreover, the high resolution imaging techniques available in SCs allowed me to demonstrate that manipulating these two regulators produces different phenotypes. The most severe AP-1 knockdown phenotypes were associated with highly enlarged non-acidic and acidic compartments. Collaborative studies with B. Kroeger suggested key Rab transition from Rab6 to Rab11 that is required for DCG biogenesis in SCs did not take place in these cells. By contrast, most of the non-acidic compartments in Arf79F knockdown cells were much closer to normal size, but they generally failed to form a DCG. Furthermore, subsequent studies from B. Kroeger suggested that neither Rab6 nor Rab11 coated these structures.

One of the roles of mammalian Arf1, the orthologue of Arf79F, is to recruit AP-1 to exiting compartments in the Golgi (Ren, Farias et al. 2013). Our data suggest that Arf79F also has AP-1-independent functions that may be important in recruiting Rab6 to these compartments. A more extended analysis of other AP-1 and Arf79F

interactors and regulators should help to dissect out the genetic basis of these different functions. Together with the identification of the Rab6/Rab11 transition in DCG biogenesis, our work to date forms the basis of a manuscript describing the process of DCG formation in SCs, which we are preparing for submission.

6.3. Future analysis of DCG biogenesis in SCs

Members of the Wilson laboratory are continuing to screen through candidate genes implicated in DCG biogenesis to extend the work described in my thesis. Some obvious possibilities are regulators of specific Rabs, most notably Rab11 and Rab6, which we already know play central roles in the process. However, screens of other genes that are known to be expressed very specifically in the accessory gland or in secondary cells (through gene trap expression studies or mRNA array data) have already identified at least one novel gene whose product is trafficked into DCG compartments and that is essential to make dense cores. Interestingly, its orthologue in humans has already been associated with diabetes, suggesting that the SC model may provide new clues to understanding the molecular processes underlying this disease. Indeed, GWAS (genome-wide association studies) screens have provided a set of genes expressed in pancreatic beta cells, which are implicated in Type 2 diabetes mellitus (McCarthy 2017), and the SC may provide a new model to test their functions *in vivo*.

One fascinating observation from my work is that DCGs in SCs are surrounded by chains of small intraluminal vesicles that appear to interact with some of the

molecules, which reach the dense core. These ILVs are also in intimate contact with highly organised fibres that surround the DCG (Rylett, Walker et al. 2007). ILVs have not previously been reported in DCG compartments of other cell types. However, it is the unique size of these compartments in SCs that has allowed us to identify this association, and this would almost certainly require an EM analysis in other cells. It will be interesting to undertake a detailed analysis of the functions of ILVs in DCG biogenesis in the SC system and, provided they can be molecularly characterised, the associated fibres. Preliminary data suggest that the ILVs do play a role (B. Kroeger, pers. comm.), perhaps providing a new route by which cargos converge and aggregate during DCG formation.

It is also clear that additional tools are already available to improve the level of analysis of knockdown phenotypes in SCs. For example, other Rabs, like Rab1 and Rab2 mark the trans-Golgi – gene traps generated for these genes (Dunst, Kazimiers et al. 2015) will be useful in determining whether non-acidic compartments in knockdown SCs that do not carry either Rab6 or Rab11 (as found in *Arf79F* knockdown) retain Golgi markers that should have been removed when they left the trans-Golgi network.

Another important development that has emerged during the course of my DPhil studies in the Wilson laboratory is the emergence of real-time imaging in SCs, which can be extended over a period of 4-6 hours, long enough to generate a new DCG compartment (B. Kroeger, DPhil thesis). One of the problems in studying the control of trafficking is that visualising a phenotype at a certain time is only a snap-shot of the cumulative events that build up as the cell's trafficking network responds to a

specific defect. Real-time imaging provides an additional tool to visualise the earliest events in DCG biogenesis at the trans-face of the Golgi at sub-compartmental resolution and this should help in determining whether some of the defects observed are primary as opposed to secondary in nature.

In summary, my thesis has made a significant contribution to the establishment of SCs as a new model for the study of DCG, as well as exosome, biogenesis. It seems likely that further studies will reveal additional parallels between the DCG biogenesis process in these cells and mammalian secretory cell types, as well as uncovering some of the previously unidentified sub-compartmental biology, involving ILVs and associated fibres, which may underpin this mechanism.

7. Bibliography

Adams, M. D., S. E. Celniker, R. A. Holt, C. A. Evans, J. D. Gocayne, P. G. Amanatides, S. E. Scherer, P. W. Li, R. A. Hoskins, R. F. Galle, R. A. George, S. E. Lewis, S. Richards and M. Ashburner, et al (2000). "The genome sequence of Drosophila melanogaster." Science **287**(5461): 2185-2195.

Aguilar, P. S., M. K. Baylies, A. Fleissner, L. Helming, N. Inoue, B. Podbilewicz, H. Wang and M. Wong (2013). "Genetic basis of cell-cell fusion mechanisms." Trends Genet **29**(7): 427-437.

Arighi, C. N., L. M. Hartnell, R. C. Aguilar, C. R. Haft and J. S. Bonifacino (2004). "Role of the mammalian retromer in sorting of the cation-independent mannose 6-phosphate receptor." J Cell Biol **165**(1): 123-133.

Avila, F. W., J. A. Sánchez-López, J. L. McGlaughon, S. Raman, M. F. Wolfner and Y. Heifetz (2016). Nature and Functions of Glands and Ducts in the Drosophila Reproductive Tract. Extracellular Composite Matrices in Arthropods. E. Cohen and B. Moussian. Cham, Springer International Publishing**:** 411-444.

Avila, F. W., L. K. Sirot, B. A. LaFlamme, C. D. Rubinstein and M. F. Wolfner (2011). "Insect seminal fluid proteins: identification and function." Annu Rev Entomol **56**: 21-40.

Avila, F. W. and M. F. Wolfner (2017). "Cleavage of the Drosophila seminal protein Acp36DE in mated females enhances its sperm storage activity." J Insect Physiol **101**: 66-72.

Avila, F. W., A. Wong, J. L. Sitnik and M. F. Wolfner (2015). "Don't pull the plug! the Drosophila mating plug preserves fertility." Fly (Austin) **9**(2): 62-67.

Avinoam, O., K. Fridman, C. Valansi, I. Abutbul, T. Zeev-Ben-Mordehai, U. E. Maurer, A. Sapir, D. Danino, K. Grunewald, J. M. White and B. Podbilewicz (2011). "Conserved eukaryotic fusogens can fuse viral envelopes to cells." Science **332**(6029): 589-592.

Bastin, P., Z. Bagherzadeh, K. R. Matthews and K. Gull (1996). "A novel epitope tag system to study protein targeting and organelle biogenesis in Trypanosoma brucei." Molecular and biochemical parasitology **77**(2): 235-239.

Benhra, N., S. Lallet, M. Cotton, S. Le Bras, A. Dussert and R. Le Borgne (2011). "AP-1 controls the trafficking of Notch and Sanpodo toward E-cadherin junctions in sensory organ precursors." Curr Biol **21**(1): 87-95.

Bertram, M. J., G. A. Akerkar, R. L. Ard, C. Gonzalez and M. F. Wolfner (1992). "Cell type-specific gene expression in the Drosophila melanogaster male accessory gland." Mechanisms of Development **38**(1): 33-40.

Binker, M. G., D. Richards, H. Y. Gaisano and L. I. Cosen-Binker (2015). "ER stress-associated CTRC mutants decrease stimulated pancreatic zymogen secretion through SIRT2-mediated microtubule dysregulation." Biochem Biophys Res Commun **463**(3): 329-335.

Bloomfield, G. (2011). "Genetics of sex determination in the social amoebae." Dev Growth Differ **53**(4): 608-616.

Boehm, M. and J. S. Bonifacino (2001). "Adaptins: the final recount." Mol Biol Cell **12**(10): 2907-2920.

Bohme, U. and G. A. Cross (2002). "Mutational analysis of the variant surface glycoprotein GPI-anchor signal sequence in Trypanosoma brucei." J Cell Sci **115**(Pt 4): 805-816.

Bolker, B. M., M. E. Brooks, C. J. Clark, S. W. Geange, J. R. Poulsen, M. H. Stevens and J. S. White (2009). "Generalized linear mixed models: a practical guide for ecology and evolution." Trends Ecol Evol **24**(3): 127-135.

Bonifacino, J. S. (2014). "Adaptor proteins involved in polarized sorting." J Cell Biol **204**(1): 7-17.

Bonnemaison, M. L., B. A. Eipper and R. E. Mains (2013). "Role of adaptor proteins in secretory granule biogenesis and maturation." Front Endocrinol (Lausanne) **4**: 101.

Brand, A. H. and N. Perrimon (1993). "Targeted gene expression as a means of altering cell fates and generating dominant phenotypes." Development **118**(2): 401-415.

Breslow, N. E. and D. G. Clayton (1993). "Approximate Inference in Generalized Linear Mixed Models." Journal of the American Statistical Association **88**(421): 9-25.

Brun, R. and Schonenberger (1979). "Cultivation and in vitro cloning or procyclic culture forms of Trypanosoma brucei in a semi-defined medium. Short communication." Acta tropica **36**(3): 289-292.

Burgess, J., M. Jauregui, J. Tan, J. Rollins, S. Lallet, P. A. Leventis, G. L. Boulianne, H. C. Chang, R. Le Borgne, H. Krämer and J. A. Brill (2011). "AP-1 and clathrin are essential for secretory granule biogenesis in Drosophila." Molecular Biology of the Cell **22**(12): 2094-2105.

Carvajal-Gonzalez, J. M., S. Balmer, M. Mendoza, A. Dussert, G. Collu, A. C. Roman, U. Weber, B. Ciruna and M. Mlodzik (2015). "The clathrin adaptor AP-1 complex and Arf1 regulate planar cell polarity in vivo." Nat Commun **6**: 6751.

Chapman, T. and S. J. Davies (2004). "Functions and analysis of the seminal fluid proteins of male Drosophila melanogaster fruit flies." Peptides **25**(9): 1477-1490.

Chen, E. H. and E. N. Olson (2005). "Unveiling the mechanisms of cell-cell fusion." Science **308**(5720): 369-373.

Chen, M., Z. Wang, M. Zhan, R. Liu, A. Nie, J. Wang, G. Ning and Q. Ma (2014). "Adiponectin regulates ACTH secretion and the HPAA in an AMPK-dependent manner in pituitary corticotroph cells." Mol Cell Endocrinol **383**(1-2): 118-125.

Chen, P. S. (1984). "The Functional Morphology and Biochemistry of Insect Male Accessory Glands and their Secretions." Annual Review of Entomology **29**(1): 233-255.

Chernomordik, L. V. and M. M. Kozlov (2008). "Mechanics of membrane fusion." Nat Struct Mol Biol **15**(7): 675-683.

Chintapalli, V. R., J. Wang and J. A. Dow (2007). "Using FlyAtlas to identify better Drosophila melanogaster models of human disease." Nat Genet **39**(6): 715-720.

Chow, C. Y., F. W. Avila, A. G. Clark and M. F. Wolfner (2015). "Induction of excessive endoplasmic reticulum stress in the Drosophila male accessory gland results in infertility." PLoS One **10**(3): e0119386.

Cole, E. S., D. Cassidy-Hanley, J. Fricke Pinello, H. Zeng, M. Hsueh, D. Kolbin, C. Ozzello, T. Giddings, Jr., M. Winey and T. G. Clark (2014). "Function of the male-gamete-specific fusion protein HAP2 in a seven-sexed ciliate." Curr Biol **24**(18): 2168-2173.

Colombo, M., G. Raposo and C. Thery (2014). "Biogenesis, secretion, and intercellular interactions of exosomes and other extracellular vesicles." Annu Rev Cell Dev Biol **30**: 255-289.

Corrigan, L., S. Redhai, A. Leiblich, S. J. Fan, S. M. Perera, R. Patel, C. Gandy, S. M. Wainwright, J. F. Morris, F. Hamdy, D. C. Goberdhan and C. Wilson (2014). "BMP-regulated exosomes from Drosophila male reproductive glands reprogram female behavior." J Cell Biol **206**(5): 671-688.

D'Souza-Schorey, C. and P. Chavrier (2006). "ARF proteins: roles in membrane traffic and beyond." Nat Rev Mol Cell Biol **7**(5): 347-358.

Day, R. and S. U. Gorr (2003). "Secretory granule biogenesis and chromogranin A: master gene, on/off switch or assembly factor?" Trends Endocrinol Metab **14**(1): 10-13.

del Valle Rodriguez, A., D. Didiano and C. Desplan (2012). "Power tools for gene expression and clonal analysis in Drosophila." Nat Methods **9**(1): 47-55.

Dietzl, G., D. Chen, F. Schnorrer, K. C. Su, Y. Barinova, M. Fellner, B. Gasser, K. Kinsey, S. Oppel, S. Scheiblauer, A. Couto, V. Marra, K. Keleman and B. J. Dickson (2007). "A genome-wide transgenic RNAi library for conditional gene inactivation in Drosophila." Nature **448**(7150): 151-156.

Dikeakos, J. D. and T. L. Reudelhuber (2007). "Sending proteins to dense core secretory granules: still a lot to sort out." J Cell Biol **177**(2): 191-196.

Donaldson, J. G. and C. L. Jackson (2011). "ARF family G proteins and their regulators: roles in membrane transport, development and disease." Nat Rev Mol Cell Biol **12**(6): 362-375.

Dunst, S., T. Kazimiers, F. von Zadow, H. Jambor, A. Sagner, B. Brankatschk, A. Mahmoud, S. Spannl, P. Tomancak, S. Eaton and M. Brankatschk (2015). "Endogenously tagged rab proteins: a resource to study membrane trafficking in Drosophila." Dev Cell **33**(3): 351-365.

Ebchuqin, E., N. Yokota, L. Yamada, Y. Yasuoka, M. Akasaka, M. Arakawa, R. Deguchi, T. Mori and H. Sawada (2014). "Evidence for participation of GCS1 in fertilization of the starlet sea anemone Nematostella vectensis: implication of a common mechanism of sperm-egg fusion in plants and animals." Biochem Biophys Res Commun **451**(4): 522-528.

Eddy, S. R. (1996). "Hidden Markov models." Curr Opin Struct Biol **6**(3): 361-365.

Edvardson, S., Y. Murakami, T. T. M. Nguyen, M. Shahrour, A. St-Denis, A. Shaag, N. Damseh, F. Le Deist, Y. Bryceson, B. Abu-Libdeh, P. M. Campeau, T. Kinoshita and O. Elpeleg (2017). "Mutations in the phosphatidylinositol glycan C (PIGC) gene are associated with epilepsy and intellectual disability." Journal of medical genetics **54**(3): 196-201.

Evans, J. P. (2012). "Sperm-egg interaction." Annu Rev Physiol **74**: 477-502.

Fedry, J., J. Forcina, P. Legrand, G. Pehau-Arnaudet, A. Haouz, M. Johnson, F. A. Rey and T. Krey (2018). "Evolutionary diversification of the HAP2 membrane insertion motifs to drive gamete fusion across eukaryotes." PLoS Biol **16**(8): e2006357.

Fedry, J., Y. Liu, G. Pehau-Arnaudet, J. Pei, W. Li, M. A. Tortorici, F. Traincard, A. Meola, G. Bricogne, N. V. Grishin, W. J. Snell, F. A. Rey and T. Krey (2017). "The Ancient Gamete Fusogen HAP2 Is a Eukaryotic Class II Fusion Protein." Cell **168**(5): 904-915 e910.

Ferguson, M. A. J., G. W. Hart and T. Kinoshita (2015). Glycosylphosphatidylinositol Anchors. Essentials of Glycobiology. A. Varki, R. D. Cummings, J. D. Esko et al. Cold Spring Harbor (NY).

Fujita, S. C., S. L. Zipursky, S. Benzer, A. Ferrus and S. L. Shotwell (1982). "Monoclonal antibodies against the Drosophila nervous system." Proc Natl Acad Sci U S A **79**(24): 7929-7933.

Gibson, W., L. Peacock, V. Ferris, K. Williams and M. Bailey (2008). "The use of yellow fluorescent hybrids to indicate mating in Trypanosoma brucei." Parasites & vectors **1**(1): 4.

Gillott, C. (2003). "Male accessory gland secretions: modulators of female reproductive physiology and behavior." Annu Rev Entomol **48**: 163-184.

Giudici, A. M., E. Sher, M. Pelagi, F. Clementi and A. Zanini (1992). "Immunolocalization of secretogranin II, chromogranin A, and chromogranin B in differentiating human neuroblastoma cells." Eur J Cell Biol **58**(2): 383-389.

Gligorov, D., J. L. Sitnik, R. K. Maeda, M. F. Wolfner and F. Karch (2013). "A novel function for the Hox gene Abd-B in the male accessory gland regulates the long-term female post-mating response in Drosophila." PLoS Genet **9**(3): e1003395.

Goberdhan, D. C., C. Wilson and A. L. Harris (2016). "Amino Acid Sensing by mTORC1: Intracellular Transporters Mark the Spot." Cell Metab **23**(4): 580-589.

Grant, B. D. and J. G. Donaldson (2009). "Pathways and mechanisms of endocytic recycling." Nat Rev Mol Cell Biol **10**(9): 597-608.

Greco, V., M. Hannus and S. Eaton (2001). "Argosomes: a potential vehicle for the spread of morphogens through epithelia." Cell **106**(5): 633-645.

Guiraudie-Capraz, G., D. B. Pho and J. M. Jallon (2007). "Role of the ejaculatory bulb in biosynthesis of the male pheromone cis-vaccenyl acetate in Drosophila melanogaster." Integr Zool **2**(2): 89-99.

Guo, Z., J. F. Linn, G. Wu, S. L. Anzick, C. F. Eisenberger, S. Halachmi, Y. Cohen, A. Fomenkov, M. O. Hoque, K. Okami, G. Steiner, J. M. Engles, M. Osada, C. Moon,

E. Ratovitski, J. M. Trent, P. S. Meltzer, W. H. Westra, L. A. Kiemeney, M. P. Schoenberg, D. Sidransky and B. Trink (2004). "CDC91L1 (PIG-U) is a newly discovered oncogene in human bladder cancer." Nat Med **10**(4): 374-381.

Gurudev, N., M. Yuan and E. Knust (2014). "chaoptin, prominin, eyes shut and crumbs form a genetic network controlling the apical compartment of Drosophila photoreceptor cells." Biol Open **3**(5): 332-341.

Hales, K. G., C. A. Korey, A. M. Larracuente and D. M. Roberts (2015). "Genetics on the Fly: A Primer on the Drosophila Model System." Genetics **201**(3): 815-842.

Happ, G. M. (1984). Structure and Development of Male Accessory Glands in Insects. Insect Ultrastructure: Volume 2. R. C. King and H. Akai. Boston, MA, Springer US**:** 365-396.

Heifetz, Y., L. N. Vandenberg, H. I. Cohn and M. F. Wolfner (2005). "Two cleavage products of the Drosophila accessory gland protein ovulin can independently induce ovulation." Proc Natl Acad Sci U S A **102**(3): 743-748.

Heigwer, F., F. Port and M. Boutros (2018). "RNA Interference (RNAi) Screening in Drosophila." Genetics **208**(3): 853-874.

Hentze, J. L., M. E. Moeller, A. F. Jorgensen, M. S. Bengtsson, A. M. Bordoy, J. T. Warren, L. I. Gilbert, O. Andersen and K. F. Rewitz (2013). "Accessory gland as a site for prothoracicotropic hormone controlled ecdysone synthesis in adult male insects." PloS one **8**(2): e55131.

Hernandez, J. M. and B. Podbilewicz (2017). "The hallmarks of cell-cell fusion." Development **144**(24): 4481-4495.

Hirai, M., M. Arai, T. Mori, S. Y. Miyagishima, S. Kawai, K. Kita, T. Kuroiwa, O. Terenius and H. Matsuoka (2008). "Male fertility of malaria parasites is determined by GCS1, a plant-type reproduction factor." Current biology : CB **18**(8): 607-613.

Hirst, J., D. A. Sahlender, M. Choma, R. Sinka, M. E. Harbour, M. Parkinson and M. S. Robinson (2009). "Spatial and functional relationship of GGAs and AP-1 in Drosophila and HeLa cells." Traffic **10**(11): 1696-1710.

Hong, Y., K. Ohishi, J. Y. Kang, S. Tanaka, N. Inoue, J. Nishimura, Y. Maeda and T. Kinoshita (2003). "Human PIG-U and yeast Cdc91p are the fifth subunit of GPI transamidase that attaches GPI-anchors to proteins." Mol Biol Cell **14**(5): 1780-1789.

Houy, S., C. Estay-Ahumada, P. Croise, V. Calco, A. M. Haeberle, Y. Bailly, P. Billuart, N. Vitale, M. F. Bader, S. Ory and S. Gasman (2015). "Oligophrenin-1 Connects Exocytotic Fusion to Compensatory Endocytosis in Neuroendocrine Cells." J Neurosci **35**(31): 11045-11055.

Hurst, D., C. M. Rylett, R. E. Isaac and A. D. Shirras (2003). "The drosophila angiotensin-converting enzyme homologue Ance is required for spermiogenesis." Dev Biol **254**(2): 238-247.

Hutagalung, A. H. and P. J. Novick (2011). "Role of Rab GTPases in membrane traffic and cell physiology." Physiol Rev **91**(1): 119-149.

Jenni, L., S. Marti, J. Schweizer, B. Betschart, R. W. Le Page, J. M. Wells, A. Tait, P. Paindavoine, E. Pays and M. Steinert (1986). "Hybrid formation between African trypanosomes during cyclical transmission." Nature **322**(6075): 173-175.

Johnson, M. A., K. von Besser, Q. Zhou, E. Smith, G. Aux, D. Patton, J. Z. Levin and D. Preuss (2004). "Arabidopsis hapless mutations define essential gametophytic functions." Genetics **168**(2): 971-982.

Kametaka, S., A. Kametaka, S. Yonekura, M. Haruta, S. Takenoshita, S. Goto and S. Waguri (2012). "AP-1 clathrin adaptor and CG8538/Aftiphilin are involved in Notch signaling during eye development in Drosophila melanogaster." J Cell Sci **125**(Pt 3): 634-648.

Kametaka, S., N. Sawada, J. S. Bonifacino and S. Waguri (2010). "Functional characterization of protein-sorting machineries at the trans-Golgi network in Drosophila melanogaster." J Cell Sci **123**(Pt 3): 460-471.

Kametaka, S. and S. Waguri (2012). "Visualization of TGN-endosome trafficking in mammalian and Drosophila cells." Methods Enzymol **504**: 255-271.

Kanie, Y., M. Yamamoto-Hino, Y. Karino, H. Yokozawa, S. Nishihara, R. Ueda, S. Goto and O. Kanie (2009). "Insight into the regulation of glycan synthesis in Drosophila chaoptin based on mass spectrometry." PLoS One **4**(5): e5434.

Kawai-Toyooka, H., T. Mori, T. Hamaji, M. Suzuki, B. J. Olson, T. Uemura, T. Ueda, A. Nakano, A. Toyoda, A. Fujiyama and H. Nozaki (2014). "Sex-specific posttranslational regulation of the gamete fusogen GCS1 in the isogamous volvocine alga Gonium pectorale." Eukaryot Cell **13**(5): 648-656.

Keller, P., D. Toomre, E. Diaz, J. White and K. Simons (2001). "Multicolour imaging of post-Golgi sorting and trafficking in live cells." Nat Cell Biol **3**(2): 140-149.

Kelly, S., J. Reed, S. Kramer, L. Ellis, H. Webb, J. Sunter, J. Salje, N. Marinsek, K. Gull, B. Wickstead and M. Carrington (2007). "Functional genomics in Trypanosoma brucei: a collection of vectors for the expression of tagged proteins from endogenous and ectopic gene loci." Molecular and biochemical parasitology **154**(1): 103-109.

Kim, J. H., P. Jin, R. Duan and E. H. Chen (2015). "Mechanisms of myoblast fusion during muscle development." Curr Opin Genet Dev **32**: 162-170.

Kim, T., M. C. Gondre-Lewis, I. Arnaoutova and Y. P. Loh (2006). "Dense-core secretory granule biogenesis." Physiology (Bethesda) **21**: 124-133.

Kinoshita, T. (2014). "Biosynthesis and deficiencies of glycosylphosphatidylinositol." Proc Jpn Acad Ser B Phys Biol Sci **90**(4): 130-143.

Kinoshita, T. and M. Fujita (2016). "Biosynthesis of GPI-anchored proteins: special emphasis on GPI lipid remodeling." J Lipid Res **57**(1): 6-24.

Kolev, N. G., K. Ramey-Butler, G. A. Cross, E. Ullu and C. Tschudi (2012). "Developmental progression to infectivity in Trypanosoma brucei triggered by an RNA-binding protein." Science **338**(6112): 1352-1353.

Krawitz, P. M., M. R. Schweiger, C. Rodelsperger, C. Marcelis, U. Kolsch, C. Meisel, F. Stephani, T. Kinoshita, Y. Murakami, S. Bauer, M. Isau, A. Fischer, A. Dahl, M. Kerick, J. Hecht, S. Kohler, M. Jager, J. Grunhagen, B. J. de Condor, S. Doelken, H. G. Brunner, P. Meinecke, E. Passarge, M. D. Thompson, D. E. Cole, D. Horn, T.

Roscioli, S. Mundlos and P. N. Robinson (2010). "Identity-by-descent filtering of exome sequence data identifies PIGV mutations in hyperphosphatasia mental retardation syndrome." Nat Genet **42**(10): 827-829.

Leiblich, A., L. Marsden, C. Gandy, L. Corrigan, R. Jenkins, F. Hamdy and C. Wilson (2012). "Bone morphogenetic protein- and mating-dependent secretory cell growth and migration in the Drosophila accessory gland." Proc Natl Acad Sci U S A **109**(47): 19292-19297.

Leopold, R. A. (1976). "The Role of Male Accessory Glands in Insect Reproduction." Annual Review of Entomology **21**(1): 199-221.

Liu, Y., M. J. Misamore and W. J. Snell (2010). "Membrane fusion triggers rapid degradation of two gamete-specific, fusion-essential proteins in a membrane block to polygamy in Chlamydomonas." Development **137**(9): 1473-1481.

Liu, Y., R. Tewari, J. Ning, A. M. Blagborough, S. Garbom, J. Pei, N. V. Grishin, R. E. Steele, R. E. Sinden, W. J. Snell and O. Billker (2008). "The conserved plant sterility gene HAP2 functions after attachment of fusogenic membranes in Chlamydomonas and Plasmodium gametes." Genes & development **22**(8): 1051-1068.

Lui-Roberts, W. W., L. M. Collinson, L. J. Hewlett, G. Michaux and D. F. Cutler (2005). "An AP-1/clathrin coat plays a novel and essential role in forming the Weibel-Palade bodies of endothelial cells." J Cell Biol **170**(4): 627-636.

Lukinavicius, G., C. Blaukopf, E. Pershagen, A. Schena, L. Reymond, E. Derivery, M. Gonzalez-Gaitan, E. D'Este, S. W. Hell, D. W. Gerlich and K. Johnsson (2015). "SiR-Hoechst is a far-red DNA stain for live-cell nanoscopy." Nat Commun **6**: 8497.

Lung, O., L. Kuo and M. F. Wolfner (2001). "Drosophila males transfer antibacterial proteins from their accessory gland and ejaculatory duct to their mates." J Insect Physiol **47**(6): 617-622.

MacGregor, P., B. Szoor, N. J. Savill and K. R. Matthews (2012). "Trypanosomal immune evasion, chronicity and transmission: an elegant balancing act." Nat Rev Microbiol **10**(6): 431-438.

Malvy, D. and F. Chappuis (2011). "Sleeping sickness." Clin Microbiol Infect **17**(7): 986-995.

Martens, S. and H. T. McMahon (2008). "Mechanisms of membrane fusion: disparate players and common principles." Nat Rev Mol Cell Biol **9**(7): 543-556.

McCarthy, M. I. (2017). "Genetics of T2DM in 2016: Biological and translational insights from T2DM genetics." Nat Rev Endocrinol **13**(2): 71-72.

McConville, M. J., K. A. Mullin, S. C. Ilgoutz and R. D. Teasdale (2002). "Secretory pathway of trypanosomatid parasites." Microbiol Mol Biol Rev **66**(1): 122-154; table of contents.

McCullagh, P. and J. A. Nelder (1989). Generalized linear models. London ; New York, Chapman and Hall.

McGraw, L. A., A. G. Clark and M. F. Wolfner (2008). "Post-mating gene expression profiles of female Drosophila melanogaster in response to time and to four male accessory gland proteins." Genetics **179**(3): 1395-1408.

Mellman, I. and W. J. Nelson (2008). "Coordinated protein sorting, targeting and distribution in polarized cells." Nat Rev Mol Cell Biol **9**(11): 833-845.

Messenger, S. W., M. A. Falkowski and G. E. Groblewski (2014). "Ca(2)(+)-regulated secretory granule exocytosis in pancreatic and parotid acinar cells." Cell Calcium **55**(6): 369-375.

Millay, D. P., J. R. O'Rourke, L. B. Sutherland, S. Bezprozvannaya, J. M. Shelton, R. Bassel-Duby and E. N. Olson (2013). "Myomaker is a membrane activator of myoblast fusion and muscle formation." Nature **499**(7458): 301-305.

Minami, R., M. Wakabayashi, S. Sugimori, K. Taniguchi, A. Kokuryo, T. Imano, T. Adachi-Yamada, N. Watanabe and H. Nakagoshi (2012). "The homeodomain protein defective proventriculus is essential for male accessory gland development to enhance fecundity in Drosophila." PloS one **7**(3): e32302.

Mori, T., M. Hirai, T. Kuroiwa and S. Y. Miyagishima (2010). "The functional domain of GCS1-based gamete fusion resides in the amino terminus in plant and parasite species." PloS one **5**(12): e15957.

Mori, T., H. Kuroiwa, T. Higashiyama and T. Kuroiwa (2006). "GENERATIVE CELL SPECIFIC 1 is essential for angiosperm fertilization." Nature cell biology **8**(1): 64-71.

Morvan, J. and S. A. Tooze (2008). "Discovery and progress in our understanding of the regulated secretory pathway in neuroendocrine cells." Histochem Cell Biol **129**(3): 243-252.

Nagarkar-Jaiswal, S., P. T. Lee, M. E. Campbell, K. Chen, S. Anguiano-Zarate, M. C. Gutierrez, T. Busby, W. W. Lin, Y. He, K. L. Schulze, B. W. Booth, M. Evans-Holm, K. J. Venken, R. W. Levis, A. C. Spradling, R. A. Hoskins and H. J. Bellen (2015). "A library of MiMICs allows tagging of genes and reversible, spatial and temporal knockdown of proteins in Drosophila." Elife **4**.

Nakamura, A., K. Takigawa, Y. Kurishita, K. Kuwata, M. Ishida, Y. Shimoda, I. Hamachi and S. Tsukiji (2014). "Hoechst tagging: a modular strategy to design synthetic fluorescent probes for live-cell nucleus imaging." Chem Commun (Camb) **50**(46): 6149-6152.

Nakatsu, F., K. Hase and H. Ohno (2014). "The Role of the Clathrin Adaptor AP-1: Polarized Sorting and Beyond." Membranes (Basel) **4**(4): 747-763.

Ni, J. Q., M. Markstein, R. Binari, B. Pfeiffer, L. P. Liu, C. Villalta, M. Booker, L. Perkins and N. Perrimon (2008). "Vector and parameters for targeted transgenic RNA interference in Drosophila melanogaster." Nat Methods **5**(1): 49-51.

Okamoto, M., L. Yamada, Y. Fujisaki, G. Bloomfield, K. Yoshida, H. Kuwayama, H. Sawada, T. Mori and H. Urushihara (2016). "Two HAP2-GCS1 homologs responsible for gamete interactions in the cellular slime mold with multiple mating types: Implication for common mechanisms of sexual reproduction shared by plants and protozoa and for male-female differentiation." Dev Biol **415**(1): 6-13.

Oren-Suissa, M., T. Gattegno, V. Kravtsov and B. Podbilewicz (2017). "Extrinsic Repair of Injured Dendrites as a Paradigm for Regeneration by Fusion in Caenorhabditis elegans." Genetics **206**(1): 215-230.

Oren-Suissa, M. and B. Podbilewicz (2007). "Cell fusion during development." Trends in Cell Biology **17**(11): 537-546.

Parton, R. M., A. M. Valles, I. M. Dobbie and I. Davis (2010). "Live cell imaging in Drosophila melanogaster." Cold Spring Harb Protoc **2010**(4): pdb top75.

Peacock, L., M. Bailey, M. Carrington and W. Gibson (2014). "Meiosis and Haploid Gametes in the Pathogen Trypanosoma brucei." Current biology : CB **24**(2): 181-186.

Peacock, L., V. Ferris, M. Bailey and W. Gibson (2009). "Intraclonal mating occurs during tsetse transmission of Trypanosoma brucei." Parasit Vectors **2**(1): 43.

Peacock, L., V. Ferris, M. Bailey and W. Gibson (2014). "Mating compatibility in the parasitic protist Trypanosoma brucei." Parasit Vectors **7**: 78.

Peacock, L., V. Ferris, R. Sharma, J. Sunter, M. Bailey, M. Carrington and W. Gibson (2011). "Identification of the meiotic life cycle stage of Trypanosoma brucei in the tsetse fly." Proc Natl Acad Sci U S A **108**(9): 3671-3676.

Perkins, L. A., L. Holderbaum, R. Tao, Y. Hu, R. Sopko, K. McCall, D. Yang-Zhou, I. Flockhart, R. Binari, H. S. Shim, A. Miller, A. Housden, M. Foos, S. Randkelv, C. Kelley, P. Namgyal, C. Villalta, L. P. Liu, X. Jiang, Q. Huan-Huan, X. Wang, A. Fujiyama, A. Toyoda, K. Ayers, A. Blum, B. Czech, R. Neumuller, D. Yan, A. Cavallaro, K. Hibbard, D. Hall, L. Cooley, G. J. Hannon, R. Lehmann, A. Parks, S. E. Mohr, R. Ueda, S. Kondo, J. Q. Ni and N. Perrimon (2015). "The Transgenic RNAi Project at Harvard Medical School: Resources and Validation." Genetics **201**(3): 843-852.

Pfeffer, S. R. (2013). "Rab GTPase regulation of membrane identity." Curr Opin Cell Biol **25**(4): 414-419.

Pinello, J. F., A. L. Lai, J. K. Millet, D. Cassidy-Hanley, J. H. Freed and T. G. Clark (2017). "Structure-Function Studies Link Class II Viral Fusogens with the Ancestral Gamete Fusion Protein HAP2." Curr Biol **27**(5): 651-660.

Poon, S. K., L. Peacock, W. Gibson, K. Gull and S. Kelly (2012). "A modular and optimized single marker system for generating Trypanosoma brucei cell lines expressing T7 RNA polymerase and the tetracycline repressor." Open Biol **2**(2): 110037.

Primakoff, P. and D. G. Myles (2007). "Cell-cell membrane fusion during mammalian fertilization." FEBS letters **581**(11): 2174-2180.

Ravi Ram, K., S. Ji and M. F. Wolfner (2005). "Fates and targets of male accessory gland proteins in mated female Drosophila melanogaster." Insect Biochem Mol Biol **35**(9): 1059-1071.

Redhai, S., J. E. Hellberg, M. Wainwright, S. W. Perera, F. Castellanos, B. Kroeger, C. Gandy, A. Leiblich, L. Corrigan, T. Hilton, B. Patel, S. J. Fan, F. Hamdy, D. C. Goberdhan and C. Wilson (2016). "Regulation of Dense-Core Granule Replenishment by Autocrine BMP Signalling in Drosophila Secondary Cells." PLoS Genet **12**(10): e1006366.

Reinke, R., D. E. Krantz, D. Yen and S. L. Zipursky (1988). "Chaoptin, a cell surface glycoprotein required for Drosophila photoreceptor cell morphogenesis, contains a repeat motif found in yeast and human." Cell **52**(2): 291-301.

Ren, X., G. G. Farias, B. J. Canagarajah, J. S. Bonifacino and J. H. Hurley (2013). "Structural basis for recruitment and activation of the AP-1 clathrin adaptor complex by Arf1." Cell **152**(4): 755-767.

Rodrigues, F. F., W. Shao and T. J. Harris (2016). "The Arf GAP Asap promotes Arf1 function at the Golgi for cleavage furrow biosynthesis in Drosophila." Mol Biol Cell **27**(20): 3143-3155.

Rosenbaum, E. E., K. S. Brehm, E. Vasiljevic, A. Gajeski and N. J. Colley (2012). "Drosophila GPI-mannosyltransferase 2 is required for GPI anchor attachment and surface expression of chaoptin." Vis Neurosci **29**(3): 143-156.

Rubinstein, C. D. and M. F. Wolfner (2013). "Drosophila seminal protein ovulin mediates ovulation through female octopamine neuronal signaling." Proc Natl Acad Sci U S A **110**(43): 17420-17425.

Rylett, C. M., M. J. Walker, G. J. Howell, A. D. Shirras and R. E. Isaac (2007). "Male accessory glands of Drosophila melanogaster make a secreted angiotensin I-converting enzyme (ANCE), suggesting a role for the peptide-processing enzyme in seminal fluid." J Exp Biol **210**(Pt 20): 3601-3606.

Sanchez-Pulido, L. and C. P. Ponting (2011). "Structure and evolutionary history of DISC1." Hum Mol Genet **20**(R2): R175-181.

Sanchez-Pulido, L. and C. P. Ponting (2011). "Structure and evolutionary history of DISC1." Human molecular genetics **20**(R2): R175-181.

Sasikumar, S. and J. K. Roy (2009). "Developmental expression of Rab11, a small GTP-binding protein in Drosophila epithelia." Genesis (New York, N Y : 2000) **47**(1): 32-39.

Satoh, T., T. Inagaki, Z. Liu, R. Watanabe and A. K. Satoh (2013). "GPI biosynthesis is essential for rhodopsin sorting at the trans-Golgi network in Drosophila photoreceptors." Development **140**(2): 385-394.

Satouh, Y., N. Inoue, M. Ikawa and M. Okabe (2012). "Visualization of the moment of mouse sperm-egg fusion and dynamic localization of IZUMO1." Journal of cell science **125**(Pt 21): 4985-4990.

Scott, C. C., F. Vacca and J. Gruenberg (2014). "Endosome maturation, transport and functions." Semin Cell Dev Biol **31**: 2-10.

Seed, B. (1987). "An LFA-3 cDNA encodes a phospholipid-linked membrane protein homologous to its receptor CD2." Nature **329**(6142): 840-842.

Sharma, R., E. Gluenz, L. Peacock, W. Gibson, K. Gull and M. Carrington (2009). "The heart of darkness: growth and form of Trypanosoma brucei in the tsetse fly." Trends in parasitology **25**(11): 517-524.

Sharma, R., L. Peacock, E. Gluenz, K. Gull, W. Gibson and M. Carrington (2008). "Asymmetric cell division as a route to reduction in cell length and change in cell morphology in trypanosomes." Protist **159**(1): 137-151.

Shemiakina, II, G. V. Ermakova, P. J. Cranfill, M. A. Baird, R. A. Evans, E. A. Souslova, D. B. Staroverov, A. Y. Gorokhovatsky, E. V. Putintseva, T. V. Gorodnicheva, T. V. Chepurnykh, L. Strukova, S. Lukyanov, A. G. Zaraisky, M. W. Davidson, D. M. Chudakov and D. Shcherbo (2012). "A monomeric red fluorescent protein with low cytotoxicity." Nat Commun **3**: 1204.

Shin, K., V. C. Fogg and B. Margolis (2006). "Tight junctions and cell polarity." Annu Rev Cell Dev Biol **22**: 207-235.

Siddhanta, A., J. M. Backer and D. Shields (2000). "Inhibition of phosphatidic acid synthesis alters the structure of the Golgi apparatus and inhibits secretion in endocrine cells." J Biol Chem **275**(16): 12023-12031.

Simarro, P. P., G. Cecchi, J. R. Franco, M. Paone, A. Diarra, J. A. Ruiz-Postigo, E. M. Fevre, R. C. Mattioli and J. G. Jannin (2012). "Estimating and mapping the population at risk of sleeping sickness." PLoS Negl Trop Dis **6**(10): e1859.

Sitnik, J. L., D. Gligorov, R. K. Maeda, F. Karch and M. F. Wolfner (2016). "The Female Post-Mating Response Requires Genes Expressed in the Secondary Cells of the Male Accessory Gland in Drosophila melanogaster." Genetics **202**(3): 1029-1041.

Steele, R. E. and C. E. Dana (2009). "Evolutionary history of the HAP2/GCS1 gene and sexual reproduction in metazoans." PloS one **4**(11): e7680.

Stoops, E. H. and M. J. Caplan (2014). "Trafficking to the apical and basolateral membranes in polarized epithelial cells." J Am Soc Nephrol **25**(7): 1375-1386.

Sturrock, E. D., R. Natesh, J. M. van Rooyen and K. R. Acharya (2004). "Structure of angiotensin I-converting enzyme." Cell Mol Life Sci **61**(21): 2677-2686.

Susic-Jung, L., C. Hornbruch-Freitag, J. Kuckwa, K. H. Rexer, U. Lammel and R. Renkawitz-Pohl (2012). "Multinucleated smooth muscles and mononucleated as

well as multinucleated striated muscles develop during establishment of the male reproductive organs of Drosophila melanogaster." Dev Biol **370**(1): 86-97.

Suster, M. L., L. Seugnet, M. Bate and M. B. Sokolowski (2004). "Refining GAL4-driven transgene expression in Drosophila with a GAL80 enhancer-trap." Genesis **39**(4): 240-245.

Takemori, N. and M. T. Yamamoto (2009). "Proteome mapping of the Drosophila melanogaster male reproductive system." Proteomics **9**(9): 2484-2493.

Trimble, W. S. and S. Grinstein (2015). "Barriers to the free diffusion of proteins and lipids in the plasma membrane." J Cell Biol **208**(3): 259-271.

Tsuchiya, M., M. Hosaka, T. Moriguchi, S. Zhang, M. Suda, H. Yokota-Hashimoto, K. Shinozuka and T. Takeuchi (2010). "Cholesterol biosynthesis pathway intermediates and inhibitors regulate glucose-stimulated insulin secretion and secretory granule formation in pancreatic beta-cells." Endocrinology **151**(10): 4705-4716.

Vagin, O., J. A. Kraut and G. Sachs (2009). "Role of N-glycosylation in trafficking of apical membrane proteins in epithelia." Am J Physiol Renal Physiol **296**(3): F459-469.

Valansi, C., D. Moi, E. Leikina, E. Matveev, M. Grana, L. V. Chernomordik, H. Romero, P. S. Aguilar and B. Podbilewicz (2017). "Arabidopsis HAP2/GCS1 is a gamete fusion protein homologous to somatic and viral fusogens." J Cell Biol **216**(3): 571-581.

van Niel, G., G. D'Angelo and G. Raposo (2018). "Shedding light on the cell biology of extracellular vesicles." Nat Rev Mol Cell Biol **19**(4): 213-228.

Van Vactor, D., Jr., D. E. Krantz, R. Reinke and S. L. Zipursky (1988). "Analysis of mutants in chaoptin, a photoreceptor cell-specific glycoprotein in Drosophila, reveals its role in cellular morphogenesis." Cell **52**(2): 281-290.

Vickerman, K. (1985). "Developmental cycles and biology of pathogenic trypanosomes." British medical bulletin **41**(2): 105-114.

Vickerman, K., L. Tetley, K. A. Hendry and C. M. Turner (1988). "Biology of African trypanosomes in the tsetse fly." Biology of the cell / under the auspices of the European Cell Biology Organization **64**(2): 109-119.

Vissers, J. H., S. A. Manning, A. Kulkarni and K. F. Harvey (2016). "A Drosophila RNAi library modulates Hippo pathway-dependent tissue growth." Nat Commun **7**: 10368.

von Besser, K., A. C. Frank, M. A. Johnson and D. Preuss (2006). "Arabidopsis HAP2 (GCS1) is a sperm-specific gene required for pollen tube guidance and fertilization." Development **133**(23): 4761-4769.

Walker, G., R. G. Dorrell, A. Schlacht and J. B. Dacks (2011). "Eukaryotic systematics: a user's guide for cell biologists and parasitologists." Parasitology **138**(13): 1638-1663.

Wasbrough, E. R., S. Dorus, S. Hester, J. Howard-Murkin, K. Lilley, E. Wilkin, A. Polpitiya, K. Petritis and T. L. Karr (2010). "The Drosophila melanogaster sperm proteome-II (DmSP-II)." J Proteomics **73**(11): 2171-2185.

Wilson, C., A. Leiblich, D. C. Goberdhan and F. Hamdy (2017). "The Drosophila Accessory Gland as a Model for Prostate Cancer and Other Pathologies." Curr Top Dev Biol **121**: 339-375.

Wirtz, E., S. Leal, C. Ochatt and G. A. Cross (1999). "A tightly regulated inducible expression system for conditional gene knock-outs and dominant-negative genetics in Trypanosoma brucei." Molecular and biochemical parasitology **99**(1): 89-101.

Wolfinger, R. and M. Oconnell (1993). "Generalized Linear Mixed Models - a Pseudo-Likelihood Approach." Journal of Statistical Computation and Simulation **48**(3-4): 233-243.

Wong, J. L. and M. A. Johnson (2010). "Is HAP2-GCS1 an ancestral gamete fusogen?" Trends in cell biology **20**(3): 134-141.

Wong, J. L., A. R. Leydon and M. A. Johnson (2010). "HAP2(GCS1)-dependent gamete fusion requires a positively charged carboxy-terminal domain." PLoS genetics **6**(3): e1000882.

Wu, M. M., M. Grabe, S. Adams, R. Y. Tsien, H. P. Moore and T. E. Machen (2001). "Mechanisms of pH regulation in the regulated secretory pathway." J Biol Chem **276**(35): 33027-33035.

Xie, Y., C. You and J. Chen (2014). "An updated meta-analysis on association between angiotensin I-converting enzyme gene insertion/deletion polymorphism and cancer risk." Tumour biology : the journal of the International Society for Oncodevelopmental Biology and Medicine **35**(7): 6567-6579.

Xue, L. and M. Noll (2000). "Drosophila female sexual behavior induced by sterile males showing copulation complementation." Proc Natl Acad Sci U S A **97**(7): 3272-3275.

Yamanaka, N., G. Marques and M. B. O'Connor (2015). "Vesicle-Mediated Steroid Hormone Secretion in Drosophila melanogaster." Cell **163**(4): 907-919.

Yoo, S. H. and J. P. Albanesi (1990). "Ca2(+)-induced conformational change and aggregation of chromogranin A." The Journal of biological chemistry **265**(24): 14414-14421.

Younus, F., N. J. Fraser, C. W. Coppin, J. W. Liu, G. J. Correy, T. Chertemps, G. Pandey, M. Maibeche, C. J. Jackson and J. G. Oakeshott (2017). "Molecular basis for the behavioral effects of the odorant degrading enzyme Esterase 6 in Drosophila." Sci Rep **7**: 46188.

Appendix 1. Candidates found with the HMMer2-based analysis for Boxes 1-3. Colour code illustrates taxonomic groups (Walker, Dorrell et al. 2011).

Box 1	Box 2	Box3	Species	Uniprot Link
A0C2L6_PART_01	A0C2L6_PARTE_01	A0C2L6_PARTE_01	*Paramecium tetraurelia*	http://www.uniprot.org/uniprot/A0C2L6
	A3FEQ2_9CNID_01		*Hydra magnipapillata*	http://www.uniprot.org/uniprot/A3FEQ2
A4GRC6_CHLRE_01	A4GRC6_CHLRE_01	A4GRC6_CHLRE_01	*Chlamydomonas reinhardtii (Chlamydomonas smithii)*	http://www.uniprot.org/uniprot/A4GRC6
A5ADU5_VITVI_01			*Vitis vinifera (Grape)*	http://www.uniprot.org/uniprot/A5ADU5
		A5K5U6_PLAVS_01	*Plasmodium vivax (strain Salvador I)*	http://www.uniprot.org/uniprot/A5K5U6
A6MD07_ORYBR_01			*Oryza brachyantha*	http://www.uniprot.org/uniprot/A6MD07
	A7ANV4_BABBO_01	A7ANV4_BABBO_01	*Babesia bovis*	http://www.uniprot.org/uniprot/A7ANV4
A7SIM4_NEMVE_01	A7SIM4_NEMVE_01		*Nematostella vectensis (Starlet sea anemone)*	http://www.uniprot.org/uniprot/A7SIM4
	A8J3B3_CHLRE_01	A8J3B3_CHLRE_01	*Chlamydomonas reinhardtii (Chlamydomonas smithii)*	http://www.uniprot.org/uniprot/A8J3B3
A9SWN6_PHYPA_01			*Physcomitrella patens subsp. patens (Moss)*	http://www.uniprot.org/uniprot/A9SWN6
A9V179_MONBE_01	A9V179_MONBE_01	A9V179_MONBE_01	*Monosiga brevicollis (Choanoflagellate)*	http://www.uniprot.org/uniprot/A9V179
B3M263_DROAN_01		B3M263_DROAN_01	*Drosophila ananassae (Fruit fly)*	http://www.uniprot.org/uniprot/B3M263
	B3L1E3_PLAKH_01	B3L1E3_PLAKH_01	*Plasmodium knowlesi (strain H)*	http://www.uniprot.org/uniprot/B3L1E3
B4QUA9_DROSI_01			*Drosophila simulans (Fruit fly)*	http://www.uniprot.org/uniprot/B4QUA9
		B4NJV9_DROWI_01	*Drosophila willistoni (Fruit fly)*	http://www.uniprot.org/uniprot/B4NJV9
	B6AB62_CRYMR_01		*Cryptosporidium muris (strain RN66)*	http://www.uniprot.org/uniprot/B6AB62
		B6KN09_TOXGO_01	*Toxoplasma gondii*	http://www.uniprot.org/uniprot/B6KN09
B7PZS5_IXOSC_01			*Ixodes scapularis (Black-legged tick) (Deer tick)*	http://www.uniprot.org/uniprot/B7PZS5
B9RC35_RICCO_01	B9RC35_RICCO_01		*Ricinus communis (Castor bean)*	http://www.uniprot.org/uniprot/B9RC35
	C0H4U8_PLAF7_01	C0H4U8_PLAF7_01	*Plasmodium falciparum (isolate 3D7)*	http://www.uniprot.org/uniprot/C0H4U8
C5X637_SORBI_01			*Sorghum bicolor (Sorghum) (Sorghum vulgare)*	http://www.uniprot.org/uniprot/C5X637
CG34027_Q2PDQ0		CG34027_Q2PDQ0	*Drosophila melanogaster (Fruit fly)*	http://www.uniprot.org/uniprot/Q2PDQ0
	D2VN83_NAEGR_01	D2VN83_NAEGR_01	*Naegleria gruberi (Amoeba)*	http://www.uniprot.org/uniprot/D2VN83
		D3B4N3_POLPA_01	*Polysphondylium pallidum*	http://www.uniprot.org/uniprot/D3B4N3
D3BGR4_POLPA_01	D3BGR4_POLPA_01		*Polysphondylium pallidum*	http://www.uniprot.org/uniprot/D3BGR4
		D3BB89_POLPA_01	*Polysphondylium pallidum*	http://www.uniprot.org/uniprot/D3BB89
D6WRF1_TRICA_01	D6WRF1_TRICA_01	D6WRF1_TRICA_01	*Tribolium castaneum (Red flour beetle)*	http://www.uniprot.org/uniprot/D6WRF1
D8RKA0_SELML_01		D8RKA0_SELML_01	*Selaginella moellendorffii (Spikemoss)*	http://www.uniprot.org/uniprot/D8RKA0
	D8U2H3_VOLCA_01	D8U2H3_VOLCA_01	*Volvox carteri (Green alga)*	http://www.uniprot.org/uniprot/D8U2H3
D8U2H4_VOLCA_01		D8U2H4_VOLCA_01	*Volvox carteri (Green alga)*	http://www.uniprot.org/uniprot/D8U2H4
E0VV28_PEDHC_01		E0VV28_PEDHC_01	*Pediculus humanus subsp. corporis (Body louse)*	http://www.uniprot.org/uniprot/E0VV28
	E1Z455_CHLVA_01	E1Z455_CHLVA_01	*Chlorella variabilis (Green alga)*	http://www.uniprot.org/uniprot/E1Z455
E9BRS7_LEIDB_01	E9BRS7_LEIDB_01	E9BRS7_LEIDB_01	*Leishmania donovani*	http://www.uniprot.org/uniprot/E9BRS7
		E9CHV8_CAPO3_01	*Capsaspora owczarzaki (strain ATCC 30864)*	http://www.uniprot.org/uniprot/E9CHV8
		F0ZLD8_DICPU_01	*Dictyostelium purpureum*	http://www.uniprot.org/uniprot/F0ZLD8
		F0ZQI2_DICPU_01	*Dictyostelium purpureum*	http://www.uniprot.org/uniprot/F0ZQI2
	F0ZW03_DICPU_01	F0ZW03_DICPU_01	*Dictyostelium purpureum*	http://www.uniprot.org/uniprot/F0ZW03
F2UNH3_SALS5_01	F2UNH3_SALS5_01	F2UNH3_SALS5_01	*Salpingoeca sp. (strain ATCC 50818)*	http://www.uniprot.org/uniprot/F2UNH3
F4PR89_DICFS_01	F4PR89_DICFS_01	F4PR89_DICFS_01	*Dictyostelium fasciculatum (strain SH3)*	http://www.uniprot.org/uniprot/F4PR89
		F4WFD7_ACREC_01	*Acromyrmex echinatior (Panamanian leafcutter ant)*	http://www.uniprot.org/uniprot/F4WFD7
		G0QL62_ICHMG_01	*Ichthyophthirius multifiliis*	http://www.uniprot.org/uniprot/G0QL62
G0U801_TRYVY_01	G0U801_TRYVY_01	G0U801_TRYVY_01	*Trypanosoma vivax (strain Y486)*	http://www.uniprot.org/uniprot/G0U801
G0UXL2_TRYCI_01	G0UXL2_TRYCI_01	G0UXL2_TRYCI_01	*Trypanosoma congolense (strain IL3000)*	http://www.uniprot.org/uniprot/G0UXL2
		G6DNV7_DANPL_01	*Danaus plexippus (Monarch butterfly)*	http://www.uniprot.org/uniprot/G6DNV7
HAP2_F4JP36	F4JP36_ARATH_01	F4JP36_ARATH_01	*Arabidopsis thaliana (Mouse-ear cress)*	http://www.uniprot.org/uniprot/F4JP36
I0Z782_9CHLO_01	I0Z782_9CHLO_01	I0Z782_9CHLO_01	*Coccomyxa subellipsoidea C-169*	http://www.uniprot.org/uniprot/I0Z782
I1FNA7_AMPQE_01		I1FNA7_AMPQE_01	*Amphimedon queenslandica (Sponge)*	http://www.uniprot.org/uniprot/I1FNA7
I1FNC0_AMPQE_01		I1FNC0_AMPQE_01	*Amphimedon queenslandica (Sponge)*	http://www.uniprot.org/uniprot/I1FNC0
I1IS14_BRADI_01			*Brachypodium distachyon (Purple false brome)*	http://www.uniprot.org/uniprot/I1IS14
I4DEF5_EIMTE_01	I4DEF5_EIMTE_01	I4DEF5_EIMTE_01	*Eimeria tenella (Coccidian parasite)*	http://www.uniprot.org/uniprot/I4DEF5
I7I9C3_BABMI_01		I7I9C3_BABMI_01	*Babesia microti strain RI*	http://www.uniprot.org/uniprot/I7I9C3
J4CDY9_THEOR_01	J4CDY9_THEOR_01		*Theileria orientalis strain Shintoku*	http://www.uniprot.org/uniprot/J4CDY9
	J9FHQ6_9SPIT_01	J9FHQ6_9SPIT_01	*Oxytricha trifallax*	http://www.uniprot.org/uniprot/J9FHQ6
J9KKT4_ACYPI_01			*Acyrthosiphon pisum (Pea aphid)*	http://www.uniprot.org/uniprot/J9KKT4
	J9M478_ACYPI_01	J9M478_ACYPI_01	*Acyrthosiphon pisum (Pea aphid)*	http://www.uniprot.org/uniprot/J9M478
K2N3W5_TRYCR_01	K2N3W5_TRYCR_01	K2N3W5_TRYCR_01	*Trypanosoma cruzi marinkellei*	http://www.uniprot.org/uniprot/K2N3W5
K4CP45_SOLLC_01	K4CP45_SOLLC_01		*Solanum lycopersicum (Tomato) (L. esculentum)*	http://www.uniprot.org/uniprot/K4CP45
		K6V7X4_9APIC_01	*Plasmodium cynomolgi strain B*	http://www.uniprot.org/uniprot/K6V7X4
	K7LCI4_SOYBN_01	K7LCI4_SOYBN_01	*Glycine max (Soybean) (Glycine hispida)*	http://www.uniprot.org/uniprot/K7LCI4
	L0B2I6_BABEQ_01	L0B2I6_BABEQ_01	*Babesia equi*	http://www.uniprot.org/uniprot/L0B2I6
		L8GEA8_ACACA_01	*Acanthamoeba castellanii str. Neff*	http://www.uniprot.org/uniprot/L8GEA8
L8H1Q8_ACACA_01	L8H1Q8_ACACA_01		*Acanthamoeba castellanii str. Neff*	http://www.uniprot.org/uniprot/L8H1Q8
M0S139_MUSAC_01			*Musa acuminata subsp. malaccensis (Wild banana)*	http://www.uniprot.org/uniprot/M0S139
M0YC72_HORVD_01	M0YC72_HORVD_01	M0YC72_HORVD_01	*Hordeum vulgare var. distichum (Two-rowed barley)*	http://www.uniprot.org/uniprot/M0YC72
		MatD_D3UFF8_01	*Dictyostelium discoideum (Slime mold)*	http://www.uniprot.org/uniprot/D3UFF8
		MatT_D3UFE1_01	*Dictyostelium discoideum (Slime mold)*	http://www.uniprot.org/uniprot/D3UFE1
Q1X7J9_LEIMA_01	Q1X7J9_LEIMA_01	Q1X7J9_LEIMA_01	*Leishmania major*	http://www.uniprot.org/uniprot/Q1X7J9
Q22C76_TETTS_01	Q22C76_TETTS_01		*Tetrahymena thermophila (strain SB210)*	http://www.uniprot.org/uniprot/Q22C76
Q2PGG5_PHYPO_01	Q2PGG5_PHYPO_01	Q2PGG5_PHYPO_01	*Physarum polycephalum (Slime mold)*	http://www.uniprot.org/uniprot/Q2PGG5
	Q4N203_THEPA_01		*Theileria parva*	http://www.uniprot.org/uniprot/Q4N203
		Q4X6I4_PLACH_01	*Plasmodium chabaudi*	http://www.uniprot.org/uniprot/Q4X6I4
		Q54T88_DICDI_01	*Dictyostelium discoideum (Slime mold)*	http://www.uniprot.org/uniprot/Q54T88
		Q559R5_DICDI_01	*Dictyostelium discoideum (Slime mold)*	http://www.uniprot.org/uniprot/Q559R5
Q5W6B9_ORYSJ_01	Q5W6B9_ORYSJ_01	Q5W6B9_ORYSJ_01	*Oryza sativa subsp. japonica (Rice)*	http://www.uniprot.org/uniprot/Q5W6B9
Q75JL6_DICDI_01	Q75JL6_DICDI_01	Q75JL6_DICDI_01	*Dictyostelium discoideum (Slime mold)*	http://www.uniprot.org/uniprot/Q75JL6
	Q8IJQ3_PLAF7_01	Q8IJQ3_PLAF7_01	*Plasmodium falciparum (isolate 3D7)*	http://www.uniprot.org/uniprot/Q8IJQ3
Q389Q2_TRYB2	Q389Q2_TRYB2	Q389Q2_TRYB2	*Trypanosoma brucei brucei (strain 927/4 GUTat10.1)*	http://www.uniprot.org/uniprot/Q389Q2

Appendix 2. Inducible Expression of HAP2(GCS1) in *T. brucei* using 29-13 and SmOxP9 cells. pDex577 illustration courtesy of Kelly, Reed et al 2007. Cell lines expressing pDex577:HAP2 were designed by E. Gluenz. Construct illustrations courtesy of E. Gluenz.

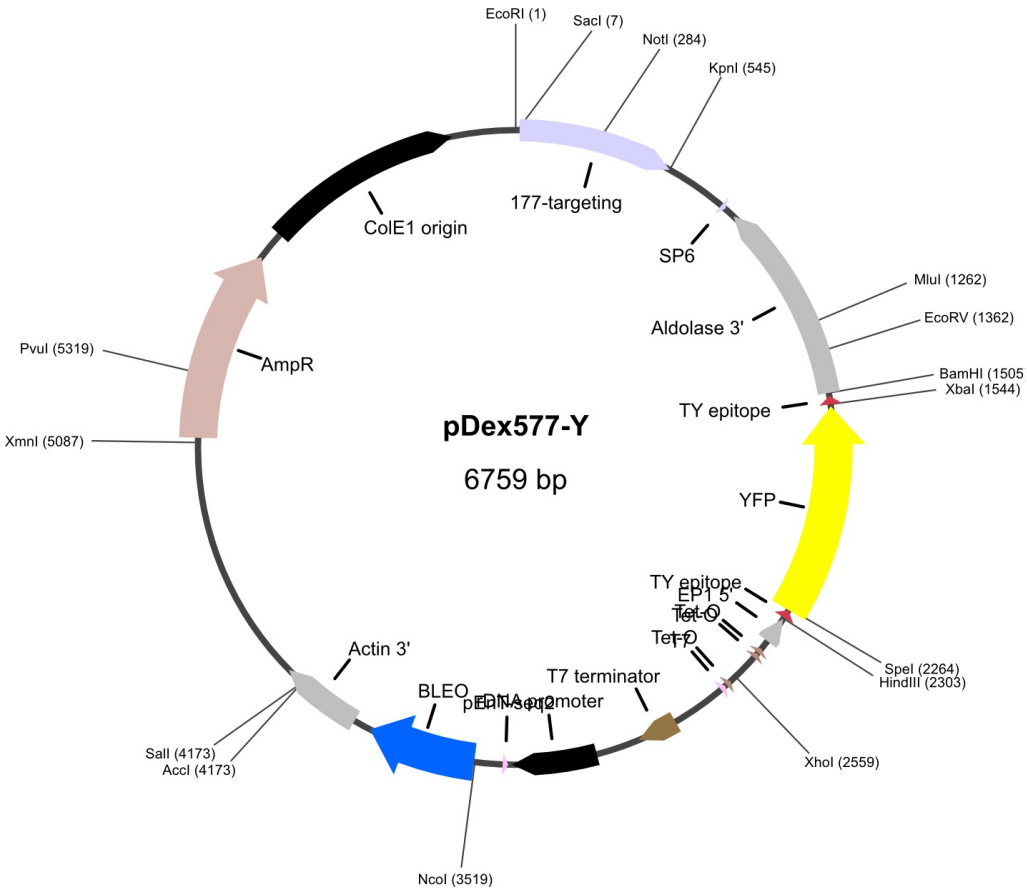

*Tb*HAP2:TY

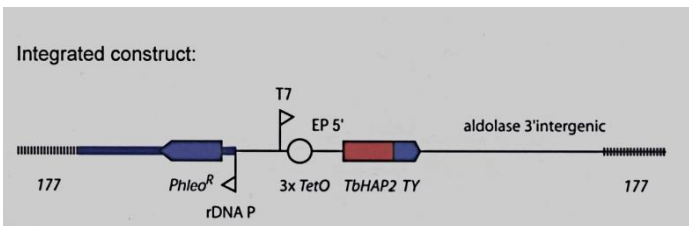

*Tb*HAP2:YFP:TY

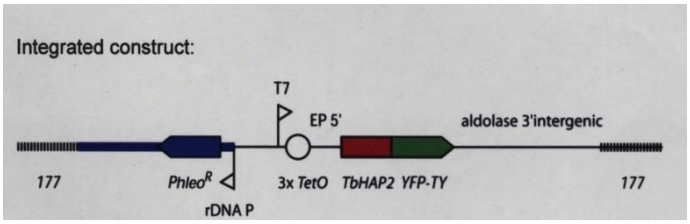

Appendix 3. Endogenous expression of HAP2(GCS1) in *T. brucei* using TREU 927/4 cells. Plasmid illustration courtesy of Kelly, Reed et al 2007. Cell lines expressing *Tb*HAP2:YFP were designed by E. Gluenz. Construct illustration courtesy of E. Gluenz.